Negative regulation of interferon lambda induced JAK-STAT signaling and development of patient-derived xenograft models from fresh human hepatocellular carcinoma biopsies

Inauguraldissertation
zur
Erlangung der Würde eines Doktors der Philosophie
vorgelegt der
Philosophisch-Naturwissenschaftlichen Fakultät
der Universität Basel

von

Tanja Blumer
aus Basel, BS

Basel, 2018

Genehmigt von der Philosophisch-Naturwissenschaftlichen Fakultät

Auf Antrag von

Prof. Dr. med. Markus Heim
Prof. Dr. Gerhard Christofori

Basel, den 27.02.2018

Prof. Dr. Martin Spiess

I dedicate my PhD thesis to my grandmothers Myrtha and Ronny, two strong women who inspire me with their energy and positive thinking.

Acknowledgments

I would like to express my gratitude to…

… Prof. Dr. med. Markus Heim for giving me the opportunity to complete my PhD thesis in his lab, for the valuable discussions about my projects and for teaching me how fascinating translational research is.

… my committee members Prof. Dr. Gerhard Christofori and Prof. Dr. Petr Broz for their time, helpful inputs and discussions during the committee meetings.

… Dr. Stefan Wieland for his support during my PhD, for the critical reading of my manuscripts and thesis, and for explaining to me the intricacies of the English language. I really appreciated it.

… Dr. François Duong for being my supervisor during the first years of my PhD. For his creative experimental ideas, endless discussions and for the daily coffee break. I really enjoyed working with you.

… all the great people from the Hepatology group for an enjoyable working atmosphere, endless support, countless laughs and lively discussions during the lunch breaks. Special thanks to Dr. Mairene Coto-Llerena, Marie-Anne Meier and Sandro Nuciforo for their support, and countless discussions which were not only about science during our daily coffee break.

… all the helpful people from the Institute of Pathology for their support during the last years. Special thanks to Dr. med. Matthias Matter, Prof. Dr. med. Luigi Tornillo and Prof. Dr. med. Luigi Terracciano for the help, and for the endless patience in explaining to me the mysteries of liver tumor histology. Special thanks to Dr. Charlotte Ng for a wonderful and very fruitful collaboration. I really appreciated working with you.

… all the people for their helpful inputs and critical reading of my PhD thesis, and manuscripts.

… my friends for supporting me during the last years, for cheering me up after failed experiments and for all the great events outside the lab. You are amazing.

… my family, especially my two sisters, my mother and my father for their endless support, love and motivation. I know that I can always count on you.

… Fabian for always supporting and believing in me and for the amazing time we spent together. You are my inspiration.

Summary

Type I and type III interferons (IFNs) act as the first line of defense against invading pathogens by inducing a fast and strong host response characterized by the expression of hundreds of interferon stimulated genes (ISGs). However, the magnitude and duration of cellular responses to viral and bacterial infections needs to be controlled properly to maintain tissue homeostasis. Ubiquitin specific peptidase 18 (USP18), suppressor of cytokine signaling 1 (SOCS1) and SOCS3 are the three known inducible negative regulators of the IFN-α induced signaling cascade. However, the role of USP18 on IFN-λ signaling is a matter of controversy. Furthermore, the physiological relevance of the relative contribution of SOCS1 and SOCS3 on *in vitro* IFN-λ signaling needs to be validated *in vivo.* Thus, we aimed to investigate the role of USP18, SOCS1 and SOCS3 on the IFN-λ induced signaling cascade both *in vitro* and *in vivo*.

Based on experiments with USP18, SOCS1 and SOCS3 knockout cells, we demonstrated that USP18 is the major negative regulator of IFN-α induced JAK-STAT signaling whereas IFN-λ is negatively regulated by SOCS1. Furthermore, using USP18 and SOCS1 knockout mice, we confirmed USP18 and SOCS1 as physiological relevant negative regulators of IFN-α and IFN-λ, respectively. Importantly, we demonstrated that negative regulation of IFN-α was strong and immediate while that for IFN-λ was more subtle both in kinetics as well as magnitude. Taken together, our results suggest that the differences in negative regulations are the basis for the distinct kinetic properties of IFN-α and IFN-λ signaling reflecting their specific functions. IFN-α signaling provides a powerful and immediate defense system against systemic infections but has to be controlled tightly to maintain tissue homeostasis. Therefore a strong negative regulator like USP18 that completely shuts down the system is needed. By contrast, IFN-λ provides a continuous first line defense in mucosal epithelial cells that are constantly exposed to pathogens. Thus, SOCS1 facilitates a maintained but controlled IFN-λ signaling that allows fighting invading pathogens without loosing tissue homeostasis.

Hepatocellular carcinoma (HCC) is the second deadliest cancer worldwide with yearly increasing incidence and unsatisfying treatment options. Thus, there is a clear need for new and more efficient drugs for the treatment of HCC. A major obstacle for the

understanding of the pathogenesis of HCC is the lack of an efficient *in vivo* model that accurately reflects the broad spectrum of human HCC. Patient-derived xenograft (PDX) models gained a lot of interest in pre-clinical studies of anti-cancer drugs. Indeed, several HCC PDX models have been established in recent years. However, all these models are derived from resected HCC specimen and therefore limited to early stage disease. Patients with advanced stage HCC are not represented, although they would benefit most from new treatment options. Therefore, we aimed to generate HCC PDX models from fresh human HCC biopsies that cover all disease stages, with special interest in advanced stage HCC.

We successfully established and passaged eleven HCC PDX mouse models from patients presenting with all major underlying liver diseases. The biopsies that successfully engrafted were representative of the spectrum of poorly differentiated HCCs, including both early and late-stage disease. Importantly, the PDX models recapitulated tumor morphology, differentiation grade and the expression pattern of known HCC markers. Finally, RNA sequencing analyses demonstrated that our PDX models maintained the transcriptomic profiles and expression of somatic mutations of their originating tumors over at least four generations. Taken together, these novel HCC PDX models do not only allow investigation of the biology of all stages of HCC but also the study of drug-induced resistance mechanisms and the development of new HCC therapies.

Abbreviations

Aa	Amino acids
AFP	Alpha-fetoprotein
BCLC	Barcelona Clinic Liver Cancer
CIS	Cytokine-inducible SH2-containing protein
CT	Computed tomography
DAA	Direct-acting antivirals
DEN	Diethylnitrosamine
ESS	Extended SH2-subdomain
GAF	Gamma activated factor
GAS	Gamma activated sequence
GEM	Genetically engineered mouse
GPC3	Glypican-3
GS	Glutamine Synthetase
H&E	Hematoxylin & Eosin
HBV	Hepatitis B virus
HBx	Hepatitis B protein X
HCC	Hepatocellular carcinoma
HCV	Hepatitis C virus
HSP70	Heat Shock protein 70
IFN	Interferon
IFNAR	Interferon-α receptor
IFNGR	Interferon-γ receptor
IFNLR	Interferon-λ receptor
IHC	Immunohistochemistry
IRF9	Interferon regulatory factor 9
ISG	Interferon stimulated gene
ISGF3	Interferon-stimulated gene factor 3
ISRE	Interferon-stimulated response element
JAK	Janus kinase
KIR	Kinase inhibitory region
LPS	Lipopolysaccharide
MRI	Magnetic resonance imaging
NAFLD	Non-alcoholic fatty liver disease
NASH	Non-alcoholic steatohepatitis
pDCs	Plasmacytoid dentritic cells
PDX	Patient-derived xenograft
pegIFN	Pegylated interferon
PIAS	Protein inhibitor of activated STAT
PTP	Protein tyrosine phosphatase
PTP1B	Protein tyrosine phosphatase 1B
RBV	Ribavirin
S.c.	Subcutaneous
SH2	Src-homology 2
SOCS	Suppressor of cytokine signaling
STAT	Signal transducers and activators of transcription
SVR	Sustained virological response
TACE	Transcatheter arterial chemoembolization
TC-PTP	T cell protein tyrosine phosphatase
TERT	Telomerase reverse-transcriptase
TVR	Telaprevir
TYK2	Tyrosine kinase 2
UBP	Ubiquitin-specific protease
USP18	Ubiquitin-specific peptidase 18

Contents

I Introduction

1 The Interferon System

1.1 Interferons

Interferons (IFNs) are cytokines, which are crucial for the induction of an efficient immune response against foreign material. Already early chordates 500 million years ago have developed IFNs as early elements of their innate and adaptive immune system[1]. In 1957, IFNs were first described by Isaacs and Lindenmann as a substance that protects cells from viral infection[2]. IFNs belong to the Class II cytokines known to be involved in minimizing the damage induced by external noninfectious agents, viruses or other microorganisms[1]. They have a broad range of biological activities, including inhibition of cell proliferation, immunomodulatory effects and induction of antiviral responses[3,4]. 10 mammalian IFN species (IFN-α, IFN-β, IFN-ε, IFN-κ, IFN-ω, IFN-δ, IFN-τ, IFN-ζ/limitin, IFN-γ and IFN-λ) have been discovered from which seven (IFN-α, IFN-β, IFN-ε, IFN-κ, IFN-ω, IFN-γ and IFN-λ) are found in humans[5,6]. Based on their structural features, receptor usage and biological activities, they are divided into three groups: type I, type II and type III IFNs[6-8]. The different IFN classes will be described in more detail in the following chapters.

1.1.1 Type I interferons

In humans, the group of type I IFNs comprises 12 functional IFN-α species and a single member each of IFN-β, IFN-ε, IFN-κ and IFN-ω[5]. All genes encoding type I IFNs are clustered on chromosome 9 and are devoid of introns[4,9]. While type I IFNs can be produced by all nucleated cells in response to invading pathogens[10,11], macrophages and plasmacytoid dendritic cells (pDCs) additionally produce type I IFNs in response to a variety of foreign material that they sample from the outside, without being infected themselves. Indeed, pDCs are considered as professional type I IFN producers[12-14]. Within the first 24 hours upon viral infection, pDCs produce 100-1000 times more type I IFN compared to other blood cell types[11,12].

Type I IFNs signal through a single cell surface receptor that is found on all nucleated cells[10]. The IFN-α/β receptor (IFNAR) is composed of the IFNAR1 and IFNAR2 subunits, the latter one harboring the major ligand binding domain[6]. The essential role of type I

IFNs in the antiviral defense has been demonstrated in mice deficient for components of the type I IFN system. These mice are highly susceptible to and unable to cope with viral infections[15]. Similarly, two infants with genetic defects in the IFN system died from viral infection despite best medical care[16].

1.1.2 Type II interferon

The only member of the type II IFN family is IFN-γ, which is encoded by a gene containing three introns located on human chromosome 12[4,9]. IFN-γ is secreted by cells of the innate and adaptive immune system such as natural killer (NK) and natural killer T cells and activated T cells, respectively[13,17]. In contrast to type I and III IFNs, IFN-γ forms homodimers and signals through a heterotetrameric receptor comprised of two IFN-γ receptor 1 (IFNGR1) and two IFNGR2 chains[18,19].

IFN-γ is involved in the innate and adaptive immune response against viruses, bacteria and parasites[8,20]. Beside its direct antiviral effect, IFN-γ has immunostimulatory and immunomodulatory roles. For example, it activates macrophages, mediators of nonspecific, cell-mediated host defense and stimulates their antigen presentation through major histocompatibility complex class I and II molecules. Furthermore, it induces the transcription of interferon stimulated genes (ISGs), many of which have antiviral activities[21-23]. Mice deficient for IFN-γ signaling have shown an impaired capacity to cope with viruses, bacteria and parasites, demonstrating the importance of IFN-γ–mediated immune responses[17,22,24].

Taken together, type I and type II IFNs work synergistically to induce innate and adaptive immune responses that contribute to the clearance of viral infections.

1.1.3 Type III interferons

Type III IFNs functionally resemble type I IFNs, inducing antiviral protection *in vitro*[9,25] and *in vivo*[26]. In humans, the type III IFN family consists of four members; IFN-λ1 (IL29), IFN-λ2 (IL28A), IFN-λ3 (IL28B) and the newly discovered IFN-λ4[27]. The distinct but closely related IFN-λ1, -λ2 and -λ3 have been discovered by two independent groups in 2003[9,25] whereas the IFN-λ4 has been identified only in 2013 in the polyI:C-induced gene expression profile of primary human hepatocytes[27]. The genes encoding IFN-λ1, -λ2 and -λ3 are clustered on human chromosome 19 and each of them is composed of

five exons[9]. The newly discovered *IFNL4* gene is also located within the *IFNL* locus, upstream of the *IFNL3* gene and, at the protein level, is only expressed in a fraction of the human population as a consequence of a genetic polymorphism that induces a deletion frameshift in the ss469415590 allele[27] (Figure 1). Paradoxically, the potential to produce the fully active IFN-λ4 is strongly associated with impaired clearance of hepatitis C virus (HCV) and a poorer response to pegylated (peg) IFN-α/ribavirin (RBV) combination treatment of chronic HCV patients[27,28]. However, the exact role of IFN-λ4 in HCV clearance remains to be elucidated.

Type I and type III IFNs are induced by similar signaling pathways[29,30] and pDCs are currently thought to be the main producers of IFN-λ[31,32]. Besides pDCs, other cells such as respiratory epithelial cells, keratinocytes, hepatocytes and primary neuronal cells have also been reported to produce IFN-λ[33]. Type III IFNs signal through a heterodimeric IFN-λ receptor (IFNLR) complex consisting of the IFN-λ specific IFNLR1 chain and the ubiquitously expressed accessory chain IL-10R2, used by IL-10 and related cytokines[9,20,25,34,35]. In contrast to the ubiquitous expression of the type I IFN receptor, the expression of the IFNLR1 chain is mostly restricted to epithelial cells, especially in the respiratory and the gastrointestinal tract[33,36-38]. Given the epithelial cell restricted IFNLR1 expression, the type III IFN system is believed to primarily protect mucosal epithelial cells from infection[38,39] and thus to serve as a defense system at the border, where virus infection is a frequent challenge[36,39]. Nevertheless, type III IFNs are also involved in the defense of hepatotropic viruses, shown for hepatitis B virus (HBV) and HCV[40,41].

1.1.3.1 Human versus mouse IFN-λ

One major difference between the human and the mouse type III interferon system is the number of functional IFN-λs. As described above in chapter 1.1.3, the human type III IFN family encompasses four members; IFN-λ1-4. In contrast, the mouse genome encodes only for functional IFN-λ2 and IFN-λ3 proteins whereas *Ifnl1* is a pseudogene[20,39]. Furthermore, it has been demonstrated that while IFN-λ4 sequences exist in most mammalian species they are absent in rodents[42]. At the protein level, human and mouse type III IFNs differ in their glycosylation. In mice, IFN-λ2 and IFN-λ3 are N-glycosylated whereas in humans, only IFN-λ4 is glycosylated[20,34,43]. Interestingly,

the IFNLR1 is weakly expressed on hepatocytes in the human[41] but not the mouse liver[38,44]. Accordingly, the mouse liver is not responsive to IFN-λ. The weak response to IFN-λ stimulation observed in mouse liver is derived from cholangiocytes, the epithelial cells forming the bile duct[44]. Despite these differences, mouse IFN-λs have strong antiviral and immunomodulatory capacities, similar to their human orthologues[20,25]. Viral infection studies in *Ifnlr1* knock out mice identified IFN-λ as a potent contributor in controlling respiratory and gastrointestinal viruses[36]. Furthermore, and unlike type I and II IFNs[45], mouse and human IFN-λs are not species specific and are able to bind the receptors of both species. Mouse IFN-λ2 and IFN-λ3 were capable of inducing antiviral protection and MHC class I antigen expression in several human cell lines. The same was true for human IFN-λ1 in mouse B16 cells[20].

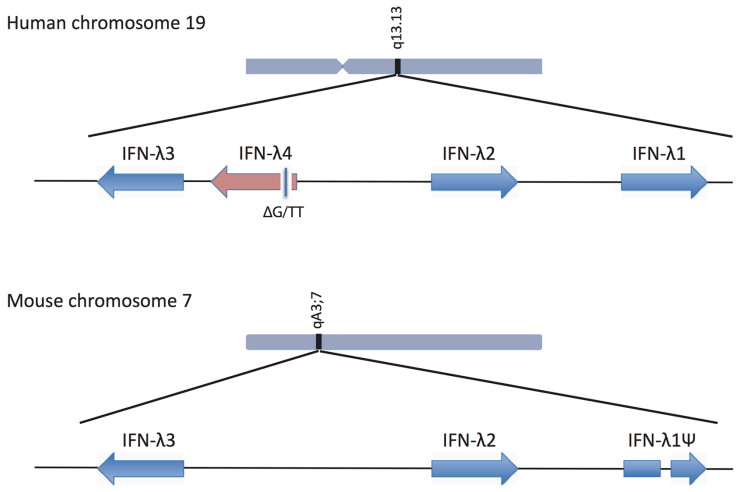

Figure 1. Schematic representation of the genomic organization of the IFN-λ genes on human chromosome 19 and mouse chromosome 7. In humans, the type III IFN family consists of four members; IFN-λ1-λ4, with their genes located on chromosome 19. An intact IFN-λ4 open reading frame is only present in the human sub-population bearing the ΔG genotype. The mouse genome encodes for only two functional IFN-λ proteins; IFN-λ2 and IFN-λ3. IFN-λ1 is a pseudogene because of a stop codon in exon 1 and lack of exon 2. Ψ, pseudogene[46].

1.1.4 Clinical relevance of interferons

After the discovery of IFNs in 1957, it was expected that they would be rapidly developed for the treatment of a variety of viral infections. However, their species specificity[47] and difficult purification[6] slowed down their therapeutic development[48]. Recombinant IFN-α-2b was first described by *Hoofnagle et al.* as potential treatment of

non-A, non-B hepatitis, even before HCV was first described[49]. Finally, IFN-α-2b was approved for the treatment of HCV in 1991[50]. The combination of IFN-α-2b with the nucleoside analogue RBV further improved the rate of sustained virological response (SVR: undetectable HCV-RNA 6 month after end of treatment) in HCV infected patients[51,52]. Later on, IFN-α-2b was replaced by IFN-α-2b conjugated to polyethylene glycol (peginterferon), extending its half-life and improving the treatment outcome in HCV infected patients[48,53]. However, the development of new direct-acting antivirals (DAAs) has revolutionized the field of hepatitis C treatment with SVRs higher than 90% for all genotypes[28,54]. Apart from its use in hepatitis C, IFN-α has been developed for the treatment of hairy cell leukemia[6,55], malignant melanoma[56] and chronic hepatitis B[57]. IFN-β underwent clinical development for multiple sclerosis and is currently still used for this treatment indication[6,48,58]. IFN-γ is approved for the treatment of chronic granulomatous disease[59,60].

Although type I IFNs are approved for the treatment of HCV, their severe side-effects, probably a function of the ubiquitously expressed IFNAR, often require dosing reductions or treatment discontinuations and thus, make it difficult to achieve a SVR[61]. Therefore IFN-λs might be an alternative to the current IFN-α therapy as it induces fewer side effects with restricted inflammatory costs for the host[39] due to the cell type specific IFNLR expression and a more restricted cell response pattern[60]. Indeed, the milder side effects of IFN-λ compared to IFN-α were confirmed in phase I[62] and II[40] clinical trials with pegIFN-λ1 on chronic HCV patients. However, the phase III study with chronic HCV patients could not demonstrate a beneficial role of pegIFN-λ/RBV/telaprevir (TVR) combination compared to pegIFN-α/RBV/TVR[63]. Although IFN-λ will most probably not become the standard of care for HCV patients, it has the potential to be used in the treatment of other diseases. Indeed, *in vivo* studies using a B16 murine melanoma model revealed antitumor activities for IFN-λ[20], suggesting a therapeutic potential in cancer treatment.

1.2 The JAK-STAT signal transduction pathway

The binding of IFNs as well as other cytokines to their cognate receptors initiates a signaling cascade involving Janus kinases (JAKs), the IFN receptor itself and transcription factors termed signal transducers and activators of transcription

(STATs)[21,64]. This signal cascade is tailored to transmit the IFN signal from the cell surface to the nucleus, resulting in transcriptional induction of hundreds of IFN induced effector genes termed interferon stimulated genes (ISGs)[21,65] (Figure 2). The so-called canonical JAK-STAT pathway is evolutionary conserved in eukaryotic organisms from slime molds to humans and is well characterized (reviewed in[23,64,66-69]).

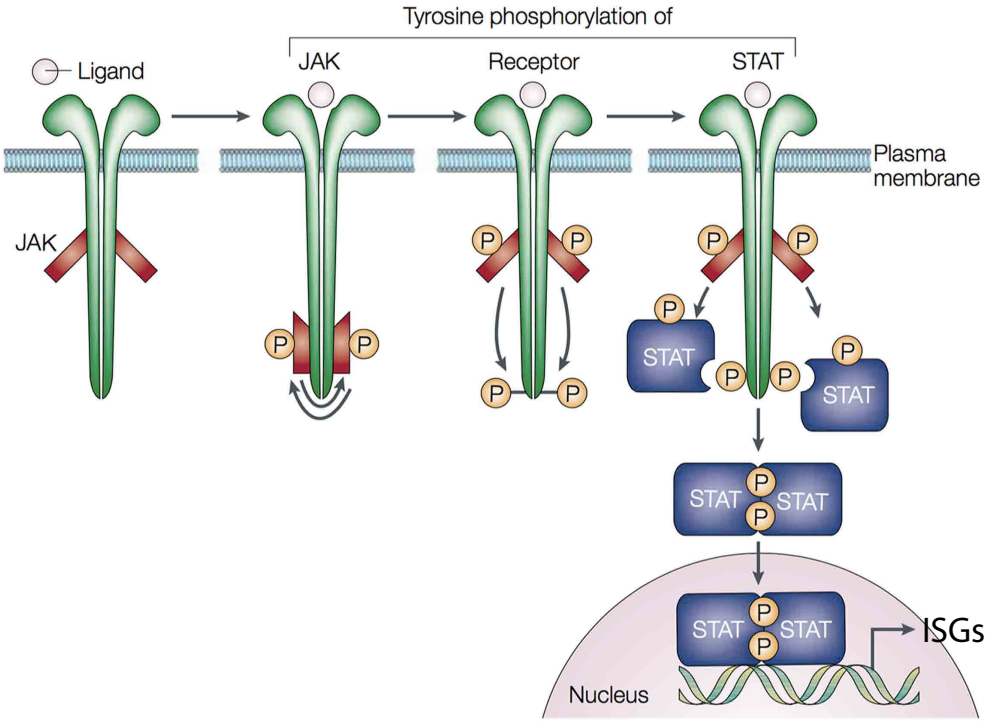

Figure 2. Canonical JAK-STAT pathway. The binding of the ligand to its corresponding receptor induces a cascade of tyrosine phosphorylation events that finally induce the expression of interferon stimulated genes (ISGs). Cytokine-receptor interaction triggers dimerization of the receptor, followed by transphosphorylation and activation of the receptor-associated Janus kinases (JAKs). This leads to the phosphorylation of the cytoplasmic receptor tails and recruitment of the signal transducers and activators of transcription (STATs) proteins. STATs become activated by phosphorylation, form dimers and translocate to the nucleus where they induce the expression of ISGs. Modified from[66].

1.2.1 Janus kinases

JAKs are evolutionary conserved tyrosine kinases that associate with cytokine receptors[67]. In mammals, the family of JAKs comprises four members; JAK1, JAK2, JAK3 and tyrosine kinase 2 (TYK2)[70-76]. While JAK1, JAK2 and TYK2 are ubiquitously expressed, JAK3 expression is mostly restricted to NK and T cells[74].

As shown in Figure 3, different cytokine receptor chains are associated with particular JAKs. Specifically, JAK1 and TYK2 associate with the type I IFN receptor chains IFNAR2

and IFNAR1[68,77,78] and also with the type III IFN receptor chains IFNLR1[28,79] and IL-10R2[35,80], respectively. The type II IFN receptor chains IFNGR1 and IFNGR2 on the other hand are complexed with JAK1 and JAK2, respectively[81,82]. Cytokine binding leads to receptor dimerization that in turn facilitates transactivation of the receptor-associated JAKs through mutual tyrosine phosphorylation. Next, the activated JAKs phosphorylate tyrosine residues on the intracellular receptor chains creating docking sites for STATs[7,67,68] (Figure 2).

1.2.2 Signal transducers and activators of transcription

STATs comprise a family of latent, cytoplasmic transcription factors that are rapidly activated upon receptor-ligand coupling. They act as both, signaling molecules and transcription factors, shuttling between cytoplasm and nucleus[21,69]. In mammals, seven STAT genes have been identified[67,83], *STAT1* and *STAT2*[84], *STAT3*[85], *STAT4*[86,87], *STAT5A*[88], *STAT5B*[89] and *STAT6*[90]. Due to differential splicing, STAT1 exists in two forms, the full length STAT1α (91kDa) and the C-terminal truncated STAT1β (84kDa)[21,91]. All STATs contain a Src-homology 2 (SH2) domain with which they specifically bind to the phospho-tyrosine residues of the intracellular part of the cytokine receptors[92] followed by JAK-mediated STAT phosphorylation[91,93]. Phosphorylated STATs form stable homo- and heterodimers and translocate to the nucleus, where they function as transcriptional activators for ISGs[65,67,68,94] (Figure 3). In the following, the most important STATs for type I, II and III IFNs will be discussed.

Type I and type III IFN primarily activate STAT1 and STAT2[9,95] that form heterodimers which associate with another transcription factor (interferon regulatory factor 9 (IRF9))[96] to form a heterotrimeric complex called interferon-stimulated gene factor 3 (ISGF3)[35,97,98]. This complex translocates to the nucleus where it binds to interferon stimulated response elements (ISREs) in the promotors of ISGs[9,97,99,100]. Alternatively, type I and type III IFNs and especially IFN-γ trigger formation of STAT1 homodimers (also designated GAF for gamma activated factor) [101] that bind to the promoter regions of ISGs containing a gamma activated sequence (GAS) [21,68,69] (Figure 3).

The central role of STAT1 in IFN regulated gene transcription is underscored by the finding that STAT1 deficient mice develop normally but their IFN-α, –β, –γ or IFN-λ responsiveness is severely compromised and they are highly sensitive to viral or bacterial infections[102-104].

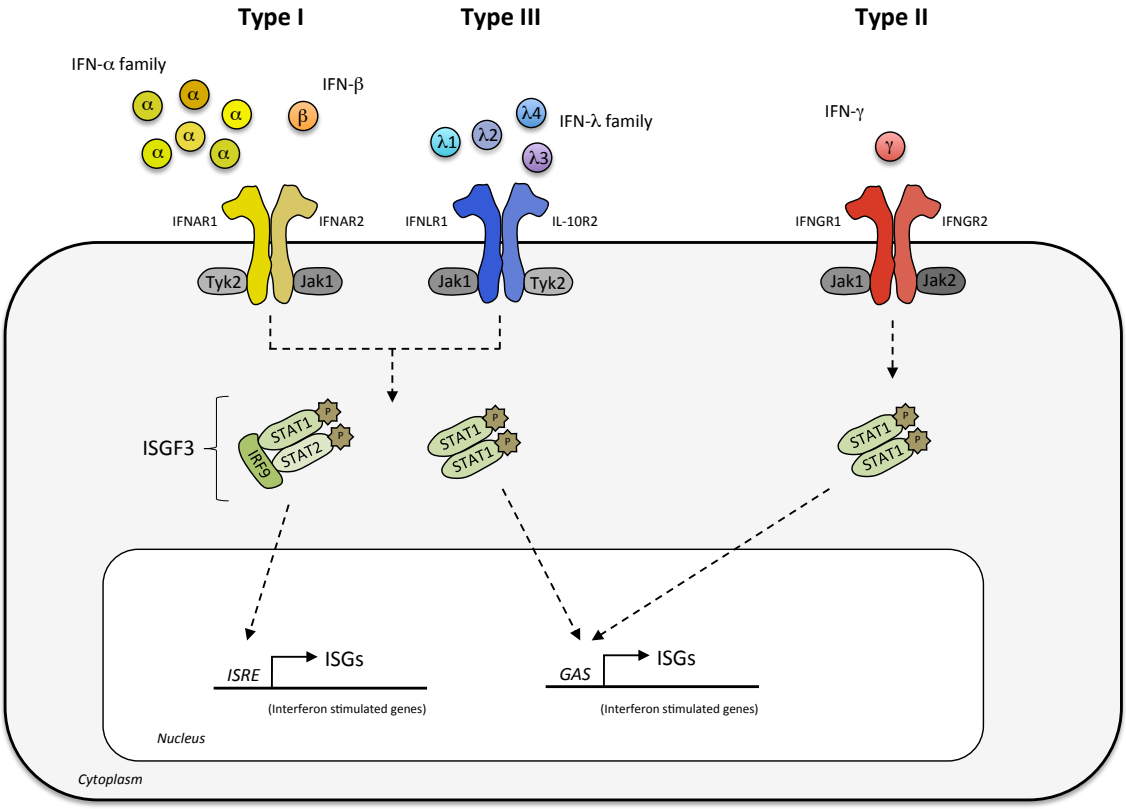

Figure 3. IFN signaling through the JAK-STAT pathway. All IFN receptors connect to the JAK-STAT pathway to transmit signals from the cell surface to the nucleus. Type I and type III IFNs signal through distinct receptors but activate the same downstream signaling cascade. They mainly induce the formation of the heterotrimeric transcription factor IFN-stimulated gene factor 3 (ISGF3) complexes and STAT1 homodimers that bind to IFN-stimulated response elements (ISRE) and gamma activated sequence (GAS) elements in the nucleus, respectively. This leads to the expression of a highly overlapping set of interferon stimulated gens (ISGs). By contrast, IFN-γ (the only type II IFN), induces STAT1 homodimers but does not activate the ISGF3 complex thus, inducing a partially overlapping but distinct set of ISGs compared to type I and III IFNs. Modified from[13].

1.3 Negative regulators of the JAK-STAT pathway

While a fast and strong activation of the IFN system is crucial to combat invading pathogens, prolonged IFN signaling is associated with auto-immune disorders such as systemic lupus erythematosus, rheumatoid arthritis and Aicardi-Goutieres syndrome[105-108] and tumor promotion[107]. Therefore, cytokine production and signaling is tightly controlled[107,109]. Several groups of proteins have been reported to be involved in the regulation of the JAK-STAT pathway targeting the receptors, signaling molecules and transcription factors (reviewed in[107,110-112]). Some of these regulatory proteins are constitutively expressed (e.g. phosphatases and protein inhibitor of activated STAT

(PIAS)), while others are ISGs themselves that are transcriptionally induced by IFNs. The latter group is represented by suppressor of cytokine signaling (SOCS) and ubiquitin-specific peptidase 18 (USP18) that act in a negative-feedback loop on the JAK-STAT cascade.

1.3.1 Constitutively expressed negative regulators of the JAK-STAT pathway

The first group of molecules identified as negative regulators of cytokine signaling were protein tyrosine phosphatases (PTPs)[113]. They encompass a large and diverse family of more than 100 enzymes with high substrate specificity[114,115].

SH2 domain-containing phosphatase 1 (SHP1) and SHP2 are two constitutively expressed cytoplasmic PTPs. SHP1 is mainly expressed in hematopoietic cells and has an important regulatory function in immune cells[116,117]. In contrast, SHP2 is ubiquitously expressed and appears to be involved in many signaling pathways downstream of growth factors and cytokines[118,119]. SHP2 serves primarily as a positive regulator during cell growth and development[119]. However, SHP2 has dual functions as it also regulates the JAK-STAT pathway upon IFN-γ and to lesser extent IFN-α induction in mouse fibroblast cells[118]. Both SHP1 and SHP2 attenuate the cytokine-mediated signal transduction by dephosphorylating the cytokine receptors, JAKs and/or STATs[107,110,111,116] (Figure 4).

Protein tyrosine phosphatase 1B (PTP1B) and T cell protein tyrosine phosphatase (TC-PTP) are two closely related PTPs involved in regulation of several signaling pathways[120]. Although closely related, knockout studies in mice suggest distinct function of the two proteins[120]. PTP1B knockout studies demonstrated that this PTP plays a role in the leptin and insulin metabolism[114,120], suggesting to be the key link between metabolic diseases and inflammation[115]. On the other hand, TC-PTP is strongly expressed in the hematopoietic system and has a critical role in the regulation of immune homeostasis[121], as shown in knockout mice that die from systemic inflammation and defects in hematopoiesis[122]. Furthermore, it was demonstrated that PTP1B and TC-PTP negatively regulate cytokine signaling at the level of the receptors by dephosphorylation of JAK2 and TYK2[114] and JAK1 and JAK3[121], respectively. Of note, TC45 (also named TC-PTPa), the nuclear isoform of TC-PTP is able to dephosphorylate STAT1 and STAT3 induced by IFN-α, IFN-γ and IL-6 within the nucleus of MEFs and primary thymocytes[123] (Figure 4).

CD45 is a another negative regulator of cytokine signaling that specifically bind to and dephosphorylates JAKs within hematopoietic cells[124]. Its role on hematopoiesis is underscored by the finding that 10% of lymphoblastic leukemia patients show a loss of CD45[125].

The mammalian PIAS family includes PIAS1, PIAS3, PIASx and PIASy[126,127]. PIAS1 and PIAS3 specifically bind to dimers of tyrosine phosphorylated STAT1[126] and STAT3[127], respectively, and block their DNA binding capacity, thereby inhibiting transcriptional activation[107,126]. PIAS proteins may act like a buffer titrating the concentration of active STAT dimers that are available within a cell upon cytokine stimulation[112] (Figure 4).

Taken together, these constitutively expressed molecules have a different physiological function compared to the inducible negative regulators that act in a classical negative feedback loop on cytokine stimulation (described in section 1.3.2).

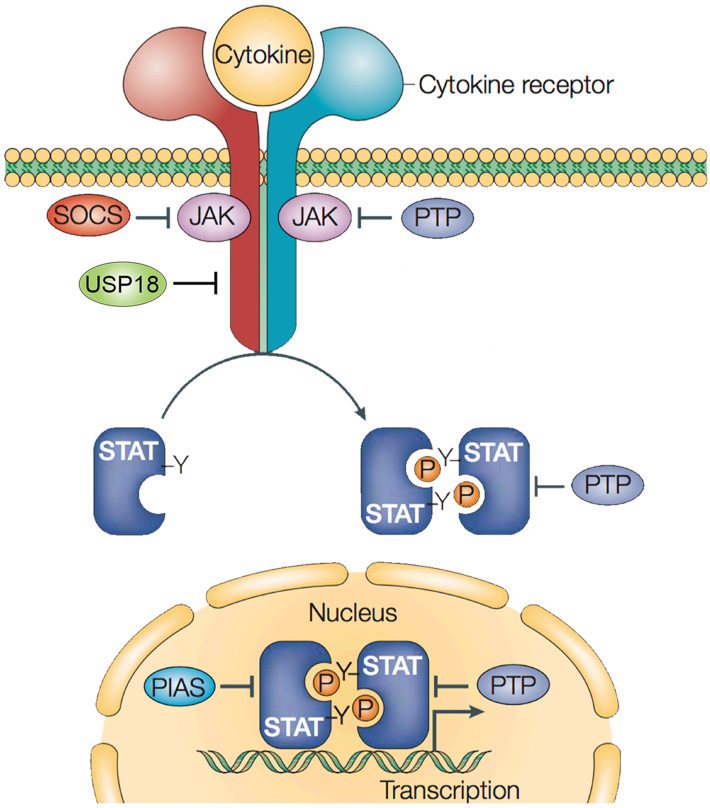

Figure 4. Negative regulation of the JAK-STAT pathway. The Janus kinase (JAK)-signal transducer and activator of transcription (STAT) pathway is regulated at the level of the receptors, signaling molecules and transcription factors. Protein tyrosine phosphatases (PTPs) and protein inhibitor of activated STAT (PIAS) represent the constitutively expressed negative regulators. In contrast, suppressor of cytokine signaling (SOCS) and ubiquitin-specific peptidase 18 (USP18) belong to the group of cytokine-inducible regulators that inhibit the JAK-STAT pathway. Modified from[111].

1.3.2 Cytokine-inducible negative regulators of the JAK-STAT pathway

As mentioned above, besides constitutively expressed regulators, there are also inducible negative regulators of the JAK-STAT signaling cascade, namely several SOCS proteins and USP18.

1.3.2.1 Suppressor of cytokine signaling

Soon after the JAK-STAT signaling transduction was delineated, several groups started to investigate the feedback mechanism responsible for switching off cytokine signaling. In 1995, the cytokine-inducible SH2-containing protein (CIS) was described as the first member of the SOCS family that could potentially function as a negative regulator of cytokine signal transduction[128]. Two years later, three independent groups discovered SOCS1 as a negative regulator of cytokine signaling[129-131]. They postulated that cytokine induced SOCS1 (also referred to as JAB and SSI-1) associates with JAK kinases and specifically inhibits their catalytic activity[130], thus providing a negative-feedback loop of the JAK-STAT pathway upon cytokine stimulation. At the same time, *Starr et al.* described SOCS2 and SOCS3 as additional members of the SOCS family[129]. By searching human DNA databases for a conserved motif of CIS and SOCS1-3 (the so called SOCS-box)[129], four additional SOCS were identified, designated as SOCS4-7[132]. Taken together, the human and mouse genome both encode eight SOCS proteins; SOCS1-7 and CIS.

All proteins of the SOCS family share a similar structure. They contain a highly conserved C-terminal region called SOCS-box[129,132], a central SH2 domain[129,130], an extended SH2-subdomain (ESS)[133] and a N-terminal region that varies in length and amino acid (aa) composition, ranging from 50-380 aa[132] (Figure 5A). SOCS1 and SOCS3 are the only members that have an additional N-terminal kinase inhibitory region (KIR) upstream of the SH2 domain[133,134] (Figure 5A).

Transcriptional induction of SOCS genes in response to cytokines follows a fast kinetics both, *in vitro* and *in vivo*[132,135] (Figure 5B, *left side*). Upon induction, individual SOCS proteins inhibit JAK-STAT signaling by multiple complementary mechanisms as described below.

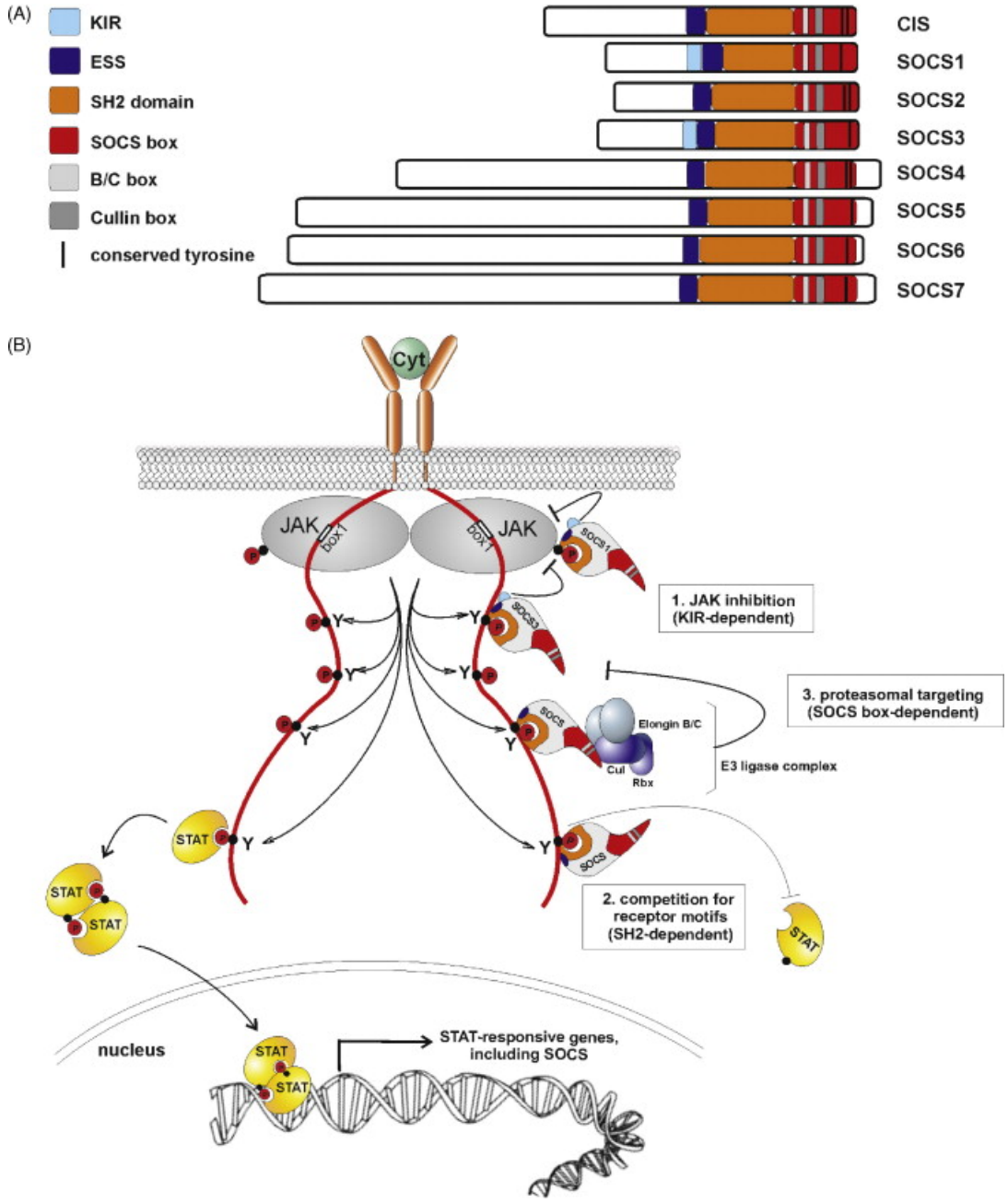

Figure 5. Structural organization and mode of action of SOCS proteins. (A) The suppressor of cytokine signaling (SOCS) family consists of 8 members, including the cytokine-inducible SH2-containing protein (CIS) and SOCS1-7. All of these proteins share a similar structure with a variable N-terminal domain, an extended SH2 domain (ESS), a SH2 domain and a C-terminal SOCS box. SOCS1 and SOCS3 are the only members that have an additional kinase inhibitory region (KIR) domain. **(B)** *Left side:* Upon binding of cytokines to the corresponding receptor, the JAK-STAT cascade becomes activated and induces the transcription of several IFN-stimulated genes (ISGs), including SOCS genes. *Right side:* SOCS proteins inhibit JAK-STAT signaling by multiple mechanisms including (1.) the KIR-dependent JAK inhibition, (2.) the SH2-dependent competition for receptor motifs and (3.) the SOCS box-dependent proteasomal targeting. The colors used for the different parts of the SOCS proteins correspond to those in Figure 5A[135].

One important mechanism is the KIR-dependent JAK inhibition (shown under 1. in Figure 5B, *right side*). The KIR domain of SOCS1 and SOCS3 directly inhibits the JAK catalytic activity[133,134]. It was demonstrated that SOCS1 directly binds to the tyrosine residue in the activation loop of JAKs[129-131] whereas SOCS3 inhibits JAKs by binding to the tyrosine residues of the cytokine receptor in close proximity of the kinase[136,137]. Furthermore, SOCS1 is able to inhibit all four known mammalian JAKs whereas SOCS3 affects only three of them; JAK1, JAK2 and Tyk2 but not JAK3[138,139].

An additional mode of action of the SOCS proteins is the SH2-dependent competition for receptor motifs (shown under 2. in Figure 5B, *right side*). For example, CIS prevents STAT5 recruitment by binding with its SH2 domain to the phosphorylated cytokine receptor[140-142].

Finally, SOCS box-dependent proteasomal targeting represents the third mode of action of SOCS proteins (shown under 3. in Figure 5B, *right side*). The SH2 and the ESS domain bind phosphorylated tyrosine motifs[133] while the SOCS box forms an E3 ubiquitin ligase complex that leads to the ubiquitination of the target proteins[135,143]. Thus, marking SOCS target proteins for proteasomal degradation[135,144].

1.3.2.1.1 Suppressor of cytokine signaling 1 and 3

SOCS family proteins are induced by cytokines and growth factors including IFN-α, IFN-β, IFN-γ and IFN-λ *in vitro* and *in vivo*[145-150] with the magnitude of induction being dependent on the cell-type and stimuli[129,151].

SOCS1 and SOCS3 are considered as the two most potent members of the SOCS family probably because their primary mode of action is mediated by the KIR domain that is absent from all other SOCS proteins[133,134]. The KIR domain enables direct SOCS-JAK interaction and thus inhibition of the JAKs enzymatic activity[152]. Of note, SOCS2, a SOCS member devoid of the KIR domain, has no inhibitory effect on the type I and II IFN-induced signaling cascade[153]. Interestingly however, the C-terminal SOCS-box, although conserved in all SOCS, seems to be dispensable for the inhibition of cytokine signaling[154].

Initially SOCS1 and SOCS3 were identified as inhibitors of the type I and II IFN-induced JAK-STAT signaling in *in vitro* studies including SOCS overexpression[153,155] with SOCS1 showing more potent inhibition than SOCS3[153]. The effect of SOCS1 on IFN-γ-induced signaling was further confirmed using SOCS1 knockout cells[156]. More recent overexpression studies established that SOCS1 and SOCS3 also act as negative regulators

on IFN-λ signaling and expression of antiviral genes[157-159]. Taken together, according to the *in vitro* data, the negative regulatory activity of SOCS1 and SOCS3 extends to type I, II and III IFN signaling.

In vivo studies with *Socs1 – Ifng* double knockout mice confirmed the effect of SOCS1 on type I and II IFN signaling observed *in vitro*[145,149,156,160]. Of note, the premature death of *Socs1* single knockout mice caused primarily by hypersensitivity to IFN-γ[161,162] is prevented by *Socs1 – Ifng* double knockout[163], demonstrating SOCS1 as a key modulator of IFN-γ signaling.

SOCS3 deficient mice exhibit embryonic lethality[164,165]. However, studies of mice with a conditional *SOCS3* deletion in the liver or in macrophages demonstrated normal STAT1 activation by IFN-γ[156], contradicting the *in vitro* results obtained with SOCS3 overexpression. Although SOCS overexpression studies showed that they have inhibitory effects on a wide range of cytokines, *in vitro* and *in vivo* knock out experiments revealed a much more specific activity for only a few cytokines[139].

Taken together, it seems clear that SOCS1 is a potent negative regulator of type I and II IFN signaling *in vitro* and *in vivo*, whereas its role on IFN-λ signaling needs to be further investigated in a more physiological experimental setting. Similarly, while SOCS3 overexpression *in vitro* inhibits IFN-λ signaling, its role *in vivo* needs to be further clarified.

1.3.2.2 Ubiquitin-specific peptidase 18

Besides the SOCS proteins discussed in the previous section, USP18 is an additional cytokine-inducible negative regulator of the JAK-STAT pathway. USP18 is known to play a dual role; as an ISG15 isopeptidase as well as a negative regulator of the IFN system[166].

USP18 (initially named UBP43 because of its molecular weight of 43kDa) was first described in 1999 as a murine protein with deubiquitinating enzyme activity[167]. The human orthologue showing 70% homology with the murine USP18 protein was identified one year later[168]. Human USP18 exists as two isoforms; the full length and the N-terminal truncated form. The translation of the full-length USP18 protein is initiated by a rare start codon CUG, characterized by a low translation initiation efficiency followed by a frequent skip by the scanning ribosome that promotes the expression of the truncated USP18[169]. USP18 belongs to a large family of ubiquitin-specific proteases, enzymes that cleave ubiquitin from ubiquitinated protein substrates[167,168]. Although

USP18 shows significant homology to well-characterized ubiquitin-specific peptidases, it only efficiently cleaves the ubiquitin-like protein ISG15 from ISGylated proteins[170,171]. Therefore, its enzymatic activity seems to be crucial for proper cellular balance of ISG15-conjugated proteins in healthy and stressed organisms[170,171].

The expression of USP18 is strongly induced by viral infection, IFNs and lipopolysaccharides (LPSs) assuming a role in processes including cell proliferation, inflammation, stress and immune responses[170,172]. However, the magnitude of induction is cell-type-specific and varies a lot in response to different stimuli[166]. Amongst others, the expression of USP18 is induced by type I and type III IFNs *in vitro* and *in vivo*[147,148,173] and is not induced by IFN-γ[147,173]. Importantly, USP18 is not only an isopeptidase but has also a role as a potent inhibitor of IFN signaling, independently of its enzymatic function towards ISG15[109,174]. USP18 was initially described as a potent negative regulator of type I IFN signaling *in vitro*[174]. For example, murine and human USP18 deficient cells were hypersensitive to IFN-α and IFN-β stimulation evident as prolonged STAT1 phosphorylation and increased ISG induction and eventual apoptosis[109,174-176]. Of note, it has been demonstrated that both human isoforms, the full length and the N-terminal truncated USP18, do not differ in the negative regulation of the IFN-α-induced signaling cascade[169]. Direct binding of the C-terminus of USP18 to the IFNAR2 subunit prevents the interaction of JAK1 with the receptor, in turn blocking downstream signaling[109]. In contrast to type I IFNs, USP18 does not modulate the IFNγ-induced JAK-STAT signaling pathway[174,177] and does not interact with the IFNGR[109]. Overexpression studies demonstrated that USP18 has a marginal inhibitory effect on IFN-λ induced JAK-STAT pathway *in vitro*[173]. Furthermore, co-immunoprecipitation experiments suggest that USP18 does not directly bind the IFNLR1[178]. Taken together, the *in vitro* data showed a negative regulatory role of USP18 on the type I IFN system, no effect on the type II IFN system and a minor effect on the type III IFN system.

Importantly, the strong inhibitory effect of USP18 on IFN-α induced JAK-STAT signaling observed *in vitro*, was confirmed in USP18 deficient mice[148] and is underscored by a rare human type I interferonopathie, the pseudo-TORCH syndrome. This disease is characterized by a USP18 deficiency leading to an uncontrolled type I IFN system that results in severe brain damage[179].

Furthermore, it was demonstrated that USP18 is responsible for the establishment of a long lasting desensitized state upon type I and III IFNs, leading to IFN-α

unresponsiveness for up to 72h. This long lasting refractoriness was not observed for IFN-β, IFN-γ or IFN-λ[147,148,173]. This suggests that the inhibitory effect of USP18 is specific to IFN-α induced signaling. In contrast, a different study postulates USP18 as an inhibitor of IFN-λ-induced signaling[178].

Taken together, USP18 is a potent negative inhibitor of the IFN-α induced JAK-STAT pathway *in vitro* and *in vivo* but has no effect on type II IFN-induced signaling. Importantly, its inhibitory role on IFN-λ-induced signaling is still a matter of controversy and needs further clarification.

2 Liver Cancer

Liver cancer is the sixth most common cancer worldwide with approximately 850'000 new cases annually with increasing incidence rates[180,181]. Around 800'000 people die of liver cancer each year which ranks this disease as the second leading cause of cancer-related deaths worldwide[181,182]. The ratio of mortality to incidence is close to one, showing a very poor prognosis for patients suffering from liver cancer[181]. The majority (80-90%) of primary liver cancers are hepatocellular carcinoma (HCC) originating from hepatocytes, the epithelial liver cells[183-185]. The second most frequent primary liver cancers accounting for 10-12% of all cases are intrahepatic cholangiocarcinomas originating from cholangiocytes, the epithelial cells that line the bile ducts[181,183]. Furthermore, hepatic angiosarcoma[186] and the pediatric neoplasm, hepatoblastoma[187] are two very rare forms of liver cancer. In the following chapters we will focus on HCC.

2.1 Etiologies of hepatocellular carcinoma

The burden of liver cancer is not evenly distributed throughout the world. Incidence and mortality rates vary between countries, reflecting the uneven distribution of major risk factors responsible for HCC development[183,185,188] as shown in Table 1 and Figure 6. Various etiologies have been linked to HCC development, including HBV and HCV infection, aflatoxin B1 intake, chronic alcohol consumption and obesity, typically conditions that induce cirrhosis[180,189]. The different risk factors and their mechanism of hepatocarcinogenesis are summarized in Figure 7 and will be described in more detail below. The highest prevalence of HCC is observed in sub-Saharan Africa and east Asia[181,183], where viral hepatitis is endemic[190], with China alone accounting for more than 50% of the total number of HCC cases and deaths worldwide[181,191] (Figure 6). Whereas in the majority of these high-rate HCC countries chronic HBV infection and aflatoxin B1 exposure are the leading risk factors, HCV infection, alcohol abuse and obesity have become important risk factors in Western Europe and Northern America[183,191] (Table 1).

Table 1: Geographical distribution of main risk factors for HCC worldwide NASH: non-alcoholic steatohepatitis. Modified from[185].

Geographic area	Risk factors			
	HCV [%]	HBV [%]	Alcohol [%]	Others [%]
Europe	60-70	10-15	20	10
North America	50-60	20	20	10 (NASH)
Asia and Africa	20	70	10	10 (Aflatoxin B1)
Japan	70	10-20	10	10
WORLD	31	54	16	

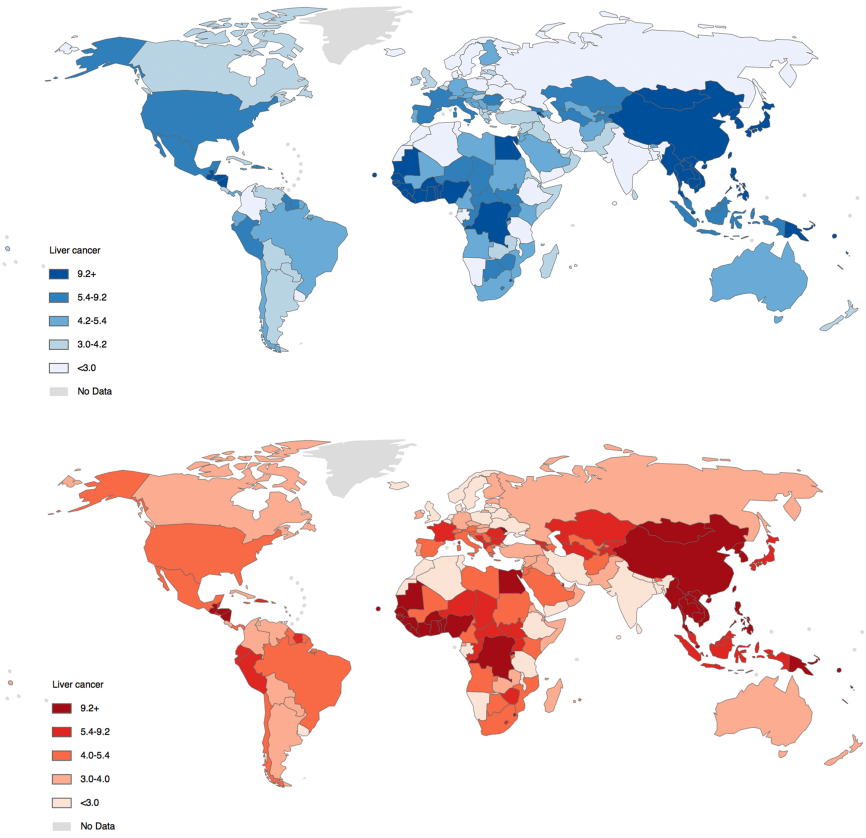

Figure 6. Regional variation in the age-standardized incidence (blue) and death (red) rates of liver cancer. Number of cases per 100'000 persons (Source: GLOBOCAN 2012 (IARC)).

Chronic HBV infection. Chronic HBV infection is one of the major risk factors that can lead to liver damage, resulting in fibrosis and cirrhosis and finally HCC[183-185,192]. Chronic HBV infection accounts for approximately 50% of all HCC cases around the world (Table 1), with the majority (70-80%) of patients with HBV-related HCC having cirrhosis[193]. At least three mechanisms by which HBV infection could contribute to HCC development have been suggested. First, viral proteins (especially the hepatitis B protein X (HBx))

have been reported to modulate cell proliferation and viability[194]. For example, it has been shown that 84% of transgenic mice with elevated levels of the HBx protein developed HCC by the age of 13-24 months[195]. However, the direct evidence from human tissues is still missing. Second, the HBV life cycle involves the presence of viral DNA in the nucleus that is prone to integration into the human genome. Such integration in cellular DNA of human HCCs was first reported in the 1980s[196-198]. The HBV DNA integration often leads to rearrangement of the targeted and flanking regions, potentially activating oncogenes and inducing chromosomal instability[199,200]. Of note, most of the observed integrations were not recurrent and appeared only in one of the analyzed samples. However, a few genes with recurrent integration sites were identified, among them the promoter region of telomerase reverse-transcriptase (*TERT*), which can activate telomerase and other oncogenes[194,201]. Third, chronic HBV infection induces hepatocyte injury and inflammation, which triggers necrosis and HCC development[200,202] (Figure 7).

Aflatoxin B1. Epidemiological studies have proven that there is a correlation between consumption of aflatoxin B1 contaminated food and HCC development[184,185,203]. Aflatoxins are fungal metabolites that contaminate food, especially in regions of Asia and sub-Saharan Africa where poor food storage condition is a problem[183,185]. Aflatoxin B1 intake was correlated with mutations in the tumor suppressor gene *TP53* and increased incidence of HCC, especially in HBV-infected individuals[204,205]. However, two case control studies suggest aflatoxin B1 as a direct risk factor for HCC development in the absence of chronic HBV infection[206,207].

Chronic HCV infection. HCV, a RNA virus, has been declared as a human carcinogen by the International Agency for Research on Cancer (IARC) in 1994. Different from HBV, HCV infection is more prevalent in Europe, the United States and Japan where it is the major risk factor for HCC development[183,208] (Table 1). About 15-35% of chronically HCV infected individuals develop HCC by the age of 75[183,192]. In most of the HCV-related HCCs, cancer development is preceded by advanced hepatic fibrosis or cirrhosis[209]. Since HCV, in contrast to HBV, does not integrate in the human genome, its HCC promoting activity most likely involves induction of hepatic inflammation and fibrosis and promoting malignant transformation of infected cells[208,210,211] (Figure 7). Of note, a meta-analysis of 21 published studies suggests that patients infected with HCV of genotype 1b have an increased risk of developing HCC compared to patients infected

with any other genotype of HCV[212]. However, it is still unclear if HCV is a direct carcinogen or whether other pathological conditions (e.g. steatosis, oxidative stress or inflammation) that are linked to chronic viral infection are the cause of HCC development and progression[213,214].

Alcohol abuse. Additional to the above mentioned risk factors, excessive alcohol consumption, is another leading cause of HCC, especially in developed countries[183,208]. Chronic alcohol intake is linked to inflammation that increases hepatocyte turnover, oxidative stress and the risk to develop cirrhosis, eventually leading to HCC[189,215] (Figure 7).

Metabolic syndrome and others. Recently, metabolic syndrome resulting from diabetes and obesity and the associated liver diseases non-alcoholic fatty liver disease (NAFLD) and non-alcoholic steatohepatits (NASH) became more important risk factors for HCC[208,216,217]. Furthermore, inherited metabolic disorders such as hemochromatosis[218] and alpha-1 antitrypsin deficiency[219] causing hepatocellular damage and necrosis can increase the risk of HCC development[183,185].

Gender. HCC is three fold more common in men than women[180,181,185]. This phenomenon is not well understood. However, it has been hypothesized that differences in sex steroid hormones, immune responses and epigenetics could be the underlying cause[188]. Indeed, a positive association between high levels of circulating testosterone and HCC has been described in the context of HBV infected men[220].

Taken together, several etiologies, such as viral hepatitis, alcohol abuse, aflatoxin B1, NASH and NAFLD can lead to hepatocarcinogenesis. Some etiologies are prone to induce mutations with higher frequency in specific genes, as observed for HBV-related HCCs that are frequently mutated in *TP53*[221]. However, although HCC risk factors are highly diverse, they induce several overlapping pathogenic pathways and processes. For example, inflammation and repeated cycles of liver damage and regeneration seem to be consistent among HBV-, HCV- and alcohol induced hepatocarcinogenesis. This suggests, that there are at least some common processes underlying HCC development and thus could represent important targets for drug development.

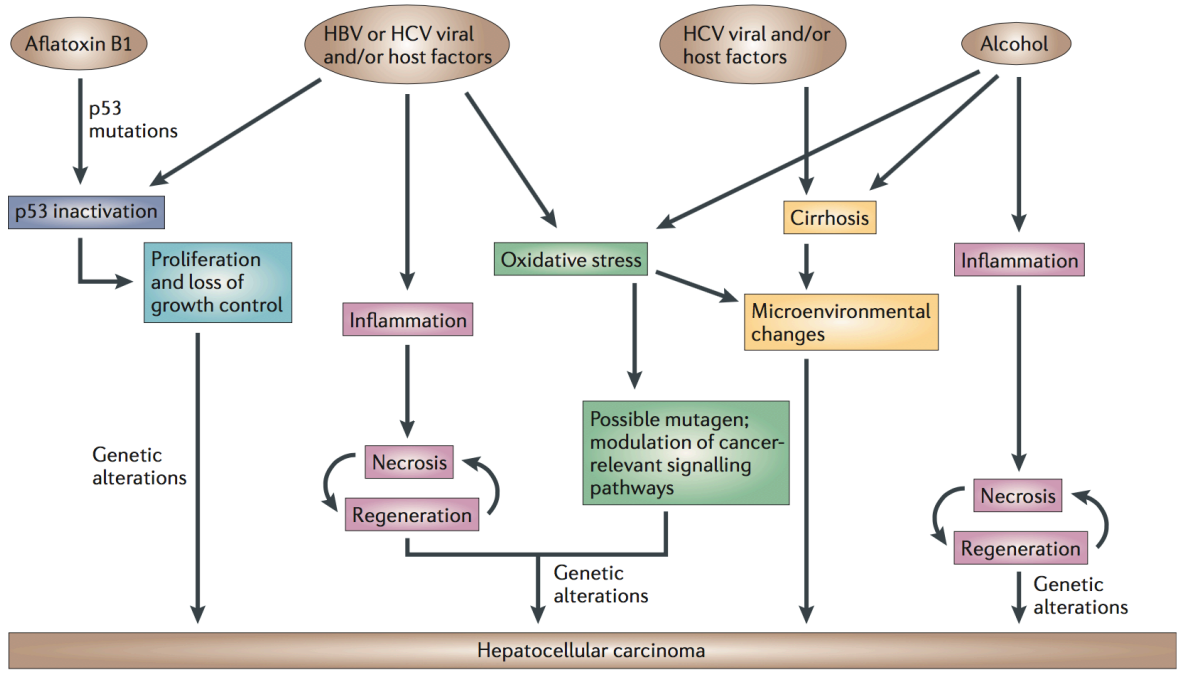

Figure 7. The different etiologies of HCC and the corresponding mechanisms of hepatocarcinogenesis. Various etiologies have been linked to HCC development, including aflatoxin B1 intake, hepatitis B virus (HBV) and hepatitis C virus (HCV) infection and chronic alcohol consumption, typically conditions that induce cirrhosis. In addition, HBV can integrate into the host genome, thus contributing to hepatocarcinogenesis. Modified from[189].

2.2 Prevention and treatment of hepatocellular carcinoma

HCC is one of the deadliest cancers worldwide and its incidence is continuously rising[185]. Furthermore, therapies for advanced HCC are limited, showing a clear need for new and more effective drugs. The lack of curative treatment options for advanced stage HCC makes prevention even more important. The different HCC prevention and treatment options are described below.

2.2.1 Prevention

The best HCC prevention strategy is the reduction of the underlying etiological factors. A major breakthrough in the field of HCC prevention was the development of a HBV vaccine. National HBV vaccination programs reduced the burden of HBV infection, which in turn lowered the incidence rates of HCC[222,223]. However, 240 million people are still chronically infected with HBV and remain at risk for the development of cirrhosis and HCC[202]. In general, effective antiviral therapies in patients with chronic HBV and HCV infection are associated with reduced HCC incidence rates[184,224]. Cohort studies showed

that the successful treatment of HCV reduces HCC incidence rates compared to untreated controls[225,226]. Furthermore, the reduction of aflatoxin 1B exposure was proposed to be highly relevant for liver cancer prevention[183].

2.2.2 Treatment

Staging of HCC patients according to prognosis and treatment options, is performed using the Barcelona Clinic Liver Cancer (BCLC) staging system[227], recommended by the European and American clinical practice guidelines[185,228]. This staging system defines five prognostic subclasses (0, A, B, C and D) that link the disease stage to the most beneficial therapy option currently available[184,185]. Class 0 represents very early, A early, B intermediate, C advanced and D terminal stage disease (Figure 8).

Alternative staging systems were proposed including the Hong Kong classification[229], the Cancer of the Liver Italian Program (CLIP) score[230], the TNM system[185] and the Japan Integrated Staging (JIS) score[231]. But in contrast to the BCLC system, they are not globally used in the clinic[185] .

To date, five different treatment options are available for patients with HCC, including surgical resection, liver transplantation, local ablation, chemoembolization and the multikinase inhibitor sorafenib[184,185]. Treatment options are divided into two groups, the potentially curative and the palliative treatments (Figure 8). About 30-40% of patients are classified as BCLC 0 or A, representing asymptomatic, early stage HCCs. These patients are considered for potential curative therapies such as resection, transplantation or local ablation, resulting in a median survival rate of five years[184]. Patients with intermediate and advanced stage disease, BCLC B-C, have two treatment options; chemoembolization and sorafenib. BCLC stage B patients with preserved liver functions benefit from chemoembolization whereas the standard of care for stage C patients is sorafenib, prolonging median survival by three months[232]. Patients with end stage disease, BCLC D, receive palliative treatment. These patients may need nutritional and psychological care and good pain management[185]. The different HCC treatment options, including liver transplantation, radiofrequency ablation, transcatheter arterial chemoembolization (TACE) and sorafenib, will be discussed in the following.

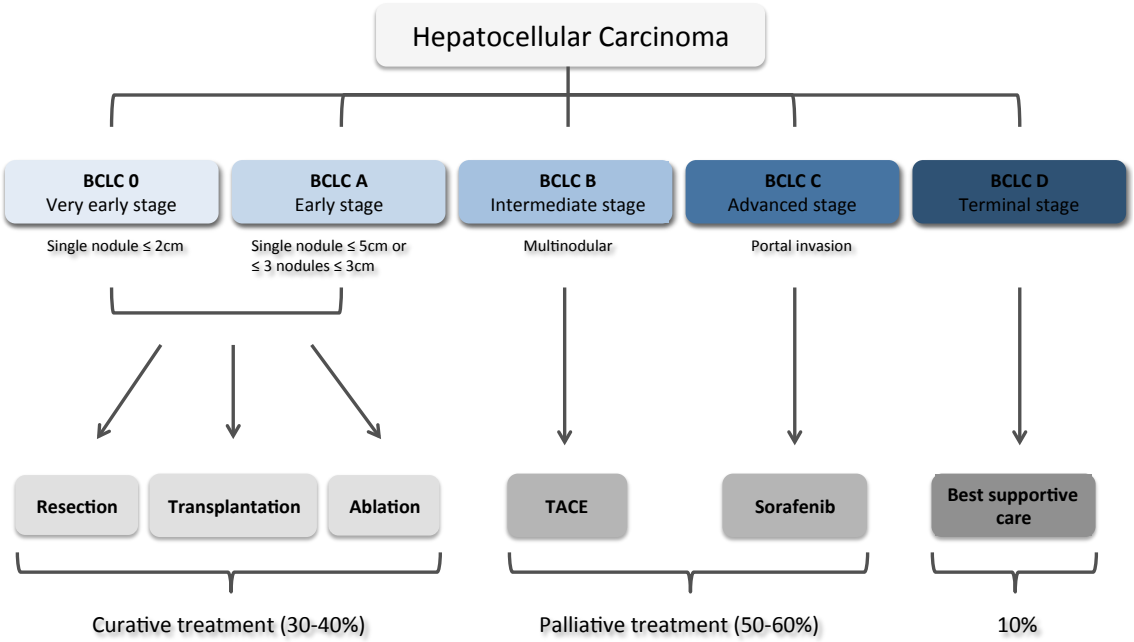

Figure 8. BCLC staging system and therapeutic strategy. The Barcelona Clinic Liver Cancer (BCLC) staging system encompasses five different stages (BCLC 0, A, B, C and D) and is used to stratify patients according to their prognosis and treatment options. Curative treatments include resection, transplantation and ablation whereas transcatheter arterial chemoembolization (TACE) and sorafenib are used as palliative treatment in patients with intermediate and advanced stage disease, respectively. Modified from[185].

Liver Resection. Patients with single tumor nodules designated BCLC 0 or A, no portal hypertension and well-preserved liver functions are considered for surgical resection. Tumor recurrence is the major complication of this treatment modality[185]. The 5-year recurrence rate of HCC is up to 70% in these patients because of either metastasis or *de novo* HCC development in the liver[185,228].

Liver Transplantation. Patients that do not qualify for resection might be candidates for liver transplantation if the HCC is defined as BCLC A and some additional criteria are met. If only one nodule is present in the liver, its size has to be ≤ 5cm. If a patient has several nodules, their number cannot exceed three and their individual sizes cannot be larger than 3cm. No vascular invasion should be present[185]. The 5-year recurrence rate of HCC is below 15%, however the scarcity of liver donors is a major drawback of this treatment option[185].

Ablation. The standard of care for patients with BCLC stage 0-A tumors not suitable for resection or transplantation is the local ablation with radiofrequency or percutaneous ethanol injection. The radiofrequency ablation is the main ablative therapy in tumors

less than 5cm, whereas ethanol injection is used when radiofrequency ablation is technically not feasible. These patients have a 5-year survival rate of 50-70%[184,185,233].

Transcatheter arterial chemoembolization (TACE). This technique is recommended in patients with an intermediate stage HCC (BCLC B). This stage is defined by preserved liver functions, several tumor nodules, no tumor-related symptoms, no vascular invasion and no extrahepatic spread[185]. TACE is a minimal invasive technique. Embolizing particles loaded with chemotherapeutic drugs (e.g. doxorubicin and cisplatin) are injected into one or more branches of the hepatic artery in close proximity of the tumor. This enables the onsite delivery of the drug and restricts tumor blood supply. Patients that receive this treatment have a median survival of 20-26 month[184,185,234].

Sorafenib. The standard of care for patients with advanced HCC (BCLC C) is the multi-kinase inhibitor sorafenib[185]. Its beneficial role was demonstrated in a randomized control trial with more than 600 patients with advanced HCC[232]. Patients treated with sorafenib benefit from an overall increased survival of three months (from 7.9 to 10.7 month). The effect of sorafenib was also confirmed in an Asian patient cohort with HBV background[235]. Despite its beneficial aspects, sorafenib has its limitations. Although it is the only first-line treatment option for patients with advanced HCC, sorafenib treatment is not curative and cannot be used in patients with impaired liver function[185,232]. Furthermore, sorafenib is associated with potentially severe side effects, including diarrhea, fatigue, hand-foot skin reactions and weight loss[228,232,235]. Sorafenib was originally identified as a Raf kinase inhibitor[236] that displayed anti-tumor activity[237]. It is now known that sorafenib affects up to 40 different kinases, including Raf-1, B-Raf, vascular endothelial growth factor receptor 2 (VEGFR2), platelet-derived growth factor receptor (PDGFR) and c-Kit receptor kinases[228]. Sorafenib acts on tumor cells and stroma[211] and has antiangiogenic, antiproliferative and/or proapoptotic effects[237]. However, its molecular mode of action is not completely understood.

Almost 10 years after the first therapy results of sorafenib were published[232], all novel systemic drugs failed in clinical phase III trials, including brivanib, sunitinib, erlotinib and linifanib[238-242]. None of these alternative treatments was superior to sorafenib in the first-line setting. Of note, regorafenib - another multikinase inhibitor – was the only drug with a beneficial outcome in a second-line setting following sorafenib failure[243]. However, it is associated with several adverse effects and is not well tolerated by many

patients[244]. Since the approval of checkpoint inhibitors such as tremelimumab and nivolumab, immunotherapy has recently gained interest in the treatment of HCC[245]. In general, cancer immunotherapy redirects the immune system of the patients against the cancer instead of targeting the cancer itself[246]. In the US, nivolumab an anti-PD-1 (programmed cell death protein 1) antibody has already been approved for the second-line treatment of HCC and is currently tested in a Phase III trial against sorafenib (ClinicalTrials. gov registry number: NCT02576509)[245]. The results from the new checkpoint inhibitors are encouraging and hold promise for potential new HCC treatments.

Taken together, despite a lot of potential therapeutic targets, sorafenib and regorafenib are the only drugs globally available for the management of advanced HCC. This could potentially be explained by the molecular heterogeneity of HCC, the lack of good biomarkers that help to stratify the patients into different treatment groups, the rapidly occurring resistance to chemotherapy and the toxicity of some compounds linked to the often bad liver condition of these patients. This indicates the urgent need for new and more effective drugs to treat HCC.

2.3 Histopathological progression and molecular features of hepatocellular carcinoma

Although HCC is one of the most lethal cancer types in humans, the precise molecular mechanisms that drive tumor initiation and progression are far from being completely understood[189,247]. Several factors play a role in hepatocyte transformation, HCC development and progression including chronic inflammation, DNA damage, epigenetic modification, senescence, telomerase reactivation and early neoangiogenesis[184,202].

HCC development is a complex, multistep process that occurs in the majority of cases on a cirrhotic background linked to inflammatory conditions induced by different underlying etiologies, including viral hepatitis, alcohol abuse and metabolic syndrome[248] (Figure 9). Each of the known risk factors can induce hepatic injury that leads to necrosis followed by regeneration due to hepatocyte proliferation. If this cycle of destruction and regeneration is repeated several times because of continuous liver damage it fosters a chronic liver disease, associated with cirrhosis. Typical for cirrhosis are the formation of collagen-surrounded nodules and the scaring of the liver (Figure 9). The early steps of HCC development, including chronic liver disease and cirrhosis, are

associated with telomere shortening[249] that correlates with chromosomal instability[250] as indicated in Figure 9. Of note, telomerase knock out mice showed an increased rate of liver cancer initiation[251]. A cirrhotic liver can subsequently develop hyperplastic nodules that further develop into dysplastic nodules and finally into HCC[189] (Figure 9).
In rare cases, HCC can also develop in normal livers without any sign of fibrosis, cirrhosis or inflammation. Some studies suggested that they might have developed in a pre-existing hepatocellular adenoma[217,252,253]. However the exact pathogenesis of these HCCs remains unclear.

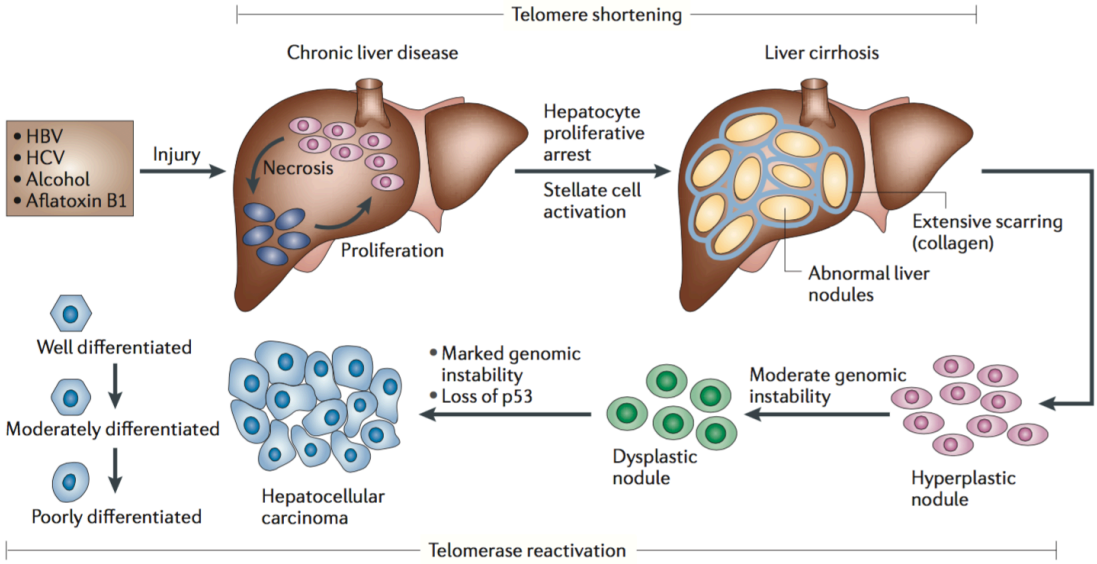

Figure 9. Histopathological progression and molecular features of HCC. The development of HCC is typically a multistep process occurring in most of the cases on a cirrhotic background. Chronic HBV and HCV infection, alcohol abuse and intake of aflatoxin B1 induce hepatic injury leading to necrosis that is followed by regeneration due to proliferation of hepatocytes. In a chronic setting, this can lead to liver cirrhosis that further develops hyperplastic nodules, followed by dysplastic nodules and finally HCC. Chronic liver disease and liver cirrhosis is associated with telomere shortening, by contrast telomerase re-activation seems to be involved in HCC development[189].

Furthermore, HCC development is the result of accumulation of mutations in passenger and driver cancer genes that leads to the alteration of multiple signaling cascades[184]. By definition, a cancer driver is a genetic event that contributes to tumor evolution at any stage by promoting functions including proliferation, survival, invasion or immune evasion[254]. In contrast, passenger mutations are of marginal relevance for cancer initiation and progression[184]. Molecular analysis of human HCC have helped to identify

the main drivers responsible for HCC development and progression[221,255]. In general, each HCC nodule has approximately 40 somatic alterations of which only a few are considered as drivers[184]. At the top of the list of the most frequently mutated driver genes in HCC (Figure 10) are *TERT, CTNNB1 and TP53* that affect telomere maintenance, WNT pathway activation and inactivation of a tumor suppressor, respectively[221].

In 90% of human HCCs Telomerase is overexpressed which is related to *TERT* promoter mutations in 45-60% of cases[201,221,248] (Figure 10). This, and data from telomerase knockout mice[251] suggest that a re-activation of telomerase is needed for HCC progression. Thus, telomere dysfunction seems to play an opposing role in the initiation versus progression of HCC. Early stages of HCC development are associated with telomere shortening, whereas telomerase re-activation is an important feature in tumor progression linked to evasion of cellular senescence and promoting uncontrolled hepatocyte proliferation[184,251] (Figure 9).

With a frequency of 11-40% (Figure 10), *CTNNB1* is one of the most frequently mutated genes in human HCCs, activating β-catenin and therefore inducing the WNT-pathway[221,248,256]. *CTNNB1* mutations are predominantly observed in well-differentiated, non-HBV-related tumors[257,258]. However, inactivating mutations or deletion in *AXIN1*, *APC* and *ZNRF3* can also result in activation of the WNT-β-catenin pathway[184].

TP53 belongs also to the top most frequently mutated gene in human HCCs (25-50% of cases) that leads to an inactivation of the tumor-suppressor p53[221,248,256]. *TP53* mutations are often associated with HBV and aflatoxin B1 related HCCs and often linked to a poor prognosis and a more aggressive phenotype[184,248,259].

Taken together, HCC development and progression is a highly complex mechanism induced by a range of different etiologies involving different molecular mechanisms and mutations. Genome wide analysis, including the recently published data from the cancer genome atlas research network[248], enhanced the understanding of important molecular events in HCC development. However, the exact role of the different etiologies, pathway alterations and mutations in HCC initiation and progression remains to be elucidated.

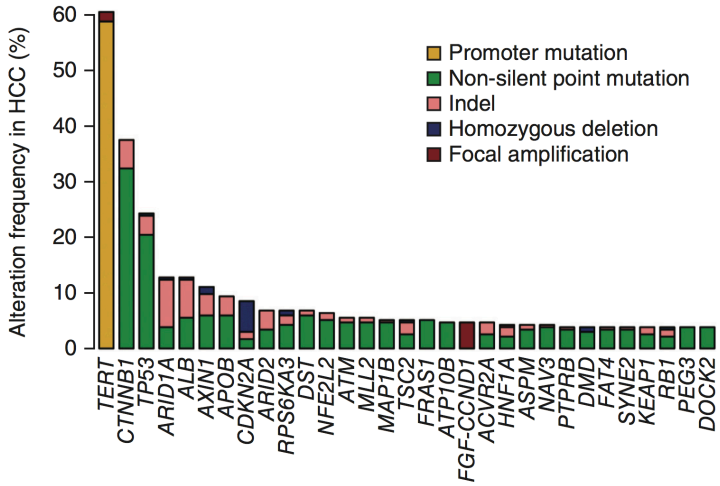

Figure 10. Most frequently altered genes in HCC, based on exome sequencing analysis of 243 human liver tumors. Genes that were altered in ≥4% of samples are shown, with *TERT, CTNNB1, TP53* being the most frequently mutated genes in HCC, affecting telomere maintenance, WNT pathway activation and inactivation of a tumor suppressor, respectively[221].

2.4 Classification of hepatocellular carcinoma

HCCs have been classified in various ways, based on etiological and molecular features, mutational landscape, prognosis and histological appearance. The histological and immunohistological as well as the different molecular classifications will be discussed in more detail in the following.

2.4.1 Histopathology and immunohistochemistry

Until 2000, the diagnosis of HCC was based only on biopsies. After that, the field of diagnosis has changed to a more non-invasive radiological approach, including computed tomography (CT), magnetic resonance imaging (MRI) and ultrasound. However, the non-invasive diagnosis of small lesions remains a challenging issue and often requires pathological confirmation on biopsy samples. Furthermore, biopsies are performed in cases with inconclusive or atypical imaging appearance in cirrhotic livers[185].

Histological assessment helps to confirm HCC and allows to define their differentiation grades and growth patterns[260]. Hematoxylin and Eosin staining of tumor sections allows for HCC growth pattern classification (f.e. trabecular, pseudoglandular and solid) and cytological subtypes (clear cell, giant cell, steato-HCC and stem cell-like)[260,261]. The Edmondson and Steiner system is the most widely used grading system for HCC[262]. It

scales the tumors into four different groups; grade I-IV. Grade I is the most differentiated group and is often difficult to distinguish from normal liver, whereas grade IV reflects highly dedifferentiated tumors. In general, the higher the Edmondson grade, the less differentiated the tumors are. Of note, a single nodule can have several differentiation grades.

In cases where the histological interpretation and diagnosis is difficult, additional tissue markers are used to improve the diagnostic accuracy[185,263]. This is often necessary in the case of small liver nodules to discriminate between high-grade dysplastic nodules and early grade I (i.e. well-differentiated) HCCs[264]. Three immunohistochemical (IHC) markers – Glutamine Synthetase (GS), Glypican-3 (GPC3) and Heat Shock Protein 70 (HSP70) – are used for the diagnosis of resected and biopsied primary liver nodules[185,264-266]. It is recommended that two out of the three markers should be positive for a pathological diagnosis of HCC[265,267].

GS catalyzes the synthesis of glutamine – the major energy source of cancer cells - from glutamate and ammonia in the mammalian liver[264]. GS is upregulated in human HCC[268] and was shown to stepwise increase from pre-cancerous lesions to early and further to advanced HCC[269]. However, this association of expression with tumor dedifferentiation was not observed in a newer study showing that early and late stage HCC similarly overexpress GS suggesting that the strong GS expression takes place in the early phases of malignant transformation[264]. Furthermore, GS is a target of β-catenin and is often overexpressed in HCC associated with a *CTNNB1* mutation[267].

GPC3 belongs to the family of Glypicans, is linked to the cell surface and is overexpressed in HCCs[270,271]. Typically, it is not expressed in normal, adult liver[272,273]. Furthermore, its expression is affected by the tumor grading with high expression levels in high grade nodules[264]. It is suggested, that GPC3 plays a role in cell growth regulation, however, its role in the pathogenesis of HCC remains poorly understood[274].

HSP70 is one of the most upregulated genes in HCC, induced by stress conditions like chronic inflammation and fibrosis[275]. Furthermore, HSP70 is a potent anti-apoptotic effector that allows the cells to survive under different conditions[264]. Of note, no correlation was observed between HSP70 immunoreactivity and HCC differentiation grade, etiology, sex, cirrhosis or tumor size[264]. Taken together, IHC can be used as an additional tool to support the diagnostic conclusions driven from morphological analysis of HCC specimen.

2.4.2 Molecular classification

Transcriptome-based molecular classification studies of human HCC are aimed at identifying tumor specific druggable targets. If successful, this would allow to determine patients that could benefit from targeted therapies[276]. Several studies analysed the gene expression profiles of HCCs from resected specimens[277-280] and biopsies[276]. Each study classified HCCs into different numbers of subclasses ranging from two to six and showing different transcriptomic profiles and clinicopathological features. However, molecular classification of HCC based on gene signatures or molecular abnormalities has not yet provided results suitable for clinical applications[184,185,247,281]. The major reason for this is probably that the most frequent mutations in HCC (*TERT*, *CTNNB1* and *TP53*) are not targetable. Nevertheless, the above mentioned molecular analysis showed that HCCs can be broadly divided into proliferative and non-proliferative tumors. The class of proliferative tumors is typically more aggressive and less differentiated[276,279]. Furthermore, these tumors are often characterized by high serum alpha-fetoprotein (AFP) levels, *TP53* mutations and are correlated with poor outcome[256,277,279,280]. The non-proliferative subclass is highly heterogeneous and harbors tumors that tend to retain hepatocyte-like features[247,256]. Around 30% of these HCCs are characterized by mutations in *CTNNB1* and show β-catenin pathway activation[276-279]. However, the remaining non-proliferative HCCs have no common distinguishing features.

Taken together, despite substantial progress, the prognostic use of molecular subclasses of HCC in the clinics is still missing. Therefore, the prognostication and decision making for HCC patients still relies mainly on the BCLC staging system.

2.5 Biomarkers of hepatocellular carcinoma

Unfortunately, at the time when HCC symptoms are evident, the disease is typically too advanced to qualify for any curative treatment attempt[185]. Additionally, life expectancy for these patients is very short, with a median survival time of less than 1 year. To date, less than 30% of HCC patients in Europe qualify for curative treatment like tumor resection or liver transplantation, mostly because of delayed HCC diagnosis[185]. In order to detect early-stage tumors, guidelines for surveillance recommend ultrasonography every 6 months for patients at risk[185,208]. However, the diagnosis of early-stage HCC by ultrasound, CT/MRI and/or liver biopsy is very challenging. Mainly because the lesions are very small, their radiological appearance might be atypical and the morphological

changes compared to the dysplastic hepatocytes could be minor[282]. Thus, biomarkers that would help to detect early stage HCC are desirable. Importantly, such biomarkers would increase the possibility for curative treatment[184,282].

AFP is one of the most frequently tested serum biomarkers for the identification of HCC[283]. However, it has been shown that only 10-20% of early-stage HCCs show high expression levels of AFP, whereas it is more often associated with advanced-stage HCC. This makes it unsuitable for the detection of tumors at an early stage[184,185,228,282]. Therefore, AFP is suboptimal for routine clinical practice[185].

An ideal biomarker would not only be helpful for diagnosing early-stage HCC but also for predicting response to sorafenib treatment. Thus, only patients would be treated that would benefit from this therapeutic approach. This would prevent patients to suffer from treatment side effects without having a therapeutic benefit. One study suggests that early increase in AFP levels is associated with disease progression and poorer outcome in patients treated with sorafenib[284]. However, these results have to be validated in a bigger cohort. Until now, no robust, predictive clinical or molecular biomarker for sorafenib response has been identified[185,281,285].

It is suggested, that a biomarker-driven selection of patients for phase II and III clinical trials could improve their outcome[286]. The tested drug could be effective in a given molecular subgroup of HCC patients, but diluted if the complete patient cohort is used. Indeed, the phase II trial of tivantinib – a small molecule MET receptor tyrosine kinase inhibitor[287] - versus placebo showed no effect when all patients were included. However, a significant effect was observed in the *post hoc* analysis when only a subgroup of patients with MET-high tumors were included[288]. A phase III clinical trial with a subgroup of only MET-positive HCC patients, that failed first line treatment with sorafenib, is currently ongoing (ClinicalTrials. gov registry number: NCT01755767). In general, a biomarker-driven selection of HCC patients for drug testing could significantly improve the identification and application of drug candidates.

2.6 Experimental models for hepatocellular carcinoma research

As described above, HCC is one of the deadliest cancers worldwide with very limited treatment options for patients with advanced stage tumors[185]. Furthermore, despite tremendous efforts over the last 10 years, sorafenib still remains the only approved drug for the first-line treatment of advanced HCC. There is a clear need for experimental

models that recapitulate key features of human HCC and therefore advance the understanding of the molecular, cellular and pathophysiological mechanisms of HCC[289]. Accordingly, a variety of different *in vitro* and *in vivo* HCC model systems have been developed. However, because HCC is a very heterogeneous disease, it is very challenging to generate a model that fully mirrors the variability and complexity of human HCC. The different *in vitro* and *in vivo* models will be described in the following.

2.6.1 *In vitro* models

Current *in vitro* studies are mainly based on two-dimensional hepatoma cell lines, derived from human or animal HCCs[290]. They mainly allow mechanistic studies of genetic alterations that could lead to abnormalities in signaling pathways. Furthermore, in the early steps of drug discovery, they are often used to evaluate the effect of potential anti-cancer compounds on cell proliferation and apoptosis[290,291]. Although they are cost-efficient, easy to handle and manipulate, they fail to recapitulate key features of HCC, including tumor architecture, cellular heterogeneity and cell-to-cell interactions. Thus, cancer cell lines do not represent the complexity of a tumor and its microenvironment[292].

Recently, the three-dimensional organoid culture system has emerged as an important tool for basic and translational research[293]. This new technology allows the long-term *in vitro* maintenance and expansion of adult stem cells from human tissues that can be further differentiated into organ-like structures[294]. Importantly, organoids can be generated from various patient-derived tumors allowing to model human diseases and testing of therapeutic compounds in a personalized medicine approach[295]. Only recently, establishing of organoid cultures from human liver cancer became possible[296](Nuciforo et al., submitted). Although clearly useful, the organoid system has some limitations, as for example the lack of a microenvironment[297]. Thus, the usage of two and three-dimensional cell culture systems are clearly helpful in the field of HCC research but some aspects of tumorigenesis, including angiogenesis and metastasis cannot be assessed[292].

2.6.2 *In vivo* models

Experimental animal models that closely mimic human HCC are important to advance the knowledge about physiological, cellular and molecular mechanisms of this

disease[289]. Furthermore, animal models may help to identify new therapeutic approaches to treat HCC. Although rats[298,299], woodchucks[300] and pigs[301] have been used to study HCC, mice are the preferred model systems in the field of HCC research. This is mainly because of their physiologic and genetic similarity to humans, their small size, short lifespan and excellent breeding capacity[292,302]. However, the appropriate modeling of liver cancer is challenging due to its different underlying etiologies and the vast genetic landscape. Several HCC mouse models have been developed but depending on whether HCC is induced by genetic manipulations, chronic liver disease, or transplantation of cancer tissue, several differences in characteristics and complexities have been observed. For example, dependent on the mouse model, tumor development can take from few weeks to more than a year[211,303]. Each model has its own advantages and disadvantages, thus it is very important to choose the most appropriate system to address specific questions[304]. The different models will be discussed in more detail in the following.

2.6.2.1 Spontaneous mouse models

Similar to humans, mice rarely develop HCCs spontaneously in the absence of chronic liver disease[303]. Interestingly, spontaneous cancer development in mice seems to be linked to the gender and the genetic background. Whereas C57BL/6 mice rarely develop HCC in their normal life span, C3H mice spontaneously develop liver cancer starting from 12 months of age[305]. Because of the low incidence rate and the high variability of tumor occurrence, size and location dependent on strain and gender, these models are not ideal for experimentation[306].

2.6.2.2 Genetically engineered mouse models

Genetically engineered mouse (GEM) models are powerful tools to study tumorigenesis, because they allow to model complex genetic alterations found in human HCCs, including point mutations, gene amplifications, deletions and translocations[303]. The most common GEM mice used to study liver carcinogenesis are generated either by overexpression (transgenic mice) or by deletion (knockout mice) of a specific gene. Furthermore, these gene modifications can target all organs (systemic) or only the liver (conditional), which may further be regulated in a time-specific manner (inducible gene expression)[303,307]. Knockout mice are often used to identify the role of tumor suppressor

genes on tumor development. For example, hepatocyte-specific deletion of phosphatase and tensin homolog (PTEN) leads to steatosis, fibrosis and finally HCC in mice at 74-78 weeks of age[308]. Similarly, deletion of *Tak1* and *Mdr2* leads to inflammation, fibrosis and eventually HCC after 4 and 16 months of age, respectively[303,309,310]. On the other side, constitutive overexpression of TGF-α induces HCC development in mice after one year of age, with the incidence rate being dependent on the genetic background and gender of the transgenic mice[307]. Likewise, transgenic mice co-expressing *Tgfa* and *Myc* show extensive chromosomal damage and develop tumors[311] with a gene expression profile similar to the subgroup of human HCCs with poor prognosis[312].

Transgenic models expressing viral genes

Chronic HBV and HCV infections are major risk factors of HCC development[185]. However, besides chimpanzees[213,313] and humanized mice[314,315] no animal model is fully permissive for human HBV and HCV infection. Of note, a recent report shows that HCV-related hepacivirus from Norway rats induces hepatotrophic infections in mice with similar immunological features observed in humans[316]. Immune competent mice mimic an acute infection with viral clearance after 3-5 weeks, whereas immune compromised mice develop a chronic infection. The usefulness of this new model for studying HCC development remains to be investigated. The pathogenicity of HCV and HBV in chimpanzees is relatively low, the humanized mice lack a functional immune system and only immune compromised mice develop chronic infection from a HCV-related rat virus, for which reasons they are poor models to study chronic liver disease and associated HCC development[213]. Thus, the study of HBV and HCV-associated liver cancer remains a challenge.

Transgenic mouse models expressing viral antigens of HBV or HCV have been established to study HBV- and HCV-induced liver carcinogenesis. For HBV, most of these models focus on the *HBx* gene that has been described to induce the expression of a broad range of oncogenes including *c-fos*, *c-myc* and *c-jun*[317]. *Kim et al.* demonstrated that HBx transgenic mice died because of clear cell HCC within 11-15 month of age[318]. Of note, in contrast to human HCC, cirrhosis and inflammation were absent in the preneoplastic stages of these mice. However, transgenic mice that overexpress HBV surface antigens[319,320], develop necrosis and inflammation during HCC development, mimicking the features of chronic hepatitis in humans. Furthermore, the presence of the

HBx gene plus an oncogene[321] or exposure to diethylnitrosamine (DEN)/aflatoxin B1[322], resulted in an accelerated HCC formation in these transgenic mouse models.

Similarly, several transgenic mouse models constitutively expressing HCV structural and/or non-structural proteins under the control of liver specific promoters have been described[323]. In some of these models HCC develops primarily in older mice (>13 month) and on an HCV mediated background of steatosis[324,325]. It is important to note however, that although these mouse models have a fully functional immune system, they are typically immune-tolerant to the viral transgene and therefore lack the inflammatory phenotype observed in humans. Furthermore, the results from mouse models that ectopically express individual viral proteins have to be taken with caution as the expression level, trafficking and cellular localization of these proteins may significantly differ from what might occur in an infected hepatocyte[213].

Taken together, GEM models are frequently used to investigate pathophysiology of HCC, especially with the focus on the identification of pathways involved in hepatocarcinogenesis. The tumors are histologically similar to human HCCs and arise in a background of a fully active immune system. However, because the mice are normally immune-tolerant to the viral transgene, they lack the immune response against the virus, which is very different from the human situation. Furthermore, the generation of GEM mice can be time consuming and the use of strong promoters results in gene overexpression not observed in the clinical setting. Furthermore, the knock out of tumor suppressor genes or the constant expression of oncogenes does not necessarily reflect the situation during natural cancer development in HCC patients.

2.6.2.3 Chemically induced mouse models

Because the liver is the main organ responsible for detoxification, it is exposed to chemical compounds, including alcohol, aflatoxin B1 and other toxins, which in constantly high concentrations can lead to liver damage and eventually HCC. Therefore, several models using genotoxic agents have been described to mimic the course of human HCC development induced by chemical compounds. DEN is the most frequently used carcinogen in the field of liver cancer research[304]. DEN-induced tumorigenesis varies with dosage, age, sex and strain of the mice[302,326] and induces tumor formation mainly in the liver but also in the respiratory tract, kidney, upper digestive tract and in the hematopoietic system[302,304]. DEN is metabolized in the liver, where it causes DNA

damage[307]. When this damage happens in proliferating hepatocytes, either during liver development in the postnatal period or following liver injury, DNA damage is transmitted to daughter cells, which accelerates HCC development[327-329]. DEN induced tumor development occurs in the absence of chronic liver injury, inflammation and fibrosis[303]. However, if it is combined with a promoting agent such as the hepatotoxin carbon tetrachloride (CCl4), it induces a multistep process, including liver injury, inflammation, fibrosis, cirrhosis and ultimately HCC development[303]. Genetically, the DEN model resembles the subclass of human HCCs with poor prognosis[312], characterized by high proliferation rate, chromosomal instability and low levels of β-catenin mutations.

As previously described, aflatoxin B1 induces genetic damage and its intake has been correlated with HCC development in humans[185,203]. Similarly, mice exposed to aflatoxin B1 administration develop HCC after 52 weeks but with an incidence rate varying from 25-90% dependent on the mouse strain[302,330].

In general, chemically induced HCC mouse models can mimic the injury-fibrosis-malignancy cycle, the background on which the majority of HCC arise[331]. However, they mainly reflect toxin-induced etiologies, which makes them suboptimal for preclinical drug screening[303].

2.6.2.4 Xenograft mouse models

For the generation of HCC xenograft mouse models, established hepatoma cell lines or fresh human tumor tissue is implanted into immunocompromised recipient mice[292,306]. According to tumor localization, ectopic and orthotopic models are distinguished. In ectopic models, tumor tissue is subcutaneously (s.c.) introduced, whereas in orthotopic models, tumor tissue is placed intrahepatically[302]. S.c. xenograft models are technically relatively easy to perform, reproducible and because the tumors are placed externally, size assessment is straightforward. This is of special interest for preclinical drug testing as it allows regular tumor volume measurements[291]. Indeed, s.c. xenograft models are most frequently used for pre-clinical studies of anti-cancer drugs *in vivo*. However, these tumors do not have a direct interaction with the liver tissue[302], preventing the interaction of the tumor cells with the proper microenvironment[292]. On the other hand, tumors of orthotopic mouse models grow in their natural environment but are technically more challenging and require sophisticated imaging technologies or serum

biomarkers to monitor tumor take rate, tumor growth and effects of therapy on tumor progression[291]. Furthermore, xenograft models lack a fully functional immune system. Thus, the process of hepatocarcinogenesis on an inflammatory and fibrotic background cannot easily be investigated in these mice[303].

Established cell lines are frequently used to generate xenograft models because they are easy to handle, can be indefinitely expanded, allow for genetic manipulation and induce rapid tumor growth when injected into mice. However, their clonal appearance hardly reflects the heterogeneity of human HCCs[302]. In contrast, fresh patient material reflects the true composition of human HCCs but is difficult to obtain with very limited possibilities of genetic manipulations. Importantly, patient-derived xenograft models (PDX) are regarded as valuable tools in the field of anti-cancer drug development and prediction of cancer therapy[332,333]. In the field of HCC, several s.c.[334-338] and orthotopic[339,340] PDX models have been generated from fresh, surgically excised human HCC specimens. However, because only patients with early stage HCCs qualify for surgical tumor resection[185], these models may not recapitulate the full spectrum of HCC including all clinical tumor stages. Furthermore, a comprehensive and in depth analysis of how well these PDX models recapitulate the original human HCC tissue on histologic, genetic and molecular level, is still missing.

II Aims of Research

1. Project: Negative regulation of the IFN-λ induced JAK-STAT pathway

Although an immediate and strong activation of signaling pathways is necessary for optimal cytokine action, it is equally important to appropriately control the magnitude and duration of cellular responses to viral and bacterial infections in order to maintain tissue homeostasis. Although type I and III IFNs signal through distinct receptors, they induce a mostly overlapping set of ISGs in cells expressing both IFN-α and IFN-λ receptors[100,341]. However, the magnitude and duration of the induction remains different. While IFN-α-induced signaling is transient and completely shut down after a few hours, IFN-λ-induced signaling persists much longer[100,342,343]. USP18 has been shown to be responsible for the strong regulation of IFN-α signaling whereas its effect on IFN-λ remains a matter of controversy. Importantly, the effect of the two known inducible negative regulators SOCS1 and SOCS3 on IFN-λ needs further clarification. Currently available data is based primarily on overexpression studies *in vitro* and therefore lacks physiological relevance. With the current study, we aimed to investigate the physiological role of SOCS1, SOCS3 and USP18 on type III IFN-induced signaling *in vitro* and *in vivo*.

2. Project: Development of patient-derived xenograft models from fresh human HCC needle biopsies

HCC is the second leading cause of cancer-related death worldwide with increasing incidence rates. The prognosis of HCC is poor, despite massive efforts by experimental and clinical research. Less than 30% of HCC patients qualify for curative treatment and therapeutic approaches for advanced stage HCC shows only limited efficacy. Thus, the identification and development of more efficient therapies for intermediate and advanced stage HCCs are required. Albeit PDX models are useful for pre-clinical drug testing, until now, only resected HCC specimens were used to generate PDX mouse models. Because surgical resection is only applied to patients with early stage HCC, these models may not reflect the full spectrum of human HCC stages. Therefore, we aimed at establishing xenograft models from fresh human HCC needle biopsy material that also includes late stage HCCs. Using this approach we could generate a pre-clinical tool suitable for personalized medicine including analysis of drug-induced resistance

mechanisms and evaluation of potential anti-cancer compounds. Furthermore, biomarkers for therapy decision or patient-specific strategies targeting driver mutations or signaling pathways could be identified.

III Results

1 Research article I

SOCS1 is an inducible negative regulator of interferon λ (IFN-λ)–induced gene expression *in vivo*

T. Blumer, M. Coto-Llerena, FHT. Duong* and MH. Heim *

*denotes equal contribution.

Accepted manuscript, *Journal of Biological Chemistry*.

Statement of contribution

I cloned the constructs for transient SOCS1, SOCS3 and USP18 overexpression and generated SOCS1, SOCS3 and USP18 knockout cell lines using the CRISPR/Cas9 system. Furthermore, I designed and performed the *in vitro* experiments for Figure 1, 2, 4 and S3 as well as the *in vivo* experiments for Figure 5, 6 and S4. Finally I wrote the manuscript together with M. Coto-Llerena, FHT. Duong and MH. Heim.

JBC ARTICLE

SOCS1 is an inducible negative regulator of interferon λ (IFN-λ)–induced gene expression *in vivo*

Received for publication, March 30, 2017, and in revised form, September 4, 2017 Published, Papers in Press, September 12, 2017, DOI 10.1074/jbc.M117.788877

Tanja Blumer[‡§], **Mairene Coto-Llerena**[‡§], **Francois H. T. Duong**[‡§1], **and Markus H. Heim**[‡§1,2]

From the [‡]*Department of Biomedicine, University of Basel, 4031 Basel, Switzerland and the* [§]*University Hospital Basel, 4031 Basel, Switzerland*

Edited by Charles E. Samuel

Type I (α and β) and type III (λ) IFNs are induced upon viral infection through host sensory pathways that activate IFN regulatory factors (IRFs) and nuclear factor κB. Secreted IFNs induce autocrine and paracrine signaling through the JAK-STAT pathway, leading to the transcriptional induction of hundreds of IFN-stimulated genes, among them sensory pathway components such as cGAS, STING, RIG-I, MDA5, and the transcription factor IRF7, which enhance the induction of IFN-αs and IFN-λs. This positive feedback loop enables a very rapid and strong host response that, at some point, has to be controlled by negative regulators to maintain tissue homeostasis. Type I IFN signaling is controlled by the inducible negative regulators suppressor of cytokine signaling 1 (SOCS1), SOCS3, and ubiquitin-specific peptidase 18 (USP18). The physiological role of these proteins in IFN-γ signaling has not been clarified. Here we used knockout cell lines and mice to show that IFN-λ signaling is regulated by SOCS1 but not by SOCS3 or USP18. These differences were the basis for the distinct kinetic properties of type I and III IFNs. We found that IFN-α signaling is transient and becomes refractory after hours, whereas IFN-λ provides a long-lasting IFN-stimulated gene induction.

Type I and type III IFNs are induced in virus-infected cells and provide an important first line of defense through the rapid induction of hundreds of IFN-stimulated genes (ISGs)[3] that collectively establish an antiviral state. Type I IFNs (IFN-αs and IFN-β) bind to the ubiquitously expressed IFN-α receptor (IFNAR), which consists of two major subunits: IFNAR1 and IFNAR2c. Each receptor subunit constitutively binds to a single specific member of the JAK family: IFNAR1 to tyrosine kinase 2 (TYK2) and IFNAR2c to JAK1. Upon binding of the two chains by type I IFNs, TYK2 and JAK1 transactivate each other by mutual tyrosine phosphorylation and then initiate a cascade of tyrosine phosphorylation events on the intracellular domains of the receptors and on STAT1 and STAT2. STAT1 and STAT2 combine with a third transcription factor, IFN regulatory factor 9 (IRF9), to form interferon-stimulated gene factor 3 (ISGF3). ISGF3 binds to interferon-stimulated response elements (ISREs) in the promoters of ISGs. Alternatively, IFN-activated STAT1 can form homodimers. These STAT dimers bind a different class of response elements, the γ-activated sequence elements (1). Activation of the JAK–STAT pathway is tightly controlled by several negative regulatory mechanisms. SOCS1 and 3 are rapidly induced and inhibit STAT activation (2). Mechanistically, SOCS proteins simultaneously bind the receptors and the JAKs and prevent STATs from access to the receptor kinase complex (3). Ubiquitin-specific peptidase 18 (USP18) is induced later but remains highly expressed for days (4). USP18 is responsible for the long-lasting refractoriness of IFN-α signaling in the liver (5). The physiological role of these inducible negative feedback loops is to prevent tissue damage caused by the potent pro-inflammatory effects of type I IFNs (6).

In humans, the type III IFN family consists of four members, IFN-λ1–4. They all bind to the IFN-λ receptor (IFNLR), consisting of the ubiquitously expressed IL-10R2 chain (shared with the IL-10 receptor) and a unique IFN-λ receptor chain (IFNλR1) whose expression is mainly restricted to epithelial cells (7–9). Activation of the IFNLR by ligand binding results in the activation of ISGF3 and STAT1 homodimers, the same transcription factor complexes that are induced by type I IFNs. As a consequence, despite using different receptors, IFN-λs induce highly similar sets of ISGs as IFN-α/βs (10–14). However, at least in cell culture, ISG induction followed distinct kinetic profiles for IFN-α and IFN-λ. Although gene induction was rapid and transient with IFN-α, IFN-λ induced a slower but more sustained increase in ISG expression (15, 16). There is indirect evidence that this difference could result from the lack of USP18 binding to the IFNLR. In cell culture and in mice, USP18 was induced by both IFN-α and IFN-λ, but only IFN-α signaling was inhibited by USP18 (17, 18). Contradictory to these findings, a more recent report identified USP18 as a novel inhibitor of IFN-λ signaling (19). The role of SOCS1 and SOCS3 in regulating IFN-λ signaling remains to be clarified as well. Overexpression of SOCS1 in Huh7 human hepatoma cells inhibited the antiviral activity of both IFN-α and IFN-λ (20). However, whether physiological expression levels of SOCS1 and/or SOCS3 can inhibit IFN-λ signaling remains to be shown.

The IFN-λ system has been intensely studied in the context of hepatitis C virus (HCV) infections because genetic variants of

This work was supported by Swiss National Science Foundation Grants 310030B_147089 and 310030_166202 (to M. H. H.). The authors declare that they have no conflicts of interest with the contents of this article.
This article contains supplemental Figs. 1–4 and Tables 1–3.
[1] Both authors contributed equally to this work.
[2] To whom correspondence should be addressed: Dept. of Biomedicine, University of Basel, Hebelstr. 20, 4031 Basel, Switzerland. Tel.: 41-612652525; Fax: 41-612655352; E-mail: markus.heim@unibas.ch.
[3] The abbreviations used are: ISG, IFN-stimulated gene; IFNAR, IFN-α receptor; ISRE, IFN-stimulated response element; SOCS, suppressor of cytokine signaling; IFNLR, IFN-λ receptor; HCV, hepatitis C virus.

the IFN-λ gene locus are strongly associated with the ability of the host response to clear the viral infection in the acute phase and with response to treatment with pegylated IFN-α and ribavirin in chronic hepatitis C (21). Genetic evidence points to IFN-λ4 as the key regulator of the host response to HCV. A variant allele (TT at position rs368234815) with an inactivating frameshift mutation in exon 1 of the IFN-λ4 gene is found with a frequency that increases from Africa (0.29–0.44) to the New World (0.51–0.65) and Europe (0.58–0.77) and reaches 0.94–0.97 in East Asia (22). Homozygosity for the functionally inactive IFN-λ4 gene (TT/TT) is associated with spontaneous clearance of HCV in the acute phase and a high cure rate of therapies with pegylated IFN-α and ribavirin (23–25). It is not entirely clear why the host benefits from lack of a functional IFN-λ4. A pertinent observation relates to the activation status of the endogenous IFN system in the liver. Patients with wild-type IFN-λ4 (encoded by the rs368234815 ΔG allele) mount a strong innate immune response and have a permanent and strong expression of hundreds of ISGs in the liver (26). Among these ISGs are also inducible negative regulators of IFN signaling such as USP18. The continuous high expression of USP18 makes it highly unlikely that type I IFNs are drivers of the innate immune response in chronic hepatitis C. Indeed, there is genetic evidence that IFN-λ4 is the driver of ISG expression in chronic hepatitis C (25). To better understand the mechanisms of ISG induction in chronic hepatitis C, differences in negative regulation of type I and type III interferons have to be elucidated.

In this work, we investigated the role of SOCS1, SOCS3, and USP18 in IFN-λ signaling in cells with physiological IFNLR expression and deletion or overexpression of all three inhibitors and in mice deficient for SOCS1 or USP18. We identify SOCS1 as a physiologically relevant inducible inhibitor of IFN-λ–induced JAK–STAT signaling. SOCS3 and USP18 are important for regulating IFN-α but not IFN-λ signaling.

Results

IFN-λ induces sustained gene expression in cells despite strong induction of USP18

The selective and restricted expression of IFNLR1 limits the biological activity range of IFN-λ primarily to mucosal epithelial tissues (27). We have previously shown very low expression of IFNLR1 in the human liver that can, however, be induced in patients with chronic hepatitis C, particularly with the IFN-λ4 wild-type genotype (TT/ΔG and ΔG/ΔG), to levels that make hepatocytes responsive to IFN-λ (28). To analyze IFN-λ signaling in a cell line with similar IFNLR1 expression, we used a clone of Huh7 cells (a widely used human hepatoma cell line) that has been stably transfected with IFNLR1, Huh7 LR clone 3 (designated Huh7 LR in this manuscript) (28). Huh7 LR cells express around 10,000 copies of IFNLR1 per 40 ng of total RNA (Fig. 1*A*). Huh7 LR cells were then stimulated with saturating concentrations of human IFN-α and human IFN-λ1 for up to 48 h. The kinetics of the activation of JAK–STAT signaling were assessed with antibodies specific for tyrosine-phosphorylated STAT1 (p-STAT1), STAT2 (p-STAT2), and STAT3 (p-STAT3). IFN-α induced strong but transient STAT1 and STAT2 activation (Fig. 1*B*). Induction of the two early ISGs, *RSAD2* and *GBP5* (4), was also transient, with an expression peak 8 h after IFN-α stimulation (Fig. 1*C*). IFN-λ1 showed prolonged activation of STAT1 and STAT2 despite an even stronger induction of USP18 at the 24 h time point (Fig. 1*B*). Consistently, ISG induction was sustained and increased compared with IFN-α (Fig. 1*C*). The induction of pSTAT3 was not significantly different between IFN-α and IFN-λ1. These results are in accordance with published data obtained with other cell lines and primary human hepatocytes (11, 15, 16).

IFN-λ signaling is inhibited in cells overexpressing SOCS1, SOCS3, or USP18

Huh7 LR cells were then transiently transfected with expression plasmids for SOCS1, SOCS3, and USP18 and stimulated with saturating concentrations of IFN-α and IFN-λ1 for 30 min. All three proteins were strongly expressed and inhibited both IFN-α– and IFN-λ1–induced STAT1 phosphorylation (Fig. 2*A*). The inhibitory effect of USP18 on IFN-λ signaling was unexpected, given the sustained p-STAT1 and ISG induction shown in Fig. 1. We therefore systematically compared the expression levels of the negative regulators obtained by physiological stimulation with IFNs *versus* those obtained in cells transfected with expression plasmid. As shown in Fig. 2*B*, transfection resulted in expression levels that were 2–3 orders of magnitude higher than those induced by maximal physiological stimulation with IFNs. The mRNA results were also confirmed at the protein level (Fig. 2*B*). We conclude that all three inhibitors have the potential to inhibit both IFN-α and IFN-λ signaling at supraphysiological expression levels.

SOCS1-deficient cells are hyperresponsive to IFN-λ

To assess the physiological relevance of SOCS1, SOCS3, and USP18 for IFN-λ signaling, we generated knockout cell lines from Huh7 LR cells using the CRISPR-Cas9 technology (supplemental Fig. 1). The rationale for this loss-of-function experiment was the expectation that loss of a physiologically relevant inhibitor of IFN signaling must result in hyperactivation of the signal transduction pathway with increased ISG induction. By definition, any inducible inhibitor of IFN signaling has to restrict ISG induction at some point and to a relevant degree. We first tested this hypothesis using a luciferase reporter gene under the control of an ISRE promoter (*i.e.* the Mx1 promoter, ISRE-Mx1-Luc). To do so, we transfected control and knockout cells with the pGL3-ISRE-Mx1-Luc plasmid together with a constitutively expressed *Renilla* luciferase construct for normalization. 20 h after transfection, they were stimulated with IFN-λ1, IFN-λ3, IFN-λ4, IFN-α, and IFN-β or left untreated, and luciferase activity was quantified 4, 8, and 24 h later. The luciferase activity in untreated cells did not differ significantly between cell lines but increased at least 15-fold within 4 h after IFN addition. At 4 h and 8 h, but not at 24 h, SOCS1 knockout cells showed significantly higher expression of the reporter constructs when stimulated with IFN-λ1, IFN-λ3, or IFN-λ4 (Fig. 3 and supplemental Fig. 2). IFN-α signaling was enhanced in USP18 knockout cells at all time points (Fig. 3), whereas IFN-β signaling was enhanced at the 8 h time point only (supplemental Fig. 2). Type I IFN–induced expression of the reporter plas-

Negative regulation of type III interferon signaling

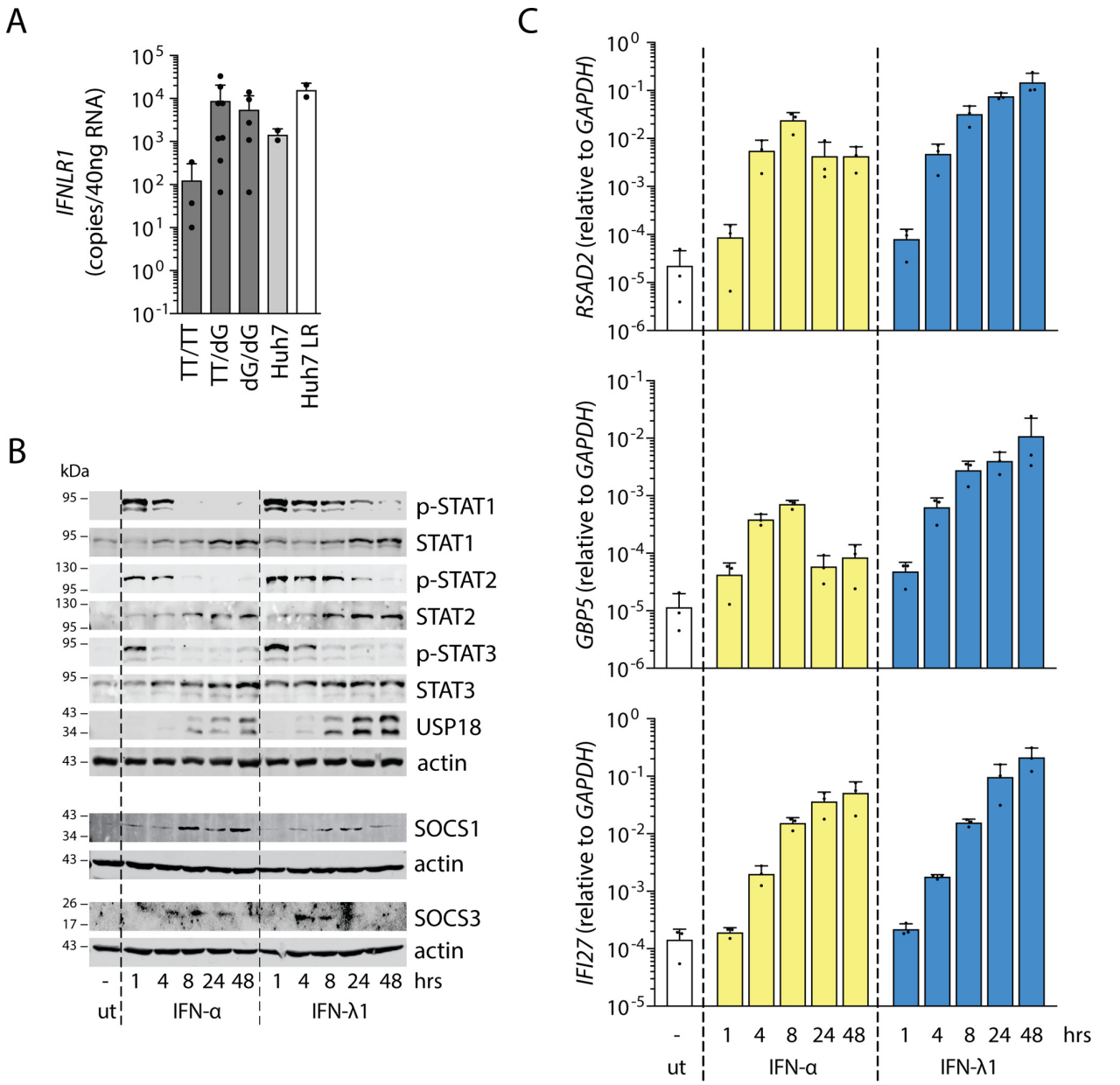

Figure 1. IFN-α– but not IFN-λ–induced STAT1 phosphorylation becomes refractory to continuous stimulation. *A*, liver biopsies from chronic hepatitis C patients ($n = 16$) were divided into three groups based on their *IFNL4* genotype (rs368234815; TT/TT, TT/dG, and dG/dG). Total RNA from biopsies and Huh7 and Huh7 LR cells were prepared. Expression of the IFNLR1 transcript was analyzed by quantitative PCR. Results (mean ± S.D.) are shown as copy numbers per 40 ng of total RNA. *B* and *C*, Huh7 LR cells were stimulated with 1000 IU/ml IFN-α or 100 ng/ml IFN-λ1 for the indicated times. *B*, p-STAT1, STAT1, p-STAT2, STAT2, p-STAT3, STAT3, USP18, SOCS1, SOCS3, and actin were visualized using specific antibodies. Shown are representative blots from two independent experiments. *C*, transcripts of interferon-stimulated genes (*RSAD2*, *IFI27*, and *GBP5*) were quantified by PCR. Results (mean ± S.D., $n = 3$) are shown as relative expression to *GAPDH*. *ut*, untreated.

mid was also significantly enhanced at some time points in SOCS1 and SOCS3 knockout cells (Fig. 3 and supplemental Fig. 2). We confirmed these findings by quantifying the expression levels of ISGs, including *RSAD2*, *GBP5*, and *IFI27*, as well as the three inducible regulators, *SOCS1*, *SOCS3*, and *USP18*, in the knockout cell lines after stimulation with IFN-λ1 and IFN-α (Fig. 4 and supplemental Fig. 3). Expression of *RSAD2*, *GBP5*, and *IFI27* in untreated control and knockout cells was detectable and did not differ significantly between the cell lines. The same ISGs were up-regulated 10- to 100-fold 4 h after IFN-α or IFN-λ1 stimulation (Fig. 4). Importantly however, IFN-λ1–induced ISG expression was significantly enhanced in SOCS1 knockout cells at 8 and 24 h, but this increase was not observed in SOCS3 or USP18 knockout cells. For *GBP5*, this enhancement could already be observed 4 h after IFN-λ1 stimulation, although it did not reach statistical significance. Furthermore, we confirmed the known negative regulatory effect of USP18 on IFN-α signaling. We conclude that, in Huh7 LR cells, SOCS1 is an inducible and physiologically relevant negative regulator of IFN-λ1, IFN-λ3, and IFN-λ4.

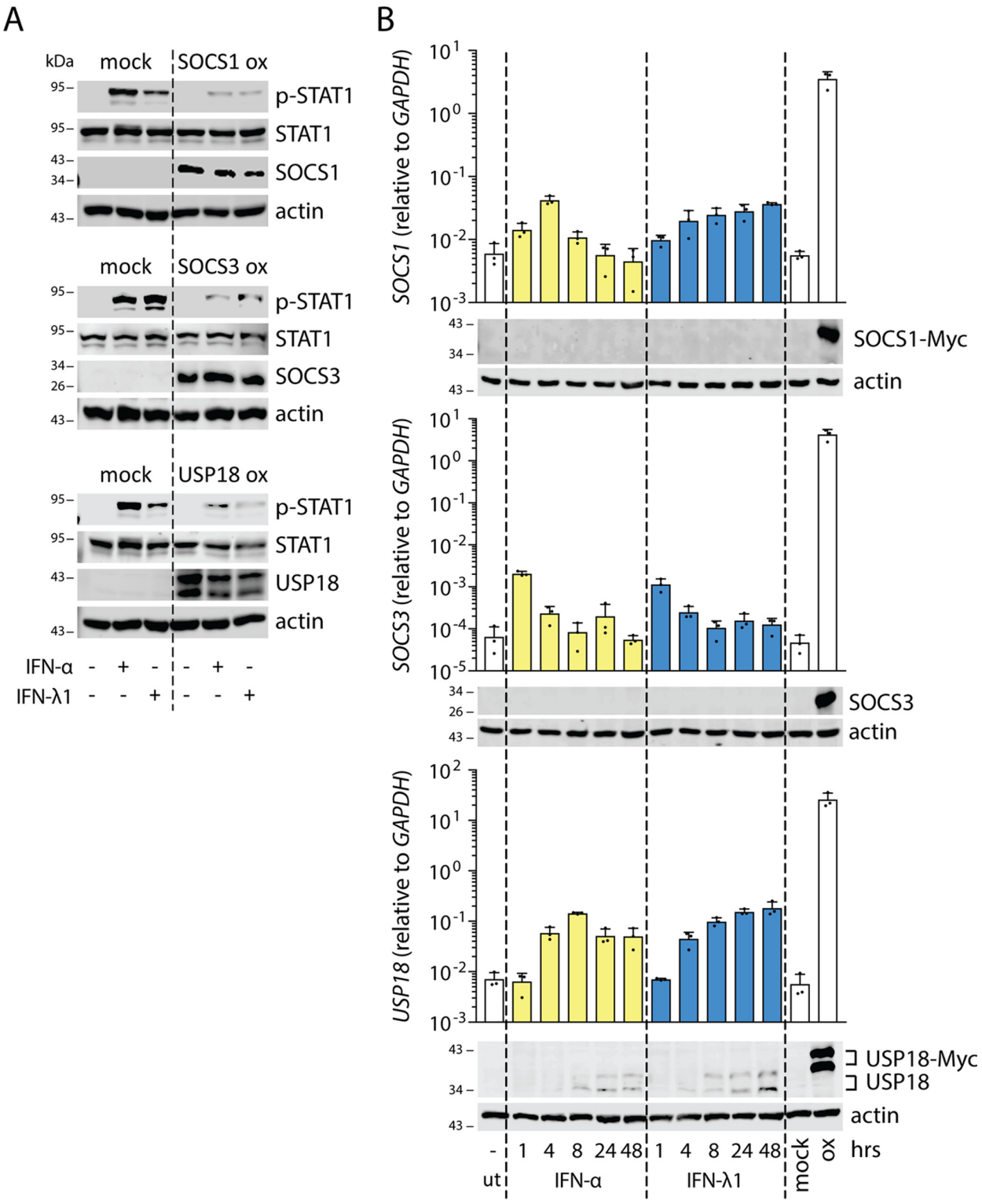

Figure 2. Overexpression of SOCS1, SOCS3, and USP18 leads to a reduction of IFN-α– and IFN-λ–mediated STAT1 phosphorylation. *A*, Huh7 LR cells were transiently transfected with control, SOCS1, SOCS3, or USP18 expression plasmids. 24 h later, cells were stimulated with 1000 IU/ml IFN-α or 100 ng/ml IFN-λ1 for 30 min, and p-STAT1, STAT1, SOCS1, SOCS3, USP18, and actin were visualized by immunoblotting. Shown are representative blots from three independent experiments. *B*, Huh7 LR cells were transfected with SOCS1, SOCS3, or USP18 expression plasmids for 24 h. The mRNA expression levels of *SOCS1*, *SOCS3*, and *USP18* were analyzed by quantitative PCR and compared with the endogenously induced *SOCS1*, *SOCS3*, or *USP18* upon IFN-α or IFN-λ1 stimulation at the indicated time points. The results (mean ± S.D., $n = 3$) are shown as relative expression to *GAPDH*. Protein levels of SOCS1, SOCS3, and USP18 and actin were visualized using specific antibodies. *ox*, overexpression; *ut*, untreated.

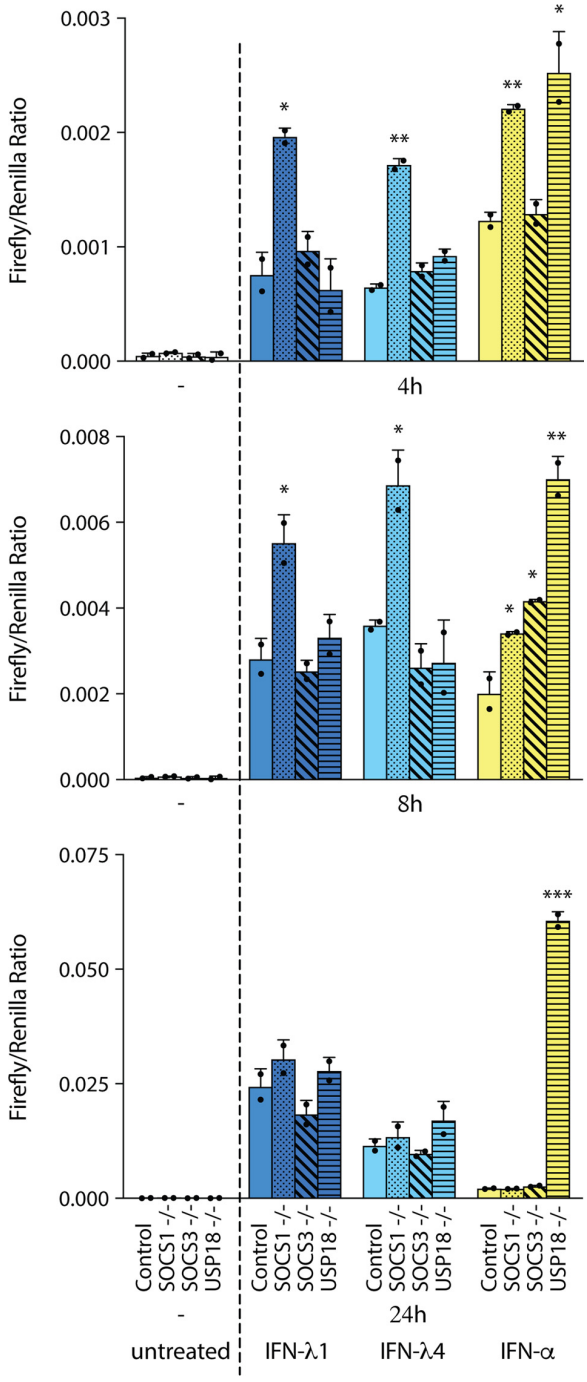

Figure 3. SOCS1 is a modulator of IFN-λ-signaling. Control, SOCS1$^{-/-}$, SOCS3$^{-/-}$, and USP18$^{-/-}$ cells were transfected with pGL3-ISRE-Mx1-Luc and pGL4-CMV-*Renilla*-Luc plasmids and, 20 h later, stimulated with 100 ng/ml IFN-λ1, 50 ng/ml IFN-λ4, or 1000 IU/ml IFN-α for 4 h, 8 h, and 24 h or left untreated. The firefly luciferase values were normalized to *Renilla* luciferase, and the results (mean ± S.D., $n = 2$) are expressed as firefly/*Renilla* ratio. Unpaired *t* test; *, $p < 0.05$; **, $p < 0.01$; ***, $p < 0.001$.

SOCS1 is a physiological inhibitor of IFN-λ signaling in vivo

To test whether the results obtained in Huh7 LR cells are valid *in vivo*, we analyzed IFN-λ and IFN-α signaling in mice deficient for *Socs1* or *Usp18* and their corresponding control mice. Because *Socs1* knockout mice suffer from IFN-γ–mediated lethal toxicity, they were bread as *Ifng/Socs1* double knockout mice, with *Ifng* knockout mice serving as controls, as described previously (5, 29). The mice were sacrificed 4 and 8 h after IFN injections, and the liver, lung, and gut were analyzed for induction of seven different ISGs (*Rsad2*, *Oas1*, *Stat1*, *Usp18*, *Gbp5*, and *Ifi27*). *Socs1* knockout resulted in significantly increased expression of all IFN-λ2–induced ISGs at 8 h in the lung and at 4 h in the gut, the two IFN-λ responsive organs, but not in the liver, which is devoid of IFNLR1 in mice (Fig. 5). Although *Socs1* knockout also resulted in enhanced expression of three of six ISGs in the lung and gut upon IFN-α injection (Fig. 5), it did not affect IFN-α–mediated ISG induction levels in the liver (Fig. 5 and supplemental Fig. 4*A*). In contrast, IFN-α induced all tested ISGs to significantly higher levels in the livers of *Usp18* knockout mice compared with control mice at all time points (Fig. 6 and supplemental Fig. 4*B*). The effect of *Usp18* knockout on IFN-α signaling in the lung occurred mainly at 8 h, and it was much less pronounced in the gut. The effect of *Usp18* knockout on IFN-λ signaling was minimal, with only *Rsad2* and *Ifi27* being significantly increased at one time point in the gut and lung, respectively (Fig. 6 and supplemental Fig. 4*B*). From these results, we conclude that IFN-α signaling in these mice is predominantly inhibited by *Usp18*, whereas IFN-λ signaling is regulated by *Socs1*.

Discussion

Type I IFNs (IFN-α/β) are potent and critically important cytokines that control innate and adaptive immune responses to infection, cancer, and other inflammatory stimuli. Positive feedback amplification through autocrine and paracrine induction of IFN-α gene transcription allows a very rapid and strong host response to infections (30). The extent and duration of this response is tightly controlled by several mechanisms to avoid adverse effects on tissue homeostasis. The fact that several clinically important autoimmune diseases, such as systemic lupus erythematosus and Aicardi-Goutières syndrome, are associated with uncontrolled type I IFN activities demonstrates the important role of negative regulators in keeping the system in balance (6, 31). SOCS1 is an inducible negative regulator of IFN-α signaling that transiently restricts phosphorylation of STATs in the first hours. However, its role as a negative regulator of IFN-α signaling is limited. The fact that the lethal phenotype of *Socs1* knockout mice is rescued by additional knockout of *Ifng* demonstrates that the main role of SOCS1 in the IFN system is to control IFN-γ (29). Furthermore, deletion of *Socs1* does not prevent the induction of refractoriness to IFN-α in the mouse liver (5). The main negative regulator of IFN-α seems to be USP18. This is demonstrated by this work, by previous work that showed that refractoriness to IFN-α stimulation is abrogated in *Usp18* knockout mice (5), and by a rare genetic interferonopathy, pseudo-TORCH syndrome, which is caused by human USP18 deficiency (32).

Negative regulation of type III IFNs is fundamentally different from type I IFNs. The inducible up-regulation of USP18 does not induce refractoriness of IFN-λ signaling (this work and Refs. 11, 15–18).). Of note, as shown in Fig. 2, USP18 indeed has the potential to inhibit IFN-λ signaling, but only at expression levels that are not achieved by physiological induction

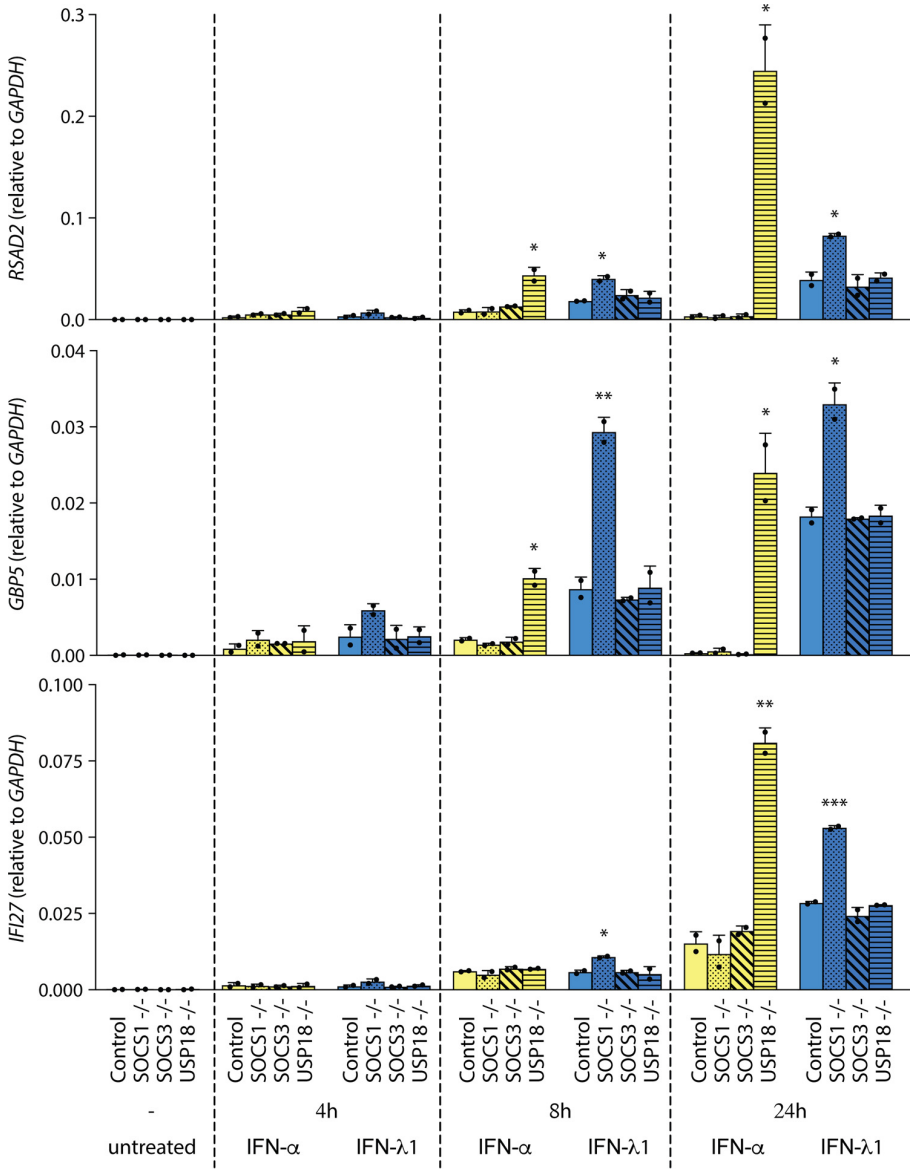

Figure 4. SOCS1 is a modulator of IFN-λ–induced ISGs expression *in vitro*. Control, SOCS1$^{-/-}$, SOCS3$^{-/-}$, and USP18$^{-/-}$ cells were stimulated with 1000 IU/ml IFN-α or 100 ng/ml IFN-λ1 for 4 h, 8 h, and 24 h or left untreated, and the expression levels of *RSAD2*, *GBP5*, and *IFI27* were analyzed by quantitative PCR. The results (mean ± S.D., $n = 2$) are shown as relative expression to *GAPDH*. Unpaired *t* test; *, $p < 0.05$; **, $p < 0.01$; ***, $p < 0.001$.

stimuli. We conclude that USP18 is not a physiological inhibitor of IFN-λ signaling. IFN-λ signaling is rather controlled by SOCS1, and contrary to IFN-α, not only in the first hours of stimulation but also at later time points (Fig. 4). Of note, a long-lasting negative regulatory effect of SOCS1 on IFN-λ1 signaling has been found previously in shRNA knockdown experiments in A549 human alveolar epithelial cells (33). SOCS1 not only controls the closely related IFN-λ1 and IFN-λ3 but also IFN-λ4. We postulate that the prolonged inhibitory effects of SOCS1 on IFN-λ signaling result from its sustained up-regulation for at least 48 h, which contrasts the transient induction of SOCS1 by IFN-α (Fig. 2*B*).

In conclusion, we show that the IFN-α and the IFN-λ systems not only differ in terms of tissue distribution of their cognate receptors (27) but are also controlled by distinct negative regulatory mechanisms of their signal transduction through the JAK–STAT pathway. IFN-α signaling is transient and shut down after 6–8 h by USP18, a very strong inhibitor of STAT tyrosine phosphorylation at the IFNAR–kinase complex. IFN-λ signaling is not affected by USP18. It is controlled by SOCS1, but SOCS1 does not shut down STAT phosphorylation completely, allowing long-lasting stimulation of ISG transcription by IFN-λ. We postulate that these differences between IFN-α and IFN-λ in the negative regulation of JAK–STAT signaling are responsible for the previously described differences in the kinetics of ISG induction. Long-lasting activation of JAK–STAT signaling allows the IFN-λ system to mount a sustained antiviral state in mucosal epithelial cells that are constantly exposed to pathogens. IFN-α is a more powerful defense system that is activated when pathogenic viruses have breached

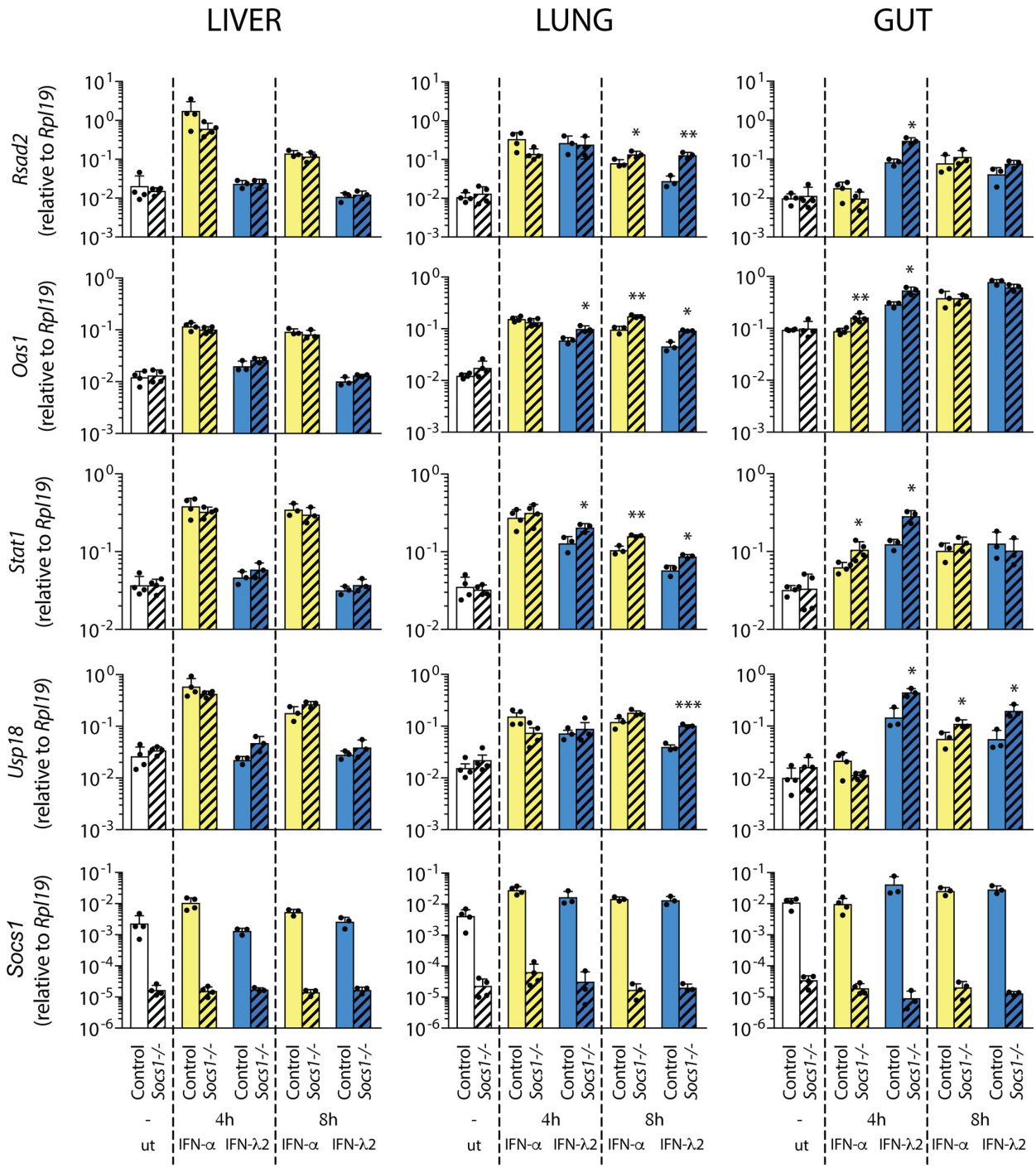

Figure 5. Depletion of *Socs-1* increased IFN-λ–induced ISGs expression *in vivo*. Control and *Socs1*$^{-/-}$ mice were subcutaneously injected with PBS, 1000 units/g mouse IFN-α, or 50 ng/g mouse IFN-λ2. The liver, the lung, and the gut were collected 4 h and 8 h after injection, and total RNA was prepared. The expression of *Rsad2*, *Oas1*, *Stat1*, *Usp18*, and *Socs1* was measured by quantitative PCR. The results (mean ± S.D.) are shown as relative expression to *Rpl19*. Three to four animals were used per time point and condition. Unpaired *t* test with Welch's correction; *, $p < 0.05$; **, $p < 0.01$; ***, $p < 0.001$. *ut*, untreated.

the mucosal surfaces and invaded the systemic circulation and other organs. In most instances, it is only transiently activated because prolonged activation of IFN-α signaling is detrimental for tissue homeostasis and can also negatively impact the cellular immune response.

Experimental procedures

Cell culture

A human hepatoma cell line (Huh7) was cultured in DMEM (Gibco) supplemented with 10% heat-inactivated FBS (Gibco) and 1% penicillin-streptomycin (Gibco). Huh7

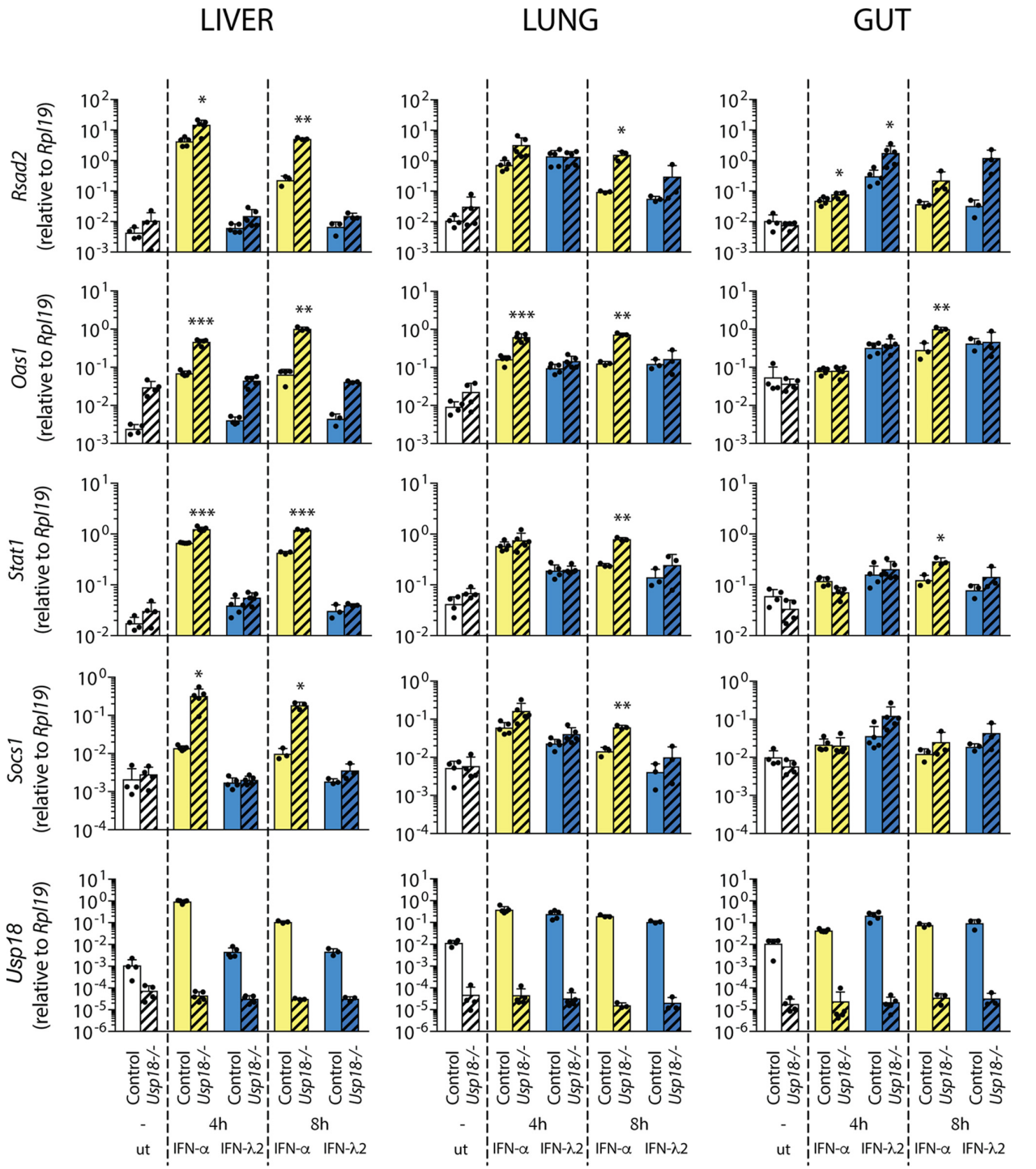

Figure 6. Depletion of *Usp18* increased IFN-α–induced ISGs expression *in vivo*. Control and *Usp18*$^{-/-}$ mice were subcutaneously injected with PBS, 1000 units/g mouse IFN-α, or 50 ng/g mouse IFN-λ2. The liver, the lung, and the gut were collected 4 h and 8 h after injection, and total RNA was prepared. The expression of *Rsad2*, *Oas1*, *Stat1*, *Socs1*, and *Usp18* was measured by quantitative PCR. The results (mean ± S.D.) are shown as relative expression to *Rpl19*. Three to five animals were used per time point and condition. Unpaired *t* test with Welch's correction; *, $p < 0.05$; **, $p < 0.01$; ***, $p < 0.001$. *ut*, untreated.

LR cells constitutively overexpressing IFNLR1 (28) and SOCS1$^{-/-}$, SOCS3$^{-/-}$, and USP18$^{-/-}$ cells were cultured in DMEM-10% FBS, 1% penicillin-streptomycin (Gibco) supplemented with 1 mg/ml G418 (Calbiochem).

Animals

Socs1$^{-/-}$ *Ifng*$^{-/-}$ (*Socs1*$^{-/-}$), *Ifng*$^{-/-}$ (control), *Ubp43*$^{-/-}$ (*Usp18*$^{-/-}$), and FVB (control) mice were described previously (29, 34–37). The animals were bred and maintained in the ani-

mal facility of the Department of Biomedicine of the University Hospital Basel under specific-pathogen-free conditions on a 12-h day and 12-h night schedule with *ad libitum* access to food and drinking water. Experiments were conducted with the approval of the Animal Care Committee of the Canton Basel-Stadt, Switzerland. Six- to eight-week-old males were used, and the animals were euthanized by CO_2 narcosis. Resected organs were immediately frozen in liquid nitrogen and kept at −70 °C until further processing. Subcutaneous injections with PBS, mouse IFN-α, or mouse IFN-λ2 were performed between 8 a.m. and 5 p.m.

Human liver biopsies

Liver biopsies from chronic HCV-infected patients ($n = 16$, patient characteristics are shown in supplemental Table 1) were obtained in the outpatient clinic of the Division of Gastroenterology and Hepatology, University Hospital Basel, Switzerland. Biopsy material that was not needed for routine histopathology was used for research purposes after obtaining written informed consent. The use of biopsy material for this project was approved by the Ethikkommission Nordwest- und Zentralschweiz, Basel, Switzerland, protocol number M989/99. Total DNA was isolated from liver biopsies using the DNeasy Blood & Tissue Kit (Qiagen, Hombrechtikon, Switzerland) according to the instructions of the manufacturer. IFN-λ4 genotype was determined as described previously (25).

Plasmids, antibodies, and reagents

Human IFN-α (Roferon-A) was purchased from Roche Pharma SA (Reinach, Switzerland). Human IFN-β (Betaferon) was obtained from Bayer HealthCare Pharmaceuticals (Bayer Consumer Care AG, Basel, Switzerland). Human IFN-λ1 and mouse IFN-λ2 were from PeproTech (LuBioScience GmbH, Luzern, Switzerland), and human IFN-γ was from Biolegend (Lucerna-Chem AG, Luzern, Switzerland). Human IFN-λ3 and human IFN-λ4 were generated as described previously (9) by Prof. Rune Hartmann (Aarhus University, Aarhus, Denmark), and mouse IFN-α was a gift from Prof. Radek Skoda (University Hospital Basel). Phospho-STAT1 (Tyr-701, 58D6), phospho-STAT3 (Tyr-705, D3A7 XP), STAT3 (124H6), and USP18 (D4E7) antibodies were from Cell Signaling Technology (BioConcept, Allschwil, Switzerland), and STAT1 (C-term) and STAT2 antibodies were from BD Biosciences (Allschwil, Switzerland). Phospho-STAT2 (Tyr689) and SOCS1 (4H1) antibodies were from EMD Millipore (Merck & Co., Schaffhausen, Switzerland). SOCS3 (H-103) and β-actin were from Santa Cruz Biotechnology (LabForce AG, Muttenz, Switzerland) and Sigma-Aldrich Chemie GmbH (Buchs, Switzerland), respectively.

Whole-cell lysates and Western blotting analysis

Whole-cell lysates and immunoblots were prepared and used as described previously (38).

Total RNA extraction and quantitative PCR

Total RNA from cell lines was isolated using NucleoSpin RNA (Macherey-Nagel AG, Oensingen, Switzerland) according to the instructions of the manufacturer. cDNA was generated from 1 μg of total RNA using Moloney murine leukemia virus reverse transcriptase (Promega AG, Dübendorf, Switzerland). Total RNA from human biopsies and mouse samples was isolated using TRIzol according to the instructions of the manufacturer. 1 μg of total RNA was incubated with rDNaseI using the DNA-free kit (Ambion). cDNA was generated using the TaqMan reverse transcription reagent kit (Applied Biosystems) according to the recommendations of the manufacturer. Real-time quantitative PCR was performed using FastStart Universal SYBR Green Master Mix (Roche Diagnostics AG, Rotkreuz, Switzerland) and the ABI 7500 detection system (Applied Biosystems, Thermo Fisher Scientific, Zug, Switzerland). Primers are listed in supplemental Table 2. The specificity of the PCR primers was assessed by sequencing the PCR product. Gene transcript expression levels were calculated using the ΔCt method. To quantitate IFNLR1 transcript levels, dilutions of plasmids containing the IFNLR1 ORF (28) were used as standard curves (dilutions ranged from 10^8 to 10^0 copies of plasmid).

SOCS1, SOCS3, and USP18 overexpression

The pCMV6 plasmid containing the SOCS1 gene (RC220847) was purchased from Origene Technologies Inc. (Rockville, MD) and used to overexpress SOCS1. Human USP18 and human SOCS3 coding sequences were cloned into the pCMV6-entry and pCMV-MIR vectors, respectively, using XhoI and BamHI restriction sites for USP18 and XhoI and KpnI restriction sites for SOCS3. Huh7 LR cells (2×10^5/well) were seeded onto a 6-well plate, and 2 μg of expression plasmid was transfected using JetPrime™ (Polyplus Transfection, VWR International GmbH, Dietikon, Switzerland) according to the instructions of the manufacturer.

Generation of SOCS1, SOCS3, and USP18 knockout cell lines

Briefly, the CRISPR design tool from the Zhang laboratory (http://crispr.mit.edu)[4] was used to design single-guide RNA constructs (supplemental Table 3). Phosphorylated and annealed single-guide RNAs were cloned into pSpCas9(BB)-2A-GFP (PX458) (Addgene, 48138, deposited by Feng Zhang) using BbsI restriction sites. Plasmids were verified by sequencing. 48 h post-transfection, GFP-positive cells were single cell–sorted by FACS. To confirm successful gene targeting in sorted clones, genomic DNA was extracted using the DNeasy Blood & Tissue Kit (Qiagen AG) and subjected to PCR amplification using specific primers for the region of interest (supplemental Table 2). PCR fragments were then cloned into a pGEMT-easy expression vector (Promega AG) and transformed into *Escherichia coli* TOP-10 chemically competent cells (Invitrogen). Colonies were analyzed by sequencing using the T7 primer. Finally, the absence of SOCS1, SOCS3, or USP18 protein was confirmed by immunoblotting.

IFN activity reporter assay

The ISRE-Mx1 firefly luciferase reporter construct (pGL3-Mx1P-FF-Luc, a gift from Rune Hartmann) and pGL4-CMV-

[4] Please note that the JBC is not responsible for the long-term archiving and maintenance of this site or any other third party–hosted site.

Renilla-Luc (a gift from Jacek Krol) were electroporated using Cytomix (39, 40) into SOCS1$^{-/-}$, SOCS3$^{-/-}$, USP18$^{-/-}$, or control cells. 20 h after electroporation, cells were treated with IFN-α (1000 UI/ml), IFN-β (1000 UI/ml), IFN-λ1 (100 ng/ml), IFN-λ3 (200 ng/ml), or IFN-λ4 (50 ng/ml) for 4, 8, and 24 h. Cells were then lysed with passive lysis buffer (Promega AG), and firefly luciferase levels were measured, followed by *Renilla* luciferase levels, using a multimode microplate reader (Centro XS^3 LB960, Berthold Technologies GmbH & Co. KG, Bad Wildbad, Germany). The firefly luciferase was normalized in each well to *Renilla* luciferase.

Statistical analysis

Prism4 (GraphPad Software Inc., La Jolla, CA) was used for statistical analysis.

Author contributions—T. B., M. C.L., and F. H. T. D. conducted the experiments, analyzed the results, and prepared the figures. M. H. H. recruited patients and obtained the liver biopsies. All authors conceived the idea for the project and wrote the manuscript.

Acknowledgments—We thank Hans Henrik Gad and Rune Hartmann for providing recombinant human IFN-λ3 and human IFN-λ4 and the ISRE luciferase reporter construct. We thank Petr Broz and Roland Dreier for excellent technical support with CRISPR/Cas9 technology. We thank Stefan Wieland for critical reading of the manuscript.

References

1. Darnell, J. E., Jr. (1997) STATs and gene regulation. *Science* **277,** 1630–1635
2. Krebs, D. L., and Hilton, D. J. (2001) SOCS proteins: negative regulators of cytokine signaling. *Stem Cells* **19,** 378–387
3. Kershaw, N. J., Murphy, J. M., Liau, N. P., Varghese, L. N., Laktyushin, A., Whitlock, E. L., Lucet, I. S., Nicola, N. A., and Babon, J. J. (2013) SOCS3 binds specific receptor-JAK complexes to control cytokine signaling by direct kinase inhibition. *Nat. Struct. Mol. Biol.* **20,** 469–476
4. Dill, M. T., Makowska, Z., Trincucci, G., Gruber, A. J., Vogt, J. E., Filipowicz, M., Calabrese, D., Krol, I., Lau, D. T., Terracciano, L., van Nimwegen, E., Roth, V., and Heim, M. H. (2014) Pegylated IFN-alpha regulates hepatic gene expression through transient Jak/STAT activation. *J. Clin. Invest.* **124,** 1568–1581
5. Sarasin-Filipowicz, M., Wang, X., Yan, M., Duong, F. H., Poli, V., Hilton, D. J., Zhang, D.-E., and Heim, M. H. (2009) α Interferon induces long-lasting refractoriness of JAK-STAT signaling in the mouse liver through induction of USP18/UBP43. *Mol. Cell. Biol.* **29,** 4841–4851
6. Porritt, R. A., and Hertzog, P. J. (2015) Dynamic control of type I IFN signalling by an integrated network of negative regulators. *Trends Immunol.* **36,** 150–160
7. Kotenko, S. V., Gallagher, G., Baurin, V. V., Lewis-Antes, A., Shen, M., Shah, N. K., Langer, J. A., Sheikh, F., Dickensheets, H., and Donnelly, R. P. (2003) IFN-λs mediate antiviral protection through a distinct class II cytokine receptor complex. *Nat. Immunol.* **4,** 69–77
8. Donnelly, R. P., Sheikh, F., Kotenko, S. V., and Dickensheets, H. (2004) The expanded family of class II cytokines that share the IL-10 receptor-2 (IL-10R2) chain. *J. Leukocyte Biol.* **76,** 314–321
9. Hamming, O. J., Terczyńska-Dyla, E., Vieyres, G., Dijkman, R., Jørgensen, S. E., Akhtar, H., Siupka, P., Pietschmann, T., Thiel, V., and Hartmann, R. (2013) Interferon λ 4 signals via the IFNλ receptor to regulate antiviral activity against HCV and coronaviruses. *EMBO J.* **32,** 3055–3065
10. Doyle, S. E., Schreckhise, H., Khuu-Duong, K., Henderson, K., Rosler, R., Storey, H., Yao, L., Liu, H., Barahmand-pour, F., Sivakumar, P., Chan, C., Birks, C., Foster, D., Clegg, C. H., Wietzke-Braun, P., *et al.* (2006) Interleukin-29 uses a type 1 interferon-like program to promote antiviral responses in human hepatocytes. *Hepatology* **44,** 896–906
11. Marcello, T., Grakoui, A., Barba-Spaeth, G., Machlin, E. S., Kotenko, S. V., MacDonald, M. R., and Rice, C. M. (2006) Interferons α and λ inhibit hepatitis C virus replication with distinct signal transduction and gene regulation kinetics. *Gastroenterology* **131,** 1887–1898
12. Lauber, C., Vieyres, G., Terczyńska-Dyla, E., Anggakusuma Dijkman, R., Gad, H. H., Akhtar, H., Geffers, R., Vondran, F. W., Thiel, V., Kaderali, L., Pietschmann, T., and Hartmann, R. (2015) Transcriptome analysis reveals a classical interferon signature induced by IFNλ4 in human primary cells. *Genes Immun.* **16,** 414–421
13. Zhou, Z., Hamming, O. J., Ank, N., Paludan, S. R., Nielsen, A. L., and Hartmann, R. (2007) Type III interferon (IFN) induces a type I IFN-like response in a restricted subset of cells through signaling pathways involving both the Jak-STAT pathway and the mitogen-activated protein kinases. *J. Virol.* **81,** 7749–7758
14. Crotta, S., Davidson, S., Mahlakoiv, T., Desmet, C. J., Buckwalter, M. R., Albert, M. L., Staeheli, P., and Wack, A. (2013) Type I and type III interferons drive redundant amplification loops to induce a transcriptional signature in influenza-infected airway epithelia. *PLoS Pathog.* **9,** e1003773
15. Jilg, N., Lin, W., Hong, J., Schaefer, E. A., Wolski, D., Meixong, J., Goto, K., Brisac, C., Chusri, P., Fusco, D. N., Chevaliez, S., Luther, J., Kumthip, K., Urban, T. J., Peng, L. F., *et al.* (2014) Kinetic differences in the induction of interferon stimulated genes by interferon-α and interleukin 28B are altered by infection with hepatitis C virus. *Hepatology* **59,** 1250–1261
16. Bolen, C. R., Ding, S., Robek, M. D., and Kleinstein, S. H. (2014) Dynamic expression profiling of type I and type III interferon-stimulated hepatocytes reveals a stable hierarchy of gene expression. *Hepatology* **59,** 1262–1272
17. François-Newton, V., Magno de Freitas Almeida, G., Payelle-Brogard, B., Monneron, D., Pichard-Garcia, L., Piehler, J., Pellegrini, S., and Uzé, G. (2011) USP18-based negative feedback control is induced by type I and type III interferons and specifically inactivates interferon α response. *PLoS ONE* **6,** e22200
18. Makowska, Z., Duong, F. H., Trincucci, G., Tough, D. F., and Heim, M. H. (2011) Interferon-β and interferon-λ signaling is not affected by interferon-induced refractoriness to interferon-α *in vivo*. *Hepatology* **53,** 1154–1163
19. Burkart, C., Arimoto, K., Tang, T., Cong, X., Xiao, N., Liu, Y. C., Kotenko, S. V., Ellies, L. G., and Zhang, D. E. (2013) Usp18 deficient mammary epithelial cells create an antitumour environment driven by hypersensitivity to IFN-λ and elevated secretion of Cxcl10. *EMBO Mol. Med.* **5,** 1035–1050
20. Liu, B., Chen, S., Guan, Y., and Chen, L. (2015) Type III interferon induces distinct SOCS1 expression pattern that contributes to delayed but prolonged activation of Jak/STAT signaling pathway: implications for treatment non-response in HCV patients. *PLoS ONE* **10,** e0133800
21. Heim, M. H., Bochud, P. Y., and George, J. (2016) Host-hepatitis C viral interactions: the role of genetics. *J. Hepatol.* **65,** S22–32
22. Key, F. M., Peter, B., Dennis, M. Y., Huerta-Sánchez, E., Tang, W., Prokunina-Olsson, L., Nielsen, R., and Andrés, A. M. (2014) Selection on a variant associated with improved viral clearance drives local, adaptive pseudogenization of interferon λ 4 (IFNL4). *PLoS Genet.* **10,** e1004681
23. Prokunina-Olsson, L., Muchmore, B., Tang, W., Pfeiffer, R. M., Park, H., Dickensheets, H., Hergott, D., Porter-Gill, P., Mumy, A., Kohaar, I., Chen, S., Brand, N., Tarway, M., Liu, L., Sheikh, F., *et al.* (2013) A variant upstream of IFNL3 (IL28B) creating a new interferon gene IFNL4 is associated with impaired clearance of hepatitis C virus. *Nat. Genet.* **45,** 164–171
24. Bibert, S., Roger, T., Calandra, T., Bochud, M., Cerny, A., Semmo, N., Duong, F. H., Gerlach, T., Malinverni, R., Moradpour, D., Negro, F., Müllhaupt, B., Bochud, P. Y., and Swiss Hepatitis C Cohort Study (2013) IL28B expression depends on a novel TT/-G polymorphism which improves HCV clearance prediction. *J. Exp. Med.* **210,** 1109–1116
25. Terczyńska-Dyla, E., Bibert, S., Duong, F. H., Krol, I., Jørgensen, S., Collinet, E., Kutalik, Z., Aubert, V., Cerny, A., Kaiser, L., Malinverni, R., Mangia, A., Moradpour, D., Müllhaupt, B., Negro, F., *et al.* (2014) Reduced IFNlambda4 activity is associated with improved HCV clearance and reduced expression of interferon-stimulated genes. *Nat. Commun.* **5,** 5699

Negative regulation of type III interferon signaling

26. Heim, M. H. (2013) Innate immunity and HCV. *J. Hepatol.* **58,** 564–574
27. Sommereyns, C., Paul, S., Staeheli, P., and Michiels, T. (2008) IFN-lambda (IFN-λ) is expressed in a tissue-dependent fashion and primarily acts on epithelial cells *in vivo*. *PLoS Pathog.* **4,** e1000017
28. Duong, F. H., Trincucci, G., Boldanova, T., Calabrese, D., Campana, B., Krol, I., Durand, S. C., Heydmann, L., Zeisel, M. B., Baumert, T. F., and Heim, M. H. (2014) IFN-λ receptor 1 expression is induced in chronic hepatitis C and correlates with the IFN-λ3 genotype and with nonresponsiveness to IFN-α therapies. *J. Exp. Med.* **211,** 857–868
29. Alexander, W. S., Starr, R., Fenner, J. E., Scott, C. L., Handman, E., Sprigg, N. S., Corbin, J. E., Cornish, A. L., Darwiche, R., Owczarek, C. M., Kay, T. W., Nicola, N. A., Hertzog, P. J., Metcalf, D., and Hilton, D. J. (1999) SOCS1 is a critical inhibitor of interferon gamma signaling and prevents the potentially fatal neonatal actions of this cytokine. *Cell* **98,** 597–608
30. Marié, I., Durbin, J. E., and Levy, D. E. (1998) Differential viral induction of distinct interferon-α genes by positive feedback through interferon regulatory factor-7. *EMBO J.* **17,** 6660–6669
31. Lee-Kirsch, M. A. (2017) The type I Interferonopathies. *Annu. Rev. Med.* **68,** 297–315
32. Meuwissen, M. E., Schot, R., Buta, S., Oudesluijs, G., Tinschert, S., Speer, S. D., Li, Z., van Unen, L., Heijsman, D., Goldmann, T., Lequin, M. H., Kros, J. M., Stam, W., Hermann, M., Willemsen, R., *et al.* (2016) Human USP18 deficiency underlies type 1 interferonopathy leading to severe pseudo-TORCH syndrome. *J. Exp. Med.* **213,** 1163–1174
33. Wei, H., Wang, S., Chen, Q., Chen, Y., Chi, X., Zhang, L., Huang, S., Gao, G. F., and Chen, J. L. (2014) Suppression of interferon λ signaling by SOCS-1 results in their excessive production during influenza virus infection. *PLoS Pathog.* **10,** e1003845
34. Starr, R., Metcalf, D., Elefanty, A. G., Brysha, M., Willson, T. A., Nicola, N. A., Hilton, D. J., and Alexander, W. S. (1998) Liver degeneration and lymphoid deficiencies in mice lacking suppressor of cytokine signaling-1. *Proc. Natl. Acad. Sci. U.S.A.* **95,** 14395–14399
35. Dalton, D. K., Pitts-Meek, S., Keshav, S., Figari, I. S., Bradley, A., and Stewart, T. A. (1993) Multiple defects of immune cell function in mice with disrupted interferon-γ genes. *Science* **259,** 1739–1742
36. Kim, K. I., Yan, M., Malakhova, O., Luo, J.-K., Shen, M.-F., Zou, W., de la Torre, J. C., and Zhang, D.-E. (2006) Ube1L and protein ISGylation are not essential for α/β interferon signaling. *Mol. Cell. Biol.* **26,** 472–479
37. Ritchie, K. J., Malakhov, M. P., Hetherington, C. J., Zhou, L., Little, M.-T., Malakhova, O. A., Sipe, J. C., Orkin, S. H., and Zhang, D.-E. (2002) Dysregulation of protein modification by ISG15 results in brain cell injury. *Genes Dev.* **16,** 2207–2212
38. Duong, F. H., Filipowicz, M., Tripodi, M., La Monica, N., and Heim, M. H. (2004) Hepatitis C virus inhibits interferon signaling through up-regulation of protein phosphatase 2A. *Gastroenterology* **126,** 263–277
39. Koutsoudakis, G., Perez-del-Pulgar, S., Coto-Llerena, M., Gonzalez, P., Dragun, J., Mensa, L., Crespo, G., Navasa, M., and Forns, X. (2011) Cell culture replication of a genotype 1b hepatitis C virus isolate cloned from a patient who underwent liver transplantation. *PLoS ONE* **6,** e23587
40. van den Hoff, M. J., Christoffels, V. M., Labruyère, W. T., Moorman, A. F., and Lamers, W. H. (1995) Electrotransfection with "intracellular" buffer. *Methods Mol. Biol.* **48,** 185–197

Figure S1. Validation of SOCS1-, SOCS3- and USP18 knockout clones by sequencing and immunoblotting.
(A) CRISPR/Cas9 technology was used to generate SOCS1, SOCS3 and USP18 knockout cells. Changes on the gene of both alleles (1a and 1b) compared to wild type (WT) are highlighted in red and blue respectively. (B) Huh7 LR cells, SOCS1, SOCS3 and USP18 knockout clones were stimulated with 1000IU/ml IFN-α or 100ng/ml IFN-γ and lysed at the indicated time points. Specific antibodies for SOCS1, SOCS3 and USP18 were used to identify knockout clones. Actin was used as a loading control.

Figure S2. SOCS1 is a modulator of IFN-λ3-mediated STATs activation *in vitro.*
Control, SOCS1 -/-, SOCS3 -/- and USP18 -/- cells were transfected with pGL3-ISRE-Mx1-Luc and pGL4-CMV-Renilla-Luc plasmids and 20h later stimulated with 200ng/ml IFN-λ3 or 1000IU/ml IFN-β for 4h, 8h and 24h or left untreated. The Firefly Luciferase values were normalized to Renilla Luciferase and the results (mean ± SD; n=2) are expressed as Firefly/Renilla Ratio. Unpaired t-test, * $p<0.05$, ** $p<0.01$, *** $p<0.001$.

Figure S3. SOCS1 is a modulator of IFN-λ-induced ISGs expression *in vitro*.
Control, SOCS1 -/-, SOCS3 -/- and USP18 -/- cells were stimulated with 1000IU/ml IFN-α or 100ng/ml IFN-λ1 for 4h, 8h and 24h or left untreated and the expression levels of *SOCS1, SOCS3* and *USP18* were analysed by quantitative PCR. The results (mean ± SD; n=2) are shown as relative expression to *GAPDH.* Unpaired t-test, * $p<0.05$, ** $p<0.01$, *** $p<0.001$.

Figure S4. Depletion of *Socs1* increased IFN-λ whereas depletion of *Usp18* increased IFN-α induced ISGs expression *in vivo*.
(A) Control and *Socs1-/-* mice were subcutaneously injected with PBS, 1000U/g mouse IFN-α or 50ng/g mouse IFN-λ2. The liver, the lung and the gut were collected 4h and 8h post injection and total RNA was prepared. The expression of *Gbp5 and Ifi27* was measured by quantitative PCR. The results (mean ± SD) are shown as relative expression to *Rpl19*. 3-4 animals were used per time point and condition. Unpaired t-test with Welch's correction, * $p<0.05$, ** $p<0.01$, *** $p<0.001$. (B) Control and *Usp18 -/-* mice were subcutaneously injected with PBS, 1000U/g mouse IFN-α or 50ng/g mouse IFN-λ2. The liver, the lung and the gut were collected 4h and 8h post injection and total RNA was prepared. The expression of *Gbp5 and Ifi27* was measured by quantitative PCR. The results (mean ± SD) are shown as relative expression to *Rpl19*. 3-5 animals were used per time point and condition. Unpaired t-test with Welch's correction, * $p<0.05$, ** $p<0.01$, *** $p<0.001$.

Figure S1

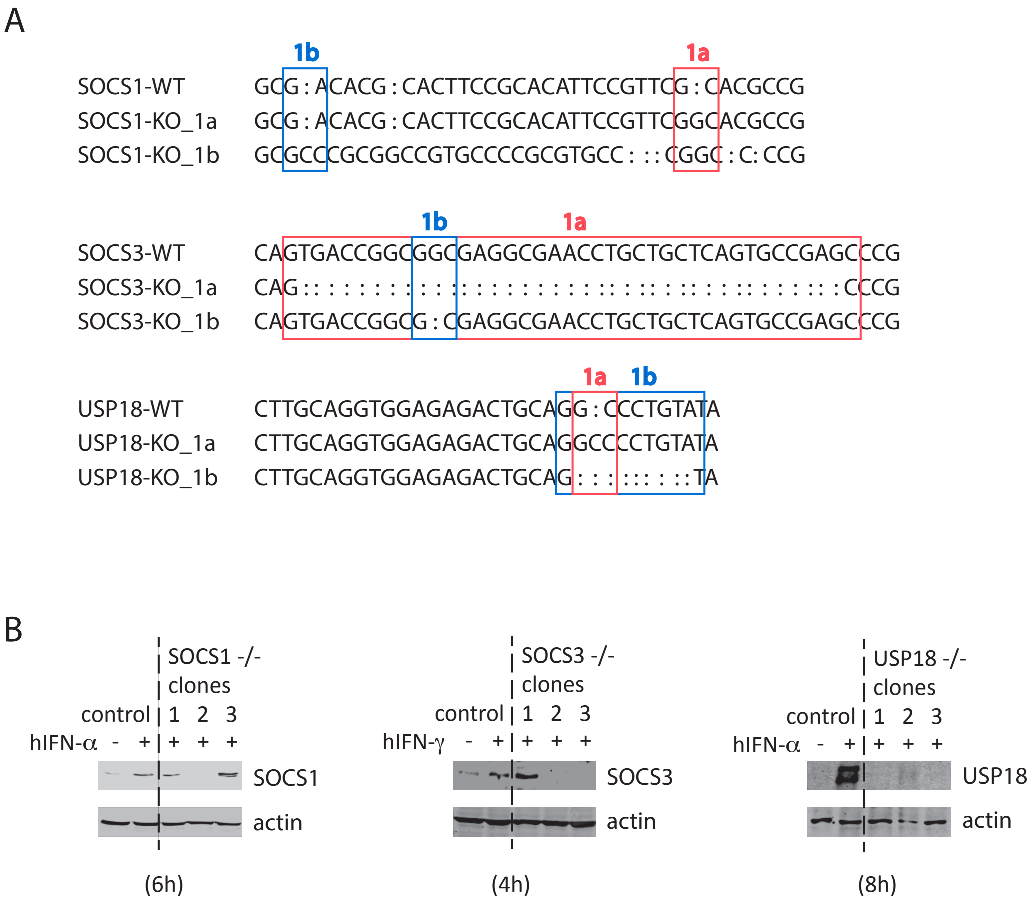
A
1b
1a
SOCS1-WT
SOCS1-KO_1a
SOCS1-KO_1b
SOCS3-WT
SOCS3-KO_1a
SOCS3-KO_1b
USP18-WT
USP18-KO_1a
USP18-KO_1b
B
SOCS1 -/- clones
control 1 2 3
hIFN-α - + + + +
SOCS1
actin
(6h)
SOCS3 -/- clones
control 1 2 3
hIFN-γ - + + + +
SOCS3
actin
(4h)
USP18 -/- clones
control 1 2 3
hIFN-α - + + + +
USP18
actin
(8h)

Figure S2

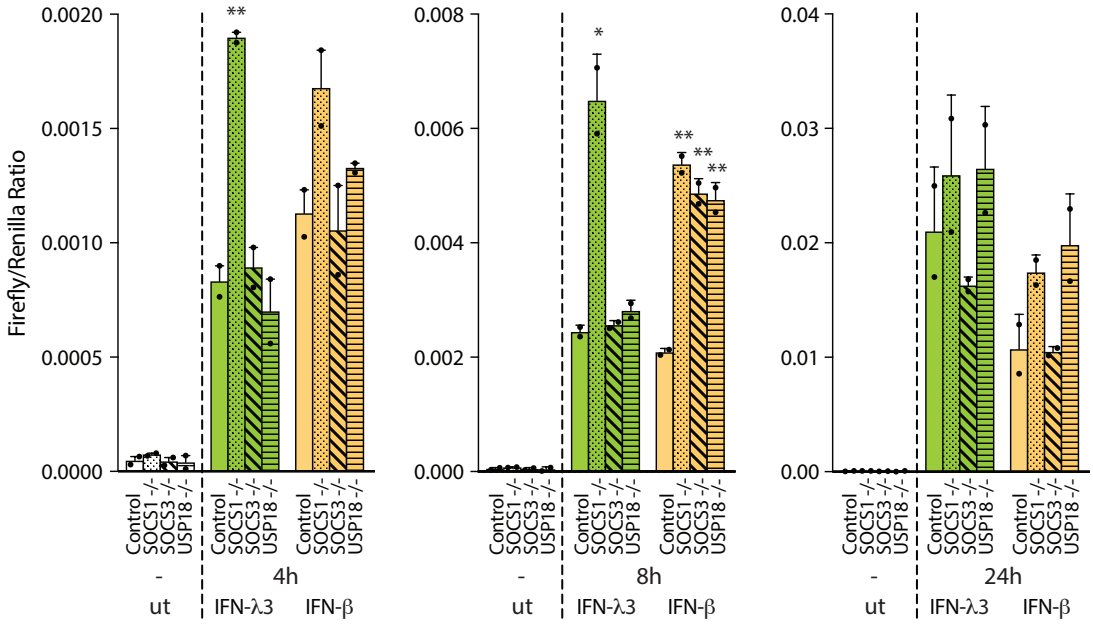
Firefly/Renilla Ratio
0.0020
0.0015
0.0010
0.0005
0.0000
0.008
0.006
0.004
0.002
0.000
0.04
0.03
0.02
0.01
0.00
**
*
**
**
**
Control
SOCS1 -/-
SOCS3 -/-
USP18 -/-
-
ut
4h
8h
24h
IFN-λ3
IFN-β

Figure S3

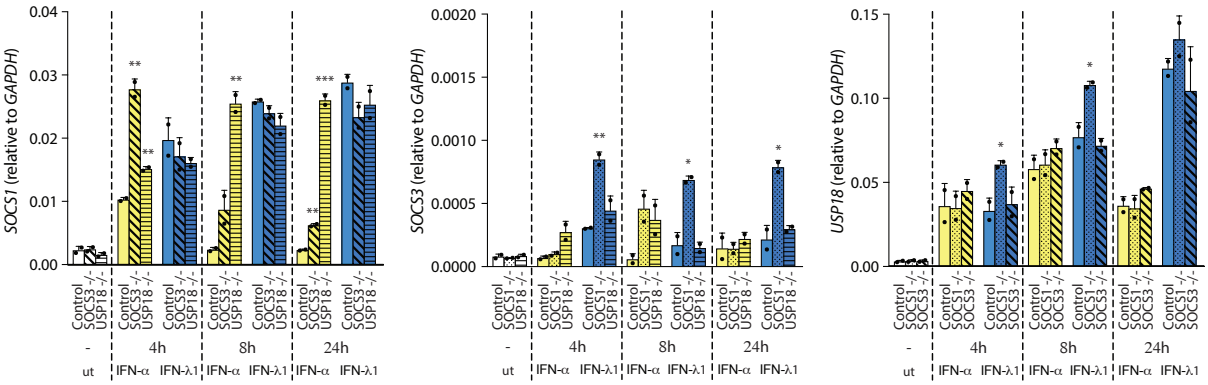
SOCS1 (relative to GAPDH)
SOCS3 (relative to GAPDH)
USP18 (relative to GAPDH)
Control
SOCS1 -/-
SOCS3 -/-
USP18 -/-
-
4h
8h
24h
ut
IFN-α
IFN-λ1

Figure S4

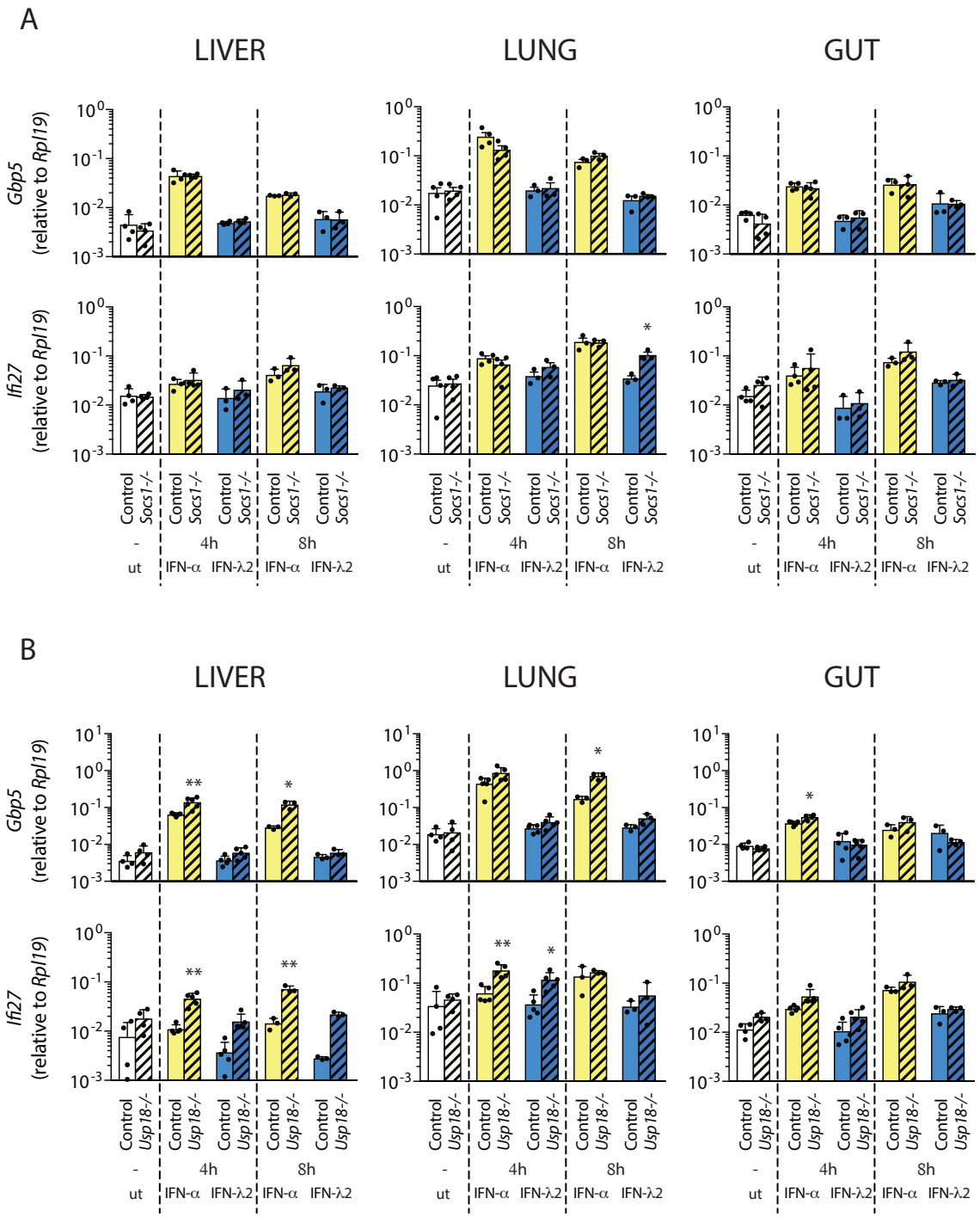
A
LIVER
LUNG
GUT
Gbp5 (relative to Rpl19)
Ifi27 (relative to Rpl19)
Control
Socs1-/-
-
4h
8h
ut
IFN-α
IFN-λ2
B
LIVER
LUNG
GUT
Gbp5 (relative to Rpl19)
Ifi27 (relative to Rpl19)
Control
Usp18-/-
-
4h
8h
ut
IFN-α
IFN-λ2

Supplementary table 1. CHC patients' characteristics

Patient's #	Gender	Age	HCV genotype	viral load	L4 genotype	IFNLR1 copies
1	m	58	1b	57'791	dG/dG	2750
2	m	60	1b	4'326'723	TT/dG	1181
3	m	45	1a	7'585'775	TT/dG	18699
4	m	43	3	1'445'439	TT/dG	1219
5	m	59	4	26'700	TT/dG	7787
6	f	48	1a	n.d.	TT/dG	7797
7	m	47	3	474'333	dG/dG	14082
8	m	52	3a	2'884'032	TT/dG	33324
9	m	24	1	64'646	dG/dG	9595
10	m	57	3	3'455'931	TT/dG	361
11	f	53	4	795'769	dG/dG	1084
12	f	47	1a	3'981'071	TT/TT	10
13	f	43	1	1'698'243	TT/TT	332
14	f	47	1	1'031'852	dG/dG	66
15	m	45	3	742'088	TT/TT	37
16	f	45	3	4'677'351	TT/dG	66

n.d: not determined

Supplementary table 2. Primer sequences for quantitative RT-PCR and PCR

Gene	Forward primer	Reverse primer	
SOCS3	ATGGTCACCCACAGCAAGTT	TCACTGCGCTCCAGTAGAAG	qRT-PCR
GAPDH	GCTCCTCCTGTTCGACAGTCA	ACCTTCCCCATGGTGTCTGA	
SOCS1	CCCCTTCTGTAGGATGGTAGCA	TGCTGTGGAGACTGCATTGTC	
USP18	CTCAGTCCCGACGTGGAACT	ATCTCTCAAGCGCCATGCA	
IFNLR1	CAGTGTCCCGAAATACAGCA	TGTGTCCAGAAAAGTCCAGGGC	
RSAD2	CTTTGTGCTGCCCCTTGAG	TCCATACCAGCTTCCTTAAGCAA	
IFI27	GGCAGCCTTGTGGCTACTCT	CCCAGGATGAACTTGGTCAATC	
GBP5	CGCAAAGGTTGGCGGCGATT	AGCTGTGCAGCCTGTTCCTGC	
Rpl19	ATCCGCAAGCCTGTGACTGT	TCGGGCCAGGGTGTTTTT	
Stat1	CGGCGCAGAGAGATTTGC	AGCTGAAACGACTGGCTCTCA	
Oas1	CACCCAGTGAGGGTCTCCAA	TTGAGTGTGGTGCCTTT	
Ifi27	TCAGCAGGGGTCCTTGGACTCTC	CATCTCCTGGGTAGTCTGTACAGGC	
Socs1	ATTACCGGCGCATCACGCGG	GATGCTCGTGGGGCCCGAAG	
Gbp5	ATTGGAGAGCCTACTAAGTGCAAA	CTCCTGCGCCACTTCTTGTT	
Usp18	CTAGAGACCTCTGCAGTGCCTGG	CCGAGGCACTGTTATCCTCTTCAAT	
Rsad2	TCTGGAGGAGAACCCTTCCT	TACTCCCCATAGTCCTTGAACC	
SOCS1	CGACAATGCAGTCTCCACA	TAGGAGGTGCGAGTTCAGGT	PCR
SOCS3	CCAAGGACGGAGACTTCGAT	CTGGATGCGCAGGTTCTTG	
UPS18	ACCTGGCTTATGGTGGTGTT	ATAATTGGGGAGGGCAAGGT	
IFN-λ4	ACTGTGTGTGCTGTGCCTTC	GGACGAGAGGGCGTTAGAG	

Supplementary table 3. SgRNA sequences for CRISPR/Cas9

Gene	Forward primer	Reverse primer
SOCS1	CACCGGCCGGTAATCGGCGTGCGAA	AAACTTCGCACGCCGATTACCGGCC
SOCS3	CACCGCAGCAGGTTCGCCTCGCCGC	AAACGCGGCGAGGCGAACCTGCTGC
USP18	CACCGCCTTCACCCGGATCGTATAC	AAACGTATACGATCCGGGTGAAGGC

2 Research article II

Hepatocellular carcinoma xenografts established from needle biopsies preserve the characteristics of the originating tumors

T. Blumer, H. Montazeri, M. S. Matter, X. Wang, I. Fofana, D. Calabrese, M. Coto-Llerena, T. Boldanova, S. Nuciforo, V. Kancherla, L. Tornillo, S. Piscuoglio, S. Wieland, L. M. Terracciano, C. K. Y. Ng, M.H. Heim

Manuscript submitted , *Journal of Hepatology*.

Statement of contribution

I established the PDX models in our laboratory and performed the subcutaneous transplantations. Furthermore, I was responsible for maintenance and analysis of the newly generated PDX models. Moreover, I was involved in data analysis and interpretation of the results. Finally I wrote the manuscript together with I. Fofana, S. Wieland, CKY. Ng and MH. Heim.

*Manuscript
Click here to view linked References

Hepatocellular carcinoma xenografts established from needle biopsies preserve the characteristics of the originating tumors.

Tanja Blumer[1], Hesam Montazeri[2], Matthias S. Matter[2], Xueya Wang[1], Isabel Fofana[1], Diego Calabrese[1], Mairene Coto-Llerena[1], Tujana Boldanova[1,3], Sandro Nuciforo[1], Venkatesh Kancherla[2], Luigi Tornillo[2], Salvatore Piscuoglio[2], Stefan Wieland[1], Luigi M. Terracciano[2], Charlotte K. Y. Ng[1,2], Markus H. Heim[1,3]

[1]Department of Biomedicine, University Hospital Basel, University of Basel, Basel CH-4031, Switzerland

[2]Institute of Pathology, University Hospital of Basel, University of Basel, Basel CH-4031, Switzerland

[3]Division of Gastroenterology and Hepatology, University Hospital Basel, University of Basel, Basel CH-4031, Switzerland

Corresponding author:

Prof. Dr. med. Markus H. Heim, Division of Gastroenterology and Hepatology, University Hospital Basel, University of Basel, Basel, Switzerland. Phone:+41612652525, E-mail: markus.heim@unibas.ch

Keywords: Hepatocellular carcinoma, Patient-derived xenograft model, biopsy, RNA sequencing, mice

Electronic word count: 5991

Number of Figures and Tables: 5 Figures, 1 Table

Conflict of interest

The authors declare no conflict of interests.

Financial support

This work was supported by European Research Council Synergy grant 609883 (MERiC), by SystemsX.ch grant MERiC and by grants from the Swiss National Science Foundation (310030B_14708 and 310030_166202) to MHH. Additional financial support was provided by the Swiss Cancer League (Oncosuisse) [KLS-3639-02-2015 to L.M.T. and KFS-3995-08-2016 to S.P.]; the Swiss National Science Foundation [Ambizione PZ00P3_168165 to S.P.]

Authors' contributions

M.H.H. and T.B. conceived the study and designed experiments; M.H.H. and Tu.B. recruited patients, performed biopsies, and collected and curated clinical annotation data; T.B., X.W., M.C. and D.C. performed the experiments; M.S.M., L.T. and L.M.T. performed the histological analysis; H.M., S.P. and C.K.Y.N. processed, computed and analysed the genomics and transcriptomics data; all authors were involved in data analysis and interpretation of the results; M.H.H. coordinated the study; T.B., I.F., S.W., S.P., C.K.Y.N. and M.H.H. wrote the manuscript.

Abstract

Background & Aims: Hepatocellular carcinoma (HCC) is the second leading cause of cancer-related deaths worldwide with limited treatment options for patients with advanced stage disease. A major obstacle in preclinical drug development is the lack of an *in vivo* model that accurately reflects the broad spectrum of human HCC. Patient derived xenograft (PDX) mouse models could overcome the limitations of cancer cell lines. PDX models have been established from surgically resected HCCs. We aimed to establish and characterize PDX models from human HCC biopsies in order to expand the spectrum of HCC xenografts to advanced HCCs not amenable to surgery.

Methods: Fifty-four human HCC needle biopsies were transplanted subcutaneously into immunodeficient NOD-SCID gamma-c (NSG) mice. Tumor growth rates, histopathological characteristics, RNA sequencing and whole exome sequencing were used to characterize the newly established mouse models and to compare them to the originating HCCs.

Results: Eleven HCCs engrafted in NSG mice. They were derived from patients with various underlying liver diseases and tumor stages. All successfully transplanted HCCs were Edmondson grade III or IV. HCC PDX tumors retained the histopathological and transcriptomic characteristics of the original HCC biopsies over at least generations of re-transplantation, including Edmondson grade, expression of tumor markers, tumor gene signature and tumor-associated mutations.

Conclusion: PDX mouse models can be established from undifferentiated HCCs with an overall success rate of about 33%. The transplanted tumors represent the entire spectrum of the molecular landscape of HCCs and

preserve the characteristics of the originating tumors. HCC PDX models are a promising tool for preclinical personalized drug development.

Abstract words: 257

Lay summary

Needle biopsies of primary liver cancer can be transplanted and grown in immunodeficient mice. They maintain the original tumor characteristics and are promising new tools for pre-clinical drug screening.

Graphical abstract

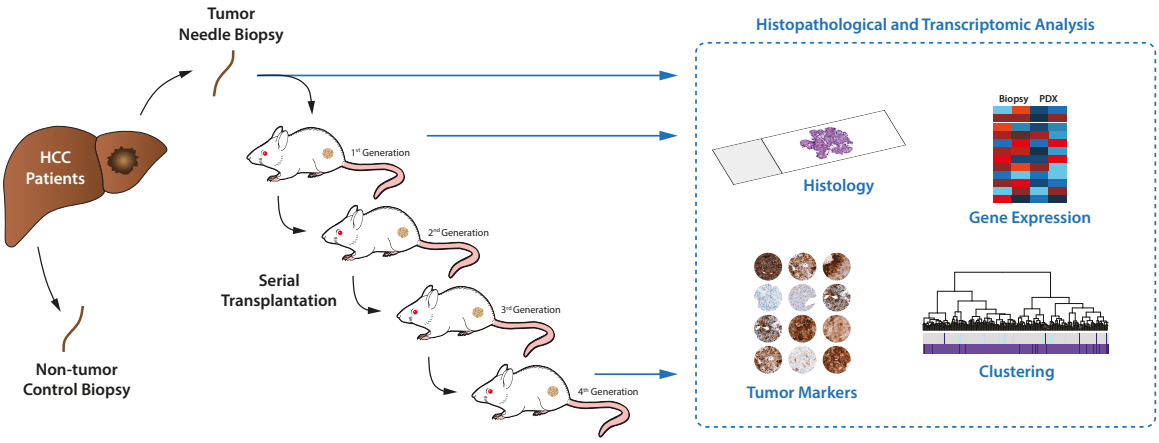

Introduction

HCC is the most common primary liver cancer and is the second most frequent cause of cancer-related mortality worldwide[1]. Current treatment options are limited with less than 30% of HCC patients in Europe qualifying for curative treatments[2]. The multikinase inhibitor sorafenib is the only first-line treatment for advanced HCC[3]. Sorafenib moderately improves survival of patients with advanced HCC but has adverse effects that preclude its use in patients with advanced cirrhosis[3, 4]. Novel therapies are urgently needed to improve treatment options for patients with advanced HCCs.

Current *in vitro* cell culture models of HCC are based on conventional hepatoma cell lines that fail to recapitulate key features of tumor tissues such as three-dimensional tumor architecture, cellular heterogeneity and cell-cell interactions. Chemically induced HCC mouse models or genetically engineered mice better reflect *in vivo* tumor biology[5]. However, they do not recapitulate the different genetic alterations present in HCCs of different patients. Patient-derived xenograft (PDX) models have the potential to overcome these limitations and are considered valuable tools in the field of anti-cancer drug development and prediction of response to cancer therapy[6, 7]. So far, all published HCC PDX models have been generated from surgically resected HCCs[8-13]. Because surgical resections are predominantly performed in patients with early stage tumors (typically BCLC stages 0/A), PDXs derived from resected tumors are heavily biased against advanced stage HCCs. Furthermore, from the published HCC PDX reports it is not clear

how much of the original tumor characteristics are preserved in the transplanted tumors. It is also not clear if successful engraftment was restricted to a subgroup of HCCs with distinct molecular characteristics. These questions need to be resolved before further developing PDX models for preclinical drug development.

In the present study we report the results of a comprehensive comparative analysis of 11 newly generated PDX models and the originating human HCCs.

Material and Methods

Human HCC Tissues and Biopsy Procedure

Fifty-four human HCC needle biopsies were obtained at the University Hospital Basel, Switzerland from 44 treatment naïve patients undergoing diagnostic liver biopsy (Table S1). A detailed description of the biopsy procedure is provided in Supplementary Material and Methods. Written informed consent was obtained from all patients. The study was approved by the Ethics committee of the north-western part of Switzerland (Protocol Number EKNZ 2014-099). One biopsy cylinder was fixed in formalin and embedded in paraffin for diagnosis and staging. Additional cylinders were immediately snap-frozen in liquid nitrogen for later use in DNA/RNA extraction or embedded in O.C.T. (Tissue-Tek) and frozen using standard procedures. For PDX model generation, biopsy pieces were placed in PBS. An additional biopsy from non-tumor liver parenchyma was also obtained from all patients.

Mice and Xenotransplantation

Needle biopsies of HCCs were transplanted subcutaneously into 6-10 weeks old NOD-SCID gamma-c (NSG) mice (Supplementary Methods). Experiments were conducted with the approval of the Ethics committee of the north-western part of Switzerland (Protocol Number EKNZ 2014-099) and the Animal Care Committee of the Canton Basel-Stadt, Switzerland.

Tumor growth rate was assessed by weekly measurement using a caliper. S.c. transplantations and injections that did not yield any measurable tumor in the

mice within eight months after intervention were considered as failed engraftments. The animals were euthanized by CO_2 narcosis as soon as the tumors reached a size of 1000-1500 mm^3. Parts of the collected tumors were immediately frozen in liquid nitrogen and kept at −70°C until further processing; embedded in O.C.T. (Tissue-Tek) and frozen using standard procedures; fixed in formalin and embedded in paraffin using standard procedures; or cryopreserved for later usage. Tumor pieces of 2x2 mm were subsequently s.c. transplanted into new mice in order to expand the tumor material for further experiments.

Lag phase and doubling time of patient-derived xenograft tumors

The PDX tumor lag phase describes the time from s.c. transplantation or injection of tumor sample until tumor growth onset (measurable tumor size; 2x2mm). Tumor doubling times were calculated based on the slope of the linear section of the log10 transformed growth curves of each tumor derived from a given biopsy. All results are shown as mean +/- SD (Figure 1B).

Histology and Immunohistochemistry

Paraffin-embedded tumor biopsies and PDX tumors were processed for Hematoxylin & Eosin or immunohistochemical staining using standard procedures (Supplementary Methods). Histopathology evaluation was carried out blindly by two board-certified hepatopathologists (L.T. and M.S.M.) at the Institute of Pathology of the University Hospital Basel. Disease stage was classified according to the BCLC staging system[14]. Histopathological grading was assigned according to the Edmondson grading system[15].

Immunofluorescence

O.C.T. (Tissue-Tek) embedded, frozen PDX tumors, mouse liver and human liver biopsy were used for vessel assessment (Supplementary Methods).

Whole exome sequencing and analysis

Paired-end 101bp sequencing was performed for the DNA extracted from 14 engrafted HCC biopsies (derived from 12 patients) and the 12 matched non-tumoral biopsies (Table S2), using the SureSelectXT Clinical Research Exome (Agilent) platform and sequenced on the Illumina HiSeq 2500 according to the manufacturers' guidelines. HCC biopsies and the matched non-tumor biopsies were sequenced to a median depth of 93x (range 61x-159x) and 51x (range 42x-75x), respectively. Whole exome data were analyzed as previously described[16], with some modifications (Supplementary Methods).

RNA sequencing and analysis

RNA extracted from 45 HCC biopsies derived from 37 patients (Table S2), 10 HCC PDX tumors and 3 lymphoma PDX tumors from 12 models (1st generation tumors) and 8 HCC PDX tumors from two models (4th generation tumors) were sequenced. Nine HCC biopsies were excluded because of low tumor cell content. Tumors from PDX models D096 and D135 were not sequenced because they were generated recently. SR126 RNA sequencing was performed using the TruSeq Stranded Total RNA Library Prep Kit with Ribo-Zero Gold (Illumina) and sequenced on the Illumina HiSeq 2500 according to the manufacturer's guidelines (Supplementary Methods).

Sequence reads from the HCC biopsy samples were aligned by STAR[17] using the two-pass approach simultaneously to the human reference genome GRCh37, HBV strain ayw genome (NC 003977.2), HCV genotype 1 genome (NC 004102.1). Sequence reads from PDX tumors were aligned as above to human, HBV, HCV and mouse genomes (GRCm38). Median numbers of reads aligning to the human genome were 71 million (range 57-106 million) for the HCC biopsies and 78 million (range 64-101 million) for the PDX tumors. Transcript quantification for human genes was performed using RSEM[18]. Differential expression analysis was performed using the edgeR R package[19]. Pathway enrichment analysis was performed using hypergeometric test for the hallmark gene sets in the Molecular Signatures Database[20]. Cluster analysis was performed using hierarchical clustering. Batch effects associated with the process of PDX establishment were removed using the edgeR R package[19], which fits a linear model to the data and removes the component associated with xenografting. The expression of somatic mutations in RNA sequencing data was determined by GATK Unified Genotyper[21], given the somatic mutations identified by whole exome sequencing. For statistical comparisons, only missense and synonymous mutations were considered. Truncating, insertions and deletions and splice site mutations were excluded, as these mutations are likely to affect transcript stability. Transcriptomic classification was performed according to Hoshida et al.[22]. See Supplementary Methods for further details.

TCGA data analysis

For unsupervised cluster analysis of HCC biopsies and HCCs from TCGA, we merged our RNA sequencing dataset with the TCGA HCC dataset RNA sequencing data ("V2_MapSpliceRSEM") retrieved from the Genomics Data Commons Data Portal[23] (Supplementary Methods). Clustering was performed as described above. Histological grading was performed according to the Edmondson grading system[15] as previously described[24] (Supplementary Methods).

Statistical analysis

Statistical analyses of the clinicopathological variables were performed in R v3.3.1. Comparisons of ordinal variables (BCLC, AFP, Edmondson grade, number of tumors, diameter of largest tumor, Hoshida subclass) were performed using Mann-Whitney U tests. Comparisons of categorical variables (all others) were performed using Fisher's exact tests. All statistical tests were two-sided and $P<0.05$ was considered statistically significant.

Data Availability

Sequencing data are available at the NCBI Sequence Read Archive under the accession SRP111479 (experiments SRX3633744- SRX3633776).

Results

Fresh human hepatocellular carcinoma needle biopsies generate xenograft tumors in immunocompromised mice.

PDX models were generated from human HCC needle biopsies as described in Material and Methods. Fifty-four needle biopsies from 44 HCC patients were included in this study (Tables S1 and S2). The patient cohort covered all major HCC risk factors and the entire spectrum of Edmondson grades (I-IV)[15] (Table S1). Additionally, in contrast to the use of resected HCC tissue, which is limited to early stage disease[9, 12, 13], our cohort comprises all four classes of the Barcelona Clinic Liver Cancer (BCLC) staging system[14]. While we typically obtained a single biopsy sample per patient, there were nine patients that were simultaneously biopsied at two locations because of the presence of multiple lesions in the liver (indicated as -A/-B, Table S1). One patient was biopsied at two different locations within the same large tumor nodule (36-I and 36-II, Table S1). In total, we successfully established eleven HCC-derived PDX models from ten patients (Table S1).

The time from subcutaneous introduction of the HCC biopsy material to onset of tumor growth ranged from 4 to 28 weeks (Figures 1A and B). Time to onset of PDX tumor growth of Edmondson grade IV derived biopsies appeared to be somewhat shorter than that of grade III biopsies, but the difference did not reach statistical significance (Figure 1; $p = 0.072$; Mann-Whitney U test). Interestingly, PDX C078b derived from s.c. injection of a biopsy cell suspension showed the latest tumor growth onset (Figures 1A and B), suggesting that the presence of an intact tumor architecture may accelerate

tumor engraftment and growth onset. Finally, the onset of tumor growth varied between mice that were transplanted with tumor tissue derived from the same biopsy cylinder (Figure S1A), suggesting that, among other factors, the tumor cell content may also influence the lag time to tumor growth. Indeed, the lag time to tumor growth was very similar when a homogenous cell suspension, generated from one biopsy cylinder, was s.c. injected into two mice (Figure S1B).

Taken together, these results demonstrate that human HCC tissue derived from fresh needle biopsies can generate xenografts upon s.c. transplantation and injection.

Growth kinetics of hepatocellular carcinoma xenograft tumors remain stable over subsequent passages.

Having successfully established eleven PDX models, we next investigated the re-transplantation capacity of the initial xenografts over at least four generations. Re-transplanted tumors showed a shortened lag phase until onset of tumor growth compared to the xenograft tumor derived from the biopsy tissue, and remained stable in subsequent PDX generations (Figures 1B and C). However, while the doubling time of tumor growth differed between PDX models, it did not change between the 1st and all subsequent PDX generations (Figures 1B and C). These data indicate that once established, PDX tumors can be expanded for several generations with stable growth kinetics over time.

PDX tumors recapitulate the histopathological features of the original human HCC tumor.

We next investigated whether the individual PDX tumors retained the histologic characteristics of the original human tumors. HCC PDX tumors maintained the differentiation grade[15], the growth pattern and the cytological subtype[25, 26] of the originating human HCC biopsies over at least four generations (Table 1, Figures 2 and S2A-J). As an example, Figure 2 shows that the PDX tumors originating from the tumor biopsy C942 displayed a solid-trabecular growth pattern with an Edmondson grade III as observed in the original tumor (Figure 2 and Table 1). Of note, only in one case (PDX model of C284b) we observed the loss of the trabecular aspect of the growth pattern that was present in the original biopsy, however the solid growth pattern and differentiation grade were maintained over subsequent passages from mouse to mouse (Table 1, Figure S2B).

Immunohistochemical analysis demonstrated that the expression and distribution of the tumoral marker alpha-fetoprotein[27] were maintained from the original tumor biopsies to the HCC xenografts over several passages (Figures 2 and S2A-J). Likewise, the expression pattern of the three most widely used markers for HCC diagnosis[28, 29], glypican 3, heat shock protein 70 and glutamine-synthetase confirmed the histological stability of the xenograft tumors compared to the original HCC biopsy (Figures 2 and S2A-J).

Taken together, these results show that the HCC PDX tumors retain the histological features of the original human tumors over several passages.

PDX tumors recapitulate the expression profile and expressed somatic mutations of the original human HCC tumors.

To investigate the transcriptomic changes induced by PDX establishment and whether the PDX models recapitulate the gene expression pattern of the tumors from which they originated, we performed RNA sequencing of 9 PDX models and the originating HCC biopsies. Differential expression analysis revealed that 1,613 were up-regulated and 1,845 genes were down-regulated in the PDX tumors compared to their matched biopsies (Table S3). The down-regulated genes were enriched in pathways of inflammatory response and angiogenesis (Figure 3A and Table S4), suggesting the loss of cells of the human immune system and vasculature. Indeed, the xenograft tumors were positive for mouse-specific CD31, suggesting that the human vascular system in the HCC tumors was replaced by mouse vessels in the xenografts (Figure S3). In contrast, up-regulated genes were associated with pathways related to cell cycle such as Myc and E2F target genes and mTORC1 signaling (Figure 3A and Table S4), likely reflecting the enrichment of tumor cells in the PDX tumors compared to the biopsies. Importantly, unsupervised clustering after correcting for the systematic effects introduced by xenografting, in effect by fitting a linear model to the data and removing the effects, demonstrated that all PDX tumors stably clustered with their corresponding HCC tumors (Figure 3B, stability as assessed by bootstrap resampling) and that the expression profile was maintained over at least four generations (Figure S4A).

To assess whether the PDX tumors retained the expression of the somatic mutations found in their originating tumors, we identified the repertoire of somatic mutations by performing whole exome sequencing (WES) of the original tumor biopsies and their non-tumoral counterparts. We then assessed the expression of these mutations by RNA sequencing in the HCC biopsies and the PDX tumors, focusing on missense and synonymous point mutations, as truncating mutations are likely to affect transcript stability. Based on WES, we identified a median of 120 (range 61-174) somatic missense and synonymous point mutations, of which 46% (range 26%-69%) were expressed in the corresponding HCC biopsies (Table S5). Of the expressed mutations in the HCC biopsies, a median of 80% (range 68%-93%) was also expressed in the respective PDX tumors (Figure 3C). Importantly, all missense mutations in HCC cancer genes, such as *TP53*, *CTNNB1*, *ALB* and *KEAP1* were expressed in the corresponding PDX tumors and their expression was maintained over at least 4 generations (Figures 3C and S4B). These results indicate that the HCC PDX tumors maintained the expression profile and the expression of somatic mutations observed in their originating tumors.

Engrafted HCC biopsies are broadly representative of the spectrum of poorly differentiated HCCs

The success rate of engraftment was 20% (10 out of 50 biopsies) and 25% (1 out of 4 biopsies) of all transplanted and injected biopsy tissues, respectively (Table S1). This success rate is in accordance with published data on s.c. PDX models derived from resected specimens[9, 11-13]. The use of HCC needle biopsies that encompasses all clinical stages offered the unique opportunity to

investigate the determinants of successful engraftment capacity into mice. When we compared the clinicopathological characteristics of the engrafted and non-engrafted biopsies we observed a clear correlation with histopathological grading; all HCC PDX tumors were derived from poorly differentiated tumors (Edmondson grades III/IV, Table S1 and Figure 4A). Indeed, differential expression analysis between engrafted and non-engrafted biopsies revealed 2,401 up-regulated and 1,440 down-regulated genes. The up-regulated genes were enriched for pathways associated with cell cycle progression, epithelial-to-mesenchymal transition, hypoxia and angiogenesis, while the down-regulated genes were enriched for liver metabolic functions (Table S6). Furthermore, molecular subtyping based on the Hoshida subclasses[22] revealed that all engrafted HCC biopsies were of subclasses S1 and S2 (Figure 4A), characterized by poor differentiation, high proliferation rate and poor survival compared to subclass S3. Besides Edmondson grading, no other available clinicopathological characteristics seemed to influence the engraftment success rate (Table S1 and Figure 4A). Indeed, when restricting the differential expression analysis to Edmondson grade III biopsies (the only histological grade that had variable successful engraftment rate), only two genes were differentially expressed (both FDR=0.04, data not shown), suggesting that, there was no systematic difference between engrafted and non-engrafted biopsies after accounting for histological grading.

To assess the distribution of our samples within a reference set from TCGA[23], we performed an unsupervised hierarchical clustering analysis of the gene expression, combining our HCC biopsy cohort with TCGA[23]. We observed that the eleven engrafted biopsies preferentially clustered together in

a subclass located at the left end of the clustering tree (Figure S5). Since all our PDX models originated from poorly differentiated HCCs, we repeated the unsupervised clustering analysis using only the subset of poorly differentiated HCCs from the TCGA. In this scenario, both the eleven engrafted samples and the non-engrafted samples broadly represented the spectrum of poorly differentiated HCCs (Figure 4B). These results demonstrate that poorly differentiated tumor cells engraft more efficiently in mice and that the HCC biopsies that engrafted are broadly representative of the diversity of poorly differentiated HCCs.

Transformation into human B-cell lymphoid neoplasms of patient-derived xenograft tumors

During histological analyses of the engrafted tumors, we observed that three PDX tumors histologically differed from the originating tumors. Specifically, they primarily contained a population of middle-sized and large lymphoid mononuclear cells with diffuse growth pattern and high mitotic index that were not present in the corresponding HCC biopsies (Figure 5A).

In fact, transcriptome-based unsupervised clustering showed that these PDX tumors did not cluster with their originating HCCs (Figure 5B) and did not express any of the mutations expressed in the corresponding biopsy (Figure 5C and Table S5). Compared to the biopsies and the HCC PDXs, these three PDX tumors overexpressed genes consistent with immune infiltration, interferon-alpha and gamma responses and the NF-kB pathway and reduced expression of genes involved in liver metabolism and liver cancer (Table S7). These results suggested the development of lymphomas in the xenografts as

has been reported in PDX studies of various cancers[30-33]. Indeed, these three PDX tumors stained positive for the human B-cell marker CD20 (Figure 5D), consistent with the presence of a B-cell lymphoma. Importantly, species-specific alignment demonstrated that CD20 mRNA expression was exclusively of human origin (Table S8). Of note, Chen et al. previously suggested that the reactivation of latent Epstein-Barr virus (EBV) of intratumoral passenger B lymphocytes led to the generation of lymphoid tumors in immunocompromised mice[30]. Consistent with this hypothesis, EBV transcripts were detected in all three of these PDX tumors, but were absent from the corresponding HCC and non-tumor biopsies, and were virtually absent from all the other PDX models (Table S8). Taken together, these results suggest that reactivation of latent EBV may lead to lymphomagenesis in some cases using our biopsy-derived xenograft system.

Discussion

During the last 10 years after the introduction of sorafenib as a first line therapy for advanced HCC, a number of additional drugs have all failed in phase 2 or phase 3 trials[34]. A major obstacle for the development of new therapies is the lack of suitable animal models, specifically animal models that reflect the heterogeneity of HCCs. PDX mice derived from human tumors offer a tool for developing anticancer therapies and personalized medicine for patients with cancer[7]. PDX models have also been established for HCCs[8-13]. However, these previously published HCC PDX mice were established from resected tumor specimens, and therefore predominantly from early stage HCCs. In the present study we expand the spectrum of HCC PDX models to advanced HCCs.

As in previously published reports[9, 11-13], we also had a limited overall success rate of about 20%. From 54 transplanted HCCs, 11 could be grown and re-transplanted as xenografts. The reasons for this low success rate remain to be fully elucidated. However, we observed that none of the well-differentiated (Edmondson grades I/II) HCCs could be engrafted in the mice. Of note, we stopped to monitor the mice for tumor growth 8 months after transplantation. Since low-grade tumors tend to grow slowly, we cannot exclude the possibility that they would have started growing beyond 8 months. However, we think that tumor cell intrinsic biological properties of undifferentiated HCCs such as growth factor independent proliferation or resistance to hypoxia are more likely reasons for the successful engraftment of undifferentiated HCCs. Another factor favoring engraftment might be an intact

tumor tissue architecture providing 3-dimensional oriented cell-cell contacts. We observed that compared to transplantations of small tumor pieces the injection of a cell suspension showed a delayed tumor growth onset. Interestingly, time to tumor growth onset was invariably shorter upon re-transplantations of all PDX tumors and then remained constant over several passages. It is possible that the presence of a mouse-derived vascular system in the PDX tumors facilitated the accelerated engraftment upon re-transplantation. Likewise, the consistent doubling time within a PDX model may reflect the intrinsic tumor growth rate once a murine vasculature system is established.

The HCC biopsy-derived PDX models maintained a striking similarity with the original human HCCs with respect to differentiation grade, growth pattern, cytological subtype and the expression pattern of typical HCC markers. Of note, only one PDX model (C284b) lost part of the histological characteristics (i.e. trabecular growth pattern) observed in the originating human HCC. This may be due to heterogeneous growth patterns in different regions of the same tumor. RNA sequencing of the HCC PDX tumors and the corresponding human HCC biopsies revealed that pathways related to angiogenesis and immune cells were generally down-regulated in the PDX models, likely a consequence of the loss of human immune cells and the presence of a murine instead of human vasculature in these PDX models. By contrast, cell cycle-related genes were up-regulated in the PDX models compared to the biopsies, suggesting an enrichment of cancer cells in the PDX tumors. Importantly, after accounting for these systematic differences, all PDX tumors clustered with

their corresponding human HCC demonstrating that they recapitulate the tumor-specific gene expression profiles. Furthermore, HCC-specific expression of somatic mutations in cancer genes was maintained in the corresponding PDX models. Of note, transcriptome-based analysis revealed that the PDX tumors are stable over several generations. Taken together, our results demonstrate that the PDX models faithfully recapitulate the histopathological and transcriptomic characteristics of the HCC tumors from which they were derived.

The diversity of our patient cohort allowed us to identify potential determinants of tumor engraftment in mice. Differentiation grade was the major determinant for successful PDX development since only poorly differentiated biopsies (Edmondson grades III/IV) and those of molecular subclasses S1 and S2[22] formed tumors in mice. Accordingly, engrafted tumors overexpressed genes related to proliferation and epithelial-to-mesenchymal transition. However, within the group of poorly differentiated HCCs, we could not identify further clinical or transcriptomic characteristics affecting engraftment.

Three HCC biopsies resulted in PDX models that did not resemble the corresponding HCC. The histological appearance of lymphocytes, the strong positivity for the human B-cell marker CD20, transcriptional up-regulation of immune cell signatures and loss of expression of the HCC-specific somatic mutations suggested that human B-cell lymphomas were formed in these PDX models. This phenomenon has already been described for PDX models derived from a number of human cancer tissues[30-33]. It has been reported

that treatment with rituximab, an anti-CD20 monoclonal antibody, prevented lymphomatous outgrowth in early-passage ovarian xenografts[33]. Whether a similar strategy would improve the success rate of HCC PDX generation and prevent lymphomagenesis remains to be investigated.

In conclusion, using needle biopsies instead of resected specimens allows to generate PDX models from advanced stages of HCC. Our model system is currently restricted to Edmondson grade III and IV tumors, but within this group, it is representative of the entire molecular spectrum of undifferentiated HCCs. The success rate is still limited to 20-30% for unknown reasons. The PDX tumors recapitulate the histopathological and transcriptomic features of the original human HCCs, and these features remain stable over at least 4 generations of re-transplantation. We conclude that PDX models from HCC needle biopsies fulfill the requirements for preclinical drug development strategies that account for the diversity of anti-cancer drug responses in HCCs.

Acknowledgements

We thank all the patients who participated in this study, Helena Antoniadis for teaching the subcutaneous transplantation, Petra Hirschmann for performing histopathological staining, Christian Beisel (Genomics Facility Basel) for performing whole exome and RNA sequencing and Sylvia Ketterer for excellent technical assistance.

References

[1] Llovet JM, Zucman-Rossi J, Pikarsky E, Sangro B, Schwartz M, Sherman M, et al. Hepatocellular carcinoma. Nat Rev Dis Primers 2016;2:16018.

[2] European Association For The Study Of The L, European Organisation For R, Treatment Of C. EASL-EORTC clinical practice guidelines: management of hepatocellular carcinoma. J Hepatol 2012;56:908-943.

[3] Llovet JM, Ricci S, Mazzaferro V, Hilgard P, Gane E, Blanc JF, et al. Sorafenib in advanced hepatocellular carcinoma. N Engl J Med 2008;359:378-390.

[4] Cheng AL, Kang YK, Chen Z, Tsao CJ, Qin S, Kim JS, et al. Efficacy and safety of sorafenib in patients in the Asia-Pacific region with advanced hepatocellular carcinoma: a phase III randomised, double-blind, placebo-controlled trial. Lancet Oncol 2009;10:25-34.

[5] Santos NP, Colaco AA, Oliveira PA. Animal models as a tool in hepatocellular carcinoma research: A Review. Tumour Biol 2017;39:1010428317695923.

[6] **Tentler JJ**, **Tan AC**, **Weekes CD**, **Jimeno A**, **Leong S**, **Pitts TM**, et al. Patient-derived tumour xenografts as models for oncology drug development. Nat Rev Clin Oncol 2012;9:338-350.

[7] Siolas D, Hannon GJ. Patient-derived tumor xenografts: transforming clinical samples into mouse models. Cancer Res 2013;73:5315-5319.

[8] **Armengol C**, **Tarafa G**, Boix L, Sole M, Queralt R, Costa D, et al. Orthotopic implantation of human hepatocellular carcinoma in mice: analysis of tumor progression and establishment of the BCLC-9 cell line. Clin Cancer Res 2004;10:2150-2157.

[9] **Gu Q**, **Zhang B**, Sun H, Xu Q, Tan Y, Wang G, et al. Genomic characterization of a large panel of patient-derived hepatocellular carcinoma xenograft tumor models for preclinical development. Oncotarget 2015;6:20160-20176.

[10] Huynh H, Soo KC, Chow PK, Panasci L, Tran E. Xenografts of human hepatocellular carcinoma: a useful model for testing drugs. Clin Cancer Res 2006;12:4306-4314.

[11] **Jiang Z**, **Jiang X**, Chen S, Lai Y, Wei X, Li B, et al. Anti-GPC3-CAR T Cells Suppress the Growth of Tumor Cells in Patient-Derived Xenografts of Hepatocellular Carcinoma. Front Immunol 2016;7:690.

[12] **Xin H**, **Wang K**, Hu G, Xie F, Ouyang K, Tang X, et al. Establishment and characterization of 7 novel hepatocellular carcinoma cell lines from patient-derived tumor xenografts. PLoS One 2014;9:e85308.

[13] Yan M, Li H, Zhao F, Zhang L, Ge C, Yao M, et al. Establishment of NOD/SCID mouse models of human hepatocellular carcinoma via subcutaneous transplantation of histologically intact tumor tissue. Chin J Cancer Res 2013;25:289-298.

[14] Llovet JM, Bru C, Bruix J. Prognosis of hepatocellular carcinoma: the BCLC staging classification. Semin Liver Dis 1999;19:329-338.

[15] Edmondson HA, Steiner PE. Primary carcinoma of the liver: a study of 100 cases among 48,900 necropsies. Cancer 1954;7:462-503.

[16] **Ng CKY**, **Piscuoglio S**, **Geyer FC**, Burke KA, Pareja F, Eberle CA, et al. The Landscape of Somatic Genetic Alterations in Metaplastic Breast Carcinomas. Clin Cancer Res 2017;23:3859-3870.

[17] Dobin A, Davis CA, Schlesinger F, Drenkow J, Zaleski C, Jha S, et al. STAR: ultrafast universal RNA-seq aligner. Bioinformatics 2013;29:15-21.

[18] Li B, Dewey CN. RSEM: accurate transcript quantification from RNA-Seq data with or without a reference genome. BMC Bioinformatics 2011;12:323.

[19] Nikolayeva O, Robinson MD. edgeR for differential RNA-seq and ChIP-seq analysis: an application to stem cell biology. Methods Mol Biol 2014;1150:45-79.

[20] Liberzon A, Birger C, Thorvaldsdottir H, Ghandi M, **Mesirov JP**, **Tamayo P**. The Molecular Signatures Database (MSigDB) hallmark gene set collection. Cell Syst 2015;1:417-425.

[21] McKenna A, Hanna M, Banks E, Sivachenko A, Cibulskis K, Kernytsky A, et al. The Genome Analysis Toolkit: a MapReduce framework for analyzing next-generation DNA sequencing data. Genome Res 2010;20:1297-1303.

[22] Hoshida Y, Nijman SM, Kobayashi M, Chan JA, Brunet JP, Chiang DY, et al. Integrative transcriptome analysis reveals common molecular subclasses of human hepatocellular carcinoma. Cancer Res 2009;69:7385-7392.

[23] Cancer Genome Atlas Research Network. Electronic address wbe, Cancer Genome Atlas Research N. Comprehensive and Integrative Genomic Characterization of Hepatocellular Carcinoma. Cell 2017;169:1327-1341 e1323.

[24] Kancherla V, Abdullazade S, Matter MS, Lanzafame M, Quagliata L, Roma G, et al. Genomic Analysis Revealed New Oncogenic Signatures in TP53-Mutant Hepatocellular Carcinoma. Frontiers in Genetics 2018;9.

[25] Schlageter M, Terracciano LM, D'Angelo S, Sorrentino P. Histopathology of hepatocellular carcinoma. World J Gastroenterol 2014;20:15955-15964.

[26] Schlageter M, Quagliata L, Matter M, Perrina V, Tornillo L, Terracciano L. Clinicopathological Features and Metastatic Pattern of Hepatocellular Carcinoma: An Autopsy Study of 398 Patients. Pathobiology 2016;83:301-307.

[27] Bruix J, Sherman M, American Association for the Study of Liver D. Management of hepatocellular carcinoma: an update. Hepatology 2011;53:1020-1022.

[28] Di Tommaso L, Franchi G, Park YN, Fiamengo B, Destro A, Morenghi E, et al. Diagnostic value of HSP70, glypican 3, and glutamine synthetase in hepatocellular nodules in cirrhosis. Hepatology 2007;45:725-734.

[29] Di Tommaso L, **Destro A**, **Seok JY**, Balladore E, Terracciano L, Sangiovanni A, et al. The application of markers (HSP70 GPC3 and GS) in liver biopsies is useful for detection of hepatocellular carcinoma. J Hepatol 2009;50:746-754.

[30] **Chen K**, **Ahmed S**, Adeyi O, Dick JE, Ghanekar A. Human solid tumor xenografts in immunodeficient mice are vulnerable to lymphomagenesis associated with Epstein-Barr virus. PLoS One 2012;7:e39294.

[31] Fujii E, Kato A, Chen YJ, Matsubara K, Ohnishi Y, Suzuki M. Characterization of EBV-related lymphoproliferative lesions arising in donor lymphocytes of transplanted human tumor tissues in the NOG mouse. Exp Anim 2014;63:289-296.

[32] **Bondarenko G**, **Ugolkov A**, Rohan S, Kulesza P, Dubrovskyi O, Gursel D, et al. Patient-Derived Tumor Xenografts Are Susceptible to Formation of Human Lymphocytic Tumors. Neoplasia 2015;17:735-741.

[33] Butler KA, Hou X, Becker MA, Zanfagnin V, Enderica-Gonzalez S, Visscher D, et al. Prevention of Human Lymphoproliferative Tumor Formation in Ovarian Cancer Patient-Derived Xenografts. Neoplasia 2017;19:628-636.

[34] Llovet JM, Hernandez-Gea V. Hepatocellular carcinoma: reasons for phase III failure and novel perspectives on trial design. Clin Cancer Res 2014;20:2072-2079.

[35] **Fujimoto A**, **Furuta M**, **Totoki Y**, **Tsunoda T**, **Kato M**, Shiraishi Y, et al. Whole-genome mutational landscape and characterization of noncoding and structural mutations in liver cancer. Nat Genet 2016;48:500-509.

[36] **Kandoth C**, **McLellan M**D, Vandin F, Ye K, Niu B, Lu C, et al. Mutational landscape and significance across 12 major cancer types. Nature 2013;502:333-339.

[37] Lawrence MS, Stojanov P, Mermel CH, Robinson JT, Garraway LA, Golub TR, et al. Discovery and saturation analysis of cancer genes across 21 tumour types. Nature 2014;505:495-501.

Table 1. Edmondson grade, growth pattern and cytological subtype of biopsies and corresponding PDX tumors.

Biopsy ID	Edmondson Grade			Growth Pattern			Cytological Subtype		
	Biopsy	PDX-1	PDX-4	Biopsy	PDX-1	PDX-4	Biopsy	PDX-1	PDX-4
C078	III	III	III	solid	solid	solid	-	-	-
C284	III	III	III	solid-trabecular	solid	solid	-	-	-
C677	IV	IV	IV	solid	solid	solid	giant cells	giant cells	giant cells
C678	IV	IV	IV	solid	solid	solid	giant cells	giant cells	giant cells
C798	III	III	III	solid-trabecular	solid-trabecular	solid-trabecular	-	-	-
C942	III	III	III	solid-trabecular	solid-trabecular	solid-trabecular	-	-	-
C949	III	III	III	solid-trabecular	solid-trabecular	solid-trabecular	-	-	-
C965	III	III	III	solid	solid	solid	-	-	-
C975	III	III	III	solid	solid	solid	-	-	-
D096	IV	IV	IV	solid	solid	solid	-	-	-
D135	IV	IV	IV	solid-trabecular	solid-trabecular	solid-trabecular	clear cell, giant cells	clear cell, giant cells	clear cell, giant cells

PDX-1: 1st generation tumor; PDX-4: 4th generation tumor

Figure Legends

Fig. 1. Xenograft tumor growth patterns

(A) Lag phase and tumor growth rate of first generation xenografts. Edmondson grade III and IV are shown in green and red, respectively. Circles and diamonds represent transplanted solid pieces and cell suspensions, respectively. **(B)** Growth characteristics of PDX models. Lag phase until detectable tumor formation, doubling time of tumors from 1st, 2nd, 3rd and 4th generation PDX and number of transplanted tumors are indicated. **(C)** Tumor growth rate over several generations (1st to 4th) in one representative PDX model (C284b). Transplantation generations are color-coded.

Fig. 2. HCC PDX mice recapitulate the histological characteristics as well as the expression patterns of HCC markers of the original tumor. Histological sections of the original HCC biopsies and their derivative PDX tumors (PDX-1 and PDX-4 corresponding to 1st and 4th transplantations, respectively) stained with Hematoxylin and Eosin (H&E), for alpha-fetoprotein (AFP) expression as well as for glypican 3 (GPC3), heat shock protein 70 (HSP70) and glutamine synthetase (GS) detected by immunohistochemistry. Scale bar: 200 µm. Representative stainings are shown for PDX model C942.

Fig. 3. HCC PDX mice recapitulate the transcriptomic features of their original tumors. (A) Heatmap of gene expression from selected differentially expressed pathways between HCC biopsies and PDX tumors (1st

transplantation). For each pathway, the top 5 genes, ranked by FDR, are shown. **(B)** Unsupervised clustering of HCC biopsies and PDX tumors, corrected for systemic biases between the two groups. **(C)** Barplot of the number of expressed somatic missense and synonymous mutations, and the repertoire of expressed somatic missense mutations affecting cancer genes[23, 35-37]. Multiple expressed mutations in the same gene are indicated by an asterisk.

Fig. 4. Clinical, histopathological and molecular features of engrafted and not engrafted HCC biopsies. (A) Patient and biopsy characteristics of all transplanted biopsies, grouped by engraftment status. Calculations of significant differences (indicated in red) between engrafted versus not engrafted biopsies are shown underneath. Two-sided Fisher's exact tests for categorical data and two-sided Mann-Whitney U tests for ordinal data. ALD: Alcoholic Liver Disease; AFP: Alpha-Fetoprotein; BCLC: Barcelona Clinic Liver Cancer; MVI: Macrovascular invasion; NAFLD: Non-Alcoholic Fatty Liver Disease. **(B)** Unsupervised hierarchical clustering analysis. Biopsy (PDX) cohort (this study) combined with high-grade (Edmondson III to IV) HCCs from the TCGA cohort.

Fig. 5. Unintended lymphoid neoplasm transformation in PDX models. (A) H&E stained sections of original HCC biopsies and their derivative lymphoma PDX tumors (PDX-1). **(B)** Unsupervised clustering of 1st generation PDX and corresponding HCC biopsies. Lymphoma PDX tumors indicated in red. **(C)** Barchart illustrating the number of expressed somatic missense and

synonymous mutations for the 9 HCC biopsies (mean) and the 10 corresponding HCC PDX tumors (mean), and for C738, C948, C951 and their corresponding lymphoma PDX tumors (C738-PDX-1, C948-PDX-1 and C951-PDX-1). **(D)** PDX tumors of the lymphoma models (C738-PDX-1, C948-PDX-1 and C951-PDX-1) stained with hCD20. Scale bar: 200 µm.

Figure 1

A

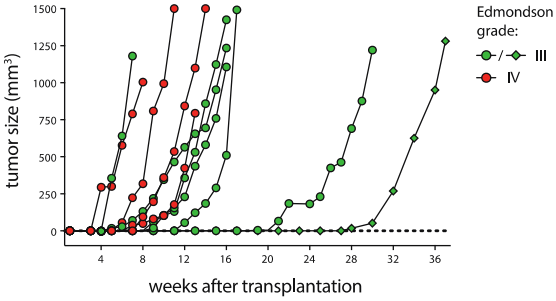

C

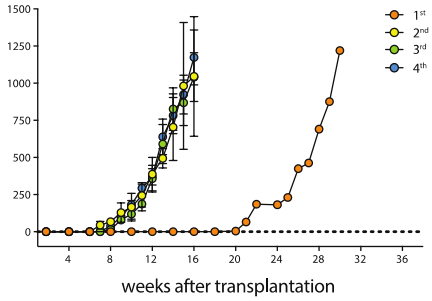

B

Biopsy ID		PDX generations			
		1st	2nd	3rd	4th
C078b	lag phase [weeks]	28 (+/- 0)	5.33 (+/-1.15)	4.67 (+/-0.99)	5.05 (+/-0.56)
	doubling time [weeks]	1,97 (+/-0,32)	2,54 (+/-0,51)	1,94 (+/-0,65)	2,07 (+/-0,72)
	# of tumors	2	8	24	22
C284b	lag phase [weeks]	21	7.0 (+/-0)	8.0 (+/-0.89)	7.43 (+/-0.49)
	doubling time [weeks]	2.30	2.02 (+/-0.07)	1.63 (+/-0.43)	2.01 (+/-0.72)
	# of tumors	1	2	5	8
C677	lag phase [weeks]	6.5 (+/-1.5)	3.5 (+/-0.5)	3.7 (+/-0.9)	3.7 (+/-1.85)
	doubling time [weeks]	1.62 (+/-0.22)	1.21 (+/-0.25)	1.18 (+/-0.33)	1.05 (+/-0.41)
	# of tumors	2	4	10	10
C678	lag phase [weeks]	5.0 (+/-1)	3.33 (+/-0.85)	3.6 (+/-1.40)	3.25 (+/-0.43)
	doubling time [weeks]	1.39 (+/-0.23)	1.37 (+/-0.44)	1.04 (+/-0.28)	1.23 (+/-0.24)
	# of tumors	2	12	15	4
C798	lag phase [weeks]	6.0	4.0	3.25 (+/-0.43)	4 (+/-2.22)
	doubling time [weeks]	2,09	1,26	2,21 (+/-0,32)	1,44 (+/-0,42)
	# of tumors	1	1	4	10
C942	lag phase [weeks]	7.5 (+/-2.50)	3.57 (+/-0.49)	4.14 (+/-2.10)	3.0 (+/-0.63)
	doubling time [weeks]	1.67 (+/-0.48)	1.59 (+/-0.27)	1.48 (+/-0.30)	1.40 (+/-0.38)
	# of tumors	2	7	10	4
C949	lag phase [weeks]	12	3.0 (+/-0)	3.89 (+/-1.45)	4 (+/-1.15)
	doubling time [weeks]	1.14	0.89 (+/-0.14)	0.88 (+/-0.2)	0.85 (+/-0.85)
	# of tumors	1	4	9	6
C965	lag phase [weeks]	9	5.67 (+/-0.47)	5.0 (+/-1.41)	5.88 (+/-2.47)
	doubling time [weeks]	1.19	1.19 (+/-0.18)	1.55 (+/-0.11)	1.35 (+/-0.39)
	# of tumors	1	3	3	8
C975	lag phase [weeks]	9.0	4.67 (+/-0.94)	4.56 (+/-0.83)	4.25 (+/-0.43)
	doubling time [weeks]	1.75	1.82 (+/-0.11)	1.06 (+/-0.21)	1.24 (+/-0.45)
	# of tumors	1	3	9	4
D096	lag phase [weeks]	7	3.33 (+/-0.47)	3.0 (+/-0.63)	2.75 (+/-0.43)
	doubling time [weeks]	1.25	1.02 (+/-0.04)	0.93 (+/-0.25)	1.04 (+/-0.21)
	# of tumors	1	3	5	4
D135	lag phase [weeks]	7.5 (+/-0.5)	5.29 (+/-1.16)	5.2 (+/-2.64)	4.5 (+/-0.87)
	doubling time [weeks]	1.94 (+/-0.21)	1.41 (+/-0.25)	1.69 (+/-0.80)	1.65 (+/-0.39)
	# of tumors	2	7	5	4

Figure 2
C942

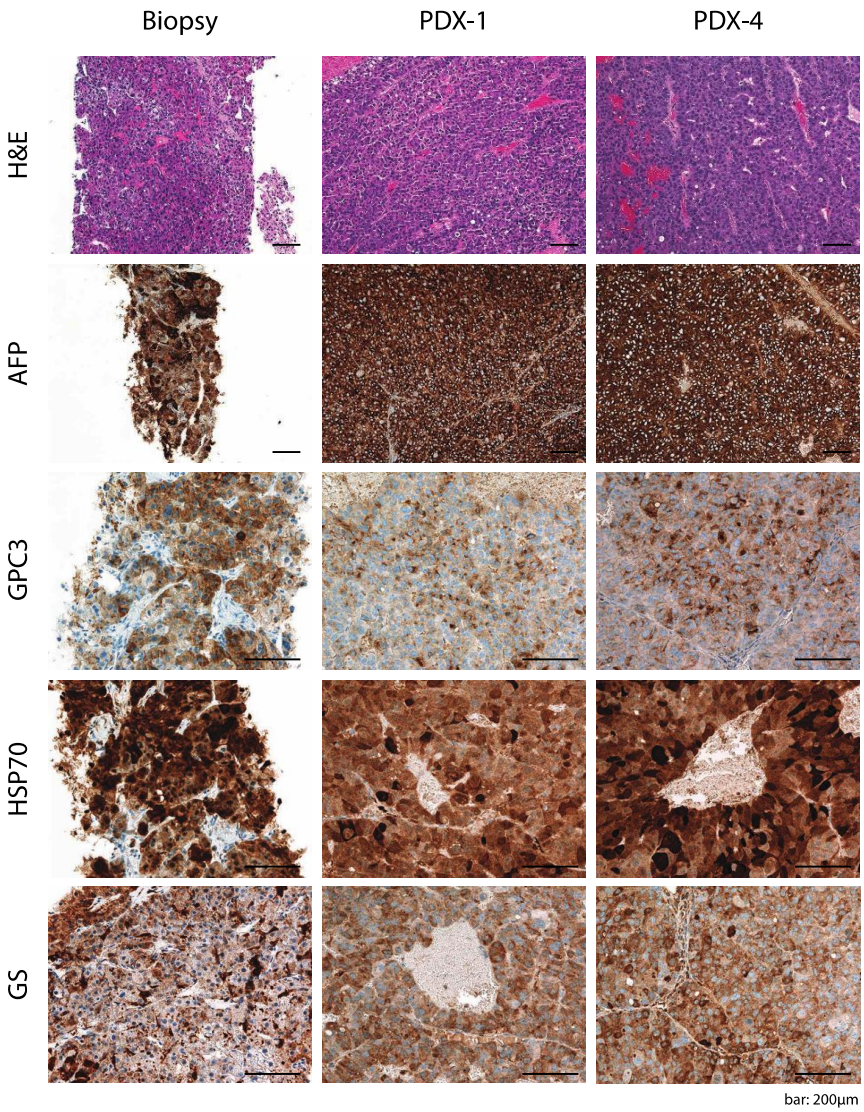

Figure 3

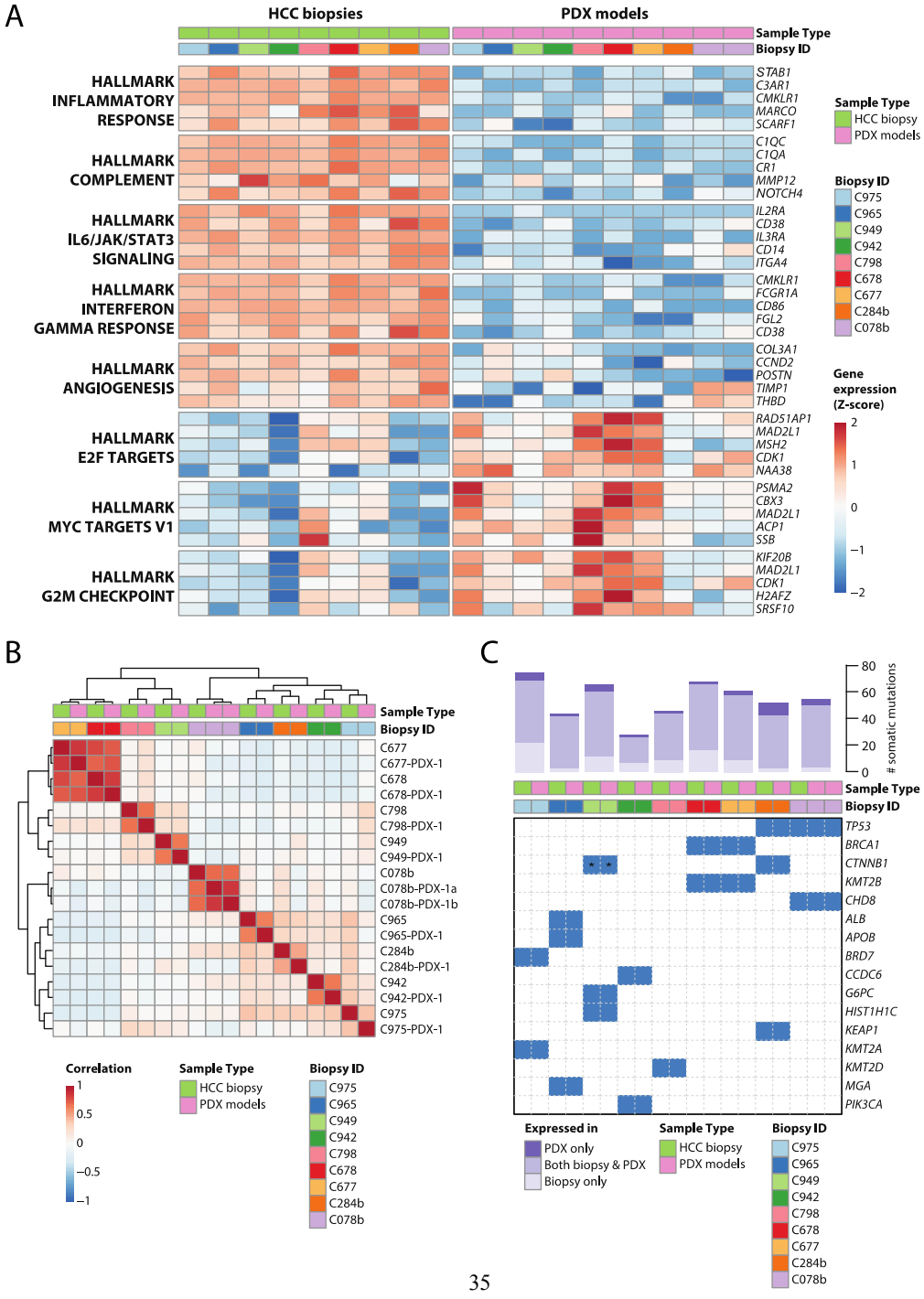
A
HCC biopsies
PDX models
Sample Type
Biopsy ID
HALLMARK INFLAMMATORY RESPONSE
STAB1
C3AR1
CMKLR1
MARCO
SCARF1
HALLMARK COMPLEMENT
C1QC
C1QA
CR1
MMP12
NOTCH4
HALLMARK IL6/JAK/STAT3 SIGNALING
IL2RA
CD38
IL3RA
CD14
ITGA4
HALLMARK INTERFERON GAMMA RESPONSE
CMKLR1
FCGR1A
CD86
FGL2
CD38
HALLMARK ANGIOGENESIS
COL3A1
CCND2
POSTN
TIMP1
THBD
HALLMARK E2F TARGETS
RAD51AP1
MAD2L1
MSH2
CDK1
NAA38
HALLMARK MYC TARGETS V1
PSMA2
CBX3
MAD2L1
ACP1
SSB
HALLMARK G2M CHECKPOINT
KIF20B
MAD2L1
CDK1
H2AFZ
SRSF10
Sample Type
HCC biopsy
PDX models
Biopsy ID
C975
C965
C949
C942
C798
C678
C677
C284b
C078b
Gene expression (Z-score)
2
1
0
−1
−2
B
Sample Type
Biopsy ID
C677
C677-PDX-1
C678
C678-PDX-1
C798
C798-PDX-1
C949
C949-PDX-1
C078b
C078b-PDX-1a
C078b-PDX-1b
C965
C965-PDX-1
C284b
C284b-PDX-1
C942
C942-PDX-1
C975
C975-PDX-1
Correlation
1
0.5
0
−0.5
−1
Sample Type
HCC biopsy
PDX models
Biopsy ID
C975
C965
C949
C942
C798
C678
C677
C284b
C078b
C
80
60
40
20
0
somatic mutations
Sample Type
Biopsy ID
TP53
BRCA1
CTNNB1
KMT2B
CHD8
ALB
APOB
BRD7
CCDC6
G6PC
HIST1H1C
KEAP1
KMT2A
KMT2D
MGA
PIK3CA
Expressed in
PDX only
Both biopsy & PDX
Biopsy only
Sample Type
HCC biopsy
PDX models
Biopsy ID
C975
C965
C949
C942
C798
C678
C677
C284b
C078b

Figure 4

A

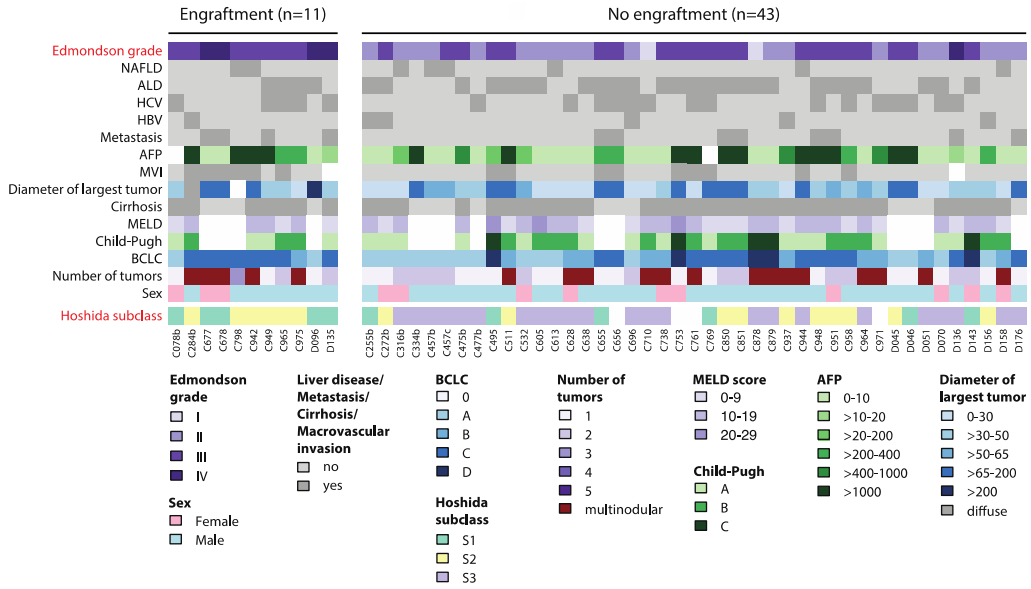

	Edmondson grade									AFP [IU/ml]						
	I	II	III	IV	NAFLD	ALD	HCV	HBV	Metastasis	0-10	10-20	20-200	200-400	400-1000	>1000	MVI
Engraftment	0/11	0/11	7/11	4/11	2/10	4/10	5/10	1/10	3/10	2/9	1/9	0/9	2/9	0/9	4/9	5/9
No engraftment	2/43	19/43	21/43	1/43	5/38	22/38	13/38	5/38	6/38	18/37	1/37	3/37	3/37	3/37	9/37	8/37
P value	<0.001				0.63	0.48	0.47	>0.99	0.37	0.17						0.09

	Diameter of largest tumor					Cirrhosis	BCLC				Number of tumors				Sex	
	0-30	>30-50	>50-65	>65-200	>200		A	B	C	D	1	2	3	multinodular	Female	Male
Engraftment	1/8	4/8	0/8	2/8	1/8	7/10	2/10	1/10	7/10	0/10	3/10	2/10	1/10	4/10	2/10	8/10
No engraftment	14/38	10/38	4/38	10/38	0/38	30/38	14/38	10/38	10/38	4/38	15/38	10/38	0/38	13/38	10/38	28/38
P value	0.30					0.68	0.23				0.54				>0.99	

	Hoshida subclass		
	S1	S2	S3
Engraftment	5/11	6/11	0/11
No engraftment	6/39	10/39	23/39
P value	<0.001		

B

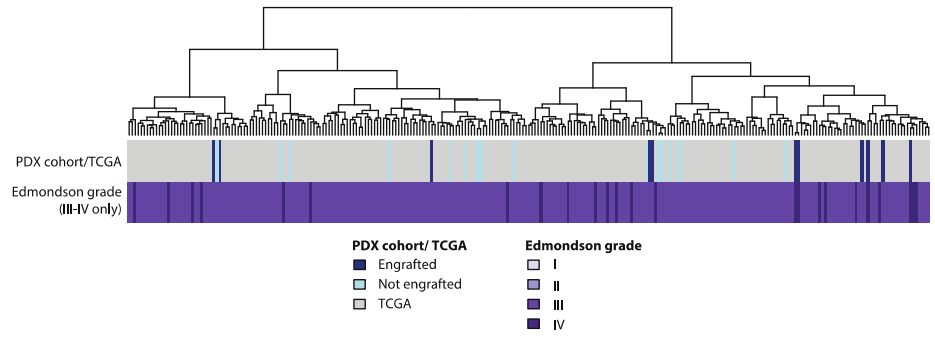

Figure 5

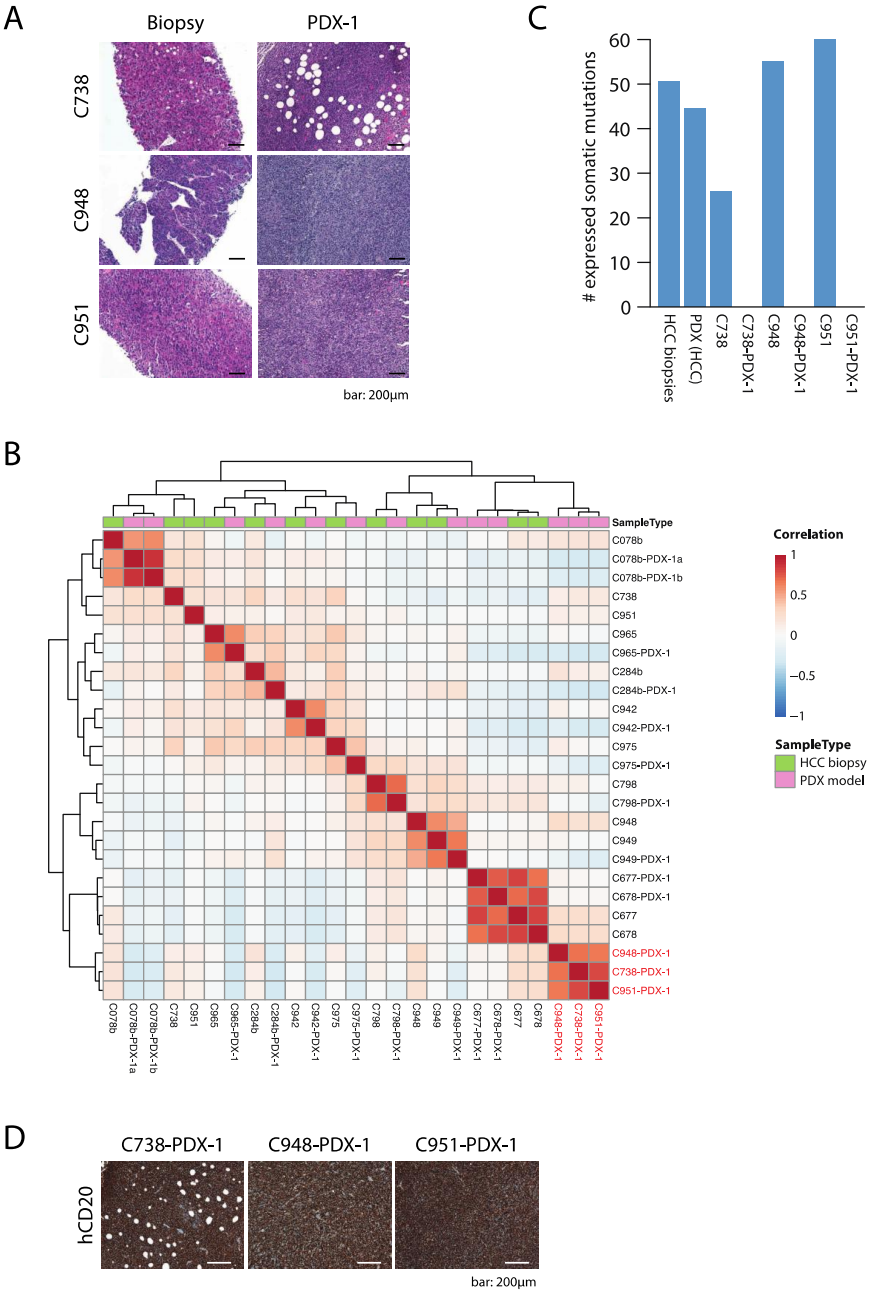
A
Biopsy
PDX-1
C738
C948
C951
bar: 200µm
C
expressed somatic mutations
60
50
40
30
20
10
0
HCC biopsies
PDX (HCC)
C738
C738-PDX-1
C948
C948-PDX-1
C951
C951-PDX-1
B
SampleType
C078b
C078b-PDX-1a
C078b-PDX-1b
C738
C951
C965
C965-PDX-1
C284b
C284b-PDX-1
C942
C942-PDX-1
C975
C975-PDX-1
C798
C798-PDX-1
C948
C949
C949-PDX-1
C677-PDX-1
C678-PDX-1
C677
C678
C948-PDX-1
C738-PDX-1
C951-PDX-1
Correlation
1
0.5
0
−0.5
−1
SampleType
HCC biopsy
PDX model
D
C738-PDX-1
C948-PDX-1
C951-PDX-1
hCD20
bar: 200µm

Supplementary Materials

Table of contents

Supplementary Material and Methods

Human HCC Biopsy Procedure

Ultrasound-guided (US) needle biopsies were obtained from tumor lesion(s) with a coaxial liver biopsy technique that allows taking several biopsy samples through a single biopsy needle tract. After local anaesthesia, the introducer needle was advanced 2-3 cm into the liver parenchyma. In case of a focal lesion, the needle was positioned precisely at the tumor border. The trocar of the introducer needle was removed, and up to five cylindrical biopsies of ~1 mm diameter and 10-30 mm length were obtained with an automatic spring-loaded biopsy needle (BioPince™). The introducer needle was kept in place during the entire procedure to ensure that all specimens came from the same area of the tumor. Finally, the needle tract was filled with absorbable gelatine sponge before removal of the introducer needle.

Mice and Xenotransplantation

NOD-SCID gamma-c (NSG) mice (The Jackson Laboratory) were bred and maintained in the animal facility of the Department of Biomedicine of the University Hospital Basel under specific-pathogen-free conditions, on a 12-h day and 12-h night schedule with *ad libitum* access to food and drinking water. The freshly obtained human HCC needle biopsy material was kept on ice during the whole procedure and was subcutaneously introduced into the mice either as pieces or cell suspension. For the subcutaneous (s.c.) transplantation of biopsy pieces, the biopsy cylinder was washed in PBS and mechanically cut into fragments of 2-3 mm, which were immediately

transplanted into the hind flank of NSG mice. For the s.c. injection of the biopsy-derived cell suspension, the biopsy material was pressed through a 70µm cell strainer (Falcon; 352350), followed by trypan blue analysis. The cells (30,000-300,000) were mixed with matrigel (BD Biosciences; 354234) and injected with a 25-gauge needle into the hind flank of NSG mice.

Histology and Immunohistochemistry

Tumor biopsies and PDX tumors were fixed in 4% phosphate buffered formalin and embedded in paraffin using standard procedures. The following primary antibodies were used for automated immunohistochemistry staining on a Benchmark XT device (Ventana Medical Systems, Inc.): Alpha-Fetoprotein (Ventana Cat. Nr. 760-2603), Glypican 3 (Ventana Cat. Nr. 790-4564), Glutamine Synthetase (Ventana Cat. Nr. 760-4898), Heat Shock Protein 70 (Biocare Medical CM407A) and human CD20 (Ventana Cat. Nr. 760-2531).

Immunofluorescence

Briefly, 10µm sections were fixed for 20 minutes in 4% formalin in phosphate-buffered saline (PBS) and incubated over night with the primary rat anti-mouse CD31 antibody (BD Pharmingen; 550274) at 4°C. Subsequently, slides were incubated with the secondary Alexa Fluor 488 donkey anti-rat antibody (Life technologies; A21208) for 1h at RT and mounted with DAPI-containing mounting solution (HP20.1; Roth).

DNA extraction

Genomic DNA from biopsies was extracted using the ZR-Duet DNA/RNA MiniPrep Plus kit (Zymo Research) following the manufacturer's instructions. Prior to extraction, biopsies were crushed in liquid nitrogen to facilitate lysis. Extracted DNA was quantified using the Qubit Fluorometer (Invitrogen).

Whole exome sequence and analysis

Whole exome sequencing was performed at the Genomics Facility of ETH Zurich Department of Biosystems Science and Engineering (Basel, Switzerland). Sequence reads were aligned to the reference human genome GRCh37 using Burrows-Wheeler Aligner (BWA, v0.7.12)[1]. Local realignment, duplicate removal and base quality adjustment were performed using the Genome Analysis Toolkit (GATK, v3.6)[2] and Picard (http://broadinstitute.github.io/picard/). Somatic single nucleotide variants (SNVs) and small insertions and deletions (indels) were detected using MuTect (v1.1.4)[3] and Strelka (v1.0.15)[4], respectively. We filtered out SNVs and indels outside of the target regions, those with variant allelic fraction (VAF) of <1% and/or those supported by <3 reads. We excluded variants for which the tumor VAF was <5 times that of the paired non-tumoral VAF. We further excluded variants identified in at least two of a panel of 123 non-tumoral samples, including the 12 matched non-tumoral biopsies included in the current study, captured and sequenced using the same protocols using the artifact detection mode of MuTect2 implemented in GATK. All indels were manually inspected using the Integrative Genomics Viewer[5].

Whole exome data were analyzed as previously described[6], with some modifications. Briefly, sequence reads were aligned to the reference human

genome GRCh37 using Burrows-Wheeler Aligner (BWA, v0.7.12)[1]. Somatic single nucleotide variants (SNVs) and small insertions and deletions (indels) were detected using MuTect (v1.1.4)[3] and Strelka (v1.0.15)[4], respectively (Supplementary Methods). Cancer genes were annotated according to the cancer gene lists described by Kandoth et al. (127 significantly mutated genes)[7], Lawrence et al., (Cancer5000-S gene set)[8], Fujimoto et al.[9] and The Cancer Genome Atlas (TCGA)[10].

RNA extraction

RNA from human tumors and xenograft tumors was extracted using the RNeasy Mini Kit (Qiagen) following the manufacturer's instructions. Extracted RNA was quantified using NanoDrop 2000 spectrophotometer (Thermo Scientific), and RNA quality/integrity was assessed with an Agilent 2100 BioAnalyzer using RNA 6000 Nano Kit (Agilent Technologies).

RNA sequencing

200 ng total RNA were used for RNA sequencing library prep with the TruSeq Stranded Total RNA Library Prep Kit with Ribo-Zero Gold (Illumina) according to manufacturer's specifications. SR126 sequencing was performed on an Illumina HiSeq 2500 using v4 SBS chemistry at the Genomics Facility Basel according to the manufacturer's guidelines. Primary data analysis was performed with the Illumina RTA version 1.18.66.3.

RNA sequence analysis

Differential expression analysis between HCC biopsies and PDX tumors was performed using the edgeR R package[11]. Specifically, genes with counts-per-million <1 in more than 5 samples were removed. Normalization was performed using the “TMM” (weighted trimmed mean) method and differential expression was assessed using the quasi-likelihood F-test, accounting for the matched pairs of HCC biopsies and PDX tumors. Genes with false discovery rate (FDR)<0.05 were considered differentially expressed. Pathway enrichment of differentially expressed genes was performed using hypergeometric test for the hallmark gene sets in the Molecular Signatures Database[12]. Pathways with FDR<0.25 were considered enriched.

For unsupervised cluster analysis of HCC biopsies and PDX tumors, we performed gene-level upper quartile normalization. Genes whose expression was quantified to be zero by RSEM[13] in >75% of the samples were removed. RSEM values were subsequently log2-transformed, adding 0.5 to RSEM values prior to transformation. To identify genes with variable expression for clustering, genes with standard deviation <2 were excluded[14]. Batch effects associated with the process of PDX establishment were removed using the edgeR R package[11], which fits a linear model to the data and removes the component associated with xenografting. Genes were centered prior to clustering. Cluster analysis was performed using hierarchical clustering using the Ward method and with a 1-Pearson correlation distance[10]. Cluster stability was assessed by bootstrap resampling using the pvclust R package[15].

Aligned reads were further processed using the GATK SplitNCigarReads tool. The expression of somatic mutations in RNA sequencing data was determined by GATK Unified Genotyper using the GENOTYPE_GIVEN_ALLELES mode[2], given the list of somatic mutations identified by whole exome sequencing. Mutations supported by at least 2 reads, VAF>1% at loci covered by at least 5 reads were considered expressed. For statistical comparisons, only missense and synonymous mutations were considered. Truncating, insertions and deletions and splice site mutations were excluded, as these mutations are likely to affect the stability of the transcripts.

Transcriptomic classification was performed according to Hoshida et al.[16], using the Nearest Template Prediction algorithm (http://software.broadinstitute.org/cancer/software/genepattern), with RSEM gene-level quantification as input.

CD20 and Epstein-Barr Virus transcripts

Sequence reads from PDX tumors were aligned by QuasR (qAlign with Rbowtie)[17] to the human and mouse CD20 reference mRNA sequences NM_152866.2 and NM_007641.5, respectively. CD20 reads were normalized to the number of total reads per sample and transcript length and are expressed as RPKM (Reads Per Kilobase Million).

Sequence reads from paired non-tumor and tumor biopsy and corresponding PDX tumors were aligned by QuasR (qAlign with Rbowtie)[17] to two Epstein-Barr virus (EBV) reference genomes (NC_009334 and NC_007605). EBV

reads were normalized to the number of total reads per sample and are expressed as RPM (Reads Per Million).

TCGA data analysis

For unsupervised cluster analysis of HCC biopsies and HCCs from TCGA, we merged our RNA sequencing dataset with the TCGA HCC dataset RNA-seq data ("V2_MapSpliceRSEM") retrieved from the Genomics Data Commons Data Portal[10]. We performed gene-level upper quartile normalization of the combined dataset to the fixed threshold 1000 as described in the TCGA study[10]. Log2-transformation and gene filtering were performed as above. Batch correction using the edgeR R package[11] was performed to correct for systematic biases between the two datasets. Gene centering and clustering were performed as described above.

For the TCGA cohort[10], images of diagnostic H&E slides were retrieved from the cbioportal (http://www.cbioportal.org; accessed December 2017)[18] and reviewed by two expert hepato-pathologists according to the Edmondson grading system[19] as previously described[20].

Supplementary References

[1] Li H, Durbin R. Fast and accurate short read alignment with Burrows-Wheeler transform. Bioinformatics 2009;25:1754-1760.

[2] McKenna A, Hanna M, Banks E, Sivachenko A, Cibulskis K, Kernytsky A, et al. The Genome Analysis Toolkit: a MapReduce framework for analyzing next-generation DNA sequencing data. Genome Res 2010;20:1297-1303.

[3] Cibulskis K, Lawrence MS, Carter SL, Sivachenko A, Jaffe D, Sougnez C, et al. Sensitive detection of somatic point mutations in impure and heterogeneous cancer samples. Nat Biotechnol 2013;31:213-219.

[4] Saunders CT, Wong WS, Swamy S, Becq J, Murray LJ, Cheetham RK. Strelka: accurate somatic small-variant calling from sequenced tumor-normal sample pairs. Bioinformatics 2012;28:1811-1817.

[5] Thorvaldsdottir H, Robinson JT, Mesirov JP. Integrative Genomics Viewer (IGV): high-performance genomics data visualization and exploration. Brief Bioinform 2013;14:178-192.

[6] **Ng CKY**, **Piscuoglio S**, **Geyer FC**, Burke KA, Pareja F, Eberle CA, et al. The Landscape of Somatic Genetic Alterations in Metaplastic Breast Carcinomas. Clin Cancer Res 2017;23:3859-3870.

[7] **Kandoth C**, **McLellan M**D, Vandin F, Ye K, Niu B, Lu C, et al. Mutational landscape and significance across 12 major cancer types. Nature 2013;502:333-339.

[8] Lawrence MS, Stojanov P, Mermel CH, Robinson JT, Garraway LA, Golub TR, et al. Discovery and saturation analysis of cancer genes across 21 tumour types. Nature 2014;505:495-501.

[9] **Fujimoto A**, **Furuta M**, **Totoki Y**, **Tsunoda T**, **Kato M**, Shiraishi Y, et al. Whole-genome mutational landscape and characterization of noncoding and structural mutations in liver cancer. Nat Genet 2016;48:500-509.

[10] Cancer Genome Atlas Research Network. Electronic address wbe, Cancer Genome Atlas Research N. Comprehensive and Integrative Genomic Characterization of Hepatocellular Carcinoma. Cell 2017;169:1327-1341 e1323.

[11] Nikolayeva O, Robinson MD. edgeR for differential RNA-seq and ChIP-seq analysis: an application to stem cell biology. Methods Mol Biol 2014;1150:45-79.

[12] Liberzon A, Birger C, Thorvaldsdottir H, Ghandi M, **Mesirov JP**, **Tamayo P**. The Molecular Signatures Database (MSigDB) hallmark gene set collection. Cell Syst 2015;1:417-425.

[13] Li B, Dewey CN. RSEM: accurate transcript quantification from RNA-Seq data with or without a reference genome. BMC Bioinformatics 2011;12:323.

[14] European Association For The Study Of The L, European Organisation For R, Treatment Of C. EASL-EORTC clinical practice guidelines: management of hepatocellular carcinoma. J Hepatol 2012;56:908-943.

[15] Suzuki R, Shimodaira H. Pvclust: an R package for assessing the uncertainty in hierarchical clustering. Bioinformatics 2006;22:1540-1542.

[16] Hoshida Y, Nijman SM, Kobayashi M, Chan JA, Brunet JP, Chiang DY, et al. Integrative transcriptome analysis reveals common molecular subclasses of human hepatocellular carcinoma. Cancer Res 2009;69:7385-7392.

[17] **Gaidatzis D**, **Lerch A**, Hahne F, Stadler MB. QuasR: quantification and annotation of short reads in R. Bioinformatics 2015;31:1130-1132.

[18] Gao J, Aksoy BA, Dogrusoz U, Dresdner G, Gross B, Sumer SO, et al. Integrative analysis of complex cancer genomics and clinical profiles using the cBioPortal. Sci Signal 2013;6:pl1.

[19] Edmondson HA, Steiner PE. Primary carcinoma of the liver: a study of 100 cases among 48,900 necropsies. Cancer 1954;7:462-503.

[20] Kancherla V, Abdullazade S, Matter MS, Lanzafame M, Quagliata L, Roma G, et al. Genomic Analysis Revealed New Oncogenic Signatures in TP53-Mutant Hepatocellular Carcinoma. Frontiers in Genetics 2018;9.

Supplementary Figures

Supplementary Figure 1

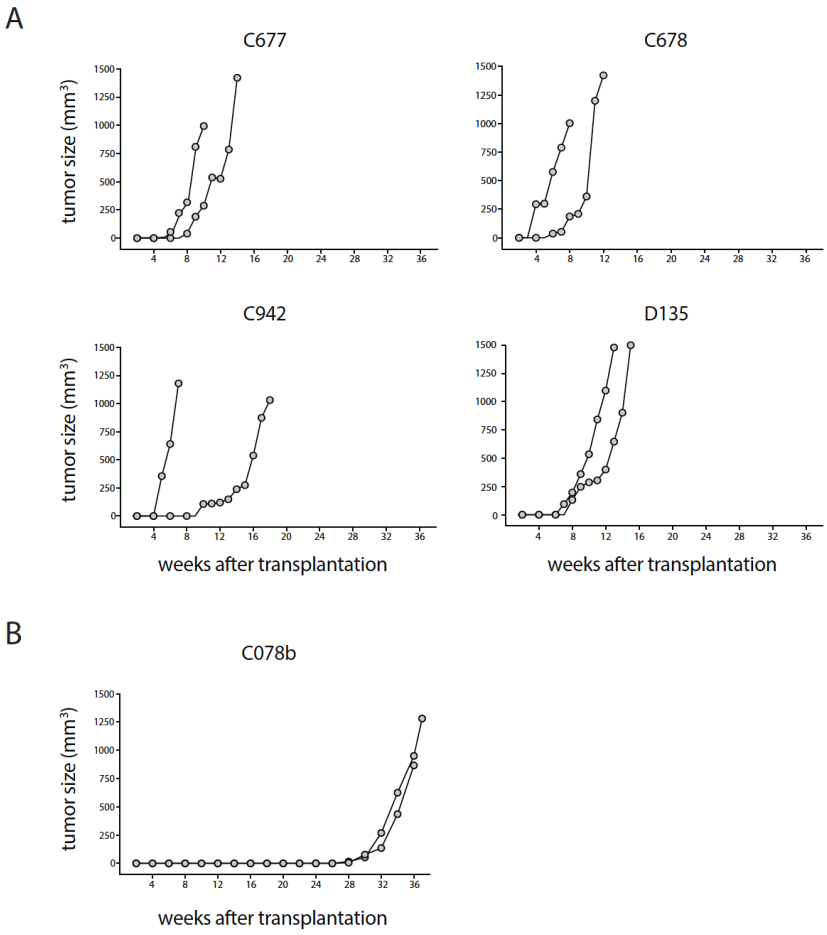

Supplementary Fig. 1. Comparative tumor growth onset of one biopsy cylinder as piece or cell-suspension. (A-B) Comparative tumor growth onset between two subcutaneously transplanted pieces **(A)** or between two suspensions subcutaneously injected from the same donor **(B)**.

Supplementary Figure 2-A
C078b

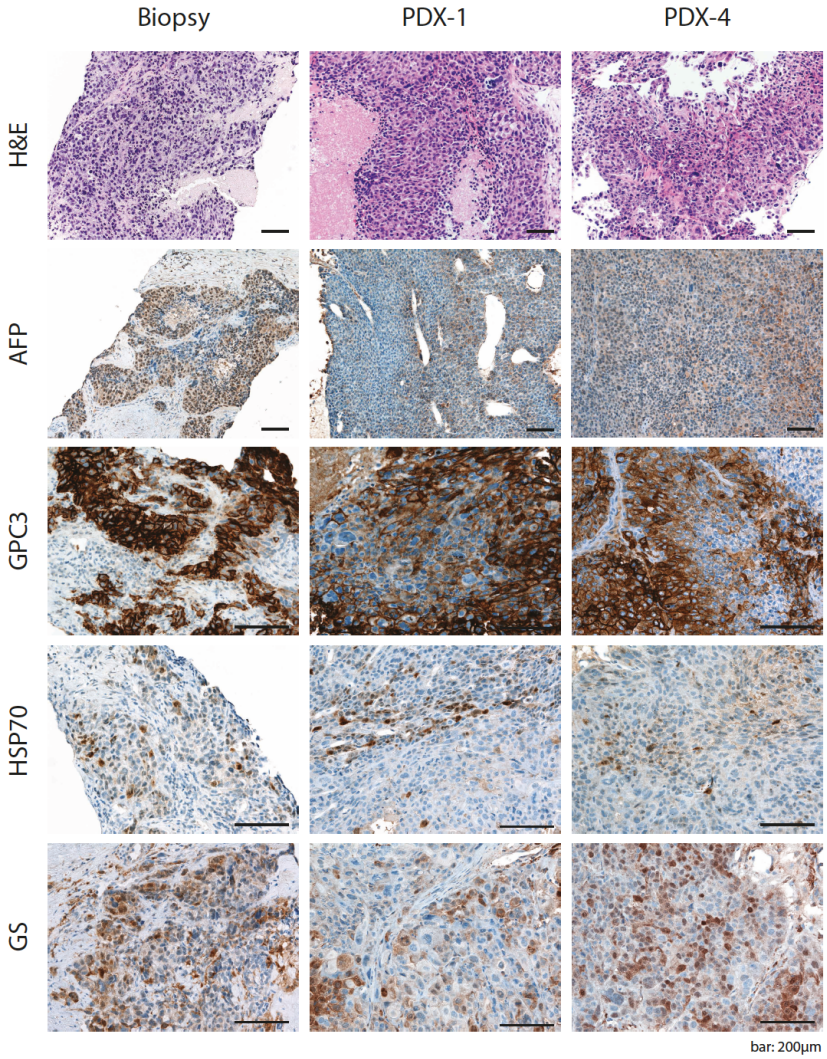

13

Supplementary Figure 2-B
C284b

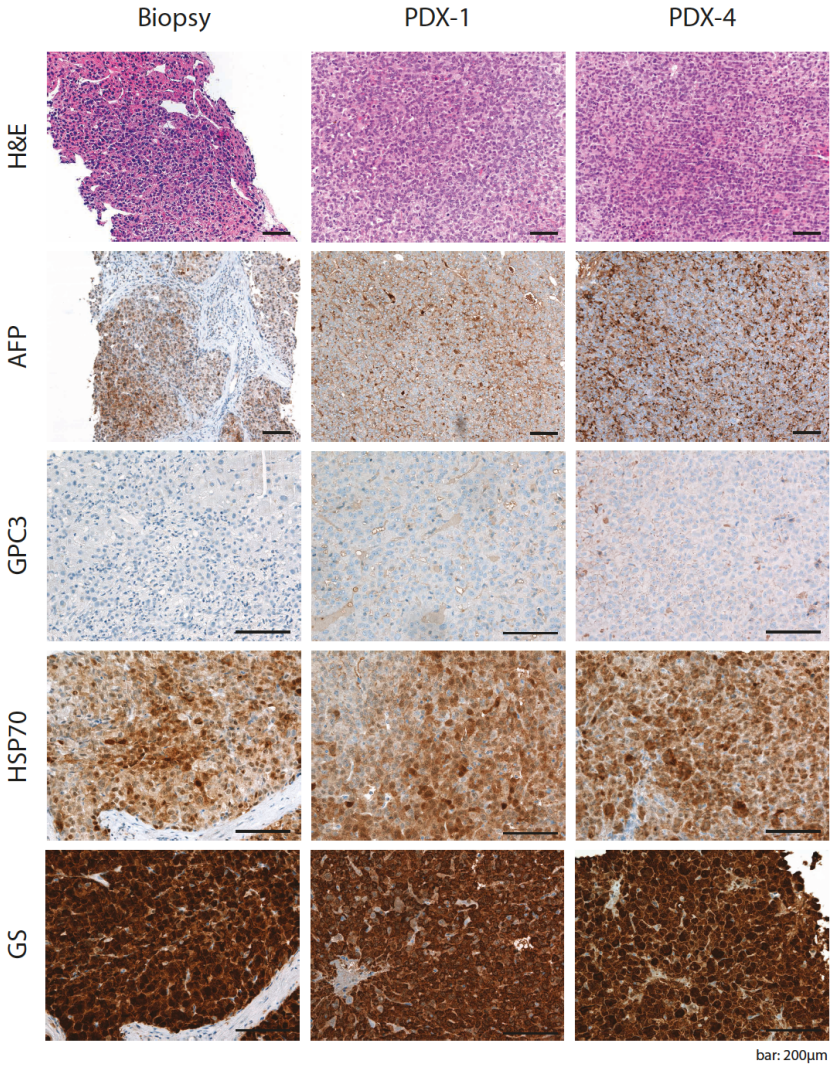

14

Supplementary Figure 2-C
C677

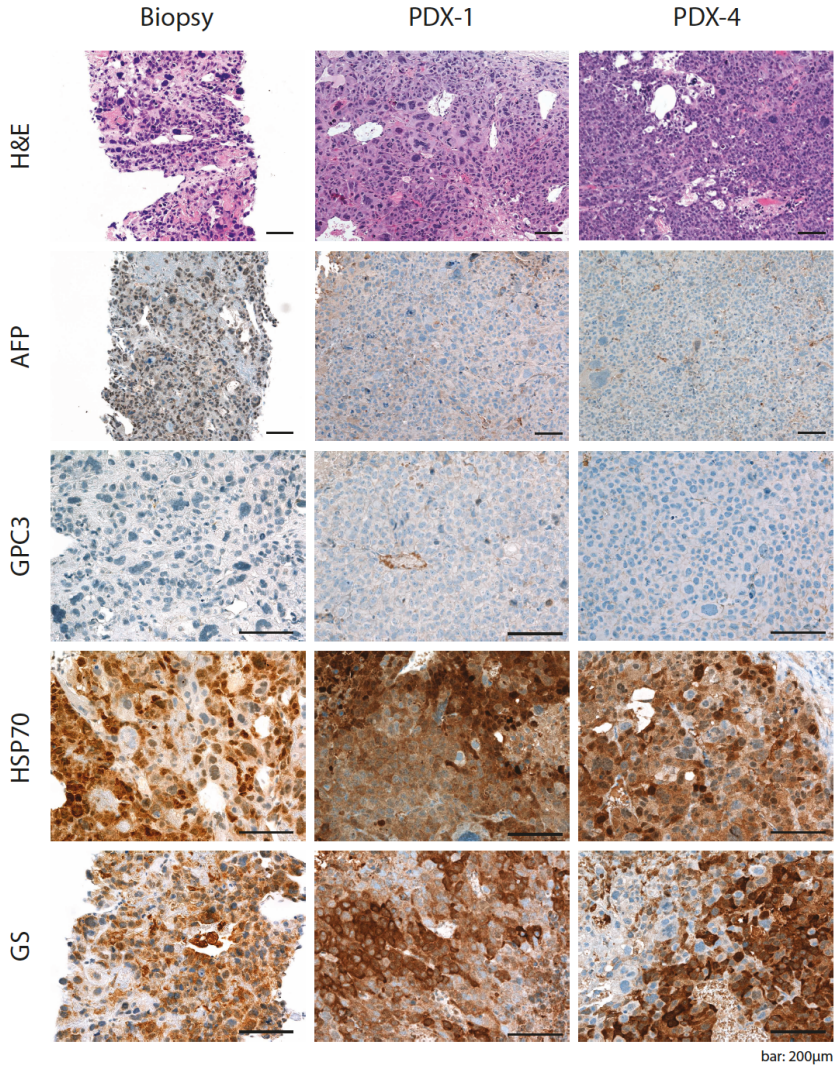

15

Supplementary Figure 2-D
C678

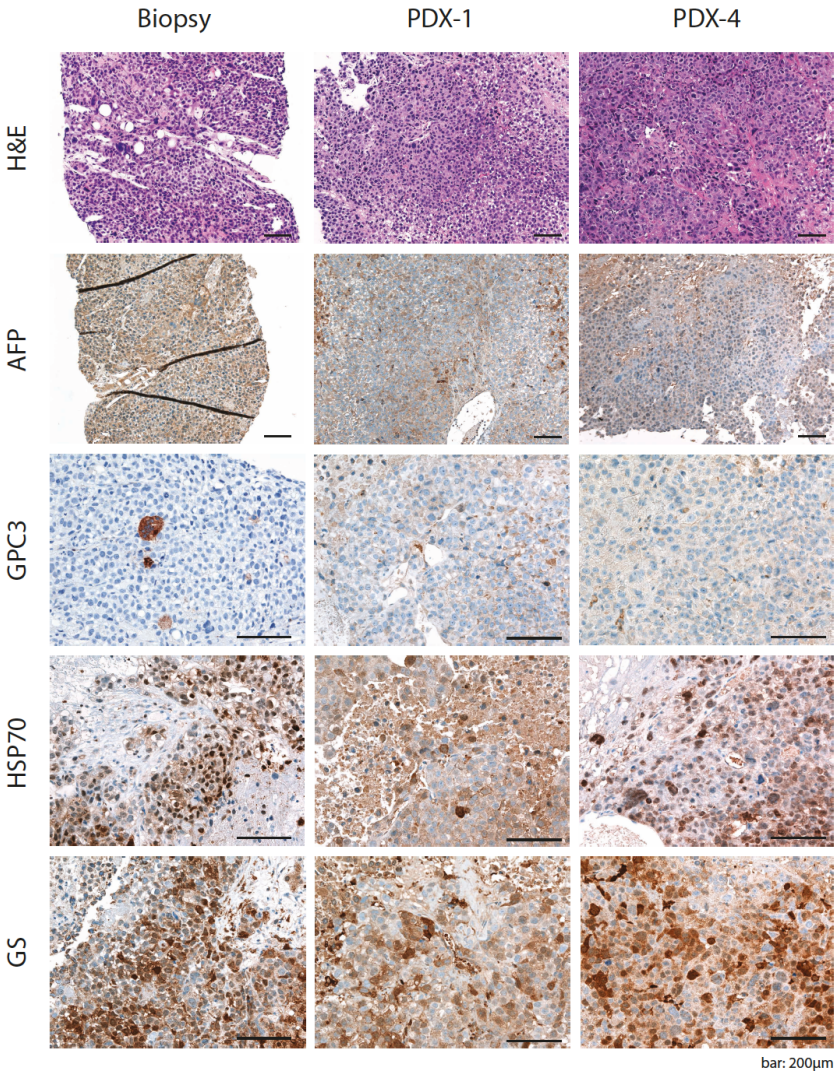

16

Supplementary Figure 2-E
C798

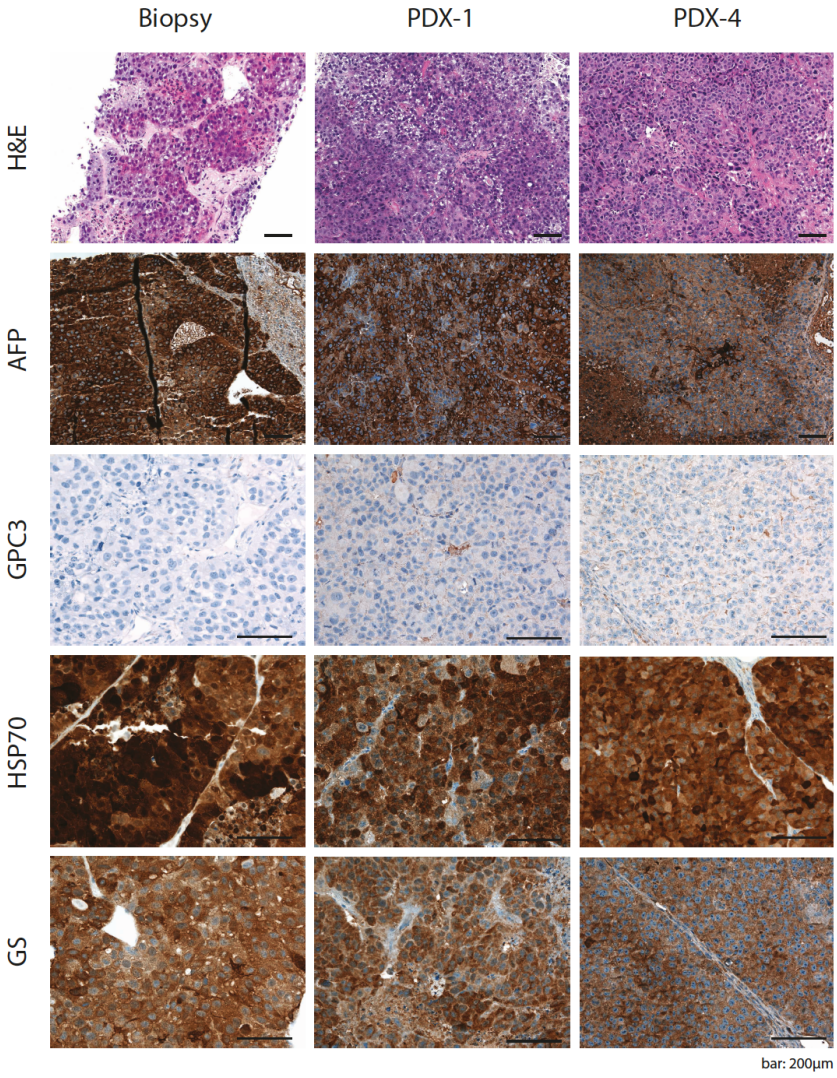

17

Supplementary Figure 2-F
C949

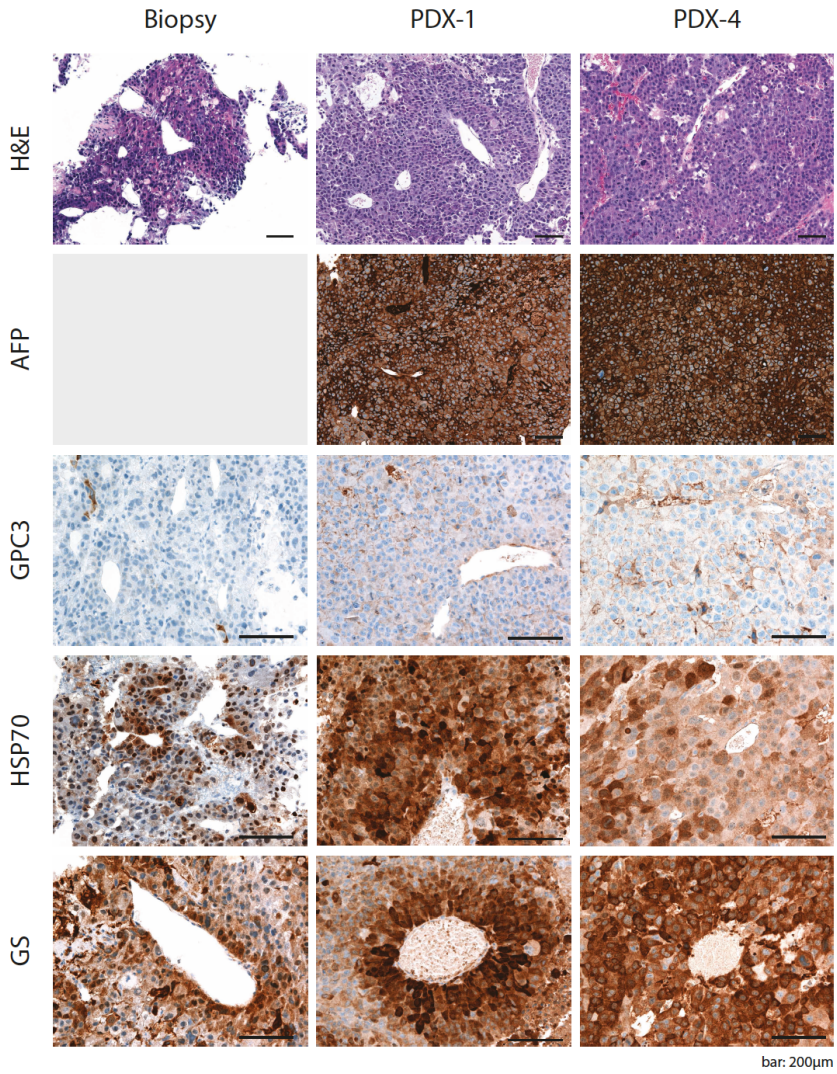

18

Supplementary Figure 2-G
C965

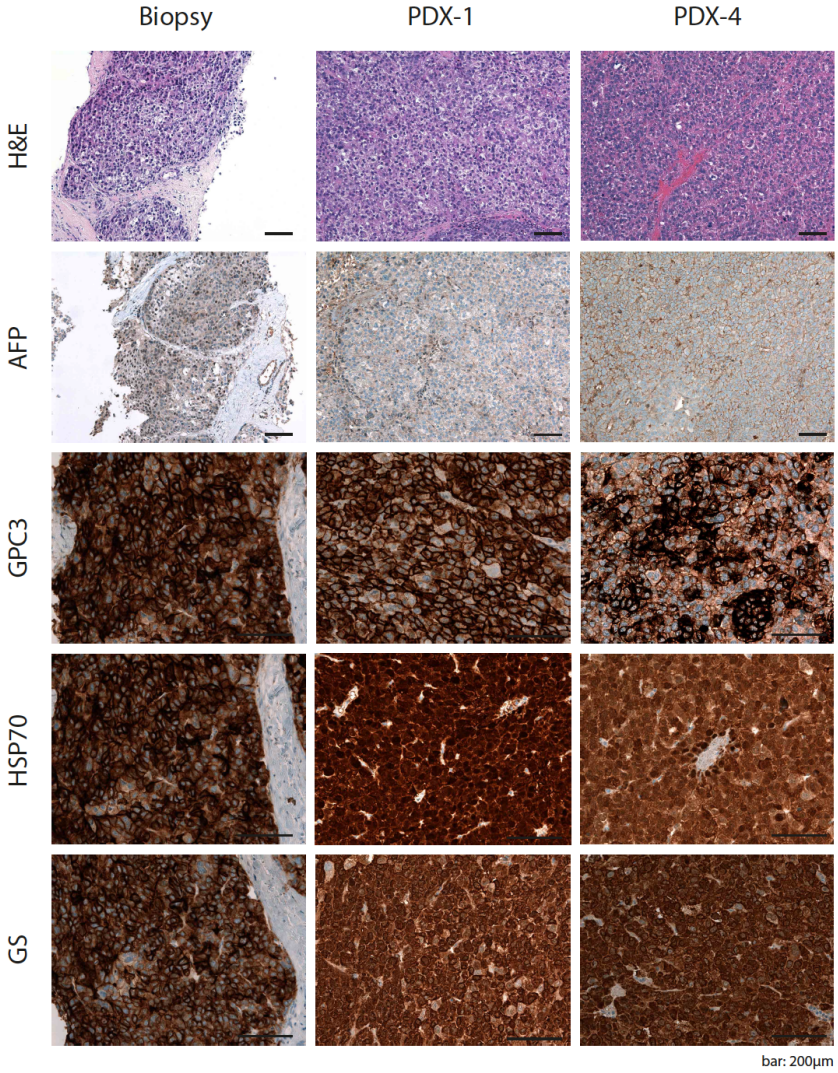

19

Supplementary Figure 2-H
C975

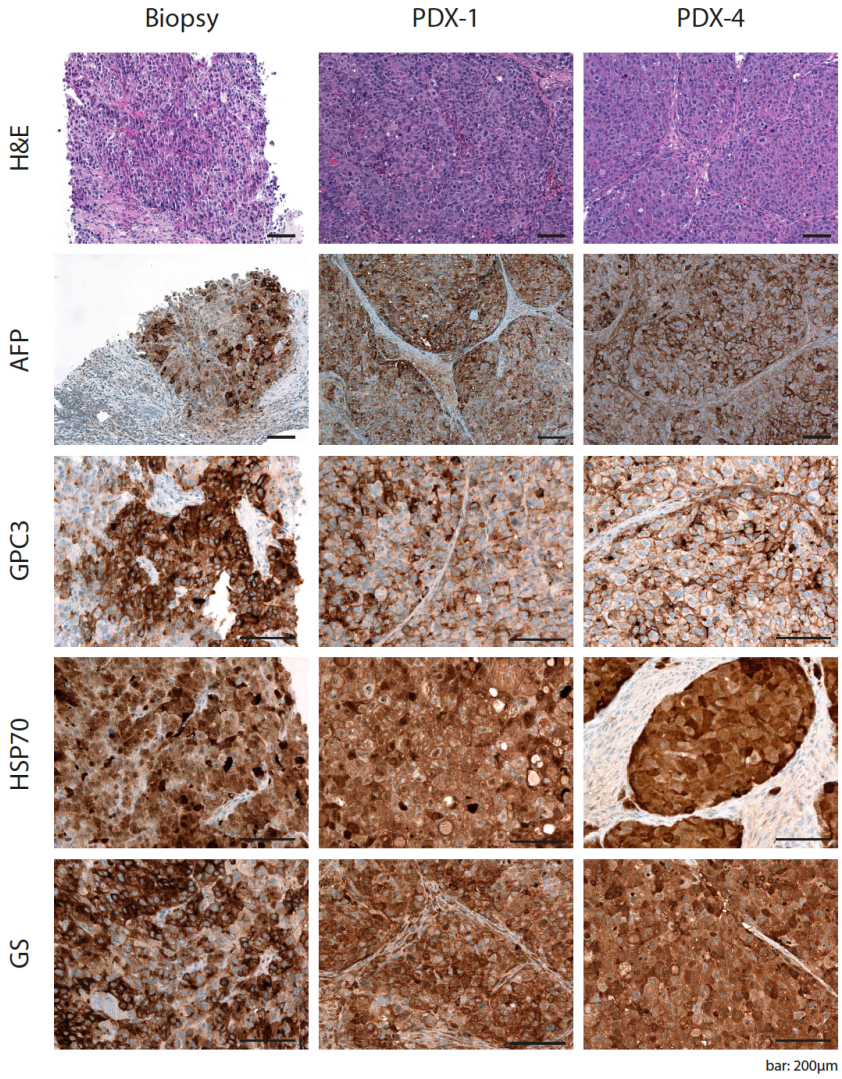

20

Supplementary Figure 2-I
D096

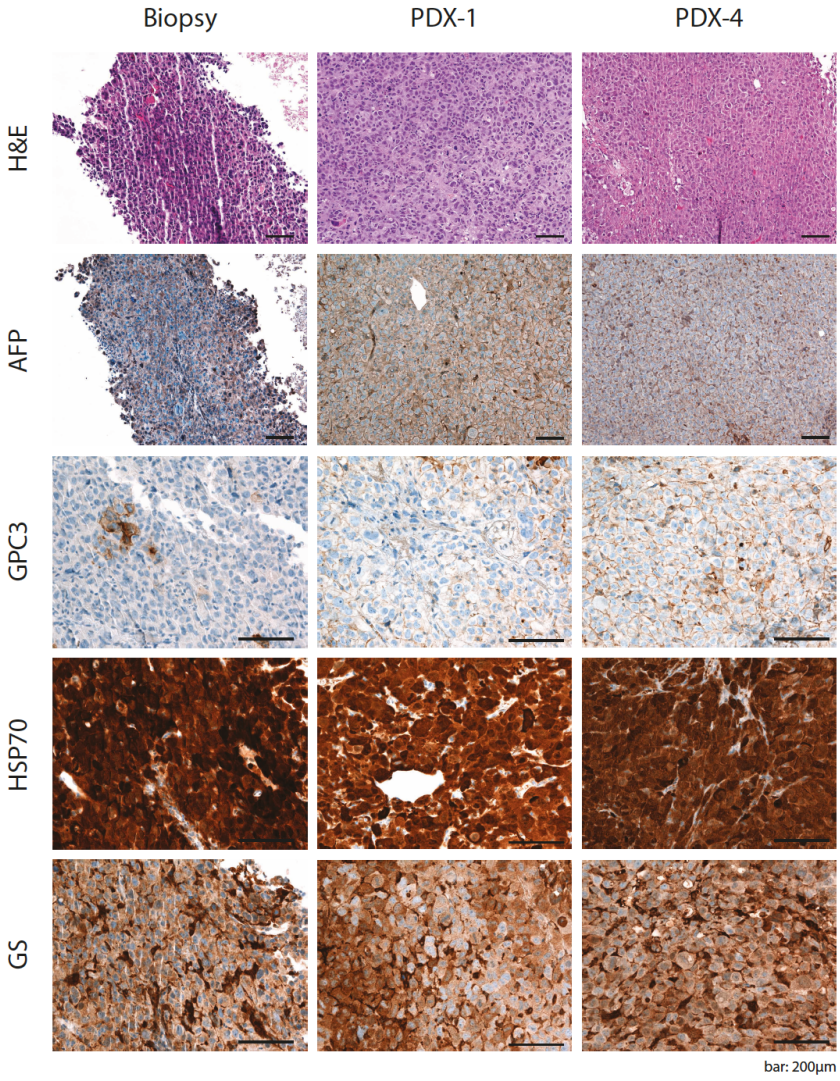

21

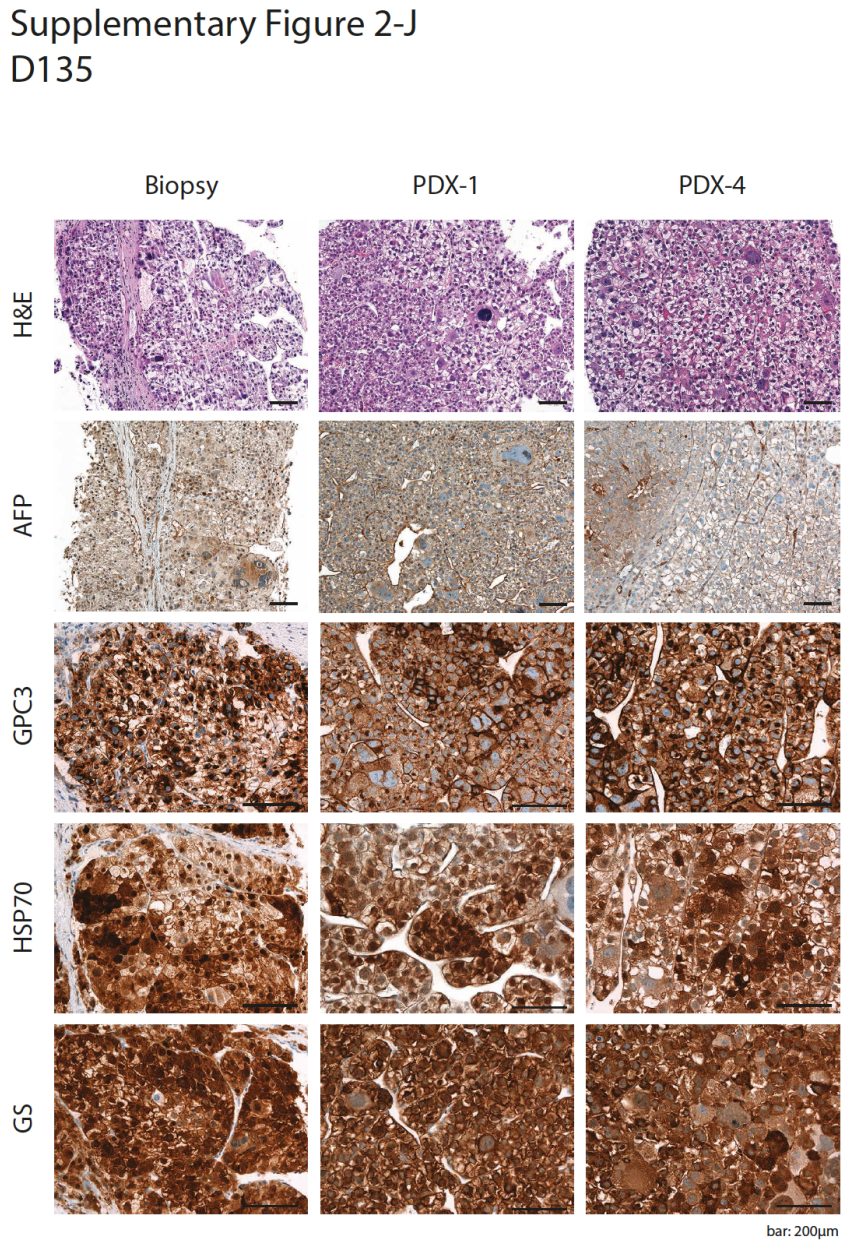

Supplementary Fig. 2A-J. HCC PDX mice retain the histology of the originating tumor. Histological sections of the original HCC biopsies and their derivative PDX tumors (PDX-1 and PDX-4 corresponding to 1st and 4th

transplantation steps, respectively) stained with H&E, for alpha-fetoprotein (AFP) expression as well as for Glypican 3 (GPC3), Heat Shock Protein 70 (HSP70) and Glutamine Synthetase (GS) detected by immunohistochemistry. Scale bar: 200 µm.

Supplementary Figure 3

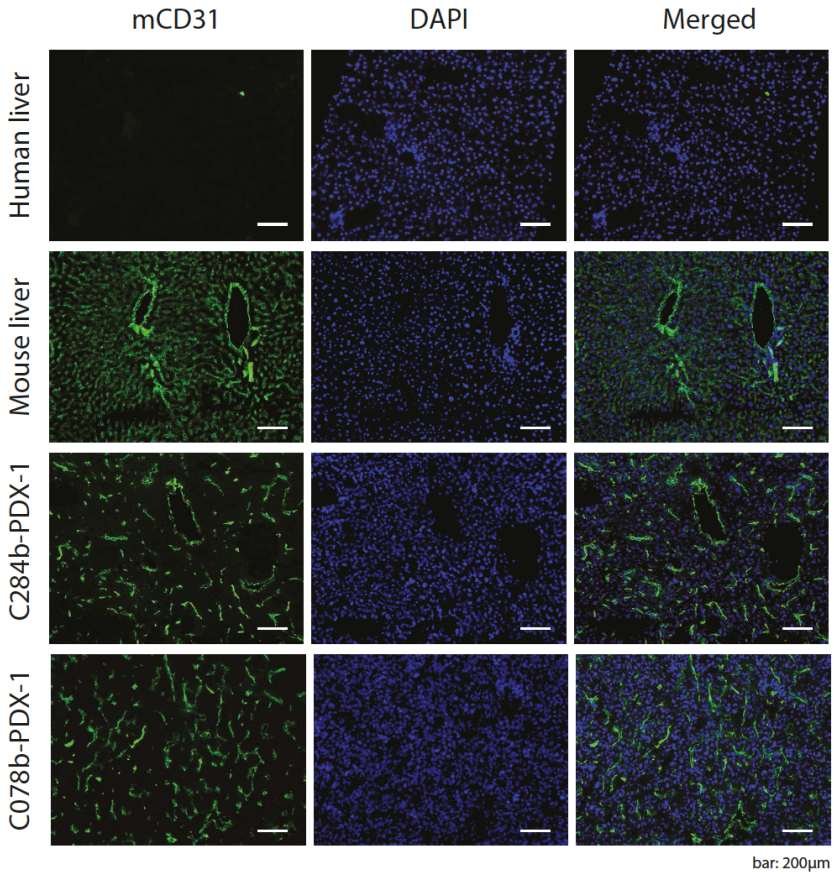

Supplementary Fig. 3. Presence of mouse vessels in HCC PDX models. Human and mouse liver, and two representative PDX tumors from model C078b and C284b were stained with mouse CD31 (mCD31) and DAPI. Scale bar: 200µm.

Supplementary Figure 4

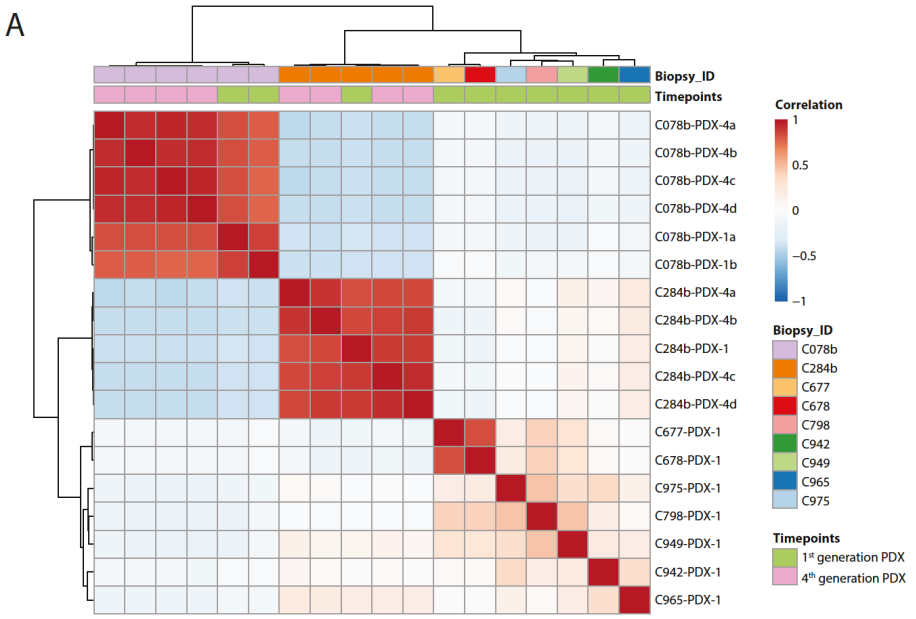

Supplementary Fig. 4. HCC PDX models are stable over at least 4 generations. (A) Unsupervised clustering of 1st and 4th transplantation PDX tumors. **(B)** Repertoire of somatic missense mutations affecting cancer genes [7-10].

References:

[7] **Kandoth C**, **McLellan M**D, Vandin F, Ye K, Niu B, Lu C, et al. Mutational landscape and significance across 12 major cancer types. Nature 2013;502:333-339.

[8] Lawrence MS, Stojanov P, Mermel CH, Robinson JT, Garraway LA, Golub TR, et al. Discovery and saturation analysis of cancer genes across 21 tumour types. Nature 2014;505:495-501.

[9] **Fujimoto A**, **Furuta M**, **Totoki Y**, **Tsunoda T**, **Kato M**, Shiraishi Y, et al. Whole-genome mutational landscape and characterization of noncoding and structural mutations in liver cancer. Nat Genet 2016;48:500-509.

[10] Cancer Genome Atlas Research Network. Electronic address wbe, Cancer Genome Atlas Research N. Comprehensive and Integrative Genomic Characterization of Hepatocellular Carcinoma. Cell 2017;169:1327-1341 e1323.

Supplementary Figure 5

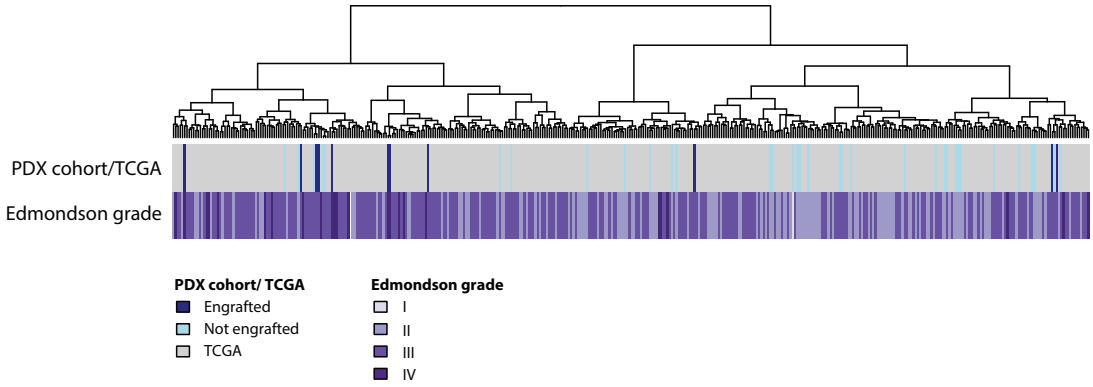

Supplementary Fig. 5. Unsupervised hierarchical clustering analysis of engrafted and not engrafted HCC biopsy (PDX) cohort (this study) combined with all HCCs from the TCGA cohort.

Supplementary Table 1. Clinical annotation and histopathological data of transplanted HCC biopsies.

Patient	Biopsy ID	Gender	Age [years]	BCLC	Cirrhosis	Liver Disease(s)	AFP [IU/ml]	Edmondson	PDX model
1	C078b	F	58	A	Yes	HCV	n.a.	III	yes
2	C255b	M	60	A	Yes	HBV, ALD	1.5	II	-
3	C272b	F	67	A	Yes	HBV, ALD	3.9	III	-
4	C284b	M	78	C	Yes	HBV	5459	III	yes
5	C316b	F	76	A	Yes	NAFLD	144	II	-
6	C334b	M	79	A	No	no liver disease	27856	II	-
7-A	C457b	M	78	A	No	NAFLD	1.7	II	-
7-B	C457c	M	78	A	No	NAFLD	1.7	III	-
8	C475b	M	66	A	Yes	ALD	541	III	-
9	C477b	M	69	A	No	HCV	4.6	II	-
10	C495	M	59	D	Yes	ALD	76	III	-
11	C511	M	66	B	Yes	ALD	4352	III	-
12	C532	F	67	A	Yes	ALD	125	II	-
13	C605	M	48	A	Yes	ALD	1.7	II	-
14	C613	M	67	A	Yes	NAFLD	1.6	II	-
15	C628	F	75	B	Yes	HCV	0.8	II	-
16	C638	M	69	B	Yes	ALD	3.2	II	-
17-A	C655	M	55	C	No	HCV, ALD	269	III	-
17-B	C656	M	55	C	No	HCV, ALD	269	III	-
18-A	C677	F	76	C	No	no liver disease	1.4	IV	yes
18-B	C678	F	76	C	No	no liver disease	1.4	IV	yes
19	C696	M	63	A	No	HCV, HBV, ALD	1.5	II	-
20	C710	M	55	B	Yes	HCV	8.4	I	-
21	C738	F	72	B	Yes	ALD	7.9	III	yes*
22	C753	F	54	D	Yes	ALD	82433	III	-
23	C761	M	61	C	Yes	HCV, ALD	10278	III	-
24	C769	M	59	C	Yes	HCV, ALD	n.a.	III	-
25	C798	M	73	C	No	NAFLD	20377	III	yes
26-A	C850	M	77	C	Yes	ALD	1882	III	-
26-B	C851	M	77	C	Yes	ALD	1882	III	-
27-A	C878	M	61	D	Yes	ALD	1.8	I	-
27-B	C879	M	61	D	Yes	ALD	1.8	II	-
28	C937	M	70	B	Yes	HBV	701	II	-
29-A	C942	M	77	C	Yes	NAFLD	>100'000	III	yes
29-B	C944	M	77	C	Yes	NAFLD	>100'000	III	-
30-A	C948	M	58	C	Yes	HCV, ALD	12054	III	yes*
30-B	C949	M	58	C	Yes	HCV, ALD	12054	III	yes
31	C951	F	71	C	Yes	ALD	1745	III	yes*
32-A	C958	M	54	C	Yes	HCV, ALD	228	III	-
33	C964	M	72	B	Yes	ALD	2.6	III	-
32-B	C965	M	54	C	Yes	HCV, ALD	228	III	yes
34	C971	M	73	B	Yes	HCV	678	II	-
35	C975	M	60	B	Yes	HCV, ALD	250	III	yes
36-I	D045	M	69	A	No	HCV	7852	III	-
36-II	D046	M	69	A	No	HCV	7852	III	-
37	D051	M	86	B	No	ALD	4.3	II	-
38	D070	F	49	A	Yes	HCV, ALD	3.1	II	-
39	D096	M	75	A	No	no liver disease	2	IV	yes
40-A	D135	M	57	C	Yes	HCV	11	IV	yes
40-B	D136	M	57	C	Yes	HCV	11	IV	-
41	D143	F	62	D	Yes	ALD	6.6	III	-
42	D156	M	67	A	Yes	HBV	204	II	-
43	D158	F	77	B	Yes	NAFLD	4.6	II	-
44	D176	M	79	C	No	no liver disease	0.9	II	-

-A/-B: different tumor nodules from same patient
-I/-II: different locations within same large tumor nodule
ALD: Alcoholic Liver Disease
AFP: Alpha-Fetoprotein
BCLC: Barcelona Clinic Liver Cancer
HCC: Hepatocellular Carcinoma
HBV: Hepatitis B Virus
HCV: Hepatitis C Virus
NAFLD: Nonalcoholic Fatty Liver Disease
n.a.: not available
* these biopsies established human B cell lymphomas in the mice

Supplementary Table 2. Histopathological analysis of biopsies. Percentage of tumor content, immune infiltrates, necrosis and non-tumoral tissue were determined in each biopsy on H&E stained sections by an experienced hepato-pathologist (M.S.M.). Biopsies used for whole exome (WES) and RNA sequencing (RNAseq) are indicated. Immune infiltrates were summarized in four different categories: - = 0-1%; + = >1-5%; ++ = >5%-15%; and +++ = >15% of immune infiltrates in the whole biopsy cylinder. n.a.: not available

Patient	Biopsy ID	Tumor content [%]	Immune infiltrates	Necrosis [%]	Non-tumoral [%]	WES	RNAseq
1	C078b	90	n.a.	n.a.	n.a.	yes	yes
2	C255b	70	++	0	30		yes
3	C272b	90	+	5	5		yes
4	C284b	50	++	5	45	yes	yes
5	C316b	90	+	2	8		yes
6	C334b	100	-	0	0		yes
7-A	C457b	60	-	0	40		yes
7-B	C457c	90	+	5	5		yes
8	C475b	95	+	0	5		yes
9	C477b	50	+	2	48		yes
10	C495	60	+	0	40		yes
11	C511	60	n.a.	n.a.	n.a.		yes
12	C532	100	-	0	0		yes
13	C605	95	+	0	5		yes
14	C613	80	-	0	20		yes
15	C628	70	+	0	30		yes
16	C638	95	+	0	5		yes
17-A	C655	10	+	80	10		
17-B	C656	5	n.a.	n.a.	n.a.		
18-A	C677	70	n.a.	n.a.	n.a.	yes	yes
18-B	C678	30	+	50	20	yes	yes
19	C696	80	+	2	18		yes
20	C710	95	+	0	5		yes
21	C738	60	+++	0	40	yes	yes
22	C753	10	-	0	90		
23	C761	10	-	45	45		
24	C769	80	+	0	20		yes
25	C798	70	-	5	25	yes	yes
26-A	C850	95	+	0	5		yes
26-B	C851	95	+	0	5		yes
27-A	C878	<5	-	25	70		
27-B	C879	<5	-	0	95		
28	C937	100	+	0	5		yes
29-A	C942	70	-	15	15	yes	yes
29-B	C944	30	++	0	70		yes
30-A	C948	80	++	0	20	yes	yes
30-B	C949	40	-	30	30	yes	yes
31	C951	80	++	0	20	yes	yes
32-A	C958	40	-	10	50		yes
33	C964	95	+	0	5		yes
32-B	C965	50	++	40	10	yes	yes
34	C971	20	++	0	80		
35	C975	50	+++	0	50	yes	yes
36-I	D045	80	++	10	10		yes
36-II	D046	70	++	20	10		yes
37	D051	90	+	2	8		yes
38	D070	70	++	0	30		yes
39	D096	40	-	60	0	yes	yes
40-A	D135	80	+	0	20	yes	yes
40-B	D136	5	+	0	95		
41	D143	40	+++	0	60		
42	D156	95	+	0	5		yes
43	D158	70	-	0	30		yes
44	D176	95	+	0	5		yes

Supplementary Table 3. List of differentially expressed genes in HCC PDX models compared to HCC biopsies.

Click here to download Supplementary material: Table S3.xlsx

Supplementary Table 4. Pathways enriched among genes down-regulated and up-regulated in HCC PDX tumors compared to HCC biopsies.

Pathways enriched among genes down-regulated in PDX			
Pathway name	**p-value**	**FDR**	**Pathway description**
HALLMARK_EPITHELIAL_MESENCHYMAL_TRANSITION	9.33E-29	4.66E-27	Genes defining epithelial-mesenchymal transition, as in wound healing, fibrosis and metastasis.
HALLMARK_INFLAMMATORY_RESPONSE	8.01E-23	2.00E-21	Genes defining inflammatory response.
HALLMARK_ALLOGRAFT_REJECTION	1.96E-21	3.27E-20	Genes up-regulated during transplant rejection.
HALLMARK_INTERFERON_GAMMA_RESPONSE	1.17E-15	1.46E-14	Genes up-regulated in response to IFNG [GeneID=3458].
HALLMARK_KRAS_SIGNALING_UP	4.55E-15	4.55E-14	Genes up-regulated by KRAS activation.
HALLMARK_IL2_STAT5_SIGNALING	8.36E-13	6.97E-12	Genes up-regulated by STAT5 in response to IL2 stimulation.
HALLMARK_IL6_JAK_STAT3_SIGNALING	1.41E-10	1.00E-09	Genes up-regulated by IL6 [GeneID=3569] via STAT3 [GeneID=6774], e.g., during acute phase response.
HALLMARK_COMPLEMENT	9.98E-10	6.24E-09	Genes encoding components of the complement system, which is part of the innate immune system.
HALLMARK_COAGULATION	1.07E-07	5.96E-07	Genes encoding components of blood coagulation system; also up-regulated in platelets.
HALLMARK_UV_RESPONSE_DN	1.01E-06	5.05E-06	Genes down-regulated in response to ultraviolet (UV) radiation.
HALLMARK_TNFA_SIGNALING_VIA_NFKB	2.94E-06	1.34E-05	Genes regulated by NF-kB in response to TNF [GeneID=7124].
HALLMARK_MYOGENESIS	7.05E-06	2.94E-05	Genes involved in development of skeletal muscle (myogenesis).
HALLMARK_APICAL_JUNCTION	0.000174	0.00067	Genes encoding components of apical junction complex.
HALLMARK_APOPTOSIS	0.000451	0.0016108	Genes mediating programmed cell death (apoptosis) by activation of caspases.
HALLMARK_ANGIOGENESIS	0.001032	0.0034392	Genes up-regulated during formation of blood vessels (angiogenesis).
HALLMARK_INTERFERON_ALPHA_RESPONSE	0.003175	0.0099234	Genes up-regulated in response to alpha interferon proteins.
HALLMARK_HYPOXIA	0.004843	0.0142442	Genes up-regulated in response to low oxygen levels (hypoxia).
HALLMARK_HEDGEHOG_SIGNALING	0.034786	0.0966285	Genes up-regulated by activation of hedgehog signaling.
HALLMARK_APICAL_SURFACE	0.04232	0.1113687	Genes encoding proteins over-represented on the apical surface of epithelial cells, e.g., important for cell polarity (apical area).
HALLMARK_MITOTIC_SPINDLE	0.060029	0.1500716	Genes important for mitotic spindle assembly.

Pathways enriched among genes up-regulated in PDX			
Pathway name	**p-value**	**FDR**	**Pathway description**
HALLMARK_E2F_TARGETS	1.36E-48	6.82E-47	Genes encoding cell cycle related targets of E2F transcription factors.
HALLMARK_MYC_TARGETS_V1	1.35E-47	3.37E-46	A subgroup of genes regulated by MYC - version 1 (v1).
HALLMARK_G2M_CHECKPOINT	3.20E-31	5.34E-30	Genes involved in the G2/M checkpoint, as in progression through the cell division cycle.
HALLMARK_OXIDATIVE_PHOSPHORYLATION	5.62E-13	7.03E-12	Genes encoding proteins involved in oxidative phosphorylation.
HALLMARK_MTORC1_SIGNALING	2.80E-09	2.80E-08	Genes up-regulated through activation of mTORC1 complex.
HALLMARK_DNA_REPAIR	3.45E-07	2.88E-06	Genes involved in DNA repair.
HALLMARK_MYC_TARGETS_V2	3.57E-06	2.55E-05	A subgroup of genes regulated by MYC - version 2 (v2).
HALLMARK_MITOTIC_SPINDLE	0.001044	0.0065221	Genes important for mitotic spindle assembly.
HALLMARK_SPERMATOGENESIS	0.015034	0.0835195	Genes up-regulated during production of male gametes (sperm), as in spermatogenesis.

Supplementary Table 5. Expression of somatic mutations in human HCC biopsy and corresponding PDX tumors. Somatic mutations were identified in the human HCC biopsies by whole exome sequencing and their expression was assessed in the HCC biopsies and their corresponding PDX tumors using RNA sequencing data. WES: whole exome sequencing. SMG: significantly mutated genes.

Click here to download Supplementary material: Table S5.xlsx

Supplementary Table 6. Pathways enriched among genes up-regulated or down-regulated in biopsies that engrafted compared to biopsies that did not engraft.

Pathways enriched among genes up-regulated in biopsies that engrafted			
Pathway name	**p-value**	**FDR**	**Pathway description**
HALLMARK_E2F_TARGETS	2.49E-52	1.24E-50	Genes encoding cell cycle related targets of E2F transcription factors.
HALLMARK_G2M_CHECKPOINT	2.30E-50	5.75E-49	Genes involved in the G2/M checkpoint, as in progression through the cell division cycle.
HALLMARK_MITOTIC_SPINDLE	2.56E-17	3.21E-16	Genes important for mitotic spindle assembly.
HALLMARK_MYC_TARGETS_V1	2.56E-17	3.21E-16	A subgroup of genes regulated by MYC - version 1 (v1).
HALLMARK_EPITHELIAL_MESENCHYMAL_TRANSITION	6.61E-14	6.61E-13	Genes defining epithelial-mesenchymal transition, as in wound healing, fibrosis and metastasis.
HALLMARK_HYPOXIA	2.26E-10	1.89E-09	Genes up-regulated in response to low oxygen levels (hypoxia).
HALLMARK_MTORC1_SIGNALING	3.33E-06	2.38E-05	Genes up-regulated through activation of mTORC1 complex.
HALLMARK_MYC_TARGETS_V2	8.73E-05	0.0005458	A subgroup of genes regulated by MYC - version 2 (v2).
HALLMARK_GLYCOLYSIS	0.00112945	0.00627471	Genes encoding proteins involved in glycolysis and gluconeogenesis.
HALLMARK_ANGIOGENESIS	0.00144402	0.00722009	Genes up-regulated during formation of blood vessels (angiogenesis).
HALLMARK_UV_RESPONSE_DN	0.00317294	0.01442248	Genes down-regulated in response to ultraviolet (UV) radiation.
HALLMARK_TNFA_SIGNALING_VIA_NFKB	0.00367897	0.01532902	Genes regulated by NF-kB in response to TNF [GeneID=7124].
HALLMARK_ESTROGEN_RESPONSE_EARLY	0.00636121	0.0244662	Genes defining early response to estrogen.
HALLMARK_UNFOLDED_PROTEIN_RESPONSE	0.01029082	0.03675292	Genes up-regulated during unfolded protein response, a cellular stress response related to the endoplasmic reticulum.
HALLMARK_UV_RESPONSE_UP	0.01270011	0.04233369	Genes up-regulated in response to ultraviolet (UV) radiation.
HALLMARK_APICAL_JUNCTION	0.01743279	0.05447747	Genes encoding components of apical junction complex.
HALLMARK_IL2_STAT5_SIGNALING	0.02761697	0.08122639	Genes up-regulated by STAT5 in response to IL2 stimulation.
HALLMARK_PI3K_AKT_MTOR_SIGNALING	0.02936448	0.081568	Genes up-regulated by activation of the PI3K/AKT/mTOR pathway.
HALLMARK_WNT_BETA_CATENIN_SIGNALING	0.04055352	0.10618775	Genes up-regulated by activation of WNT signaling through accumulation of beta catenin CTNNB1 [GeneID=1499].
HALLMARK_ESTROGEN_RESPONSE_LATE	0.0424751	0.10618775	Genes defining late response to estrogen.
HALLMARK_TGF_BETA_SIGNALING	0.08688163	0.20686102	Genes up-regulated in response to TGFB1 [GeneID=7040].

Pathways enriched among genes down-regulated in biopsies that engrafted			
Pathway name	**p-value**	**FDR**	**Pathway description**
HALLMARK_XENOBIOTIC_METABOLISM	7.84E-30	3.92E-28	Genes encoding proteins involved in processing of drugs and other xenobiotics.
HALLMARK_FATTY_ACID_METABOLISM	1.86E-21	4.65E-20	Genes encoding proteins involved in metabolism of fatty acids.
HALLMARK_BILE_ACID_METABOLISM	7.49E-18	1.25E-16	Genes involve in metabolism of bile acids and salts.
HALLMARK_COAGULATION	1.58E-13	1.97E-12	Genes encoding components of blood coagulation system; also up-regulated in platelets.
HALLMARK_ADIPOGENESIS	3.75E-13	3.13E-12	Genes up-regulated during adipocyte differentiation (adipogenesis).
HALLMARK_OXIDATIVE_PHOSPHORYLATION	3.75E-13	3.13E-12	Genes encoding proteins involved in oxidative phosphorylation.
HALLMARK_PEROXISOME	1.93E-10	1.38E-09	Genes encoding components of peroxisome.
HALLMARK_INTERFERON_ALPHA_RESPONSE	5.23E-05	0.00032687	Genes up-regulated in response to alpha interferon proteins.
HALLMARK_INTERFERON_GAMMA_RESPONSE	0.00019358	0.00107546	Genes up-regulated in response to IFNG [GeneID=3458].
HALLMARK_HEME_METABOLISM	0.00384143	0.01920713	Genes involved in metabolism of heme (a cofactor consisting of iron and porphyrin) and erythroblast differentiation.
HALLMARK_COMPLEMENT	0.02401692	0.10916784	Genes encoding components of the complement system, which is part of the innate immune system.

Supplementary Table 7. Pathways enriched among genes up-regulated or down-regulated in the lymphoid PDX tumor compared to HCC biopsies and HCC PDX tumors.

Pathways enriched among genes up-regulated in the lymphoid PDX tumors			
Pathway name	**p-value**	**FDR**	**Pathway description**
HALLMARK_INTERFERON_GAMMA_RESPONSE	5.22E-25	2.61E-23	Genes up-regulated in response to IFNG [GeneID=3458].
HALLMARK_ALLOGRAFT_REJECTION	2.79E-24	6.97E-23	Genes up-regulated during transplant rejection.
HALLMARK_INTERFERON_ALPHA_RESPONSE	1.35E-12	2.25E-11	Genes up-regulated in response to alpha interferon proteins.
HALLMARK_TNFA_SIGNALING_VIA_NFKB	8.08E-09	1.01E-07	Genes regulated by NF-kB in response to TNF [GeneID=7124].
HALLMARK_E2F_TARGETS	2.29E-08	2.29E-07	Genes encoding cell cycle related targets of E2F transcription factors.
HALLMARK_INFLAMMATORY_RESPONSE	4.42E-07	3.68E-06	Genes defining inflammatory response.
HALLMARK_G2M_CHECKPOINT	6.67E-06	4.76E-05	Genes involved in the G2/M checkpoint, as in progression through the cell division cycle.
HALLMARK_IL2_STAT5_SIGNALING	3.53E-05	0.00022042	Genes up-regulated by STAT5 in response to IL2 stimulation.
HALLMARK_IL6_JAK_STAT3_SIGNALING	9.83E-05	0.00054632	Genes up-regulated by IL6 [GeneID=3569] via STAT3 [GeneID=6774], e.g., during acute phase response.
HALLMARK_COMPLEMENT	0.00016591	0.00075412	Genes encoding components of the complement system, which is part of the innate immune system.
HALLMARK_P53_PATHWAY	0.00016591	0.00075412	Genes involved in p53 pathways and networks.
HALLMARK_PI3K_AKT_MTOR_SIGNALING	0.00026204	0.00109182	Genes up-regulated by activation of the PI3K/AKT/mTOR pathway.
HALLMARK_MYC_TARGETS_V1	0.00069163	0.00266012	A subgroup of genes regulated by MYC - version 1 (v1).
HALLMARK_APOPTOSIS	0.00091846	0.00328023	Genes mediating programmed cell death (apoptosis) by activation of caspases.

Pathways enriched among genes down-regulated in the lymphoid PDX tumors			
Pathway name	**p-value**	**FDR**	**Pathway description**
HALLMARK_XENOBIOTIC_METABOLISM	7.31E-26	3.66E-24	Genes encoding proteins involved in processing of drugs and other xenobiotics.
HALLMARK_COAGULATION	8.58E-25	2.15E-23	Genes encoding components of blood coagulation system; also up-regulated in platelets.
HALLMARK_EPITHELIAL_MESENCHYMAL_TRANSITION	8.87E-22	1.48E-20	Genes defining epithelial-mesenchymal transition, as in wound healing, fibrosis and metastasis.
HALLMARK_ESTROGEN_RESPONSE_EARLY	1.07E-15	1.34E-14	Genes defining early response to estrogen.
HALLMARK_ESTROGEN_RESPONSE_LATE	5.02E-11	5.02E-10	Genes defining late response to estrogen.
HALLMARK_BILE_ACID_METABOLISM	6.23E-09	5.19E-08	Genes involve in metabolism of bile acids and salts.
HALLMARK_HYPOXIA	8.94E-09	6.39E-08	Genes up-regulated in response to low oxygen levels (hypoxia).
HALLMARK_APICAL_JUNCTION	2.35E-08	1.47E-07	Genes encoding components of apical junction complex.
HALLMARK_GLYCOLYSIS	6.03E-08	3.35E-07	Genes encoding proteins involved in glycolysis and gluconeogenesis.
HALLMARK_ANGIOGENESIS	2.85E-07	1.42E-06	Genes up-regulated during formation of blood vessels (angiogenesis).
HALLMARK_ADIPOGENESIS	3.70E-07	1.68E-06	Genes up-regulated during adipocyte differentiation (adipogenesis).
HALLMARK_UV_RESPONSE_DN	6.13E-07	2.55E-06	Genes down-regulated in response to ultraviolet (UV) radiation.
HALLMARK_MYOGENESIS	2.05E-06	7.89E-06	Genes involved in development of skeletal muscle (myogenesis).
HALLMARK_ANDROGEN_RESPONSE	8.65E-05	0.00030895	Genes defining response to androgens.
HALLMARK_KRAS_SIGNALING_UP	9.61E-05	0.00032027	Genes up-regulated by KRAS activation.
HALLMARK_COMPLEMENT	0.00019191	0.00059972	Genes encoding components of the complement system, which is part of the innate immune system.
HALLMARK_UV_RESPONSE_UP	0.00022469	0.00066084	Genes up-regulated in response to ultraviolet (UV) radiation.
HALLMARK_CHOLESTEROL_HOMEOSTASIS	0.0003467	0.00096305	Genes involved in cholesterol homeostasis.
HALLMARK_PEROXISOME	0.00086454	0.00227511	Genes encoding components of peroxisome.
HALLMARK_FATTY_ACID_METABOLISM	0.00093519	0.00233798	Genes encoding proteins involved in metabolism of fatty acids.
HALLMARK_TGF_BETA_SIGNALING	0.00221892	0.00528314	Genes up-regulated in response to TGFB1 [GeneID=7040].
HALLMARK_P53_PATHWAY	0.00408748	0.00928974	Genes involved in p53 pathways and networks.
HALLMARK_APOPTOSIS	0.00469039	0.01019651	Genes mediating programmed cell death (apoptosis) by activation of caspases.
HALLMARK_APICAL_SURFACE	0.01514561	0.03155336	Genes encoding proteins over-represented on the apical surface of epithelial cells, e.g., important for cell polarity (apical area).
HALLMARK_HEME_METABOLISM	0.01843099	0.03544422	Genes involved in metabolism of heme (a cofactor consisting of iron and porphyrin) and erythroblast differentiation.
HALLMARK_IL2_STAT5_SIGNALING	0.01843099	0.03544422	Genes up-regulated by STAT5 in response to IL2 stimulation.
HALLMARK_NOTCH_SIGNALING	0.02746076	0.05085326	Genes up-regulated by activation of Notch signaling.
HALLMARK_REACTIVE_OXIGEN_SPECIES_PATHWAY	0.03428877	0.06122995	Genes up-regulated by reactive oxigen species (ROS).
HALLMARK_IL6_JAK_STAT3_SIGNALING	0.05438653	0.09376988	Genes up-regulated by IL6 [GeneID=3569] via STAT3 [GeneID=6774], e.g., during acute phase response.
HALLMARK_WNT_BETA_CATENIN_SIGNALING	0.06006921	0.10011536	Genes up-regulated by activation of WNT signaling through accumulation of beta catenin CTNNB1 [GeneID=1499].
HALLMARK_TNFA_SIGNALING_VIA_NFKB	0.06449537	0.10402479	Genes regulated by NF-kB in response to TNF [GeneID=7124].
HALLMARK_HEDGEHOG_SIGNALING	0.12035863	0.18806035	Genes up-regulated by activation of hedgehog signaling.

Supplementary Table 8. Summary of RNA sequencing reads aligned against human and mouse CD20, and to the genome of EBV.

Read Counts per QuasR Rbowtie alignment to mRNA sequence

RPKM

	CD20	
	human	**mouse**
Xenograft	NM_152866.2	NM_007641.5
C738-PDX-1	0.10073	0.00004
C948-PDX-1	0.06149	0.00003
C951-PDX-1	0.09700	neg
C975-PDX-1	0.00002	neg

			EBV* HHV-4	
Biopsy/Xenograft		**Total Reads**	NC_009334 / NC_007605	RPM
C736	non Tumor	100'851'444	0	neg
C738	Tumor	78'938'981	0	neg
C738-PDX-1	Xenograft	50'203'401	12'760	254.17
C947	non Tumor	52'983'481	0	neg
C948	Tumor	60'538'859	0	neg
C948-PDX-1	Xenograft	45'460'391	6'210	136.60
C950	non Tumor	49'377'190	0	neg
C951	Tumor	51'071'193	0	neg
C951-PDX-1	Xenograft	56'915'236	2'098	36.86
C078-PDX-1a	Xenograft	58'263'254	0	neg
C078-PDX-1b	Xenograft	69'004'021	0	neg
C284-PDX-1	Xenograft	57'165'620	0	neg
C677-PDX-1	Xenograft	49'633'842	3	0.06
C678-PDX-1	Xenograft	40'100'082	1	0.02
C798-PDX-1	Xenograft	52'227'184	16	0.31
C942-PDX-1	Xenograft	47'495'346	0	neg
C949-PDX-1	Xenograft	43'840'074	1	0.02
C965-PDX-1	Xenograft	44'723'122	3	0.07
C975-PDX-1	Xenograft	49'521'217	1	0.02

Remarks:

- no alignment quality control

* alignment to EBV genomic DNA, spliced transcripts not included

EBV aligned reads cover regions of EBNA-2; EBNA-3A,B,C and LF3 and also LMP1

PubMed: 20494113. **Klein G**, **Klein E**, **Kashuba E**. 2010. Interaction of Epstein-Barr virus (EBV) with human B-lymphocytes. Biochem Biophys Res Commun **396**:67–73.

IV Discussion

1 Research article I

IFNs are produced upon viral infection and induce an antiviral state to block viral replication and spread. Type I and III IFNs provide an important first line of defence through the fast induction of hundreds of ISGs who collectively establish an antiviral state[100]. This host response has to be negatively regulated at some point to maintain tissue homeostasis. Several clinical autoimmune diseases, such as Aicardi-Goutieres syndrome, systemic erythematosus and pseudo-TORCH syndrome, are associated with an uncontrolled type I IFN system highlighting the importance of negative regulation to maintain equiblibrium[107,108,179].

Despite extensive literature on the negative regulation of the IFN signaling, several aspects are still unclear or a matter of controversy, especially concerning the regulation of type III IFNs. For example, the role of SOCS1 and SOCS3 on IFN-λ signaling was only addressed in overexpression experiments, showing that both are negative regulators of IFN-λ signaling[157-159]. However, whether physiological expression levels of SOCS1 and/or SOCS3 are sufficient to inhibit IFN-λ signaling remained to be investigated. Furthermore, the role of USP18 on type III IFN is still a matter of debate[147,173,178] and needed further clarification. In the present study, we investigated the negative regulatory role of SOCS1, SOCS3 and USP18 in type I and III IFN signaling.

Although type I and type III IFNs signal through distinct receptors, they induce largely overlapping sets of ISGs[342]. However, at least in cell culture, IFN-α and IFN-λ mediated ISG induction followed distinct kinetic profiles. IFN-α triggers an immediate and strong but very transient ISG response, while IFN-λ provides long-lasting JAK-STAT activation and ISG induction[100,342,343]. The different activation patterns can in part be attributed to differences in negative regulation. SOCS1 and SOCS3 were shown to be early negative regulators of IFN-α induced JAK-STAT signaling[145,153]. Nevertheless, their role on IFN-α induced signaling is limited as shown in the present study and by previous reports[148,344]. Using knockout cells, and mice, we demonstrated that USP18, rather than SOCS1 and SOCS3 play a major role in regulating the IFN-α induced signaling cascade (Figures 3, 4, 5 and 6, research article I). With a luciferase reporter assay, we demonstrated that IFN-α signaling was enhanced in USP18 knockout compared to control cells at 4, 8 and 24

hours (Figure 3, research article I). Furthermore, we show significantly higher ISG expression levels in USP18 knockout cells compared to control cells upon IFN-α stimulation at 8 and 24 hours (Figures 4 and S3, research article I). To further test if our results obtained in cell lines are also valid *in vivo*, we investigated the IFN-α signaling in mice deficient for Usp18 and the corresponding control mice. We analysed the ISG induction upon IFN-α injection in the mouse liver, lung and gut. All tested ISGs were significantly higher expressed in the liver and the lung of Usp18 deficient mice compared to control mice (Figures 6 and S4, research article I). This effect was visible but less pronounced in the gut. This could be explained by lower Usp18 expression levels in the gut compared to the liver and the lung at the time points analyzed. In contrast to USP18, the effect of SOCS1 on IFN-α induced signaling was minor (Figures 3, 4 and 5, research article I). These results fit to the finding that *Socs1* knockout mice are hypersensitive to IFN-γ, demonstrating the main role of SOCS1 is the negative regulation of IFN-γ signaling[160,163]. Furthermore, refractoriness to IFN-α is not impaired in the liver of Socs1 deficient mice, whereas deletion of Usp18 completely restored the refractory phenotype to IFN-α stimulation[148]. Of note, the previously mentioned type I interferonopathy pseudo-TORCH syndrome is caused by a human USP18 deficiency[179]. Thus, our results together with the previously published data define USP18 as the main negative regulator of the IFN-α induced signaling cascade *in vitro* and *in vivo*.

In contrast to IFN-α, the effect of USP18 on IFN-β was marginal and only significant at 8 hours post stimulation *in vitro* (Figure S2, research article I). Of note, although IFN-β belongs to the type I IFNs and signals through the same receptor as IFN-α, the long-lasting refractoriness was not observed for IFN-β stimulation[147,173]. This goes in line with the fact that IFN-β was effective in some chronic hepatitis C patients who did not respond to previous therapies with IFN-α[345]. Furthermore, IFN-α and IFN-β induce distinct mRNA expression profiles in human cells[100,342,346,347]. In contrast to IFN-α, IFN-β induces long-lasting ISG expression[342]. This and the data from our study suggest that the negative regulatory role of USP18 on IFN-β is much weaker compared to its effect on IFN-α signaling. The reason for that is not entirely clear; especially given the fact that USP18 inhibits the IFN-α signaling by binding to the IFNAR2[109] chain that is also used by IFN-β. It can be speculated, that the interaction of USP18 with the IFNAR2 chain may lead to reorganization of the type I IFN receptor that could weaken the interaction with

IFN-α, while not affecting the binding of IFN-β that has a higher receptor affinity[173,348,349]. This would allow IFN-β to maintain activity in cells desensitized for IFN-α, which could be important for the stimulation of adaptive immune responses, critical to eradicate pathogen infest cells. However, solid experimental evidence supporting such a model is still lacking. Taken together, IFN-α and IFN-β induce the same set of ISGs but only IFN-α response is subject to a significant negative feedback by USP18.

The negative regulation of IFN-λs is fundamentally different from that of IFN-α signaling. The upregulation of USP18 does not induce refractoriness of IFN-λ signaling as shown in the present study and in previous studies[147,173]. We demonstrate that in contrast to IFN-α, IFN-λ induces a prolonged activation of STAT1 and 2 as well as sustained ISG expression despite strong induction of USP18 (Figures 1B and 1C, research article I). Importantly, we used a hepatoma cell line with IFNLR1 expression levels comparable to the expression levels in the liver of chronic hepatitis C patients, especially with the IFN-λ4 wildtype genotype (TT/ΔG and ΔG/ΔG) (Figure 1A, research article I). We have previously demonstrated that the initially very low IFNLR1 expression in human livers seems to be induced to levels sufficient for IFN-λ signaling during chronic hepatitis C infection[350]. Again using USP18 knockout cells, we show that USP18, while being the main negative regulator of the IFN-α signaling, has no effect on IFN-λ signaling (Figure 3, 4, S2 and S3 of research article I). Of note, USP18 has the potential to inhibit IFN-λ signaling but only at supra-physiological expression levels as demonstrated in our overexpression experiments (Figure 2, research article I). In this setting, the transiently transfected cells showed USP18 expression levels 2-3 order of magnitude higher than those induced by maximal physiological stimulation with IFN-λ. These experiments showed that the results from overexpression studies have to be cautiously interpreted, especially in the case of the inducible SOCS and USP18 proteins. Not only can the negative regulators be expressed at non-physiological levels, but also in a temporally inappropriate manner (i.e. already present prior to the onset of signaling rather than induced as a consequence of signal transduction). Indeed, while several SOCS proteins inhibit a number of different cytokines when artificially overexpressed, under normal conditions their activity is usually highly specific for only a few cytokines[152]. This was shown for example for SOCS1 that, despite being discovered on

the basis of its ability to inhibit IL-6 when overexpressed[129,131], has little, if any, role in inhibiting IL-6 *in vivo* based on studies in knockout mice[165]. Thus, knockout experiments are more reliable for investigating the negative regulatory role of SOCS1, SOCS3 and USP18 on the IFN-λ induced signaling cascade. Accordingly, we show that SOCS1 deficient cells are hyper-responsive to type III IFNs *in vitro* whereas IFN-λ signaling was not affected in SOCS3 and USP18 knockout cells (Figures 3, 4, S2 and S3, research article I). This led us to conclude that SOCS1 is an inducible and physiological relevant negative regulator of IFN-λ1, IFN-λ3 and IFN-λ4 in human hepatoma cells. Furthermore, we confirmed this inhibitory role of SOCS1 on IFN-λ signaling *in vivo*. IFN-λ-induced ISG expression in the lung and the gut, tissues known to express IFNLR1[38,351], was significantly increased in Socs1 knockout mice compared to control mice (Figures 5 and S4, research article I).

We demonstrated that the IFN-α and IFN-λ systems are negatively regulated in different ways. Whereas USP18 is the main negative regulator of the IFN-α signaling cascade, IFN-λ signaling is regulated by SOCS1. However, not only the regulation is different but also the distribution of their cognate receptors. Almost all nucleated cells express the IFNAR, whereas the IFNLR1 expression is mostly restricted to epithelial cells of the respiratory and gastrointestinal tracts[10,36,38]. This leads to the hypothesis that type III IFNs serve as the first line of defense at the borders where viral infection is a frequent challenge. Our data also shows that SOCS1, while negatively regulating IFN-λ induced signaling, does not completely abolish it. This probably enables a long-lasting activation of the JAK-STAT signaling, crucial for a sustained antiviral state at mucosal surfaces that are constantly exposed to pathogens. In contrast, IFN-α is a more powerful defense system that is induced fast but only transiently[5]. It is induced after viruses breached the mucosal surfaces and invade the systemic circulation and other organs. Although powerful in fighting invading pathogens, IFN-α induced signaling needs to be tightly controlled to maintain tissue homeostasis. This could explain why USP18 shuts down IFN-α signaling completely.

Taken together, we demonstrate SOCS1 as a physiologically relevant inducible inhibitor of the IFN-λ signaling, whereas USP18 represents the main negative regulator of IFN-α induced JAK-STAT signaling.

1. Research article II

HCC is the second deadliest cancer worldwide with yearly increasing incidence[181,182,185]. Treatment options for HCC patients are unsatisfactory with less than 30 percent of HCC patients in Europe qualifying for curative treatment such as resection and transplantation[185]. Due to advanced disease stages and unfavorable patient conditions at the time of diagnosis, the majority of HCC cases are unresectable. The only treatment option for patients with advanced disease is the multikinase inhibitor sorafenib, prolonging median survival by three months[232]. Although beneficial, sorafenib has its limitations mostly because of its side effects and resistance to treatment, showing a clear need for new and more effective drugs. Novel systemic drugs developed after sorafenib was approved for the treatment of advanced HCC failed in clinical phase II or III trials because of liver toxicity or marginal antitumor potency[286]. A major obstacle for the understanding of the pathogenesis of HCC and the molecular mechanisms leading to drug resistance is the lack of *in vivo* models that recapitulate key features of human HCC. In recent years, PDX models have gained interest and are regarded as valuable tools in the field of pre-clinical drug testing and prediction of cancer therapy[332,333]. Indeed, several HCC PDX mouse models have been described[334-340]. However, all of these models have been generated from surgically removed HCC tumors. Because liver resection is typically performed in patients with early stage disease, these models may not recapitulate the full spectrum of HCC stages. Importantly, none of the above mentioned PDX models includes advanced stage HCC, although this would be desired as sorafenib treatment is mainly used in patients with advanced stage disease.

We report here for the first time the establishment of s.c. PDX models from fresh human HCC needle biopsies that cover early and late stage tumors. We generated eleven PDX models from tumor biopsies of HCC patients with different etiologies and disease stages (Table S1, research article II) with an engraftment success rate of 20% (11 out of 54 biopsies). This is in accordance with published data from HCC PDX models from resected specimens[334,337,338]. The use of HCC biopsies covering the full spectrum of disease stages and etiologies enabled us to assess potential determinants for the generation of PDX models. We show that the tumor differentiation grade according to Edmondson[262] was a clear determinant for engraftment success, with only high grade biopsies (grades III and IV) engrafting in the mice (Table S1 and Figure 4A, research article II). Besides the differentiation grade, no other clinical patient characteristics

seemed to influence the engraftment success rate (Figure 4A, research article II). This suggests, that mainly dedifferentiated and thus more aggressive HCCs are able to form tumors in mice whereas those of low Edmondson grade (i.e. retaining hepatocyte differentiation) do not. This is supported by the fact that previously reported HCC PDX models, generated from early stage tumors, were mainly derived from high Edmondson grade samples[335-338]. Furthermore, in the case of well differentiated originating tumor samples, the corresponding PDX were of poor differentiation grades[340]. This is consistent with our finding that according to the Hoshida classification[279], all our engrafted biopsies were of molecular subtype S1 and S2, characterized by poor differentiation, high proliferation rate and poor survival (Figure 4A, research article II). In contrast, none of the subtype S3 biopsies, characterized as well differentiated tumors retaining a hepatocyte-like phenotype and associated with good survival gave rise to PDX models. However, although only high grade HCC biopsies resulted in PDX models, they largely represented the entire spectrum of poorly differentiated HCCs by unsupervised clustering against the poorly differentiated HCCs from the TCGA HCC reference cohort[248] (Figure 4B, research article II).

Of note, because we consider all transplanted biopsies as failed engraftments if no tumor growth was visible within eight months after transplantation, we can not exclude that slow-growing, low-grade tumors would have started growing after the cut off of eight months. This potential scenario is further supported by the observation that Edmondson grade IV biopsies tend to have an earlier tumor growth onset compared to grade III biopsies (Figure 1A, research article II). Furthermore, while transplantation of different pieces obtained from the same biopsy cylinder showed different tumor growth onsets in the mice (Figure S1A, research article II), injection of equal amounts of biopsy-derived cell suspension led to identical, but delayed tumor growth onset (Figure S1B, research article II). Although not proven, these data suggest that the cell number and tissue integrity of the tumor tissue used probably influence the time to tumor growth onset. The use of a cell-suspension generated by disruption of the tumor could promote cell death because of matrix detachment[340,352] and also requires complete revascularization, thus leading to a delayed tumor growth onset.

First generation PDX tumors were re-transplanted in order to expand the tumor material and maintain the models for further analysis. The lag phase to onset of tumor growth in the second PDX generations was shorter for all models and remained constant

over several generations (Figures 1B and 1C, research article II). The finding of a shifted onset of tumor growth in the second PDX generation is in line with a report of PDX mice derived from resected HCC specimens[334]. It can be speculated that the presence of a mouse derived vascular system in the PDX tumors facilitates the accelerated engraftment upon re-transplantation. Furthermore, the doubling time of the PDX tumors was consistent in all generations within a given model (Figure 1B, research article II). Thus, tumor growth might be primarily dependent on the tumor cells once a murine vasculature system is established.

The established PDX tumors were highly similar to their originating human tumors. They maintained the tumor differentiation grade, growth pattern, cytological subtype as well as the expression of AFP and typical HCC markers such as GPC3, HSP70 and GS over at least four generations (Figures 2, S2A-J and Table 1, research article II). Of note, only one PDX model (C284b) lost part of the histological characteristics (i.e. the trabecular growth pattern) observed in the originating human HCC. This may be due to heterogeneous growth patterns in different regions of the same tumor.

Three xenografts however, differed histologically from the corresponding human tumors (Figure 5A, research article II). Further analysis revealed the histological appearance of lymphocytes, strong positivity for the human B-cell marker CD20, transcriptional up-regulation of human immune cell signatures and loss of expression of HCC specific somatic mutations in these PDX tumors (Figure 5 and Table S7, research article II). This suggests that human B-cell lymphomas were formed in these models. This phenomena has been previously described for PDX models derived from a number of human cancer tissues[353], including HCC[354]. It was previously suggested that the reactivation of latent EBV of intratumoral passenger B lymphocytes may be the cause of lymphoma development in PDX mice[353,354]. Indeed, we detected EBV transcripts in all three lymphoma PDX models, but not in the originating HCC and matched non-tumor biopsies (Table S8, research article II). The effect of EBV reactivation may be linked to the level of immunodeficiency of the mice, as the percentage of lymphoma development was high in NSG, NOG and NOD/SCID mice, whereas no lymphoma development has been described in nude mice[355,356]. Therefore, the use of nude instead of NSG mice for PDX development might help to avoid lymphoma generation probably because of the presence of functional NK cells[355]. Interestingly, two biopsies derived from the same patient but from two distinct HCC nodules gave rise to one HCC and one lymphoma PDX

model (C948 and C949 of Table S1, research article II). This is in accordance with a report for breast and pancreatic cancer PDX models, where transplantation of the tumor pieces from the same human tumor graft could grow as a lymphocytic tumor in one mouse and as an adenocarcinoma in another mouse[355]. Butler et al. reported that treatment with rituximab, an anti-CD20 monoclonal antibody, at the time of transplantation, prevented the occurrence of lymphomatous outgrowth in early-passage ovarian xenografts[353]. If this strategy could be applied to prevent lymphoma development and improve the success rate of HCC PDX generation has to be investigated.

Because PDX models are frequently used in pre-clinical drug testing, it is important to understand to what extent they recapitulate the human tumor signatures. Based on RNA sequencing data, we showed that pathways related to immune cells and angiogenesis were generally down-regulated in the PDX models compared to their originating human HCC biopsies (Figure 3A and Table S4, research article II), most likely a consequence of the loss of human immune cells and the presence of a murine instead of human vasculature in these PDX models (Figure S3 and Table S4, research article II). In contrast, pathways related to cell cycle were up-regulated in the PDX models compared to the human HCC biopsies, suggesting an enrichment of cancer cells in the PDX tumors (Figure 3A and Table S4, research article II). Martinez-Garcia et al. suggested that the lack of human stromal components in PDX models is most probably the major difference between them and their originating human tumor[357]. After accounting for the systemic differences mentioned above, all PDX tumors clustered together with the corresponding HCC biopsy. This demonstrates that the HCC PDX models recapitulate the tumor-specific gene expression profile of the originating tumor (Figure 3B, research article II). Furthermore, we demonstrated that the HCC specific expression of somatic mutations in cancer genes was maintained in the corresponding PDX models (Figure 3C, research article II). Moreover, transcriptome based analysis revealed that the PDX tumors are stable over several generations and retain expression of somatic mutations of the biopsied tumor (Figures S4A and S4B, research article II). This suggests that the gene expression differences between the PDX tumors and their corresponding biopsies is mainly due to the substitution of human by mouse stromal cells and that this adaptation happens in an early phase of PDX establishment[357].

Taken together, we successfully generated PDX models from human HCC needle biopsies of early and late-stage disease, including unresectable tumors. Importantly, the HCC PDX models maintain the histologic features and transcriptomic characteristics of the originating tumors. Thus, these models will not only serve as valuable tools for investigating HCC biology but will also be very useful in studying drug-induced resistance mechanisms and identification of novel drug targets.

V References

1 Krause, C. D. & Pestka, S. Evolution of the Class 2 cytokines and receptors, and discovery of new friends and relatives. *Pharmacol Ther* **106**, 299-346, doi:10.1016/j.pharmthera.2004.12.002 (2005).

2 Isaacs, A. & Lindenmann, J. Virus interference. I. The interferon. *Proc R Soc Lond B Biol Sci* **147**, 258-267 (1957).

3 Stark, G. R., Kerr, I. M., Williams, B. R., Silverman, R. H. & Schreiber, R. D. How cells respond to interferons. *Annu Rev Biochem* **67**, 227-264, doi:10.1146/annurev.biochem.67.1.227 (1998).

4 Pestka, S., Langer, J. A., Zoon, K. C. & Samuel, C. E. Interferons and their actions. *Annu Rev Biochem* **56**, 727-777, doi:10.1146/annurev.bi.56.070187.003455 (1987).

5 Pestka, S., Krause, C. D. & Walter, M. R. Interferons, interferon-like cytokines, and their receptors. *Immunol Rev* **202**, 8-32, doi:10.1111/j.0105-2896.2004.00204.x (2004).

6 Pestka, S. The interferons: 50 years after their discovery, there is much more to learn. *J Biol Chem* **282**, 20047-20051, doi:10.1074/jbc.R700004200 (2007).

7 Heim, M. H. Interferons and hepatitis C virus. *Swiss Med Wkly* **142**, w13586, doi:10.4414/smw.2012.13586 (2012).

8 Donnelly, R. P. & Kotenko, S. V. Interferon-lambda: a new addition to an old family. *J Interferon Cytokine Res* **30**, 555-564, doi:10.1089/jir.2010.0078 (2010).

9 Kotenko, S. V. *et al.* IFN-lambdas mediate antiviral protection through a distinct class II cytokine receptor complex. *Nat Immunol* **4**, 69-77, doi:10.1038/ni875 (2003).

10 Hall, J. C. & Rosen, A. Type I interferons: crucial participants in disease amplification in autoimmunity. *Nat Rev Rheumatol* **6**, 40-49, doi:10.1038/nrrheum.2009.237 (2010).

11 Liu, Y. J. IPC: professional type 1 interferon-producing cells and plasmacytoid dendritic cell precursors. *Annu Rev Immunol* **23**, 275-306, doi:10.1146/annurev.immunol.23.021704.115633 (2005).

12 Siegal, F. P. *et al.* The nature of the principal type 1 interferon-producing cells in human blood. *Science* **284**, 1835-1837 (1999).

13 Heim, M. H. Innate immunity and HCV. *J Hepatol* **58**, 564-574, doi:10.1016/j.jhep.2012.10.005 (2013).

14 Asselin-Paturel, C. & Trinchieri, G. Production of type I interferons: plasmacytoid dendritic cells and beyond. *J Exp Med* **202**, 461-465, doi:10.1084/jem.20051395 (2005).

15 Muller, U. *et al.* Functional role of type I and type II interferons in antiviral defense. *Science* **264**, 1918-1921 (1994).

16 Dupuis, S. *et al.* Impaired response to interferon-alpha/beta and lethal viral disease in human STAT1 deficiency. *Nat Genet* **33**, 388-391, doi:10.1038/ng1097 (2003).

17 Lu, B. *et al.* Targeted disruption of the interferon-gamma receptor 2 gene results in severe immune defects in mice. *Proc Natl Acad Sci U S A* **95**, 8233-8238 (1998).

18 Bach, E. A., Aguet, M. & Schreiber, R. D. The IFN gamma receptor: a paradigm for cytokine receptor signaling. *Annu Rev Immunol* **15**, 563-591, doi:10.1146/annurev.immunol.15.1.563 (1997).
19 Walter, M. R. *et al.* Crystal structure of a complex between interferon-gamma and its soluble high-affinity receptor. *Nature* **376**, 230-235, doi:10.1038/376230a0 (1995).
20 Lasfar, A. *et al.* Characterization of the mouse IFN-lambda ligand-receptor system: IFN-lambdas exhibit antitumor activity against B16 melanoma. *Cancer Res* **66**, 4468-4477, doi:10.1158/0008-5472.CAN-05-3653 (2006).
21 Darnell, J. E., Jr., Kerr, I. M. & Stark, G. R. Jak-STAT pathways and transcriptional activation in response to IFNs and other extracellular signaling proteins. *Science* **264**, 1415-1421 (1994).
22 Dalton, D. K. *et al.* Multiple defects of immune cell function in mice with disrupted interferon-gamma genes. *Science* **259**, 1739-1742 (1993).
23 Heim, M. H. Intracellular signalling and antiviral effects of interferons. *Dig Liver Dis* **32**, 257-263 (2000).
24 Huang, S. *et al.* Immune response in mice that lack the interferon-gamma receptor. *Science* **259**, 1742-1745 (1993).
25 Sheppard, P. *et al.* IL-28, IL-29 and their class II cytokine receptor IL-28R. *Nat Immunol* **4**, 63-68, doi:10.1038/ni873 (2003).
26 Ank, N. *et al.* Lambda interferon (IFN-lambda), a type III IFN, is induced by viruses and IFNs and displays potent antiviral activity against select virus infections in vivo. *J Virol* **80**, 4501-4509, doi:10.1128/JVI.80.9.4501-4509.2006 (2006).
27 Prokunina-Olsson, L. *et al.* A variant upstream of IFNL3 (IL28B) creating a new interferon gene IFNL4 is associated with impaired clearance of hepatitis C virus. *Nat Genet* **45**, 164-171, doi:10.1038/ng.2521 (2013).
28 Heim, M. H., Bochud, P. Y. & George, J. Host - hepatitis C viral interactions: The role of genetics. *J Hepatol* **65**, S22-32, doi:10.1016/j.jhep.2016.07.037 (2016).
29 Osterlund, P. I., Pietila, T. E., Veckman, V., Kotenko, S. V. & Julkunen, I. IFN regulatory factor family members differentially regulate the expression of type III IFN (IFN-lambda) genes. *J Immunol* **179**, 3434-3442 (2007).
30 Onoguchi, K. *et al.* Viral infections activate types I and III interferon genes through a common mechanism. *J Biol Chem* **282**, 7576-7581, doi:10.1074/jbc.M608618200 (2007).
31 Coccia, E. M. *et al.* Viral infection and Toll-like receptor agonists induce a differential expression of type I and lambda interferons in human plasmacytoid and monocyte-derived dendritic cells. *Eur J Immunol* **34**, 796-805, doi:10.1002/eji.200324610 (2004).
32 Heim, M. H. & Thimme, R. Innate and adaptive immune responses in HCV infections. *J Hepatol* **61**, S14-25, doi:10.1016/j.jhep.2014.06.035 (2014).
33 Hermant, P. & Michiels, T. Interferon-lambda in the context of viral infections: production, response and therapeutic implications. *J Innate Immun* **6**, 563-574, doi:10.1159/000360084 (2014).
34 Hamming, O. J. *et al.* Interferon lambda 4 signals via the IFNlambda receptor to regulate antiviral activity against HCV and coronaviruses. *EMBO J* **32**, 3055-3065, doi:10.1038/emboj.2013.232 (2013).

35 Donnelly, R. P., Sheikh, F., Kotenko, S. V. & Dickensheets, H. The expanded family of class II cytokines that share the IL-10 receptor-2 (IL-10R2) chain. *J Leukoc Biol* **76**, 314-321, doi:10.1189/jlb.0204117 (2004).
36 Mordstein, M. *et al.* Lambda interferon renders epithelial cells of the respiratory and gastrointestinal tracts resistant to viral infections. *J Virol* **84**, 5670-5677, doi:10.1128/JVI.00272-10 (2010).
37 Mordstein, M., Michiels, T. & Staeheli, P. What have we learned from the IL28 receptor knockout mouse? *J Interferon Cytokine Res* **30**, 579-584, doi:10.1089/jir.2010.0061 (2010).
38 Sommereyns, C., Paul, S., Staeheli, P. & Michiels, T. IFN-lambda (IFN-lambda) is expressed in a tissue-dependent fashion and primarily acts on epithelial cells in vivo. *PLoS Pathog* **4**, e1000017, doi:10.1371/journal.ppat.1000017 (2008).
39 Wack, A., Terczynska-Dyla, E. & Hartmann, R. Guarding the frontiers: the biology of type III interferons. *Nat Immunol* **16**, 802-809, doi:10.1038/ni.3212 (2015).
40 Muir, A. J. *et al.* A randomized phase 2b study of peginterferon lambda-1a for the treatment of chronic HCV infection. *J Hepatol* **61**, 1238-1246, doi:10.1016/j.jhep.2014.07.022 (2014).
41 Doyle, S. E. *et al.* Interleukin-29 uses a type 1 interferon-like program to promote antiviral responses in human hepatocytes. *Hepatology* **44**, 896-906, doi:10.1002/hep.21312 (2006).
42 Key, F. M. *et al.* Selection on a variant associated with improved viral clearance drives local, adaptive pseudogenization of interferon lambda 4 (IFNL4). *PLoS Genet* **10**, e1004681, doi:10.1371/journal.pgen.1004681 (2014).
43 Uze, G. & Monneron, D. IL-28 and IL-29: newcomers to the interferon family. *Biochimie* **89**, 729-734, doi:10.1016/j.biochi.2007.01.008 (2007).
44 Hermant, P. *et al.* Human but not mouse hepatocytes respond to interferon-lambda in vivo. *PLoS One* **9**, e87906, doi:10.1371/journal.pone.0087906 (2014).
45 Pestka, S. The human interferon alpha species and receptors. *Biopolymers* **55**, 254-287, doi:10.1002/1097-0282(2000)55:4<254::AID-BIP1001>3.0.CO;2-1 (2000).
46 Galani, I. E., Koltsida, O. & Andreakos, E. Type III interferons (IFNs): Emerging Master Regulators of Immunity. *Adv Exp Med Biol* **850**, 1-15, doi:10.1007/978-3-319-15774-0_1 (2015).
47 Tyrrell, D. A. Interferon produced by cultures of calf kidney cells. *Nature* **184(Suppl 7)**, 452-453 (1959).
48 Friedman, R. M. Clinical uses of interferons. *Br J Clin Pharmacol* **65**, 158-162, doi:10.1111/j.1365-2125.2007.03055.x (2008).
49 Hoofnagle, J. H. *et al.* Treatment of chronic non-A,non-B hepatitis with recombinant human alpha interferon. A preliminary report. *N Engl J Med* **315**, 1575-1578, doi:10.1056/NEJM198612183152503 (1986).
50 Hoofnagle, J. H. & Seeff, L. B. Peginterferon and ribavirin for chronic hepatitis C. *N Engl J Med* **355**, 2444-2451, doi:10.1056/NEJMct061675 (2006).
51 McHutchison, J. G. *et al.* Interferon alfa-2b alone or in combination with ribavirin as initial treatment for chronic hepatitis C. Hepatitis Interventional Therapy Group. *N Engl J Med* **339**, 1485-1492, doi:10.1056/NEJM199811193392101 (1998).
52 Poynard, T. *et al.* Randomised trial of interferon alpha2b plus ribavirin for 48 weeks or for 24 weeks versus interferon alpha2b plus placebo for 48 weeks for

treatment of chronic infection with hepatitis C virus. International Hepatitis Interventional Therapy Group (IHIT). *Lancet* **352**, 1426-1432 (1998).
53 Manns, M. P. *et al.* Peginterferon alfa-2b plus ribavirin compared with interferon alfa-2b plus ribavirin for initial treatment of chronic hepatitis C: a randomised trial. *Lancet* **358**, 958-965 (2001).
54 Holmes, J. A. & Thompson, A. J. Interferon-free combination therapies for the treatment of hepatitis C: current insights. *Hepat Med* **7**, 51-70, doi:10.2147/HMER.S55864 (2015).
55 Quesada, J. R., Reuben, J., Manning, J. T., Hersh, E. M. & Gutterman, J. U. Alpha interferon for induction of remission in hairy-cell leukemia. *N Engl J Med* **310**, 15-18, doi:10.1056/NEJM198401053100104 (1984).
56 Tsao, H., Atkins, M. B. & Sober, A. J. Management of cutaneous melanoma. *N Engl J Med* **351**, 998-1012, doi:10.1056/NEJMra041245 (2004).
57 Ganem, D. & Prince, A. M. Hepatitis B virus infection--natural history and clinical consequences. *N Engl J Med* **350**, 1118-1129, doi:10.1056/NEJMra031087 (2004).
58 Jacobs, L. D. *et al.* Intramuscular interferon beta-1a therapy initiated during a first demyelinating event in multiple sclerosis. CHAMPS Study Group. *N Engl J Med* **343**, 898-904, doi:10.1056/NEJM200009283431301 (2000).
59 Errante, P. R., Frazao, J. B. & Condino-Neto, A. The use of interferon-gamma therapy in chronic granulomatous disease. *Recent Pat Antiinfect Drug Discov* **3**, 225-230 (2008).
60 Lasfar, A., Zloza, A. & Cohen-Solal, K. A. IFN-lambda therapy: current status and future perspectives. *Drug Discov Today* **21**, 167-171, doi:10.1016/j.drudis.2015.10.021 (2016).
61 Ghany, M. G., Strader, D. B., Thomas, D. L., Seeff, L. B. & American Association for the Study of Liver, D. Diagnosis, management, and treatment of hepatitis C: an update. *Hepatology* **49**, 1335-1374, doi:10.1002/hep.22759 (2009).
62 Muir, A. J. *et al.* Phase 1b study of pegylated interferon lambda 1 with or without ribavirin in patients with chronic genotype 1 hepatitis C virus infection. *Hepatology* **52**, 822-832, doi:10.1002/hep.23743 (2010).
63 Flisiak, R. *et al.* A Randomized Study of Peginterferon Lambda-1a Compared to Peginterferon Alfa-2a in Combination with Ribavirin and Telaprevir in Patients with Genotype-1 Chronic Hepatitis C. *PLoS One* **11**, e0164563, doi:10.1371/journal.pone.0164563 (2016).
64 Stark, G. R. & Darnell, J. E., Jr. The JAK-STAT pathway at twenty. *Immunity* **36**, 503-514, doi:10.1016/j.immuni.2012.03.013 (2012).
65 Larner, A. C. *et al.* Transcriptional induction of two genes in human cells by beta interferon. *Proc Natl Acad Sci U S A* **81**, 6733-6737 (1984).
66 Levy, D. E. & Darnell, J. E., Jr. Stats: transcriptional control and biological impact. *Nat Rev Mol Cell Biol* **3**, 651-662, doi:10.1038/nrm909 (2002).
67 Aaronson, D. S. & Horvath, C. M. A road map for those who don't know JAK-STAT. *Science* **296**, 1653-1655, doi:10.1126/science.1071545 (2002).
68 Heim, M. H. The Jak-STAT pathway: cytokine signalling from the receptor to the nucleus. *J Recept Signal Transduct Res* **19**, 75-120, doi:10.3109/10799899909036638 (1999).
69 Darnell, J. E., Jr. STATs and gene regulation. *Science* **277**, 1630-1635 (1997).
70 Wilks, A. F. Two putative protein-tyrosine kinases identified by application of the polymerase chain reaction. *Proc Natl Acad Sci U S A* **86**, 1603-1607 (1989).

71 Wilks, A. F. *et al.* Two novel protein-tyrosine kinases, each with a second phosphotransferase-related catalytic domain, define a new class of protein kinase. *Mol Cell Biol* **11**, 2057-2065 (1991).
72 Firmbach-Kraft, I., Byers, M., Shows, T., Dalla-Favera, R. & Krolewski, J. J. tyk2, prototype of a novel class of non-receptor tyrosine kinase genes. *Oncogene* **5**, 1329-1336 (1990).
73 Velazquez, L., Fellous, M., Stark, G. R. & Pellegrini, S. A protein tyrosine kinase in the interferon alpha/beta signaling pathway. *Cell* **70**, 313-322 (1992).
74 Johnston, J. A. *et al.* Phosphorylation and activation of the Jak-3 Janus kinase in response to interleukin-2. *Nature* **370**, 151-153, doi:10.1038/370151a0 (1994).
75 Rane, S. G. & Reddy, E. P. JAK3: a novel JAK kinase associated with terminal differentiation of hematopoietic cells. *Oncogene* **9**, 2415-2423 (1994).
76 Witthuhn, B. A. *et al.* Involvement of the Jak-3 Janus kinase in signalling by interleukins 2 and 4 in lymphoid and myeloid cells. *Nature* **370**, 153-157, doi:10.1038/370153a0 (1994).
77 Muller, M. *et al.* The protein tyrosine kinase JAK1 complements defects in interferon-alpha/beta and -gamma signal transduction. *Nature* **366**, 129-135, doi:10.1038/366129a0 (1993).
78 Colamonici, O. R., Uyttendaele, H., Domanski, P., Yan, H. & Krolewski, J. J. p135tyk2, an interferon-alpha-activated tyrosine kinase, is physically associated with an interferon-alpha receptor. *J Biol Chem* **269**, 3518-3522 (1994).
79 Kotenko, S. V. & Durbin, J. E. Contribution of Type III Interferons to Antiviral Immunity; Location, Location, Location. *J Biol Chem*, doi:10.1074/jbc.R117.777102 (2017).
80 Kotenko, S. V. *et al.* Identification and functional characterization of a second chain of the interleukin-10 receptor complex. *EMBO J* **16**, 5894-5903, doi:10.1093/emboj/16.19.5894 (1997).
81 Igarashi, K. *et al.* Interferon-gamma induces tyrosine phosphorylation of interferon-gamma receptor and regulated association of protein tyrosine kinases, Jak1 and Jak2, with its receptor. *J Biol Chem* **269**, 14333-14336 (1994).
82 Kotenko, S. V. *et al.* Interaction between the components of the interferon gamma receptor complex. *J Biol Chem* **270**, 20915-20921 (1995).
83 Copeland, N. G. *et al.* Distribution of the mammalian Stat gene family in mouse chromosomes. *Genomics* **29**, 225-228 (1995).
84 Schindler, C., Fu, X. Y., Improta, T., Aebersold, R. & Darnell, J. E., Jr. Proteins of transcription factor ISGF-3: one gene encodes the 91-and 84-kDa ISGF-3 proteins that are activated by interferon alpha. *Proc Natl Acad Sci U S A* **89**, 7836-7839 (1992).
85 Zhong, Z., Wen, Z. & Darnell, J. E., Jr. Stat3: a STAT family member activated by tyrosine phosphorylation in response to epidermal growth factor and interleukin-6. *Science* **264**, 95-98 (1994).
86 Zhong, Z., Wen, Z. & Darnell, J. E., Jr. Stat3 and Stat4: members of the family of signal transducers and activators of transcription. *Proc Natl Acad Sci U S A* **91**, 4806-4810 (1994).
87 Yamamoto, K. *et al.* Stat4, a novel gamma interferon activation site-binding protein expressed in early myeloid differentiation. *Mol Cell Biol* **14**, 4342-4349 (1994).

88 Wakao, H., Gouilleux, F. & Groner, B. Mammary gland factor (MGF) is a novel member of the cytokine regulated transcription factor gene family and confers the prolactin response. *EMBO J* **13**, 2182-2191 (1994).
89 Mui, A. L., Wakao, H., O'Farrell, A. M., Harada, N. & Miyajima, A. Interleukin-3, granulocyte-macrophage colony stimulating factor and interleukin-5 transduce signals through two STAT5 homologs. *EMBO J* **14**, 1166-1175 (1995).
90 Hou, J. *et al.* An interleukin-4-induced transcription factor: IL-4 Stat. *Science* **265**, 1701-1706 (1994).
91 Shuai, K., Stark, G. R., Kerr, I. M. & Darnell, J. E., Jr. A single phosphotyrosine residue of Stat91 required for gene activation by interferon-gamma. *Science* **261**, 1744-1746 (1993).
92 Heim, M. H., Kerr, I. M., Stark, G. R. & Darnell, J. E., Jr. Contribution of STAT SH2 groups to specific interferon signaling by the Jak-STAT pathway. *Science* **267**, 1347-1349 (1995).
93 Schindler, C., Shuai, K., Prezioso, V. R. & Darnell, J. E., Jr. Interferon-dependent tyrosine phosphorylation of a latent cytoplasmic transcription factor. *Science* **257**, 809-813 (1992).
94 Shuai, K. *et al.* Interferon activation of the transcription factor Stat91 involves dimerization through SH2-phosphotyrosyl peptide interactions. *Cell* **76**, 821-828 (1994).
95 Zhou, Z. *et al.* Type III interferon (IFN) induces a type I IFN-like response in a restricted subset of cells through signaling pathways involving both the Jak-STAT pathway and the mitogen-activated protein kinases. *J Virol* **81**, 7749-7758, doi:10.1128/JVI.02438-06 (2007).
96 Veals, S. A. *et al.* Subunit of an alpha-interferon-responsive transcription factor is related to interferon regulatory factor and Myb families of DNA-binding proteins. *Mol Cell Biol* **12**, 3315-3324 (1992).
97 Levy, D. E., Kessler, D. S., Pine, R., Reich, N. & Darnell, J. E., Jr. Interferon-induced nuclear factors that bind a shared promoter element correlate with positive and negative transcriptional control. *Genes Dev* **2**, 383-393 (1988).
98 Levy, D. E., Kessler, D. S., Pine, R. & Darnell, J. E., Jr. Cytoplasmic activation of ISGF3, the positive regulator of interferon-alpha-stimulated transcription, reconstituted in vitro. *Genes Dev* **3**, 1362-1371 (1989).
99 Levy, D., Larner, A., Chaudhuri, A., Babiss, L. E. & Darnell, J. E., Jr. Interferon-stimulated transcription: isolation of an inducible gene and identification of its regulatory region. *Proc Natl Acad Sci U S A* **83**, 8929-8933 (1986).
100 Marcello, T. *et al.* Interferons alpha and lambda inhibit hepatitis C virus replication with distinct signal transduction and gene regulation kinetics. *Gastroenterology* **131**, 1887-1898, doi:10.1053/j.gastro.2006.09.052 (2006).
101 Decker, T., Lew, D. J., Mirkovitch, J. & Darnell, J. E., Jr. Cytoplasmic activation of GAF, an IFN-gamma-regulated DNA-binding factor. *EMBO J* **10**, 927-932 (1991).
102 Meraz, M. A. *et al.* Targeted disruption of the Stat1 gene in mice reveals unexpected physiologic specificity in the JAK-STAT signaling pathway. *Cell* **84**, 431-442 (1996).
103 Durbin, J. E., Hackenmiller, R., Simon, M. C. & Levy, D. E. Targeted disruption of the mouse Stat1 gene results in compromised innate immunity to viral disease. *Cell* **84**, 443-450 (1996).
104 Dickensheets, H., Sheikh, F., Park, O., Gao, B. & Donnelly, R. P. Interferon-lambda (IFN-lambda) induces signal transduction and gene expression in human

hepatocytes, but not in lymphocytes or monocytes. *J Leukoc Biol* **93**, 377-385, doi:10.1189/jlb.0812395 (2013).
105 Ronnblom, L. The type I interferon system in the etiopathogenesis of autoimmune diseases. *Ups J Med Sci* **116**, 227-237, doi:10.3109/03009734.2011.624649 (2011).
106 Ronnblom, L. The importance of the type I interferon system in autoimmunity. *Clin Exp Rheumatol* **34**, 21-24 (2016).
107 Porritt, R. A. & Hertzog, P. J. Dynamic control of type I IFN signalling by an integrated network of negative regulators. *Trends Immunol* **36**, 150-160, doi:10.1016/j.it.2015.02.002 (2015).
108 Lee-Kirsch, M. A. The Type I Interferonopathies. *Annu Rev Med* **68**, 297-315, doi:10.1146/annurev-med-050715-104506 (2017).
109 Malakhova, O. A. *et al.* UBP43 is a novel regulator of interferon signaling independent of its ISG15 isopeptidase activity. *EMBO J* **25**, 2358-2367, doi:10.1038/sj.emboj.7601149 (2006).
110 Wormald, S. & Hilton, D. J. Inhibitors of cytokine signal transduction. *J Biol Chem* **279**, 821-824, doi:10.1074/jbc.R300030200 (2004).
111 Shuai, K. & Liu, B. Regulation of JAK-STAT signalling in the immune system. *Nat Rev Immunol* **3**, 900-911, doi:10.1038/nri1226 (2003).
112 Greenhalgh, C. J. & Hilton, D. J. Negative regulation of cytokine signaling. *J Leukoc Biol* **70**, 348-356 (2001).
113 Greenhalgh, C. J., Miller, M. E., Hilton, D. J. & Lund, P. K. Suppressors of cytokine signaling: Relevance to gastrointestinal function and disease. *Gastroenterology* **123**, 2064-2081, doi:10.1053/gast.2002.37068 (2002).
114 Myers, M. P. *et al.* TYK2 and JAK2 are substrates of protein-tyrosine phosphatase 1B. *J Biol Chem* **276**, 47771-47774, doi:10.1074/jbc.C100583200 (2001).
115 Feldhammer, M., Uetani, N., Miranda-Saavedra, D. & Tremblay, M. L. PTP1B: a simple enzyme for a complex world. *Crit Rev Biochem Mol Biol* **48**, 430-445, doi:10.3109/10409238.2013.819830 (2013).
116 Abram, C. L. & Lowell, C. A. Shp1 function in myeloid cells. *J Leukoc Biol*, doi:10.1189/jlb.2MR0317-105R (2017).
117 Neel, B. G., Gu, H. & Pao, L. The 'Shp'ing news: SH2 domain-containing tyrosine phosphatases in cell signaling. *Trends Biochem Sci* **28**, 284-293, doi:10.1016/S0968-0004(03)00091-4 (2003).
118 You, M., Yu, D. H. & Feng, G. S. Shp-2 tyrosine phosphatase functions as a negative regulator of the interferon-stimulated Jak/STAT pathway. *Mol Cell Biol* **19**, 2416-2424 (1999).
119 Qu, C. K. Role of the SHP-2 tyrosine phosphatase in cytokine-induced signaling and cellular response. *Biochim Biophys Acta* **1592**, 297-301 (2002).
120 Bourdeau, A., Dube, N. & Tremblay, M. L. Cytoplasmic protein tyrosine phosphatases, regulation and function: the roles of PTP1B and TC-PTP. *Curr Opin Cell Biol* **17**, 203-209, doi:10.1016/j.ceb.2005.02.001 (2005).
121 Simoncic, P. D., Lee-Loy, A., Barber, D. L., Tremblay, M. L. & McGlade, C. J. The T cell protein tyrosine phosphatase is a negative regulator of janus family kinases 1 and 3. *Curr Biol* **12**, 446-453 (2002).
122 Heinonen, K. M. *et al.* T-cell protein tyrosine phosphatase deletion results in progressive systemic inflammatory disease. *Blood* **103**, 3457-3464, doi:10.1182/blood-2003-09-3153 (2004).

123 ten Hoeve, J. *et al.* Identification of a nuclear Stat1 protein tyrosine phosphatase. *Mol Cell Biol* **22**, 5662-5668 (2002).
124 Irie-Sasaki, J. *et al.* CD45 is a JAK phosphatase and negatively regulates cytokine receptor signalling. *Nature* **409**, 349-354, doi:10.1038/35053086 (2001).
125 Ratei, R. *et al.* Immunophenotype and clinical characteristics of CD45-negative and CD45-positive childhood acute lymphoblastic leukemia. *Ann Hematol* **77**, 107-114 (1998).
126 Liu, B. *et al.* Inhibition of Stat1-mediated gene activation by PIAS1. *Proc Natl Acad Sci U S A* **95**, 10626-10631 (1998).
127 Chung, C. D. *et al.* Specific inhibition of Stat3 signal transduction by PIAS3. *Science* **278**, 1803-1805 (1997).
128 Yoshimura, A. *et al.* A novel cytokine-inducible gene CIS encodes an SH2-containing protein that binds to tyrosine-phosphorylated interleukin 3 and erythropoietin receptors. *EMBO J* **14**, 2816-2826 (1995).
129 Starr, R. *et al.* A family of cytokine-inducible inhibitors of signalling. *Nature* **387**, 917-921, doi:10.1038/43206 (1997).
130 Endo, T. A. *et al.* A new protein containing an SH2 domain that inhibits JAK kinases. *Nature* **387**, 921-924, doi:10.1038/43213 (1997).
131 Naka, T. *et al.* Structure and function of a new STAT-induced STAT inhibitor. *Nature* **387**, 924-929, doi:10.1038/43219 (1997).
132 Hilton, D. J. *et al.* Twenty proteins containing a C-terminal SOCS box form five structural classes. *Proc Natl Acad Sci U S A* **95**, 114-119 (1998).
133 Sasaki, A. *et al.* Cytokine-inducible SH2 protein-3 (CIS3/SOCS3) inhibits Janus tyrosine kinase by binding through the N-terminal kinase inhibitory region as well as SH2 domain. *Genes Cells* **4**, 339-351 (1999).
134 Yasukawa, H. *et al.* The JAK-binding protein JAB inhibits Janus tyrosine kinase activity through binding in the activation loop. *EMBO J* **18**, 1309-1320, doi:10.1093/emboj/18.5.1309 (1999).
135 Piessevaux, J., Lavens, D., Peelman, F. & Tavernier, J. The many faces of the SOCS box. *Cytokine Growth Factor Rev* **19**, 371-381, doi:10.1016/j.cytogfr.2008.08.006 (2008).
136 Nicholson, S. E. *et al.* Suppressor of cytokine signaling-3 preferentially binds to the SHP-2-binding site on the shared cytokine receptor subunit gp130. *Proc Natl Acad Sci U S A* **97**, 6493-6498, doi:10.1073/pnas.100135197 (2000).
137 Giordanetto, F. & Kroemer, R. T. A three-dimensional model of Suppressor Of Cytokine Signalling 1 (SOCS-1). *Protein Eng* **16**, 115-124 (2003).
138 Babon, J. J. *et al.* Suppression of cytokine signaling by SOCS3: characterization of the mode of inhibition and the basis of its specificity. *Immunity* **36**, 239-250, doi:10.1016/j.immuni.2011.12.015 (2012).
139 Krebs, D. L. & Hilton, D. J. SOCS proteins: negative regulators of cytokine signaling. *Stem Cells* **19**, 378-387, doi:10.1634/stemcells.19-5-378 (2001).
140 Yoshimura, A., Suzuki, M., Sakaguchi, R., Hanada, T. & Yasukawa, H. SOCS, Inflammation, and Autoimmunity. *Front Immunol* **3**, 20, doi:10.3389/fimmu.2012.00020 (2012).
141 Matsumoto, A. *et al.* Suppression of STAT5 functions in liver, mammary glands, and T cells in cytokine-inducible SH2-containing protein 1 transgenic mice. *Mol Cell Biol* **19**, 6396-6407 (1999).

142 Ram, P. A. & Waxman, D. J. Role of the cytokine-inducible SH2 protein CIS in desensitization of STAT5b signaling by continuous growth hormone. *J Biol Chem* **275**, 39487-39496, doi:10.1074/jbc.M004755200 (2000).
143 Kile, B. T. *et al.* The SOCS box: a tale of destruction and degradation. *Trends Biochem Sci* **27**, 235-241 (2002).
144 Babon, J. J. *et al.* The SOCS box domain of SOCS3: structure and interaction with the elonginBC-cullin5 ubiquitin ligase. *J Mol Biol* **381**, 928-940, doi:10.1016/j.jmb.2008.06.038 (2008).
145 Fenner, J. E. *et al.* Suppressor of cytokine signaling 1 regulates the immune response to infection by a unique inhibition of type I interferon activity. *Nat Immunol* **7**, 33-39, doi:10.1038/ni1287 (2006).
146 Egli, A., Santer, D. M., O'Shea, D., Tyrrell, D. L. & Houghton, M. The impact of the interferon-lambda family on the innate and adaptive immune response to viral infections. *Emerg Microbes Infect* **3**, e51, doi:10.1038/emi.2014.51 (2014).
147 Makowska, Z., Duong, F. H., Trincucci, G., Tough, D. F. & Heim, M. H. Interferon-beta and interferon-lambda signaling is not affected by interferon-induced refractoriness to interferon-alpha in vivo. *Hepatology* **53**, 1154-1163, doi:10.1002/hep.24189 (2011).
148 Sarasin-Filipowicz, M. *et al.* Alpha interferon induces long-lasting refractoriness of JAK-STAT signaling in the mouse liver through induction of USP18/UBP43. *Mol Cell Biol* **29**, 4841-4851, doi:10.1128/MCB.00224-09 (2009).
149 Wormald, S. *et al.* The comparative roles of suppressor of cytokine signaling-1 and -3 in the inhibition and desensitization of cytokine signaling. *J Biol Chem* **281**, 11135-11143, doi:10.1074/jbc.M509595200 (2006).
150 Brand, S. *et al.* IL-28A and IL-29 mediate antiproliferative and antiviral signals in intestinal epithelial cells and murine CMV infection increases colonic IL-28A expression. *Am J Physiol Gastrointest Liver Physiol* **289**, G960-968, doi:10.1152/ajpgi.00126.2005 (2005).
151 Nicholson, S. E. & Hilton, D. J. The SOCS proteins: a new family of negative regulators of signal transduction. *J Leukoc Biol* **63**, 665-668 (1998).
152 Babon, J. J., Varghese, L. N. & Nicola, N. A. Inhibition of IL-6 family cytokines by SOCS3. *Semin Immunol* **26**, 13-19, doi:10.1016/j.smim.2013.12.004 (2014).
153 Song, M. M. & Shuai, K. The suppressor of cytokine signaling (SOCS) 1 and SOCS3 but not SOCS2 proteins inhibit interferon-mediated antiviral and antiproliferative activities. *Journal of Biological Chemistry* **273**, 35056-35062 (1998).
154 Nicholson, S. E. *et al.* Mutational analyses of the SOCS proteins suggest a dual domain requirement but distinct mechanisms for inhibition of LIF and IL-6 signal transduction. *EMBO J* **18**, 375-385, doi:10.1093/emboj/18.2.375 (1999).
155 Vlotides, G. *et al.* SOCS-1 and SOCS-3 inhibit IFN-alpha-induced expression of the antiviral proteins 2,5-OAS and MxA. *Biochem Biophys Res Commun* **320**, 1007-1014, doi:10.1016/j.bbrc.2004.06.051 (2004).
156 Croker, B. A. *et al.* SOCS3 negatively regulates IL-6 signaling in vivo. *Nat Immunol* **4**, 540-545, doi:10.1038/ni931 (2003).
157 Brand, S. *et al.* SOCS-1 inhibits expression of the antiviral proteins 2',5'-OAS and MxA induced by the novel interferon-lambdas IL-28A and IL-29. *Biochem Biophys Res Commun* **331**, 543-548, doi:10.1016/j.bbrc.2005.04.004 (2005).
158 Zitzmann, K. *et al.* Novel interferon-lambdas induce antiproliferative effects in neuroendocrine tumor cells. *Biochem Biophys Res Commun* **344**, 1334-1341, doi:10.1016/j.bbrc.2006.04.043 (2006).

159 Liu, B., Chen, S., Guan, Y. & Chen, L. Type III Interferon Induces Distinct SOCS1 Expression Pattern that Contributes to Delayed but Prolonged Activation of Jak/STAT Signaling Pathway: Implications for Treatment Non-Response in HCV Patients. *PLoS One* **10**, e0133800, doi:10.1371/journal.pone.0133800 (2015).
160 Brysha, M. *et al.* Suppressor of cytokine signaling-1 attenuates the duration of interferon gamma signal transduction in vitro and in vivo. *J Biol Chem* **276**, 22086-22089, doi:10.1074/jbc.M102737200 (2001).
161 Marine, J. C. *et al.* SOCS1 deficiency causes a lymphocyte-dependent perinatal lethality. *Cell* **98**, 609-616 (1999).
162 Starr, R. *et al.* Liver degeneration and lymphoid deficiencies in mice lacking suppressor of cytokine signaling-1. *Proc Natl Acad Sci U S A* **95**, 14395-14399 (1998).
163 Alexander, W. S. *et al.* SOCS1 is a critical inhibitor of interferon gamma signaling and prevents the potentially fatal neonatal actions of this cytokine. *Cell* **98**, 597-608 (1999).
164 Marine, J. C. *et al.* SOCS3 is essential in the regulation of fetal liver erythropoiesis. *Cell* **98**, 617-627 (1999).
165 Roberts, A. W. *et al.* Placental defects and embryonic lethality in mice lacking suppressor of cytokine signaling 3. *Proc Natl Acad Sci U S A* **98**, 9324-9329, doi:10.1073/pnas.161271798 (2001).
166 Honke, N., Shaabani, N., Zhang, D. E., Hardt, C. & Lang, K. S. Multiple functions of USP18. *Cell Death Dis* **7**, e2444, doi:10.1038/cddis.2016.326 (2016).
167 Liu, L. Q. *et al.* A novel ubiquitin-specific protease, UBP43, cloned from leukemia fusion protein AML1-ETO-expressing mice, functions in hematopoietic cell differentiation. *Mol Cell Biol* **19**, 3029-3038 (1999).
168 Schwer, H. *et al.* Cloning and characterization of a novel human ubiquitin-specific protease, a homologue of murine UBP43 (Usp18). *Genomics* **65**, 44-52, doi:10.1006/geno.2000.6148 (2000).
169 Burkart, C., Fan, J. B. & Zhang, D. E. Two independent mechanisms promote expression of an N-terminal truncated USP18 isoform with higher DeISGylation activity in the nucleus. *J Biol Chem* **287**, 4883-4893, doi:10.1074/jbc.M111.255570 (2012).
170 Malakhov, M. P., Malakhova, O. A., Kim, K. I., Ritchie, K. J. & Zhang, D. E. UBP43 (USP18) specifically removes ISG15 from conjugated proteins. *J Biol Chem* **277**, 9976-9981, doi:10.1074/jbc.M109078200 (2002).
171 Malakhova, O., Malakhov, M., Hetherington, C. & Zhang, D. E. Lipopolysaccharide activates the expression of ISG15-specific protease UBP43 via interferon regulatory factor 3. *J Biol Chem* **277**, 14703-14711, doi:10.1074/jbc.M111527200 (2002).
172 Malakhov, M. P. *et al.* High-throughput immunoblotting. Ubiquitiin-like protein ISG15 modifies key regulators of signal transduction. *J Biol Chem* **278**, 16608-16613, doi:10.1074/jbc.M208435200 (2003).
173 Francois-Newton, V. *et al.* USP18-based negative feedback control is induced by type I and type III interferons and specifically inactivates interferon alpha response. *PLoS One* **6**, e22200, doi:10.1371/journal.pone.0022200 (2011).
174 Malakhova, O. A. *et al.* Protein ISGylation modulates the JAK-STAT signaling pathway. *Genes Dev* **17**, 455-460, doi:10.1101/gad.1056303 (2003).

175 Potu, H., Sgorbissa, A. & Brancolini, C. Identification of USP18 as an important regulator of the susceptibility to IFN-alpha and drug-induced apoptosis. *Cancer Res* **70**, 655-665, doi:10.1158/0008-5472.CAN-09-1942 (2010).
176 Kim, K. I. *et al.* Ube1L and protein ISGylation are not essential for alpha/beta interferon signaling. *Mol Cell Biol* **26**, 472-479, doi:10.1128/MCB.26.2.472-479.2006 (2006).
177 Dill, M. T. *et al.* Interferon-gamma-stimulated genes, but not USP18, are expressed in livers of patients with acute hepatitis C. *Gastroenterology* **143**, 777-786 e771-776, doi:10.1053/j.gastro.2012.05.044 (2012).
178 Burkart, C. *et al.* Usp18 deficient mammary epithelial cells create an antitumour environment driven by hypersensitivity to IFN-lambda and elevated secretion of Cxcl10. *EMBO Mol Med* **5**, 967-982, doi:10.1002/emmm.201201864 (2013).
179 Meuwissen, M. E. *et al.* Human USP18 deficiency underlies type 1 interferonopathy leading to severe pseudo-TORCH syndrome. *J Exp Med* **213**, 1163-1174, doi:10.1084/jem.20151529 (2016).
180 Torre, L. A. *et al.* Global cancer statistics, 2012. *CA Cancer J Clin* **65**, 87-108, doi:10.3322/caac.21262 (2015).
181 Ferlay, J. *et al.* Cancer incidence and mortality worldwide: sources, methods and major patterns in GLOBOCAN 2012. *Int J Cancer* **136**, E359-386, doi:10.1002/ijc.29210 (2015).
182 Mortality, G. B. D. & Causes of Death, C. Global, regional, and national age-sex specific all-cause and cause-specific mortality for 240 causes of death, 1990-2013: a systematic analysis for the Global Burden of Disease Study 2013. *Lancet* **385**, 117-171, doi:10.1016/S0140-6736(14)61682-2 (2015).
183 Gelband, H. *et al.* in *Cancer: Disease Control Priorities, Third Edition (Volume 3)* (eds H. Gelband, P. Jha, R. Sankaranarayanan, & S. Horton) (2015).
184 Llovet, J. M. *et al.* Hepatocellular carcinoma. *Nat Rev Dis Primers* **2**, 16018, doi:10.1038/nrdp.2016.18 (2016).
185 European Association For The Study Of The, L., European Organisation For, R. & Treatment Of, C. EASL-EORTC clinical practice guidelines: management of hepatocellular carcinoma. *J Hepatol* **56**, 908-943, doi:10.1016/j.jhep.2011.12.001 (2012).
186 Rothweiler, S. *et al.* Generation of a murine hepatic angiosarcoma cell line and reproducible mouse tumor model. *Lab Invest* **95**, 351-362, doi:10.1038/labinvest.2014.141 (2015).
187 Bissig-Choisat, B. *et al.* Novel patient-derived xenograft and cell line models for therapeutic testing of pediatric liver cancer. *J Hepatol*, doi:10.1016/j.jhep.2016.04.009 (2016).
188 McGlynn, K. A., Petrick, J. L. & London, W. T. Global epidemiology of hepatocellular carcinoma: an emphasis on demographic and regional variability. *Clin Liver Dis* **19**, 223-238, doi:10.1016/j.cld.2015.01.001 (2015).
189 Farazi, P. A. & DePinho, R. A. Hepatocellular carcinoma pathogenesis: from genes to environment. *Nat Rev Cancer* **6**, 674-687, doi:10.1038/nrc1934 (2006).
190 de Martel, C. *et al.* Global burden of cancers attributable to infections in 2008: a review and synthetic analysis. *Lancet Oncol* **13**, 607-615, doi:10.1016/S1470-2045(12)70137-7 (2012).
191 El-Serag, H. B. & Rudolph, K. L. Hepatocellular carcinoma: epidemiology and molecular carcinogenesis. *Gastroenterology* **132**, 2557-2576, doi:10.1053/j.gastro.2007.04.061 (2007).

192 El-Serag, H. B. Epidemiology of viral hepatitis and hepatocellular carcinoma. *Gastroenterology* **142**, 1264-1273 e1261, doi:10.1053/j.gastro.2011.12.061 (2012).
193 El-Serag, H. B. Hepatocellular carcinoma. *N Engl J Med* **365**, 1118-1127, doi:10.1056/NEJMra1001683 (2011).
194 Sung, W. K. *et al.* Genome-wide survey of recurrent HBV integration in hepatocellular carcinoma. *Nat Genet* **44**, 765-769, doi:10.1038/ng.2295 (2012).
195 Koike, K. *et al.* High-level expression of hepatitis B virus HBx gene and hepatocarcinogenesis in transgenic mice. *Hepatology* **19**, 810-819 (1994).
196 Brechot, C., Pourcel, C., Louise, A., Rain, B. & Tiollais, P. Presence of integrated hepatitis B virus DNA sequences in cellular DNA of human hepatocellular carcinoma. *Nature* **286**, 533-535 (1980).
197 Chakraborty, P. R., Ruiz-Opazo, N., Shouval, D. & Shafritz, D. A. Identification of integrated hepatitis B virus DNA and expression of viral RNA in an HBsAg-producing human hepatocellular carcinoma cell line. *Nature* **286**, 531-533 (1980).
198 Shafritz, D. A., Shouval, D., Sherman, H. I., Hadziyannis, S. J. & Kew, M. C. Integration of hepatitis B virus DNA into the genome of liver cells in chronic liver disease and hepatocellular carcinoma. Studies in percutaneous liver biopsies and post-mortem tissue specimens. *N Engl J Med* **305**, 1067-1073, doi:10.1056/NEJM198110293051807 (1981).
199 Wang, J., Chenivesse, X., Henglein, B. & Brechot, C. Hepatitis B virus integration in a cyclin A gene in a hepatocellular carcinoma. *Nature* **343**, 555-557, doi:10.1038/343555a0 (1990).
200 Lok, A. S. Prevention of hepatitis B virus-related hepatocellular carcinoma. *Gastroenterology* **127**, S303-309 (2004).
201 Nault, J. C. *et al.* High frequency of telomerase reverse-transcriptase promoter somatic mutations in hepatocellular carcinoma and preneoplastic lesions. *Nat Commun* **4**, 2218, doi:10.1038/ncomms3218 (2013).
202 Levrero, M. & Zucman-Rossi, J. Mechanisms of HBV-induced hepatocellular carcinoma. *J Hepatol* **64**, S84-101, doi:10.1016/j.jhep.2016.02.021 (2016).
203 Zhang, W. *et al.* Genetic Features of Aflatoxin-Associated Hepatocellular Carcinoma. *Gastroenterology* **153**, 249-262 e242, doi:10.1053/j.gastro.2017.03.024 (2017).
204 Hsu, I. C. *et al.* Mutational hotspot in the p53 gene in human hepatocellular carcinomas. *Nature* **350**, 427-428, doi:10.1038/350427a0 (1991).
205 Wild, C. P. & Gong, Y. Y. Mycotoxins and human disease: a largely ignored global health issue. *Carcinogenesis* **31**, 71-82, doi:10.1093/carcin/bgp264 (2010).
206 Omer, R. E. *et al.* Population-attributable risk of dietary aflatoxins and hepatitis B virus infection with respect to hepatocellular carcinoma. *Nutr Cancer* **48**, 15-21, doi:10.1207/s15327914nc4801_3 (2004).
207 Wu, H. C. *et al.* Aflatoxin B1 exposure, hepatitis B virus infection, and hepatocellular carcinoma in Taiwan. *Cancer Epidemiol Biomarkers Prev* **18**, 846-853, doi:10.1158/1055-9965.EPI-08-0697 (2009).
208 Mittal, S. & El-Serag, H. B. Epidemiology of hepatocellular carcinoma: consider the population. *J Clin Gastroenterol* **47 Suppl**, S2-6, doi:10.1097/MCG.0b013e3182872f29 (2013).

209 Albeldawi, M., Soliman, M., Lopez, R. & Zein, N. N. Hepatitis C virus-associated primary hepatocellular carcinoma in non-cirrhotic patients. *Dig Dis Sci* **57**, 3265-3270, doi:10.1007/s10620-012-2260-y (2012).
210 Lemon, S. M. & McGivern, D. R. Is hepatitis C virus carcinogenic? *Gastroenterology* **142**, 1274-1278, doi:10.1053/j.gastro.2012.01.045 (2012).
211 Hernandez-Gea, V., Toffanin, S., Friedman, S. L. & Llovet, J. M. Role of the microenvironment in the pathogenesis and treatment of hepatocellular carcinoma. *Gastroenterology* **144**, 512-527, doi:10.1053/j.gastro.2013.01.002 (2013).
212 Raimondi, S., Bruno, S., Mondelli, M. U. & Maisonneuve, P. Hepatitis C virus genotype 1b as a risk factor for hepatocellular carcinoma development: a meta-analysis. *J Hepatol* **50**, 1142-1154, doi:10.1016/j.jhep.2009.01.019 (2009).
213 Rusyn, I. & Lemon, S. M. Mechanisms of HCV-induced liver cancer: what did we learn from in vitro and animal studies? *Cancer Lett* **345**, 210-215, doi:10.1016/j.canlet.2013.06.028 (2014).
214 Yoon, E. J. & Hu, K. Q. Hepatitis C virus (HCV) infection and hepatic steatosis. *Int J Med Sci* **3**, 53-56 (2006).
215 McClain, C. J., Hill, D. B., Song, Z., Deaciuc, I. & Barve, S. Monocyte activation in alcoholic liver disease. *Alcohol* **27**, 53-61 (2002).
216 Mittal, S. *et al.* Temporal trends of nonalcoholic fatty liver disease-related hepatocellular carcinoma in the veteran affairs population. *Clin Gastroenterol Hepatol* **13**, 594-601 e591, doi:10.1016/j.cgh.2014.08.013 (2015).
217 Karagozian, R., Derdak, Z. & Baffy, G. Obesity-associated mechanisms of hepatocarcinogenesis. *Metabolism* **63**, 607-617, doi:10.1016/j.metabol.2014.01.011 (2014).
218 Deugnier, Y. M. *et al.* Primary liver cancer in genetic hemochromatosis: a clinical, pathological, and pathogenetic study of 54 cases. *Gastroenterology* **104**, 228-234 (1993).
219 Perlmutter, D. H. Pathogenesis of chronic liver injury and hepatocellular carcinoma in alpha-1-antitrypsin deficiency. *Pediatr Res* **60**, 233-238, doi:10.1203/01.pdr.0000228350.61496.90 (2006).
220 Yu, M. W. & Chen, C. J. Elevated serum testosterone levels and risk of hepatocellular carcinoma. *Cancer Res* **53**, 790-794 (1993).
221 Schulze, K. *et al.* Exome sequencing of hepatocellular carcinomas identifies new mutational signatures and potential therapeutic targets. *Nat Genet* **47**, 505-511, doi:10.1038/ng.3252 (2015).
222 Chang, M. H. *et al.* Decreased incidence of hepatocellular carcinoma in hepatitis B vaccinees: a 20-year follow-up study. *J Natl Cancer Inst* **101**, 1348-1355, doi:10.1093/jnci/djp288 (2009).
223 Romano, L., Paladini, S., Van Damme, P. & Zanetti, A. R. The worldwide impact of vaccination on the control and protection of viral hepatitis B. *Dig Liver Dis* **43 Suppl 1**, S2-7, doi:10.1016/S1590-8658(10)60685-8 (2011).
224 Singal, A. K. *et al.* Antiviral therapy reduces risk of hepatocellular carcinoma in patients with hepatitis C virus-related cirrhosis. *Clin Gastroenterol Hepatol* **8**, 192-199, doi:10.1016/j.cgh.2009.10.026 (2010).
225 Lok, A. S. *et al.* Incidence of hepatocellular carcinoma and associated risk factors in hepatitis C-related advanced liver disease. *Gastroenterology* **136**, 138-148, doi:10.1053/j.gastro.2008.09.014 (2009).

226 Baumert, T. F., Juhling, F., Ono, A. & Hoshida, Y. Hepatitis C-related hepatocellular carcinoma in the era of new generation antivirals. *BMC Med* **15**, 52, doi:10.1186/s12916-017-0815-7 (2017).

227 Llovet, J. M., Bru, C. & Bruix, J. Prognosis of hepatocellular carcinoma: the BCLC staging classification. *Semin Liver Dis* **19**, 329-338, doi:10.1055/s-2007-1007122 (1999).

228 Bruix, J., Sherman, M. & American Association for the Study of Liver, D. Management of hepatocellular carcinoma: an update. *Hepatology* **53**, 1020-1022, doi:10.1002/hep.24199 (2011).

229 Yau, T. *et al.* Development of Hong Kong Liver Cancer staging system with treatment stratification for patients with hepatocellular carcinoma. *Gastroenterology* **146**, 1691-1700 e1693, doi:10.1053/j.gastro.2014.02.032 (2014).

230 A new prognostic system for hepatocellular carcinoma: a retrospective study of 435 patients: the Cancer of the Liver Italian Program (CLIP) investigators. *Hepatology* **28**, 751-755, doi:10.1002/hep.510280322 (1998).

231 Kudo, M., Chung, H. & Osaki, Y. Prognostic staging system for hepatocellular carcinoma (CLIP score): its value and limitations, and a proposal for a new staging system, the Japan Integrated Staging Score (JIS score). *J Gastroenterol* **38**, 207-215, doi:10.1007/s005350300038 (2003).

232 Llovet, J. M. *et al.* Sorafenib in advanced hepatocellular carcinoma. *N Engl J Med* **359**, 378-390, doi:10.1056/NEJMoa0708857 (2008).

233 Livraghi, T. *et al.* Sustained complete response and complications rates after radiofrequency ablation of very early hepatocellular carcinoma in cirrhosis: Is resection still the treatment of choice? *Hepatology* **47**, 82-89, doi:10.1002/hep.21933 (2008).

234 Llovet, J. M. *et al.* Arterial embolisation or chemoembolisation versus symptomatic treatment in patients with unresectable hepatocellular carcinoma: a randomised controlled trial. *Lancet* **359**, 1734-1739, doi:10.1016/S0140-6736(02)08649-X (2002).

235 Cheng, A. L. *et al.* Efficacy and safety of sorafenib in patients in the Asia-Pacific region with advanced hepatocellular carcinoma: a phase III randomised, double-blind, placebo-controlled trial. *Lancet Oncol* **10**, 25-34, doi:10.1016/S1470-2045(08)70285-7 (2009).

236 Wilhelm, S. M. *et al.* BAY 43-9006 exhibits broad spectrum oral antitumor activity and targets the RAF/MEK/ERK pathway and receptor tyrosine kinases involved in tumor progression and angiogenesis. *Cancer Res* **64**, 7099-7109, doi:10.1158/0008-5472.CAN-04-1443 (2004).

237 Wilhelm, S. M. *et al.* Preclinical overview of sorafenib, a multikinase inhibitor that targets both Raf and VEGF and PDGF receptor tyrosine kinase signaling. *Mol Cancer Ther* **7**, 3129-3140, doi:10.1158/1535-7163.MCT-08-0013 (2008).

238 Cheng, A. L. *et al.* Sunitinib versus sorafenib in advanced hepatocellular cancer: results of a randomized phase III trial. *J Clin Oncol* **31**, 4067-4075, doi:10.1200/JCO.2012.45.8372 (2013).

239 Johnson, P. J. *et al.* Brivanib versus sorafenib as first-line therapy in patients with unresectable, advanced hepatocellular carcinoma: results from the randomized phase III BRISK-FL study. *J Clin Oncol* **31**, 3517-3524, doi:10.1200/JCO.2012.48.4410 (2013).

240 Cainap, C. *et al.* Linifanib versus Sorafenib in patients with advanced hepatocellular carcinoma: results of a randomized phase III trial. *J Clin Oncol* **33**, 172-179, doi:10.1200/JCO.2013.54.3298 (2015).
241 Zhu, A. X. *et al.* SEARCH: a phase III, randomized, double-blind, placebo-controlled trial of sorafenib plus erlotinib in patients with advanced hepatocellular carcinoma. *J Clin Oncol* **33**, 559-566, doi:10.1200/JCO.2013.53.7746 (2015).
242 Worns, M. A. & Galle, P. R. HCC therapies--lessons learned. *Nat Rev Gastroenterol Hepatol* **11**, 447-452, doi:10.1038/nrgastro.2014.10 (2014).
243 Bruix, J. *et al.* Regorafenib for patients with hepatocellular carcinoma who progressed on sorafenib treatment (RESORCE): a randomised, double-blind, placebo-controlled, phase 3 trial. *Lancet* **389**, 56-66, doi:10.1016/S0140-6736(16)32453-9 (2017).
244 Feun, L. G., Li, Y.-Y., Wangpaichitr, M., Wu, C.-J. & Savaraj, N. Immunotherapy for hepatocellular carcinoma: the force awakens in HCC? *Hepatoma Research* **3**, 43, doi:10.20517/2394-5079.2016.45 (2017).
245 Greten, T. F. & Sangro, B. Targets for immunotherapy of liver cancer. *J Hepatol*, doi:10.1016/j.jhep.2017.09.007 (2017).
246 Buttner, N., Schmidt, N. & Thimme, R. Perspectives of immunotherapy in hepatocellular carcinoma (HCC). *Z Gastroenterol* **54**, 1334-1342, doi:10.1055/s-0042-120417 (2016).
247 Zucman-Rossi, J., Villanueva, A., Nault, J. C. & Llovet, J. M. Genetic Landscape and Biomarkers of Hepatocellular Carcinoma. *Gastroenterology* **149**, 1226-1239 e1224, doi:10.1053/j.gastro.2015.05.061 (2015).
248 Cancer Genome Atlas Research Network. Electronic address, w. b. e. & Cancer Genome Atlas Research, N. Comprehensive and Integrative Genomic Characterization of Hepatocellular Carcinoma. *Cell* **169**, 1327-1341 e1323, doi:10.1016/j.cell.2017.05.046 (2017).
249 Wiemann, S. U. *et al.* Hepatocyte telomere shortening and senescence are general markers of human liver cirrhosis. *FASEB J* **16**, 935-942, doi:10.1096/fj.01-0977com (2002).
250 Plentz, R. R. *et al.* Hepatocellular telomere shortening correlates with chromosomal instability and the development of human hepatoma. *Hepatology* **40**, 80-86, doi:10.1002/hep.20271 (2004).
251 Farazi, P. A. *et al.* Differential impact of telomere dysfunction on initiation and progression of hepatocellular carcinoma. *Cancer Res* **63**, 5021-5027 (2003).
252 Nault, J. C., Bioulac-Sage, P. & Zucman-Rossi, J. Hepatocellular benign tumors-from molecular classification to personalized clinical care. *Gastroenterology* **144**, 888-902, doi:10.1053/j.gastro.2013.02.032 (2013).
253 Zucman-Rossi, J. *et al.* Genotype-phenotype correlation in hepatocellular adenoma: new classification and relationship with HCC. *Hepatology* **43**, 515-524, doi:10.1002/hep.21068 (2006).
254 Alizadeh, A. A. *et al.* Toward understanding and exploiting tumor heterogeneity. *Nat Med* **21**, 846-853, doi:10.1038/nm.3915 (2015).
255 Totoki, Y. *et al.* Trans-ancestry mutational landscape of hepatocellular carcinoma genomes. *Nat Genet* **46**, 1267-1273, doi:10.1038/ng.3126 (2014).
256 Calderaro, J. *et al.* Histological subtypes of hepatocellular carcinoma are related to gene mutations and molecular tumour classification. *J Hepatol* **67**, 727-738, doi:10.1016/j.jhep.2017.05.014 (2017).

257 de La Coste, A. *et al.* Somatic mutations of the beta-catenin gene are frequent in mouse and human hepatocellular carcinomas. *Proc Natl Acad Sci U S A* **95**, 8847-8851 (1998).
258 Audard, V. *et al.* Cholestasis is a marker for hepatocellular carcinomas displaying beta-catenin mutations. *J Pathol* **212**, 345-352, doi:10.1002/path.2169 (2007).
259 Minouchi, K., Kaneko, S. & Kobayashi, K. Mutation of p53 gene in regenerative nodules in cirrhotic liver. *J Hepatol* **37**, 231-239 (2002).
260 Schlageter, M., Terracciano, L. M., D'Angelo, S. & Sorrentino, P. Histopathology of hepatocellular carcinoma. *World J Gastroenterol* **20**, 15955-15964, doi:10.3748/wjg.v20.i43.15955 (2014).
261 Schlageter, M. *et al.* Clinicopathological Features and Metastatic Pattern of Hepatocellular Carcinoma: An Autopsy Study of 398 Patients. *Pathobiology* **83**, 301-307, doi:10.1159/000446245 (2016).
262 Edmondson, H. A. & Steiner, P. E. Primary carcinoma of the liver: a study of 100 cases among 48,900 necropsies. *Cancer* **7**, 462-503 (1954).
263 Bruix, J., Sherman, M. & Practice Guidelines Committee, A. A. f. t. S. o. L. D. Management of hepatocellular carcinoma. *Hepatology* **42**, 1208-1236, doi:10.1002/hep.20933 (2005).
264 Di Tommaso, L. *et al.* Diagnostic value of HSP70, glypican 3, and glutamine synthetase in hepatocellular nodules in cirrhosis. *Hepatology* **45**, 725-734, doi:10.1002/hep.21531 (2007).
265 Di Tommaso, L. *et al.* The application of markers (HSP70 GPC3 and GS) in liver biopsies is useful for detection of hepatocellular carcinoma. *J Hepatol* **50**, 746-754, doi:10.1016/j.jhep.2008.11.014 (2009).
266 Tremosini, S. *et al.* Prospective validation of an immunohistochemical panel (glypican 3, heat shock protein 70 and glutamine synthetase) in liver biopsies for diagnosis of very early hepatocellular carcinoma. *Gut* **61**, 1481-1487, doi:10.1136/gutjnl-2011-301862 (2012).
267 International Consensus Group for Hepatocellular NeoplasiaThe International Consensus Group for Hepatocellular, N. Pathologic diagnosis of early hepatocellular carcinoma: a report of the international consensus group for hepatocellular neoplasia. *Hepatology* **49**, 658-664, doi:10.1002/hep.22709 (2009).
268 Christa, L. *et al.* Overexpression of glutamine synthetase in human primary liver cancer. *Gastroenterology* **106**, 1312-1320 (1994).
269 Osada, T. *et al.* Acquisition of glutamine synthetase expression in human hepatocarcinogenesis: relation to disease recurrence and possible regulation by ubiquitin-dependent proteolysis. *Cancer* **85**, 819-831 (1999).
270 Capurro, M. *et al.* Glypican-3: a novel serum and histochemical marker for hepatocellular carcinoma. *Gastroenterology* **125**, 89-97 (2003).
271 Zhu, Z. W. *et al.* Enhanced glypican-3 expression differentiates the majority of hepatocellular carcinomas from benign hepatic disorders. *Gut* **48**, 558-564 (2001).
272 Sung, Y. K. *et al.* Glypican-3 is overexpressed in human hepatocellular carcinoma. *Cancer Sci* **94**, 259-262 (2003).
273 Baumhoer, D. *et al.* Glypican 3 expression in human nonneoplastic, preneoplastic, and neoplastic tissues: a tissue microarray analysis of 4,387 tissue samples. *Am J Clin Pathol* **129**, 899-906, doi:10.1309/HCQWPWD50XHD2DW6 (2008).

274 Gao, W. & Ho, M. The role of glypican-3 in regulating Wnt in hepatocellular carcinomas. *Cancer Rep* **1**, 14-19 (2011).
275 Chuma, M. *et al.* Expression profiling in multistage hepatocarcinogenesis: identification of HSP70 as a molecular marker of early hepatocellular carcinoma. *Hepatology* **37**, 198-207, doi:10.1053/jhep.2003.50022 (2003).
276 Makowska, Z. *et al.* Gene expression analysis of biopsy samples reveals critical limitations of transcriptome-based molecular classifications of hepatocellular carcinoma. *J Pathol Clin Res* **2**, 80-92, doi:10.1002/cjp2.37 (2016).
277 Boyault, S. *et al.* Transcriptome classification of HCC is related to gene alterations and to new therapeutic targets. *Hepatology* **45**, 42-52, doi:10.1002/hep.21467 (2007).
278 Chiang, D. Y. *et al.* Focal gains of VEGFA and molecular classification of hepatocellular carcinoma. *Cancer Res* **68**, 6779-6788, doi:10.1158/0008-5472.CAN-08-0742 (2008).
279 Hoshida, Y. *et al.* Integrative transcriptome analysis reveals common molecular subclasses of human hepatocellular carcinoma. *Cancer Res* **69**, 7385-7392, doi:10.1158/0008-5472.CAN-09-1089 (2009).
280 Lee, J. S. *et al.* Classification and prediction of survival in hepatocellular carcinoma by gene expression profiling. *Hepatology* **40**, 667-676, doi:10.1002/hep.20375 (2004).
281 Ng, C. K. Y., Piscuoglio, S. & Terracciano, L. M. Molecular classification of hepatocellular carcinoma: The view from metabolic zonation. *Hepatology* **66**, 1377-1380, doi:10.1002/hep.29311 (2017).
282 Lok, A. S. *et al.* Des-gamma-carboxy prothrombin and alpha-fetoprotein as biomarkers for the early detection of hepatocellular carcinoma. *Gastroenterology* **138**, 493-502, doi:10.1053/j.gastro.2009.10.031 (2010).
283 Marrero, J. A. *et al.* Alpha-fetoprotein, des-gamma carboxyprothrombin, and lectin-bound alpha-fetoprotein in early hepatocellular carcinoma. *Gastroenterology* **137**, 110-118, doi:10.1053/j.gastro.2009.04.005 (2009).
284 Nakazawa, T. *et al.* Early increase in alpha-fetoprotein for predicting unfavorable clinical outcomes in patients with advanced hepatocellular carcinoma treated with sorafenib. *Eur J Gastroenterol Hepatol* **25**, 683-689, doi:10.1097/MEG.0b013e32835d913b (2013).
285 Llovet, J. M. *et al.* Plasma biomarkers as predictors of outcome in patients with advanced hepatocellular carcinoma. *Clin Cancer Res* **18**, 2290-2300, doi:10.1158/1078-0432.CCR-11-2175 (2012).
286 Llovet, J. M. & Hernandez-Gea, V. Hepatocellular carcinoma: reasons for phase III failure and novel perspectives on trial design. *Clin Cancer Res* **20**, 2072-2079, doi:10.1158/1078-0432.CCR-13-0547 (2014).
287 Munshi, N. *et al.* ARQ 197, a novel and selective inhibitor of the human c-Met receptor tyrosine kinase with antitumor activity. *Mol Cancer Ther* **9**, 1544-1553, doi:10.1158/1535-7163.MCT-09-1173 (2010).
288 Santoro, A. *et al.* Tivantinib for second-line treatment of advanced hepatocellular carcinoma: a randomised, placebo-controlled phase 2 study. *Lancet Oncol* **14**, 55-63, doi:10.1016/S1470-2045(12)70490-4 (2013).
289 Aravalli, R. N., Steer, C. J., Sahin, M. B. & Cressman, E. N. Stem cell origins and animal models of hepatocellular carcinoma. *Dig Dis Sci* **55**, 1241-1250, doi:10.1007/s10620-009-0861-x (2010).

290 Arellanes-Robledo, J., Hernández, C., Camacho, J. & Pérez-Carreón, J. I. In Vitro Models of HCC. 563-579, doi:10.1016/b978-0-12-804274-8.00042-4 (2017).
291 Bagi, C. M. & Andresen, C. J. Models of hepatocellular carcinoma and biomarker strategy. *Cancers (Basel)* **2**, 1441-1452, doi:10.3390/cancers2031441 (2010).
292 Frese, K. K. & Tuveson, D. A. Maximizing mouse cancer models. *Nat Rev Cancer* **7**, 645-658, doi:10.1038/nrc2192 (2007).
293 Clevers, H. Modeling Development and Disease with Organoids. *Cell* **165**, 1586-1597, doi:10.1016/j.cell.2016.05.082 (2016).
294 Huch, M. *et al.* Long-term culture of genome-stable bipotent stem cells from adult human liver. *Cell* **160**, 299-312, doi:10.1016/j.cell.2014.11.050 (2015).
295 Huch, M., Knoblich, J. A., Lutolf, M. P. & Martinez-Arias, A. The hope and the hype of organoid research. *Development* **144**, 938-941, doi:10.1242/dev.150201 (2017).
296 Broutier, L. *et al.* Human primary liver cancer-derived organoid cultures for disease modeling and drug screening. *Nat Med*, doi:10.1038/nm.4438 (2017).
297 Fatehullah, A., Tan, S. H. & Barker, N. Organoids as an in vitro model of human development and disease. *Nat Cell Biol* **18**, 246-254, doi:10.1038/ncb3312 (2016).
298 Gross, C. *et al.* Model Matters: Differences in Orthotopic Rat Hepatocellular Carcinoma Physiology Determine Therapy Response to Sorafenib. *Clin Cancer Res* **21**, 4440-4450, doi:10.1158/1078-0432.CCR-14-2018 (2015).
299 Alshareeda, A. T., Sakaguchi, K., Abumaree, M., Mohd Zin, N. K. & Shimizu, T. The potential of cell sheet technique on the development of hepatocellular carcinoma in rat models. *PLoS One* **12**, e0184004, doi:10.1371/journal.pone.0184004 (2017).
300 Mulrooney-Cousins, P. M., Chauhan, R., Churchill, N. D. & Michalak, T. I. Primary seronegative but molecularly evident hepadnaviral infection engages liver and induces hepatocarcinoma in the woodchuck model of hepatitis B. *PLoS Pathog* **10**, e1004332, doi:10.1371/journal.ppat.1004332 (2014).
301 Mitchell, J. *et al.* Validation of a Preclinical Model of Diethylnitrosamine-Induced Hepatic Neoplasia in Yucatan Miniature Pigs. *Oncology* **91**, 90-100, doi:10.1159/000446074 (2016).
302 Heindryckx, F., Colle, I. & Van Vlierberghe, H. Experimental mouse models for hepatocellular carcinoma research. *Int J Exp Pathol* **90**, 367-386, doi:10.1111/j.1365-2613.2009.00656.x (2009).
303 Caviglia, J. M. & Schwabe, R. F. Mouse models of liver cancer. *Methods Mol Biol* **1267**, 165-183, doi:10.1007/978-1-4939-2297-0_8 (2015).
304 Santos, N. P., Colaco, A. A. & Oliveira, P. A. Animal models as a tool in hepatocellular carcinoma research: A Review. *Tumour Biol* **39**, 1010428317695923, doi:10.1177/1010428317695923 (2017).
305 Dragani, T. A., Manenti, G., Gariboldi, M., De Gregorio, L. & Pierotti, M. A. Genetics of liver tumor susceptibility in mice. *Toxicol Lett* **82-83**, 613-619 (1995).
306 Wu, L., Tang, Z. Y. & Li, Y. Experimental models of hepatocellular carcinoma: developments and evolution. *J Cancer Res Clin Oncol* **135**, 969-981, doi:10.1007/s00432-009-0591-7 (2009).
307 Fausto, N. & Campbell, J. S. Mouse models of hepatocellular carcinoma. *Semin Liver Dis* **30**, 87-98, doi:10.1055/s-0030-1247135 (2010).

308 Horie, Y. *et al.* Hepatocyte-specific Pten deficiency results in steatohepatitis and hepatocellular carcinomas. *J Clin Invest* **113**, 1774-1783, doi:10.1172/JCI20513 (2004).

309 Mauad, T. H. *et al.* Mice with homozygous disruption of the mdr2 P-glycoprotein gene. A novel animal model for studies of nonsuppurative inflammatory cholangitis and hepatocarcinogenesis. *Am J Pathol* **145**, 1237-1245 (1994).

310 Bettermann, K. *et al.* TAK1 suppresses a NEMO-dependent but NF-kappaB-independent pathway to liver cancer. *Cancer Cell* **17**, 481-496, doi:10.1016/j.ccr.2010.03.021 (2010).

311 Calvisi, D. F., Factor, V. M., Ladu, S., Conner, E. A. & Thorgeirsson, S. S. Disruption of beta-catenin pathway or genomic instability define two distinct categories of liver cancer in transgenic mice. *Gastroenterology* **126**, 1374-1386 (2004).

312 Lee, J. S. *et al.* Application of comparative functional genomics to identify best-fit mouse models to study human cancer. *Nat Genet* **36**, 1306-1311, doi:10.1038/ng1481 (2004).

313 Dandri, M. & Petersen, J. Animal models of HBV infection. *Best Pract Res Clin Gastroenterol* **31**, 273-279, doi:10.1016/j.bpg.2017.04.014 (2017).

314 Dorner, M. *et al.* Completion of the entire hepatitis C virus life cycle in genetically humanized mice. *Nature* **501**, 237-241, doi:10.1038/nature12427 (2013).

315 Dandri, M. *et al.* Repopulation of mouse liver with human hepatocytes and in vivo infection with hepatitis B virus. *Hepatology* **33**, 981-988, doi:10.1053/jhep.2001.23314 (2001).

316 Billerbeck, E. *et al.* Mouse models of acute and chronic hepacivirus infection. *Science* **357**, 204-208, doi:10.1126/science.aal1962 (2017).

317 Li, Y., Tang, Z. Y. & Hou, J. X. Hepatocellular carcinoma: insight from animal models. *Nat Rev Gastroenterol Hepatol* **9**, 32-43, doi:10.1038/nrgastro.2011.196 (2011).

318 Kim, C. M., Koike, K., Saito, I., Miyamura, T. & Jay, G. HBx gene of hepatitis B virus induces liver cancer in transgenic mice. *Nature* **351**, 317-320, doi:10.1038/351317a0 (1991).

319 Dunsford, H. A., Sell, S. & Chisari, F. V. Hepatocarcinogenesis due to chronic liver cell injury in hepatitis B virus transgenic mice. *Cancer Res* **50**, 3400-3407 (1990).

320 Chisari, F. V. *et al.* A transgenic mouse model of the chronic hepatitis B surface antigen carrier state. *Science* **230**, 1157-1160 (1985).

321 Lakhtakia, R. *et al.* Hepatocellular carcinoma in a hepatitis B 'x' transgenic mouse model: A sequential pathological evaluation. *J Gastroenterol Hepatol* **18**, 80-91 (2003).

322 Sell, S., Hunt, J. M., Dunsford, H. A. & Chisari, F. V. Synergy between hepatitis B virus expression and chemical hepatocarcinogens in transgenic mice. *Cancer Res* **51**, 1278-1285 (1991).

323 Koike, K., Moriya, K. & Matsuura, Y. Animal models for hepatitis C and related liver disease. *Hepatol Res* **40**, 69-82, doi:10.1111/j.1872-034X.2009.00593.x (2010).

324 Moriya, K. *et al.* The core protein of hepatitis C virus induces hepatocellular carcinoma in transgenic mice. *Nat Med* **4**, 1065-1067, doi:10.1038/2053 (1998).

325 Koike, K., Moriya, K. & Kimura, S. Role of hepatitis C virus in the development of hepatocellular carcinoma: transgenic approach to viral hepatocarcinogenesis. *J Gastroenterol Hepatol* **17**, 394-400 (2002).

326 Rao, K. V. & Vesselinovitch, S. D. Age- and sex-associated diethylnitrosamine dealkylation activity of the mouse liver and hepatocarcinogenesis. *Cancer Res* **33**, 1625-1627 (1973).
327 Bakiri, L. & Wagner, E. F. Mouse models for liver cancer. *Mol Oncol* **7**, 206-223, doi:10.1016/j.molonc.2013.01.005 (2013).
328 Hacker, H. J., Mtiro, H., Bannasch, P. & Vesselinovitch, S. D. Histochemical profile of mouse hepatocellular adenomas and carcinomas induced by a single dose of diethylnitrosamine. *Cancer Res* **51**, 1952-1958 (1991).
329 Binato, M. *et al.* Mouse model of diethylnitrosamine-induced gastric cancer. *J Surg Res* **148**, 152-157, doi:10.1016/j.jss.2007.12.748 (2008).
330 McGlynn, K. A. *et al.* Susceptibility to aflatoxin B1-related primary hepatocellular carcinoma in mice and humans. *Cancer Res* **63**, 4594-4601 (2003).
331 Weber, A., O'Connor, T. & Heikenwalder, M. Next Generation of Preclinical Liver Cancer Models. *Clin Cancer Res* **21**, 4254-4256, doi:10.1158/1078-0432.CCR-15-1152 (2015).
332 Tentler, J. J. *et al.* Patient-derived tumour xenografts as models for oncology drug development. *Nat Rev Clin Oncol* **9**, 338-350, doi:10.1038/nrclinonc.2012.61 (2012).
333 Siolas, D. & Hannon, G. J. Patient-derived tumor xenografts: transforming clinical samples into mouse models. *Cancer Res* **73**, 5315-5319, doi:10.1158/0008-5472.CAN-13-1069 (2013).
334 Yan, M. *et al.* Establishment of NOD/SCID mouse models of human hepatocellular carcinoma via subcutaneous transplantation of histologically intact tumor tissue. *Chin J Cancer Res* **25**, 289-298, doi:10.3978/j.issn.1000-9604.2013.05.02 (2013).
335 Huynh, H., Soo, K. C., Chow, P. K., Panasci, L. & Tran, E. Xenografts of human hepatocellular carcinoma: a useful model for testing drugs. *Clin Cancer Res* **12**, 4306-4314, doi:10.1158/1078-0432.CCR-05-2568 (2006).
336 Xin, H. *et al.* Establishment and characterization of 7 novel hepatocellular carcinoma cell lines from patient-derived tumor xenografts. *PLoS One* **9**, e85308, doi:10.1371/journal.pone.0085308 (2014).
337 Gu, Q. *et al.* Genomic characterization of a large panel of patient-derived hepatocellular carcinoma xenograft tumor models for preclinical development. *Oncotarget* **6**, 20160-20176, doi:10.18632/oncotarget.3969 (2015).
338 Jiang, Z. *et al.* Anti-GPC3-CAR T Cells Suppress the Growth of Tumor Cells in Patient-Derived Xenografts of Hepatocellular Carcinoma. *Front Immunol* **7**, 690, doi:10.3389/fimmu.2016.00690 (2016).
339 Sun, F. X. *et al.* Establishment of a metastatic model of human hepatocellular carcinoma in nude mice via orthotopic implantation of histologically intact tissues. *Int J Cancer* **66**, 239-243, doi:10.1002/(SICI)1097-0215(19960410)66:2<239::AID-IJC17>3.0.CO;2-7 (1996).
340 Armengol, C. *et al.* Orthotopic implantation of human hepatocellular carcinoma in mice: analysis of tumor progression and establishment of the BCLC-9 cell line. *Clin Cancer Res* **10**, 2150-2157 (2004).
341 Kotenko, S. V. IFN-lambdas. *Curr Opin Immunol* **23**, 583-590, doi:10.1016/j.coi.2011.07.007 (2011).
342 Bolen, C. R., Ding, S., Robek, M. D. & Kleinstein, S. H. Dynamic expression profiling of type I and type III interferon-stimulated hepatocytes reveals a stable hierarchy of gene expression. *Hepatology* **59**, 1262-1272, doi:10.1002/hep.26657 (2014).

343 Jilg, N. *et al.* Kinetic differences in the induction of interferon stimulated genes by interferon-alpha and interleukin 28B are altered by infection with hepatitis C virus. *Hepatology* **59**, 1250-1261, doi:10.1002/hep.26653 (2014).
344 Lupberger, J. *et al.* Epidermal growth factor receptor signaling impairs the antiviral activity of interferon-alpha. *Hepatology* **58**, 1225-1235, doi:10.1002/hep.26404 (2013).
345 Barbaro, G. *et al.* Intravenous recombinant interferon-beta versus interferon-alpha-2b and ribavirin in combination for short-term treatment of chronic hepatitis C patients not responding to interferon-alpha. Multicenter Interferon Beta Italian Group Investigators. *Scand J Gastroenterol* **34**, 928-933 (1999).
346 Der, S. D., Zhou, A., Williams, B. R. & Silverman, R. H. Identification of genes differentially regulated by interferon alpha, beta, or gamma using oligonucleotide arrays. *Proc Natl Acad Sci U S A* **95**, 15623-15628 (1998).
347 Pulverer, J. E. *et al.* Temporal and spatial resolution of type I and III interferon responses in vivo. *J Virol* **84**, 8626-8638, doi:10.1128/JVI.00303-10 (2010).
348 Jaks, E., Gavutis, M., Uze, G., Martal, J. & Piehler, J. Differential receptor subunit affinities of type I interferons govern differential signal activation. *J Mol Biol* **366**, 525-539, doi:10.1016/j.jmb.2006.11.053 (2007).
349 Uze, G., Schreiber, G., Piehler, J. & Pellegrini, S. The receptor of the type I interferon family. *Curr Top Microbiol Immunol* **316**, 71-95 (2007).
350 Duong, F. H. *et al.* IFN-lambda receptor 1 expression is induced in chronic hepatitis C and correlates with the IFN-lambda3 genotype and with nonresponsiveness to IFN-alpha therapies. *J Exp Med* **211**, 857-868, doi:10.1084/jem.20131557 (2014).
351 Mordstein, M. *et al.* Interferon-lambda contributes to innate immunity of mice against influenza A virus but not against hepatotropic viruses. *PLoS Pathog* **4**, e1000151, doi:10.1371/journal.ppat.1000151 (2008).
352 Grossmann, J. Molecular mechanisms of "detachment-induced apoptosis--Anoikis". *Apoptosis* **7**, 247-260 (2002).
353 Butler, K. A. *et al.* Prevention of Human Lymphoproliferative Tumor Formation in Ovarian Cancer Patient-Derived Xenografts. *Neoplasia* **19**, 628-636, doi:10.1016/j.neo.2017.04.007 (2017).
354 Chen, K., Ahmed, S., Adeyi, O., Dick, J. E. & Ghanekar, A. Human solid tumor xenografts in immunodeficient mice are vulnerable to lymphomagenesis associated with Epstein-Barr virus. *PLoS One* **7**, e39294, doi:10.1371/journal.pone.0039294 (2012).
355 Bondarenko, G. *et al.* Patient-Derived Tumor Xenografts Are Susceptible to Formation of Human Lymphocytic Tumors. *Neoplasia* **17**, 735-741, doi:10.1016/j.neo.2015.09.004 (2015).
356 Choi, Y. Y. *et al.* Establishment and characterisation of patient-derived xenografts as paraclinical models for gastric cancer. *Sci Rep* **6**, 22172, doi:10.1038/srep22172 (2016).
357 Martinez-Garcia, R. *et al.* Transcriptional dissection of pancreatic tumors engrafted in mice. *Genome Med* **6**, 27, doi:10.1186/gm544 (2014).

VI Curriculum Vitae

Name: *Tanja Blumer*
Nationality: *Swiss*
Date of Birth: *13.09.1988*
Phone: *+41 79 853 52 25*
e-mail: *t.blumer@unibas.ch*

EDUCATION AND EXPERIENCE

09/2012 - 02/2018 *PhD; Cell Biology - Liver cancer and interferon signaling*
Hepatology group, Department Biomedicine, University Hospital Basel

02/2012 – 06/2012 *Research Associate*
Bernhard-Nocht Institute for Tropical Medicine Hamburg, Germany

09/2010 – 01/2012 *MSc; Infection Biology and Epidemiology*
Joint program of the Bernhard-Nocht Institute for Tropical Medicine of Hamburg, Germany and the Swiss Tropical and Public Health Institute of Basel

09/2007 – 08/2010 *BSc; Biology*
University of Basel

LANGUAGES

(Swiss-) German	*native*
English	*fluent*
French	*basic*

COMPUTATIONAL SKILLS

MS Office, Prism, Illustrator, Photoshop and Endnote

COURSES

LTK Module 1: Introductory Course in Laboratory Animal Science; Basel, Switzerland

PyRAT – Animal Management System

GCP-Basiskurs; Clinical Trial Unit, University Hospital Basel

GCP-Aufbaukurs: Clinical Trial Unit, University Hospital Basel

---

PUBLICATIONS

2017 **SOCS1 is an inducible negative regulator of interferon λ (IFN- λ)-induced gene expression *in vivo.***

Blumer T, Coto-Llerena M, Duong FHT, Heim MH. **J Biol Chem**

2015 **YAP promotes proliferation, chemoresistance, and angiogenesis in human cholangiocarcinoma through TEAD transcription factors.**

Marti P, Stein C, Blumer T, Abraham Y, Dill MT, Pikiolek M, Orsini V, Jurisic G, Megel P, Makowska Z, Agarinis C, Tornillo L, Bouwmeester T, Ruffner H, Bauer A, Parker CN, Schmelzle T, Terracciano LM, Heim MH, Tchorz JS. **Hepatology**

2014 **WASH-driven actin polmerization is required for efficient mycrobacterial phagosome maturation arrest.**

Kolonko M, Geffken AC, Blumer T, Hagens K, Schaible UE, Hagedorn M. **Cell Microbiol**

2013 **Sequential induction of type I and II interferons mediates a long-lasting gene induction in the liver in response to a novel toll-like receptor 9 agonist.**

Makowska Z, Blumer T, Duong FH, La Monica N, Kandimalla ER, Heim MH. **J Hepatol**